



# **[<sup>18</sup>F]Fluoride as a Nucleophile for the Ring Opening of Cyclic Ammonium Salts**

Inaugural-Dissertation  
zur  
Erlangung des Doktorgrades  
der Mathematischen-Naturwissenschaftlichen Fakultät  
der Universität zu Köln

Vorgelegt von  
Yannick Keuthen  
Aus Dortmund

Köln, 2025

Berichtersteller (Gutachter):

Prof. Dr. Boris D. Zlatopolskiy

Prof. Dr. Bernd Goldfuß

Tag der mündlichen Prüfung:

13.03.2025

## Danksagung

An dieser Stelle möchte ich mich bei allen Menschen bedanken, die mich während der Entstehung dieser Dissertation unterstützt und begleitet haben. Ohne ihre Hilfe wäre diese Arbeit nicht in der vorliegenden Form möglich gewesen.

Mein besonderer Dank gilt Herrn Prof. Dr. Bernd Neumaier, für die Gelegenheit diese Dissertation am INM-5: Nuklearchemie durchführen zu dürfen, für seine stetige Unterstützung, hilfreichen Ratschläge und permanente Ermutigung sowie für die Bereitstellung hervorragender Arbeitsbedingungen.

Besonders möchte ich auch meinem Doktorvater Professor Dr. Boris Zlatopolskiy, für die stets kompetente Betreuung sowie für die unermüdliche Unterstützung und das Vertrauen, das er mir entgegengebracht hat, danken. Seine fachliche Expertise und Ideen haben maßgeblich zu dieser Arbeit beigetragen.

Zudem danke ich Professor Dr. Bernd Goldfuß für die freundliche Übernahme des Zweitgutachtens und Professor Dr. Ines Neundorf für die Zweitbetreuung im Thesis Advisory Committee und den Prüfungsvorsitz.

Des Weiteren danke ich allen Mitgliedern des INM-5 für das freundliche Arbeitsumfeld. Besonders möchte ich Dr. Birte Drewes und Dr. Marcus Holschbach für die Messung meiner NMR-Proben sowie Dr. Swen Humpert, Dr. Dirk Bier und Tobias Wachten für die Messung meiner Masse-Proben danken.

Ebenfalls danke ich Dr. Felix Neumaier für seine schnelle und gründliche Hilfe bei der Verfassung und Korrektur von wissenschaftlichen Texten.

Besonders wertvoll war die Zusammenarbeit mit meinen Mitdoktoranden, die mir durch ihre Anregungen, ihr Feedback und ihre freundliche Unterstützung immer wieder neue Perspektiven eröffnet haben.

Ein herzliches Dankeschön gilt auch meiner Familie, die mir in allen Phasen dieser Dissertation bedingungslos den Rücken gestärkt hat. Ihr Vertrauen und Ihre Geduld haben mir die nötige Kraft gegeben, auch in schwierigen Momenten weiterzumachen. Besonders meiner Frau danke ich für die unerschütterliche Unterstützung und Liebe, die mir über die Jahre hinweg stets Halt gegeben haben.

## 1 Abstract

This thesis describes the development of novel methods for the preparation of radiofluorinated aliphatic amines. Specifically, DABCO (1,4-diazabicyclo[2.2.2]octane) and 3-hydroxyazetidinium salts were investigated as precursors for nucleophilic ring opening with [ $^{18}\text{F}$ ]fluoride under “minimalist” conditions.

The nucleophilic ring opening of DABCO salts was investigated. Starting with a 3-phenylpropyl DABCO salt as an aliphatic model compound for optimization studies, the radiofluorinated ring opening product, the corresponding *N'*-2- [ $^{18}\text{F}$ ]fluoroethylpiperazine could be prepared with RCCs of  $96 \pm 4\%$ . Thereafter, aliphatic DABCO salts with alkyne and azide motifs were synthesized and evaluated as radiofluorination precursors, which afforded the  $^{18}\text{F}$ -labeled products with RCCs of  $63 \pm 4\%$  and  $48 \pm 2\%$ , respectively. Furthermore, several *N'*-2- [ $^{18}\text{F}$ ]fluoroethylpiperazines were synthesized by ring-opening of suitable DABCO salt intermediates, which were prepared *in situ* by treating benzoyl chloride, tosyl chloride, bromo-iodo-pyridine or 4-trifluoromethanesulfonate benzaldehyde with DABCO in tetrahydrofuran (THF). Subsequent radiofluorination under minimalist conditions demonstrated that the DABCO motif in these salts acts as an effective leaving group, affording the respective *N'*-2- [ $^{18}\text{F}$ ]fluoroethylpiperazines with RCCs of  $28 \pm 1\%$ ,  $32 \pm 1\%$ ,  $46 \pm 3\%$ , and  $47 \pm 3\%$ , respectively.

Next, a phenyl DABCO salt was synthesized as aromatic model compound and radiofluorinated under reaction conditions optimized to account for the higher reactivity. This afforded the corresponding  $^{18}\text{F}$ -labeled product with RCCs of up to  $98 \pm 1\%$ . Subsequent screening of additional DABCO salts confirmed excellent radiolabeling efficiencies, with RCCs of  $66 \pm 5\%$  to  $98 \pm 1\%$  for various aromatic model compounds, and  $38 \pm 1\%$  for an azide-substituted compound.

Several attempts were made to apply this method to the radiolabeling of pharmaceutical compounds. Synthesis of amino acids and PSMA (prostate-specific membrane antigen) ligand precursors containing the *N*-alkyl-substituted DABCO motif was explored but proved unsuccessful. Further efforts to prepare and radiofluorinate DABCO-substituted prosthetic groups and linkers for conjugation with pharmacophores also failed. Likewise, attempts to prepare a DABCO-based precursor for the radiosynthesis of PSMA ligands did not yield viable results.

## 1 Abstract

Next, the radiofluorination of a model 3-hydroxyazetidinium salt was optimized with regard to the heating method (conventional vs. inductive) and other reaction parameters. The best radiochemical conversions (RCCs) of  $65 \pm 10\%$  were obtained in MeCN with an inductive heater at  $110\text{ }^{\circ}\text{C}$  for 5 minutes. These conditions were then applied for the preparation of  $^{18}\text{F}$ -labeled more complex, clickable azetidines. The radiofluorination of a 3-propargoxy-substituted 3-hydroxyazetidinium salt did not yield any radiolabeled product, while the corresponding azide-substituted salt was successfully radiolabeled with RCCs of  $26 \pm 1\%$ .

In conclusion, while the methods developed in this study show significant potential, their practical application to radiopharmaceutical synthesis remains not unfold. The challenges encountered in their application for PET-tracer synthesis underscore the need for further optimization and refinement to make them viable for practical radiopharmaceutical applications.

### 2 Kurzzusammenfassung

Diese Arbeit behandelt die Entwicklung neuartiger Methoden zur Herstellung von radiofluorierten aliphatischen Aminen. Konkret wurden DABCO (1,4-Diazabicyclo[2.2.2]octan)- und 3-Hydroxyazetidiniumsalze als Vorstufen für die nukleophile Ringöffnung mit [<sup>18</sup>F]Fluorid unter „minimalistischen“ Bedingungen untersucht.

Es wurde mit der Untersuchung der nukleophilen Ringöffnung von DABCO-Salzen begonnen. Ausgehend von einem 3-Phenylpropyl-DABCO-Salz als aliphatische Modellverbindung für Optimierungen konnte das radiofluorierte Ringöffnungsprodukt, das entsprechende *N'*-2-[<sup>18</sup>F]Fluorethylpiperazin, mit RCCs von 96 ± 4% hergestellt werden. Danach wurden aliphatische DABCO-Salze mit Alkin- und Azid-Gruppen synthetisiert und als Radiofluorierungsvorläufer bewertet, die radiofluorierte Produkte mit RCCs von 63 ± 4 % bzw. 48 ± 2 % lieferten. Darüber hinaus wurden mehrere *N'*-2-[<sup>18</sup>F]Fluorethylpiperazine durch Ringöffnung geeigneter DABCO-Salz-Vorläufer synthetisiert. Diese wurden *in situ* durch das Versetzen von Benzoylchlorid, Tosylchlorid, Bromiodpyridin oder 4-Trifluormethansulfonat-Benzaldehyd mit DABCO in Tetrahydrofuran (THF) hergestellt. Die anschließende Radiofluorierung unter minimalistischen Bedingungen zeigte, dass das DABCO-Motiv in diesen Salzen eine effektive Abgangsgruppe ist und die entsprechenden *N'*-2-[<sup>18</sup>F]Fluorethylpiperazine mit RCCs von 28 ± 1 %, 32 ± 1 %, 46 ± 3 % bzw. 47 ± 3 % liefert.

Als nächstes wurde ein Phenyl-DABCO-Salz als aromatische Modellverbindung synthetisiert und unter milderer Reaktionsbedingungen radiofluoriert, die im Hinblick auf die höhere Reaktivität optimiert wurden. Dadurch wurde das entsprechende <sup>18</sup>F-markierte Produkt mit RCCs von bis zu 98 ± 1 % erhalten. Ein anschließendes Screening weiterer DABCO-Salze bestätigte eine ausgezeichnete Radiomarkierungseffizienz dieser, mit RCCs von 66 ± 5 % bis 98 ± 1 % für verschiedene aromatische Modellverbindungen und 38 ± 1 % für eine azidsubstituierte Verbindung.

Es wurden mehrere Versuche unternommen, diese Methode für die Radiomarkierung von pharmazeutischen Verbindungen anzuwenden. Die Synthese von Aminosäuren und PSMA (Prostata-spezifisches Membranantigen)-Ligandenvorläufern, die das N-Alkyl-substituierte DABCO-Motiv enthalten, wurde erprobt, blieb aber erfolglos. Weitere Versuche, DABCO-substituierte prosthetische Gruppen und Linker für die Konjugation mit Pharmakophoren herzustellen und zu radiofluorieren, schlugen ebenfalls fehl. Auch die Versuche, einen DABCO-

## 2 Kurzzusammenfassung

basierten Vorläufer für die Radiosynthese von PSMA-Liganden herzustellen, brachten keine brauchbaren Ergebnisse.

Anschließend wurde die Radiofluorierung eines modellhaften 3-Hydroxyazetidiniumsalzes im Hinblick auf die Heizmethode (konventionell vs. induktiv) und andere Reaktionsparameter optimiert. Die besten radiochemischen Umsätze (RCCs) von  $65 \pm 10 \%$  wurden in MeCN mit einer induktiven Heizung bei  $110 \text{ }^\circ\text{C}$  für 5 Minuten erzielt. Diese Bedingungen wurden dann für die Herstellung von  $^{18}\text{F}$ -markierten komplexeren, klickbaren 3-Hydroxyazetidiniumsalzen verwendet. Die Radiofluorierung eines 3-Propargoxy-substituierten 3-Hydroxyazetidiniumsalzes ergab kein radioaktiv markiertes Produkt, während das entsprechende Azid-substituierte Salz mit RCCs von  $26 \pm 1\%$  erfolgreich radioaktiv markiert wurde.

Zusammenfassend lässt sich sagen, dass die in dieser Studie entwickelten Methoden zwar ein erhebliches Potenzial aufweisen, ihre praktische Anwendung für die radiopharmazeutische Synthese jedoch noch nicht ausgereift ist. Die Herausforderungen, die bei ihrer Anwendung für die PET-Tracer-Synthese aufgetreten sind, unterstreichen die Notwendigkeit einer weiteren Optimierung und Verfeinerung, um sie für praktische radiopharmazeutische Anwendungen nutzbar zu machen.

## Table of Contents

<b>1</b>	<b>Abstract .....</b>	<b>1</b>
<b>2</b>	<b>Kurzzusammenfassung .....</b>	<b>3</b>
<b>3</b>	<b>Introduction .....</b>	<b>7</b>
3.1	Beta plus decay .....	7
3.2	Electrophilic Radiofluorination .....	10
3.3	Nucleophilic Radiofluorination .....	10
3.3.1	Minimalist Radiofluorination .....	14
3.4	Onium Salts as Substrates for Nucleophilic Aromatic Radiofluorination .....	18
3.4.1	Nitrogen Salts as Precursors for Radiolabeling.....	18
3.4.2	Iodonium Salts .....	20
3.4.3	Sulfonium Salts .....	24
3.5	Ring Opening Radiofluorinations of Cyclic Ammonium Salts .....	26
3.5.1	Azetidinium Salts.....	26
3.5.2	DABCO Salts as Targets for Ring Opening Nucleophilic Attacks .....	28
<b>4</b>	<b>Aim of this Work .....</b>	<b>33</b>
<b>5</b>	<b>Results and Discussion.....</b>	<b>34</b>
5.1	Manuscript Part .....	34
5.2	DABCO Salts .....	44
5.2.1	Optimization of Ring Opening Reaction.....	44
5.2.2	Influence of Solvent on Ring Opening Ratio .....	47
5.2.3	Attempts to Prepare DABCO Salts Containing Pharmacophores .....	49
5.3	3-Hydroxyazetidinium Salts .....	60
5.3.1	Optimization of Reaction Conditions.....	60
5.3.2	Preparation of Radiolabeled Prosthetic Groups for Click Labeling.....	64
<b>6</b>	<b>Summary and Outlook.....</b>	<b>66</b>
<b>7</b>	<b>Experimental Part.....</b>	<b>67</b>
7.1	Supporting Information of the Manuscript .....	67
7.2	Experimental Part for DABCO Salts.....	145
7.3	Experimental Part for 3-Hydroxyazetidinium Salts.....	159
<b>8</b>	<b>References .....</b>	<b>166</b>
<b>9</b>	<b>List of Abbreviations.....</b>	<b>169</b>

<b>10 List of Figures .....</b>	<b>170</b>
<b>11 List of Tables .....</b>	<b>176</b>
<b>12 Attachment: Erklärung gemäß § 7 Absatz 8.....</b>	<b>177</b>

### 3 Introduction

#### 3.1 $\beta^+$ Decay

The decay of proton-rich radionuclides occurs through two distinct mechanisms: electron capture ( $\epsilon$ ) and  $\beta^+$  decay. A nuclide can undergo  $\beta^+$  decay only if the energy difference between the parent and daughter nuclides, plus the energy of all emitted particles, exceeds 1022 eV—the combined rest mass energy of two electrons or positrons. Nuclides with insufficient mass defect to account for the energy of two electrons can only undergo electron capture. For nuclides capable of  $\beta^+$  decay, electron capture may also occur, with the ratio of these two decay modes depending on the specific nuclide<sup>[1]</sup>.

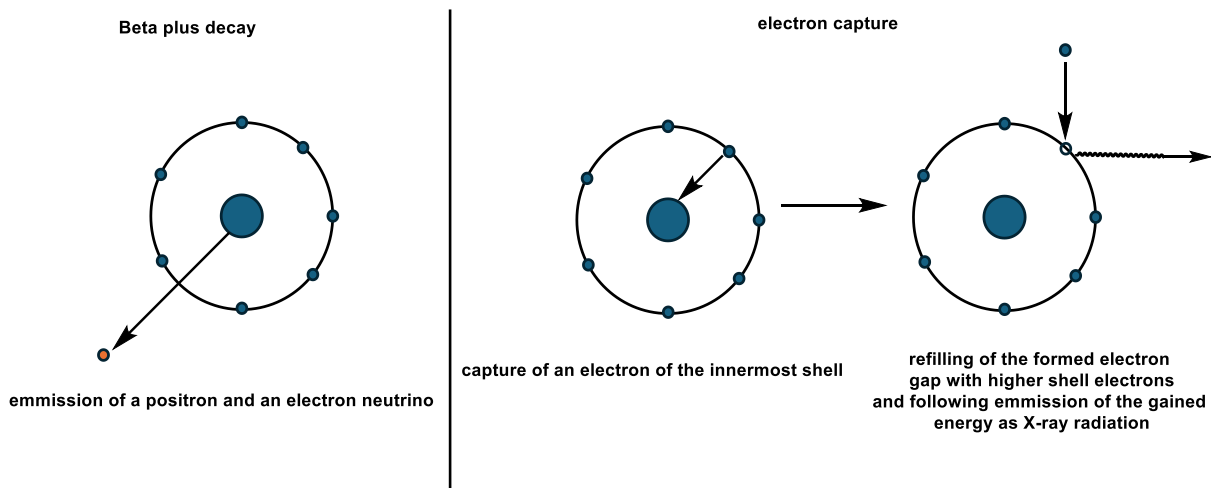


Figure 1: Radioactive decay options for proton rich nuclides.

In electron capture, an inner-shell electron, typically from the K-shell due to its close proximity to the nucleus, is captured by the nucleus. The captured electron combines with a proton to form a neutron, thus reducing the proton richness of the nucleus. The electron vacancy resulting from the capture is filled by an electron from a higher-energy shell, and the energy released in this process is either emitted as X-ray radiation or in the form of an Auger electron. In  $\beta^+$  decay, the nucleus is stabilized by conversion of a proton into a neutron, releasing a positron and an electron antineutrino. For  $\beta^+$  decay to occur, the available energy must be sufficient to produce the positron and account for the mass and charge balance resulting from proton-to-neutron conversion (Figure 1).

After emission, the positron loses kinetic energy and may either combine with an electron to form a positronium or undergo direct annihilation under emission of two gamma photons at

### 3 Introduction

an angle of  $180^\circ$ . In biological tissues, direct annihilation occurs in approximately 60% of events, with positronium formation occurring in the remaining 40%<sup>[2]</sup>.

Positronium can exist in two configurations: as *ortho*-positronium with parallel spins and a mean lifetime of approximately 142 ns in a vacuum, or as *para*-positronium with antiparallel spins and a mean lifetime of approximately 125 ps in a vacuum<sup>[3]</sup>. The ratio of *ortho*- to *para*-positronium formation in biological tissues amounts to 3:1<sup>[4]</sup>. Only about 0.5% of *ortho*-positronium undergoes decay into three gamma photons<sup>[4]</sup>. Instead, *ortho*-positronium primarily undergoes pick-off annihilation by reacting with nearby electrons, or it interacts with biomolecules like oxygen to form a *para*-positronium (Figure 2)<sup>[3,2,4]</sup>. The pick-off annihilation and the decay of *para*-positronium result in the emission of two gamma photons at an angle of  $180^\circ$ . Therefore, this emission is the predominantly observed one, providing the basis for nuclear imaging methods that rely on coincidence detection of the two photons.

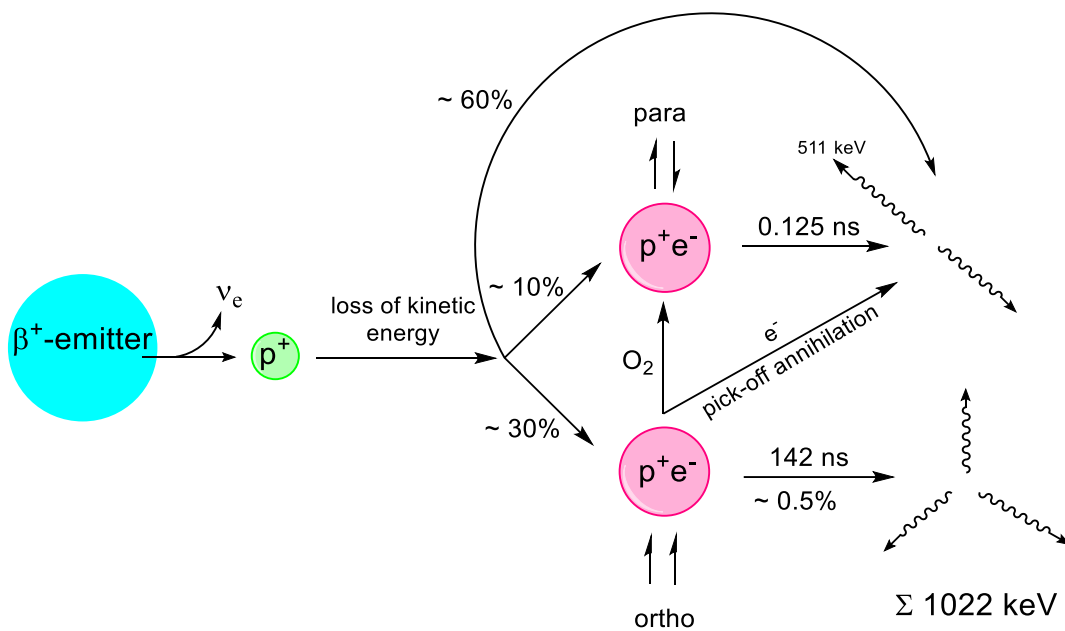


Figure 2: Scheme of  $\beta^+$ -decay with positronium variants<sup>[3,2,4]</sup>.

In particular, nuclides that undergo  $\beta^+$  decay are used as radiolabels for positron emission tomography (PET) tracers. The most commonly used PET nuclides and their properties are summarized in Table 1.

### 3 Introduction

Table 1: Physical properties of radionuclides commonly used in positron emission tomography<sup>[5]</sup>.

Nuclide	Half-life / min	Decay Mode	Maximum positron energy / keV	Mean positron range (in water) /mm
<sup>18</sup> F	109.8	$\beta^+$ : 96.9% $\epsilon$ : 3.1%	634	0.6
<sup>68</sup> Ga	67.8	$\beta^+$ : 88.9% $\epsilon$ : 11.1%	1899	3.5
<sup>11</sup> C	20.4	$\beta^+$ : 99.8% $\epsilon$ : 0.2%	960	1.2
<sup>13</sup> N	10.0	$\beta^+$ : 100% $\epsilon$ : 0%	1199	1.8
<sup>15</sup> O	2.0	$\beta^+$ : 99.9% $\epsilon$ : 0.1%	1732	3.0
<sup>82</sup> Rb	1.3	$\beta^+$ : 81.8% $\epsilon$ : 13.1%	3378	7.1

Among these, fluorine-18 (<sup>18</sup>F) is the most widely used PET nuclide due to its favorable physical properties and high availability in large quantities in the form of [<sup>18</sup>F]fluoride. A <sup>18</sup>F half-life of approximately 110 minutes enables the transportation of radiofluorinated tracers from specialized facilities to surrounding hospitals. Additionally, its relatively low maximum positron energy enhances the achievable PET image resolution relative to other PET nuclides by minimizing the positron range before annihilation. Furthermore, since many pharmaceuticals contain fluorine atoms, <sup>19</sup>F in these compounds can be replaced by <sup>18</sup>F without altering their physicochemical and biological properties.

### 3.2 Electrophilic Radiofluorination

In radiofluorination it is often differentiated between electrophilic and nucleophilic fluorine-18, depending on the chemical species of the resulting nuclide which is determined by the selection of the nuclear reaction used for the production of the fluorine-18. So called electrophilic fluorine-18 is obtained using the  $^{20}\text{Ne}(d,\alpha)^{18}\text{F}$  reaction, which yields anhydrous  $^{18}\text{F}\text{F}_2$  gas. However, extraction of these gases without addition of a carrier results in low and inconsistent recoveries<sup>[6]</sup>. Adding  $^{19}\text{F}\text{F}_2$  as a carrier improves the reproducibility and recovery yield but reduces the maximum radiochemical yields (RCYs) and significantly decreases the molar activity ( $A_m$ ), which is critical for many radiopharmaceutical applications. The  $^{20}\text{Ne}(d,\alpha)^{18}\text{F}$  reaction has a production yield of 0.40 GBq/ $\mu\text{Ah}$  and the molar activity of  $^{18}\text{F}\text{F}_2$  produced via the  $^{20}\text{Ne}(d,\alpha)^{18}\text{F}$  route is around 100 MBq/ $\mu\text{mol}$ <sup>[7]</sup>.

### 3.3 Nucleophilic Radiofluorination

Fluorine-18 used in nucleophilic radiofluorination is produced via the  $^{18}\text{O}(p,n)^{18}\text{F}$  reaction with  $^{18}\text{O}\text{H}_2\text{O}$  as the target, this reaction provides a high production yield of 2.22 GBq/ $\mu\text{Ah}$  and a high molar activity of approximately 600 GBq/ $\mu\text{mol}$ <sup>[7]</sup>. In recent years, nucleophilic radiofluorination has become more prevalent than electrophilic radiofluorination due to several inherent advantages. These include the use of no-carrier-added nucleophilic  $^{18}\text{F}$ fluoride, easier handling of dissolved  $^{18}\text{F}$ fluoride as opposed to gaseous  $^{18}\text{F}\text{F}_2$ , and the superior efficiency of the  $^{18}\text{O}(p,n)^{18}\text{F}$  reaction. Nucleophilic radiofluorination typically begins with the isolation of  $^{18}\text{F}$ fluoride from the aqueous phase generated during extraction of the target water. This step is critical for enhancing the reactivity of  $^{18}\text{F}$ fluoride, since formation of a hydrated complex due to the high Lewis acidity of fluoride substantially reduces its nucleophilicity (Figure 3)<sup>[8,9]</sup>.

### 3 Introduction

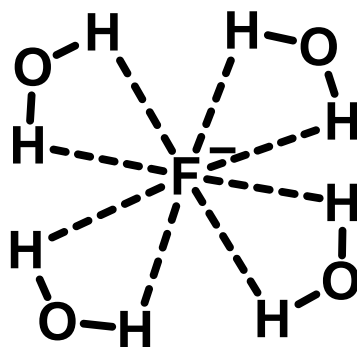


Figure 3: Coordination of water molecules around fluorine in water.

Firstly, the target water is given through an anion exchange cartridge trapping the [ $^{18}\text{F}$ ]fluoride and separating it from unwanted metallic trace impurities originating from the target and the surrounding tubing<sup>[10]</sup>. Afterwards, the [ $^{18}\text{F}$ ]fluoride is eluted with an aqueous (or organic aqueous) solution of  $\text{K}_2\text{CO}_3$  as an elution salt and Kryptofix[2.2.2] is added as a phase transfer catalyst increasing the solubility of [ $^{18}\text{F}$ ]KF in organic solvents. The water shell surrounding the [ $^{18}\text{F}$ ]fluoride anion can now be removed by repeated azeotropic distillation of the aqueous phase with acetonitrile, which is typically performed at 70–110 °C under reduced pressure. Following this, a solution of the labeling precursor in reaction solvent is added, and the reaction mixture is stirred under appropriate temperature for appropriate time, followed by removal of any protecting groups if needed (Figure 4).

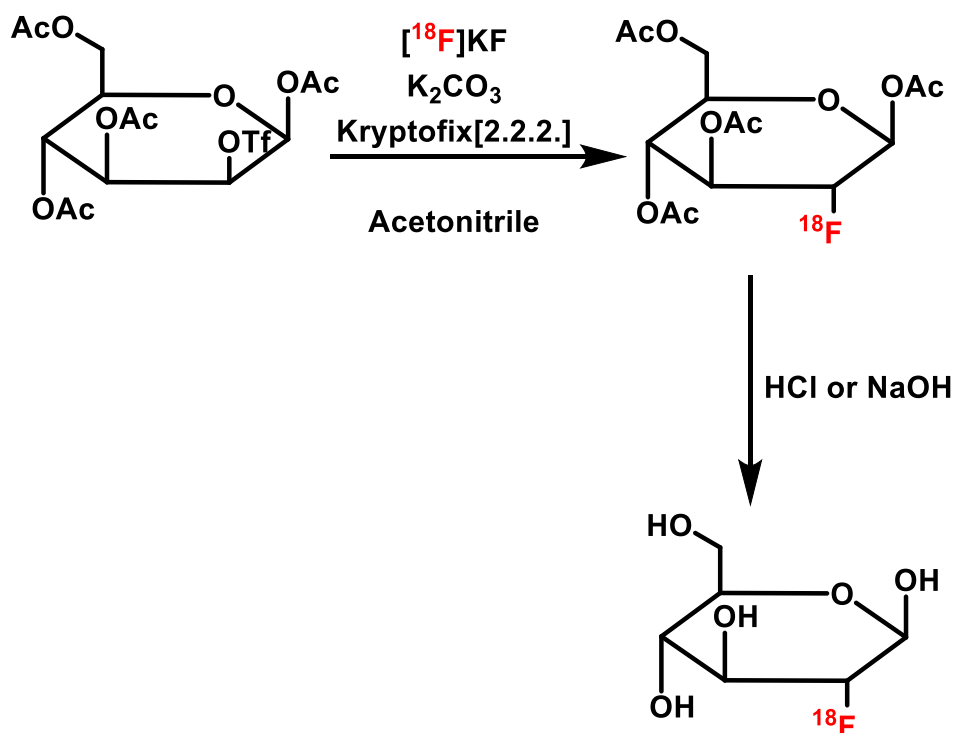


Figure 4: Preparation of [ $^{18}\text{F}$ ]FDG by nucleophilic radiofluorination<sup>[11]</sup>.

### 3 Introduction

Nucleophilic radiofluorination is primarily performed using  $S_N2$  and  $S_NAr$  reactions.  $S_N2$  reactions proceed through a backside attack of the nucleophile on the electrophilic carbon opposite to the leaving group. This results in inversion of the stereoconfiguration of the substrate, allowing for predictable stereochemical outcomes (Figure 5). The starting materials for  $S_N2$  reactions are aliphatic compounds with leaving groups like sulfonates or halides, which are readily available or can be synthesized in a single step from the corresponding alcohols. In contrast, the  $S_N1$  reaction is less suitable for radiofluorinations, as formation of the flat carbocation compromises the stereochemical integrity, producing a pair of stereoisomers that would necessitate cumbersome separation — an impractical requirement for the synthesis of compounds containing short-lived radionuclides.  $S_N1$  reactions are the dominant reaction pathway at tertiary carbons as the backside attack is heavily limited or outright impossible due to steric limitations and the carbocation formed as part of the  $S_N1$  reaction is stabilized. At secondary carbons, both  $S_N1$  and  $S_N2$  substitutions are possible. To control the selectivity, in these cases the selection of appropriate conditions is crucial. Polar aprotic solvents, low temperatures and good nucleophiles favor the  $S_N2$  reaction. Polar aprotic solvents are able to separate the charged nucleophiles from their counter ions allowing for “naked” nucleophiles, which are favorable for nucleophilic attacks and therefore for the  $S_N2$  reaction. Polar protic solvents stabilize the carbocation and deactivate the nucleophile promoting the  $S_N1$  reaction. Low temperatures favor the  $S_N2$  reaction as well, as high temperatures are favorable or outright necessary for the formation of the carbocation. A high nucleophilicity of the nucleophile favors the  $S_N2$  reaction as the rate determining step of the  $S_N2$  reaction is the backside attack of the nucleophile while in the  $S_N1$  reaction the rate determining step consists of the formation of the carbocation and is wholly independent of the nucleophilicity of the nucleophile. For primary carbons the  $S_N2$  reaction is nearly exclusively prevalent as the carbocation is not sufficiently stabilized. Aside from the  $S_N1$  reactions, eliminations are the most common occurring side reactions. The  $E1$  reaction occurs as a side reaction during  $S_N1$  reactions. The  $E2$  reaction is a side reaction of the  $S_N2$  reaction and therefore has to be taken into account. Generally, the  $E2$  reaction is favored over the  $S_N2$  reaction when a strong base is used, or steric hindrance is present either in the nucleophile or at the carbon center. In radiofluorination the change of the nucleophile is not feasible, therefore, the prominent avenues to suppress the undesired  $E2$  are the choice of leaving group (better leaving groups promote eliminations), reaction temperature and the substitution of the target carbon.

### 3 Introduction

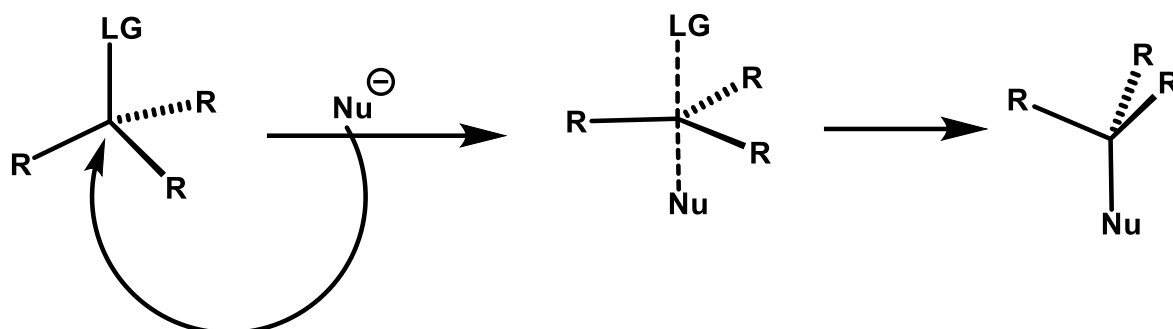
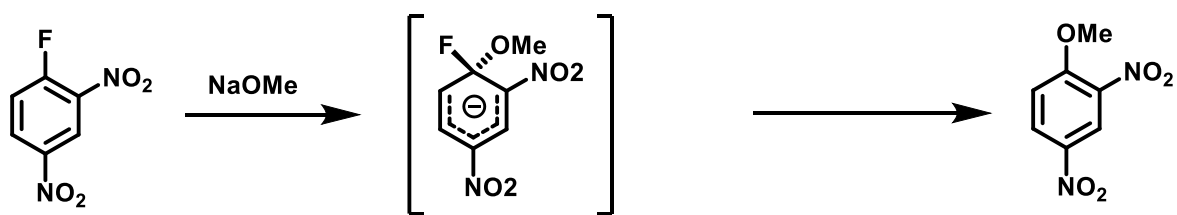


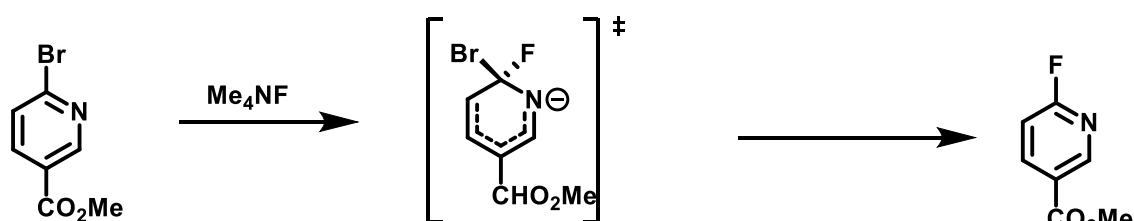
Figure 5: Mechanism of the S<sub>N</sub>2 reaction.

S<sub>N</sub>Ar reactions are another widely used approach for nucleophilic radiofluorination. However, in the case of the utilization of the conventional leaving groups like NO<sub>2</sub>, Me<sub>3</sub>N<sup>+</sup> or Hal, S<sub>N</sub>Ar radiofluorinations are only applicable to highly activated aromatic rings, e.g., aromatics substituted with strongly electron-withdrawing groups like nitro or chloro substituents<sup>[9]</sup>.

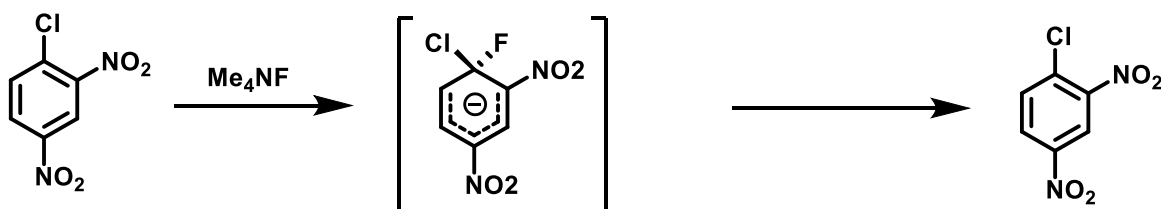
The mechanism of S<sub>N</sub>Ar reactions at highly activated aromatic compounds was long believed to consist of the attack of the nucleophile on the aromatic ring forming the so called Meisenheimer complex which can be even isolatable in some cases. Afterwards, the leaving group is cleaved under rearomatization forming the S<sub>N</sub>Ar product. However, Kwan et al. showed in 2018 that this reaction mechanism is feasible only for electron poor arenes, which bear poor leaving groups, and whose Meisenheimer complexes are stabilized<sup>[12]</sup>. In arenes with better leaving groups, the reaction proceeds mainly via a concerted mechanism, in which the addition of the nucleophile directly leads to the elimination of the leaving group. Arenes, which contain good leaving groups, and are stabilized concerning the formation of the transition state, react via a borderline mechanism between the concerted mechanism and the formation of a Meisenheimer complex, showing that these two mechanisms are examples of two extremes of a continuum of reaction mechanisms (Figure 6).



Typical reaction via Meisenheimer complex



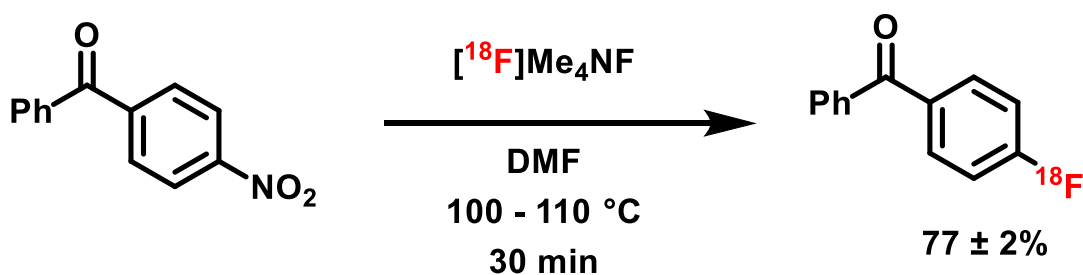
Concerted reaction mechanism



Borderline reaction mechanism between concerted and Meisenheimer complex mechanism

Figure 6: Mechanisms of the  $S_NAr$  reaction.

An example of aromatic radiofluorination is shown in Figure 7. In this case, the radiofluorinating reagent  $^{18}\text{F}\text{Me}_4\text{NF}$  was generated *in situ* by treating  $^{18}\text{F}\text{KF}/\text{K}_2\text{CO}_3/\text{K}_2.2.2$  with  $\text{Me}_4\text{NHCO}_3$ . This approach resulted in an RCC of 77%, whereas reaction with  $^{18}\text{F}\text{KF}/\text{K}_2\text{CO}_3/\text{K}_2.2.2$  without  $\text{Me}_4\text{NHCO}$  yielded no product<sup>[9]</sup>.

Figure 7: Example for  $S_NAr$  radiofluorination<sup>[9]</sup>.

### 3.3.1 Minimalist Radiofluorination

In recent years, several approaches have been developed to simplify nucleophilic radiofluorination and to eliminate the need for repeated azeotropic drying of  $^{18}\text{F}$ fluoride.

### 3 Introduction

The minimalist method simplifies radiofluorination even further by eliminating the need for external elution salts and phase-transfer catalysts<sup>[13]</sup>. Instead, it uses solutions of onium salt precursors, like ammonium, iodonium or sulfonium salts in alcohols, typically MeOH, for elution of [<sup>18</sup>F]fluoride from an anion exchange resin (Figure 8). Afterwards, the low-boiling MeOH is evaporated, affording dried [<sup>18</sup>F]fluoride salt of the precursor that can be directly used for radiofluorination. The simplicity of this reaction leads to easier purification of the radiofluorinated product as well as higher activity yields as such radiolabeling can be carried out far faster than the classical radiofluorination with Kryptofix and K<sub>2</sub>CO<sub>3</sub>. An example of a minimalist reaction is shown in Figure 9<sup>[13]</sup>.

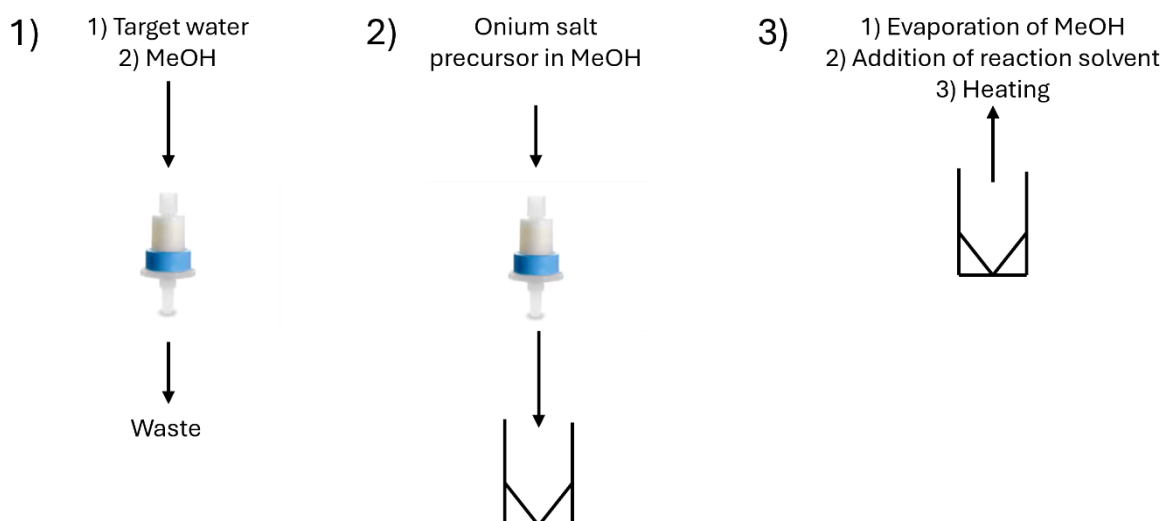


Figure 8: [<sup>18</sup>F]Fluoride workup with onium salt precursors as elution salts.

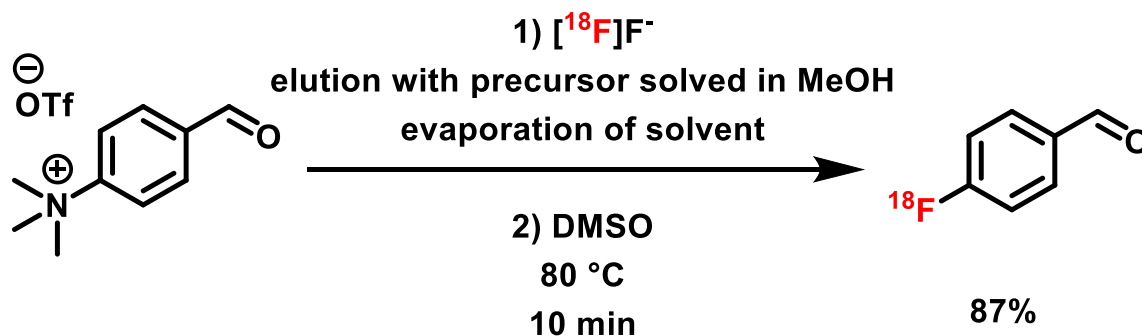


Figure 9: Minimalist radiofluorination of trimethylammonium benzaldehyde triflate.

The minimalist approach eliminates the need for an external base, and, consequently, can be applied for radiolabeling of base-sensitive precursors and preparation of base-sensitive radiofluorinated compounds. Exemplary, it allows for direct radiofluorination of base-

sensitive active esters (Figure 10), which is impossible using the conventional protocol for  $^{18}\text{F}$ -fluorination.

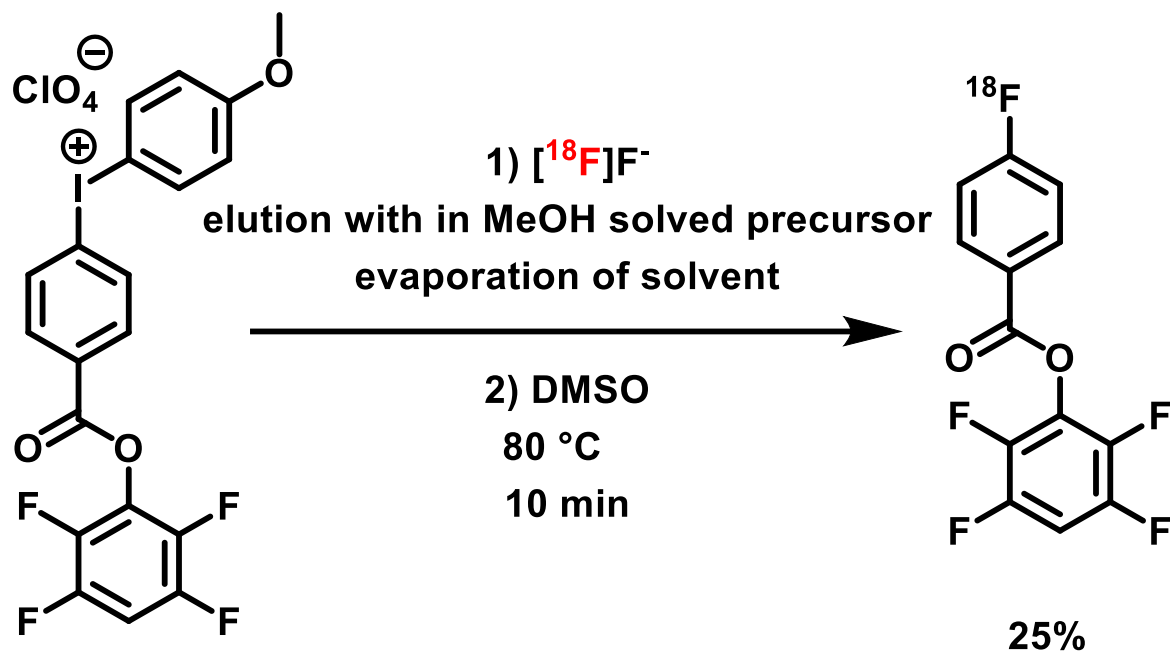


Figure 10: Minimalist radiofluorination of an active ester.

Moreover, the minimalist approach enables “green” radiolabeling of highly activated substrates simply by elution of  $[^{18}\text{F}]\text{F}^-$  from a anion exchange resin with ethanolic solution of the appropriate onium salt precursor followed by heating of the resulting solution (Figure 11)<sup>[14]</sup>.

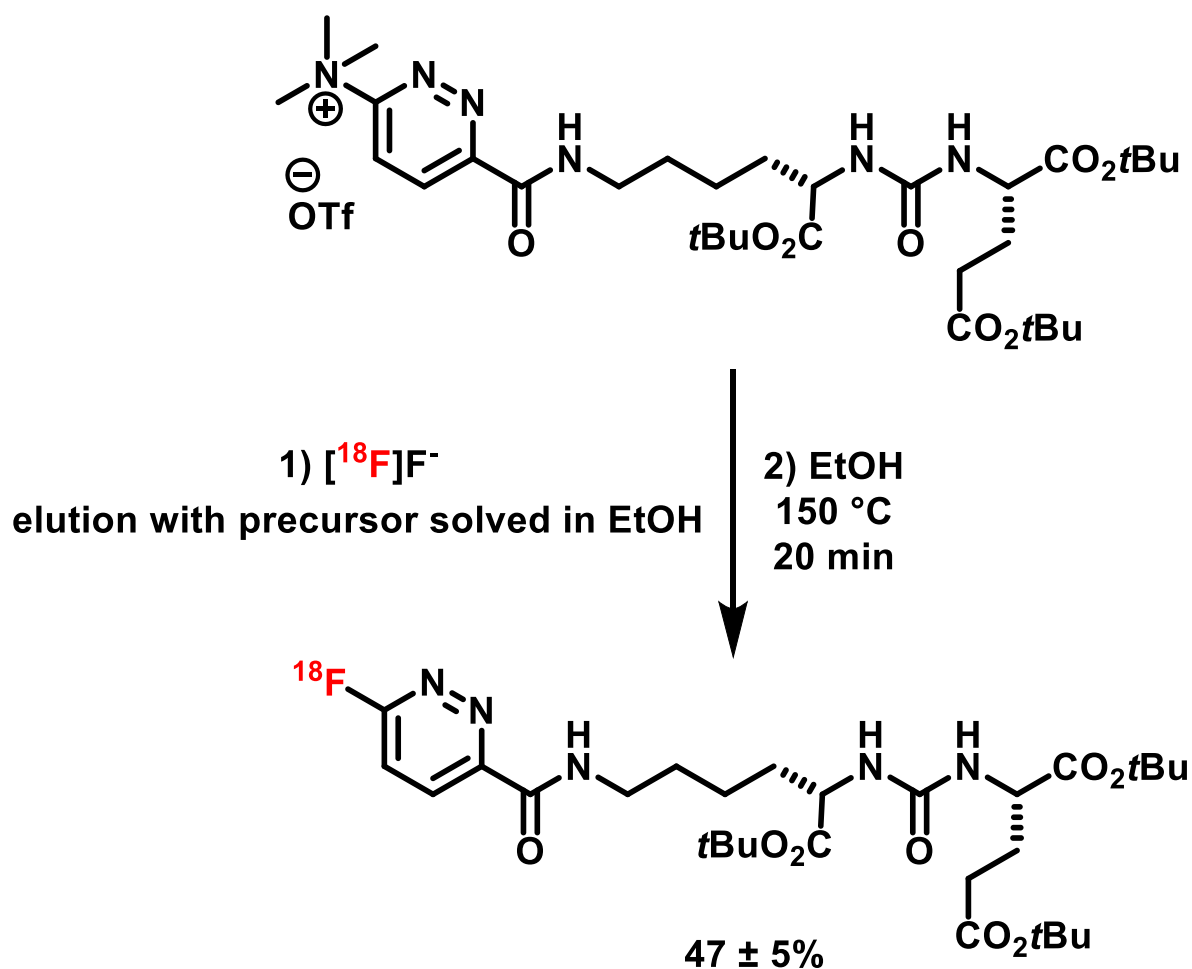


Figure 11: Radiofluorination of a derivative of a PSMA inhibitor with the green minimalist approach.

In summary, the minimalist approach offers a streamlined and more rapid protocol than conventional nucleophilic radiofluorination methods by eliminating the need for azeotropic drying and a base as well as any additives. This results in higher RCYs and molar activities, and enables application of base-sensitive substrates.

### 3.4 Onium Salts as Substrates for Nucleophilic Aromatic Radiofluorination

Onium salts are excellent substrates for nucleophilic aromatic radiofluorination due to their straightforward synthesis and stability under standard conditions. Common types of onium salt precursors include *N, N, N*-trialkylammonium, triarylsulfonium and diaryliodonium salts (Figure 12).

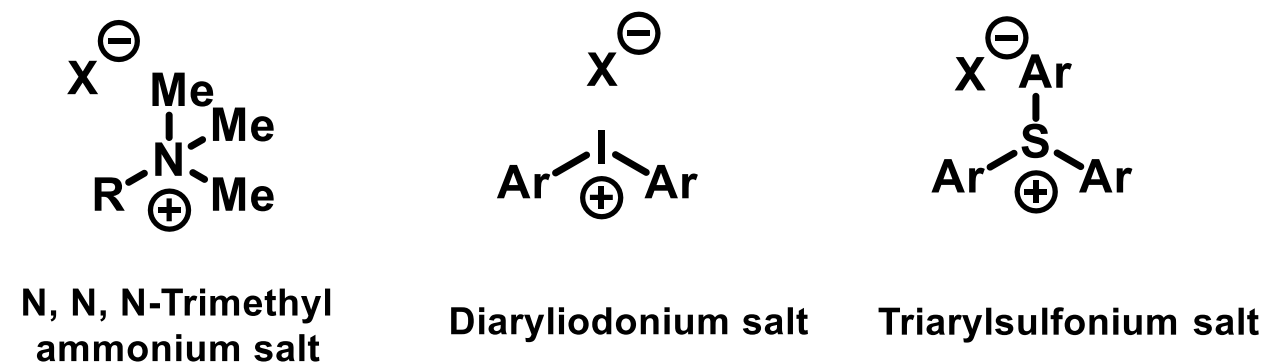


Figure 12: Overview of onium salt precursors conveniently used for nucleophilic aromatic radiofluorination.

#### 3.4.1 Nitrogen Salts as Precursors for Radiolabeling

*N, N, N*-Trimethylammonium salt precursors remain the most widely used members of this family, while pyridinium, quinuclidinium and DABCO salts have been employed in some specific cases. *N, N, N*-Trimethylammonium salts can be readily synthesized by treating the corresponding amines with methyl iodide or methyl triflate. However, depending on the activation of the aromatic ring, radiofluorination of these salts can result in the formation of [<sup>18</sup>F]methyl fluoride as an undesired side product of the concurrent S<sub>N</sub>2 substitution (Figure 13)<sup>[15]</sup>.

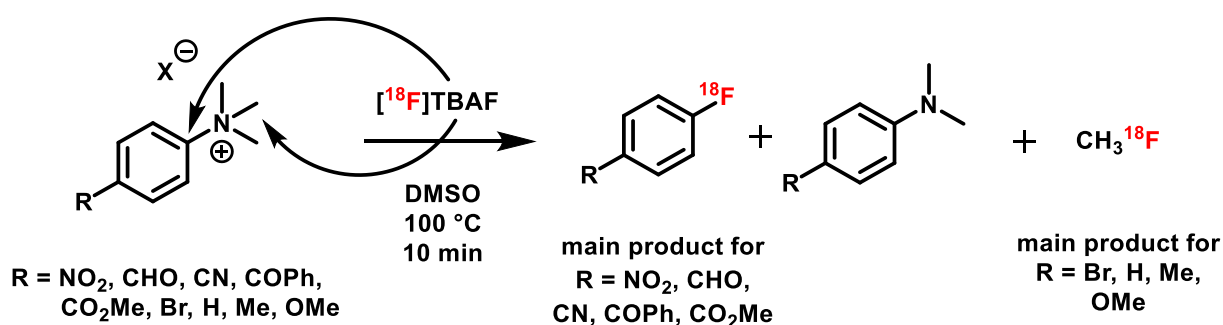


Figure 13: Formation of undesired side products in radiofluorination of *N, N, N*-trimethylammonium salts<sup>[15]</sup>. In addition to trimethylammonium salts, pyridinium salts can act as leaving groups for the nucleophilic radiofluorination of heteroaromatic compounds. These salts are accessible through various synthetic routes, such as treatment of the corresponding amines with pyrylium tetrafluoroborate (Figure 14). Pyridinium salts offer the advantage of avoiding the

### 3 Introduction

[<sup>18</sup>F]methyl fluoride side reaction and are compatible with base-sensitive substrates. They can also be utilized in automated radiolabeling protocols, making them suitable for use in commercial radiosynthesis modules<sup>[16]</sup>. Unfortunately, the substrate scope of the protocol is limited exclusively to the highly activated heteroaromatics like pyrimidines (at the second or fourth position).

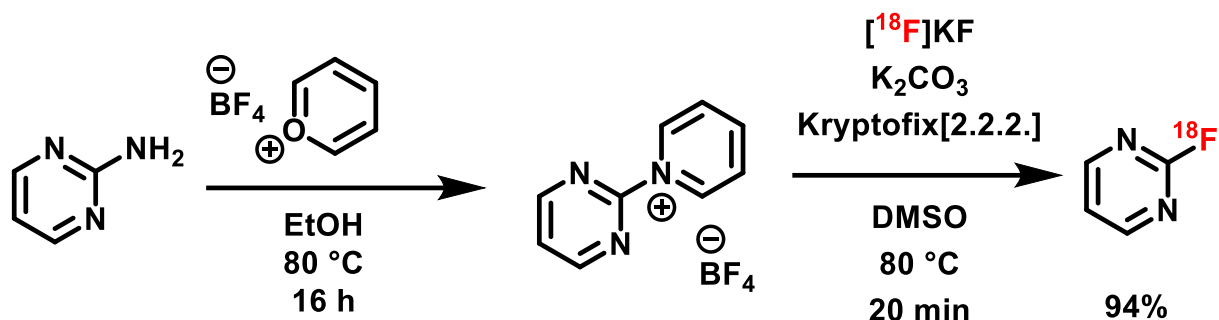


Figure 14: Use of a pyridinium salt as precursor for nucleophilic radiofluorination<sup>[16]</sup>.

Alternatively, DABCO salts can serve as precursors for nucleophilic aromatic radiofluorinations. The synthesis of DABCO salts precursors is rather challenging due to the potential for an S<sub>N</sub>2 ring-opening side reaction involving either nucleophilic leaving groups or DABCO itself. This necessitates precise control of the reaction conditions to avoid side reactions, which can be achieved by selecting non-nucleophilic leaving groups, lowering the DABCO equivalents, or reducing the reaction temperature<sup>[17,18]</sup>. A DABCO salt precursor has been successfully used for the preparation of 5-iodo-2-[<sup>18</sup>F]fluoropyridine, which proved to be a valuable prosthetic group for indirect radiofluorination of thiol-containing substrates via Pd-catalyzed *S*-arylation (Figure 15). This approach has been applied for the indirect radiofluorination of several pharmacologically relevant structures, including a PSMA ligand, polypeptides and BSA protein<sup>[18]</sup>.

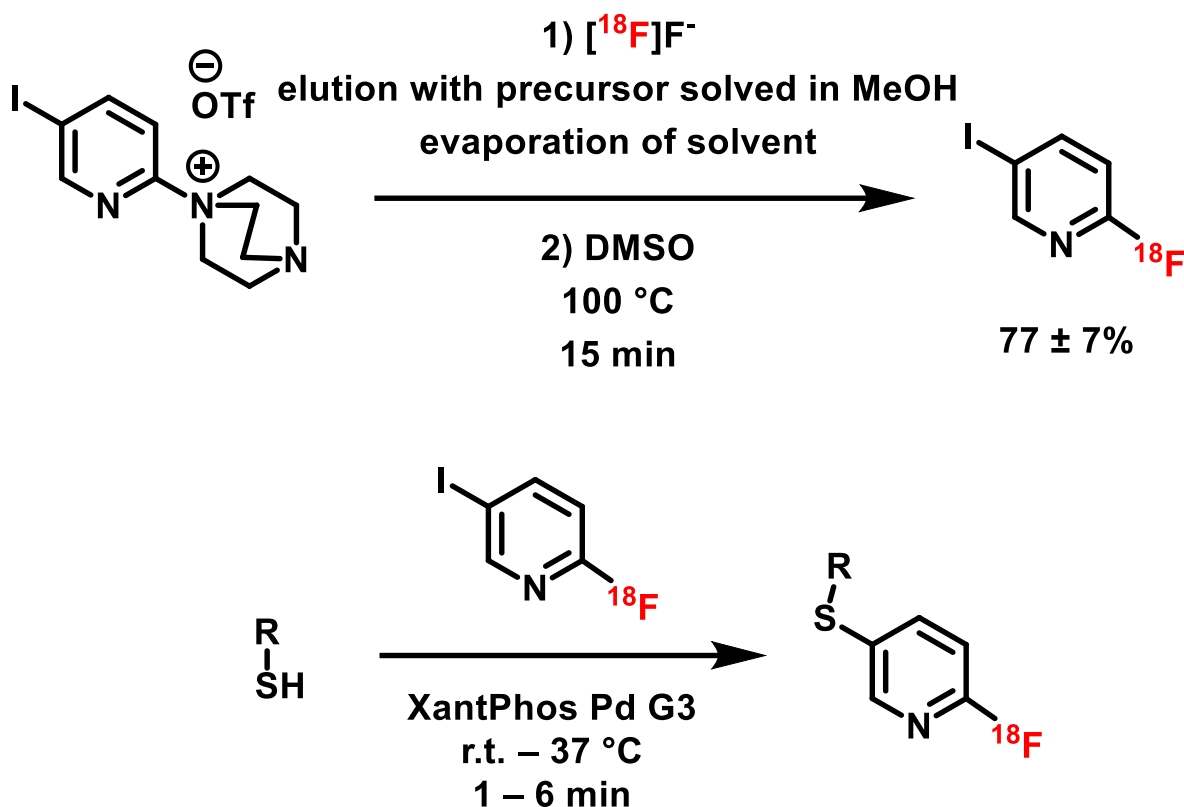


Figure 15: Use of a DABCO salt as leaving group for nucleophilic radiofluorination<sup>[18]</sup>.

In summary, nitrogen salts provide a diverse range of options for nucleophilic radiofluorination. While trimethylammonium salts are frequently used, their limited commercial availability, narrow application scope, the potential for formation of undesired side products, and specific precursor requirements have led to the exploration of alternative onium salt precursors.

### 3.4.2 Iodonium Salts

Iodonium salts are an attractive class of bench-stable radiolabeling precursors that are readily available in high yields and on large scales. They can be classified as either symmetric or asymmetric. In symmetric iodonium salts, the ligands attached to the iodine are identical, which minimizes the formation of undesirable radiofluorinated by-products. However, the use of two identical ligands can be a disadvantage in the case of costly or complex starting materials. Asymmetric iodonium salts address this issue by combining a target ligand (the desired radiofluorination site) with an inexpensive, readily available second ligand.

### 3 Introduction

To avoid the formation of undesired side products, the regioselectivity of the radiofluorination reaction must be carefully controlled. This is achieved by incorporating “spectator ligands” that resist radiofluorination, such as electron-rich arenes (e.g., anisole) or sterically hindered aromatic rings. However, *ortho*-substituted spectator ligands can sometimes undergo radiofluorination due to the ortho effect of the radiofluorination mechanism (Figure 16).

Upon addition of [<sup>18</sup>F]fluoride, the counterion of the iodonium salt is exchanged with [<sup>18</sup>F]fluoride. The iodonium salt adopts a hexagonal geometry, where the two lone electron pairs of iodine occupy equatorial positions, the [<sup>18</sup>F]fluoride occupies an axial position, and the two ligands occupy equatorial and axial positions, respectively.

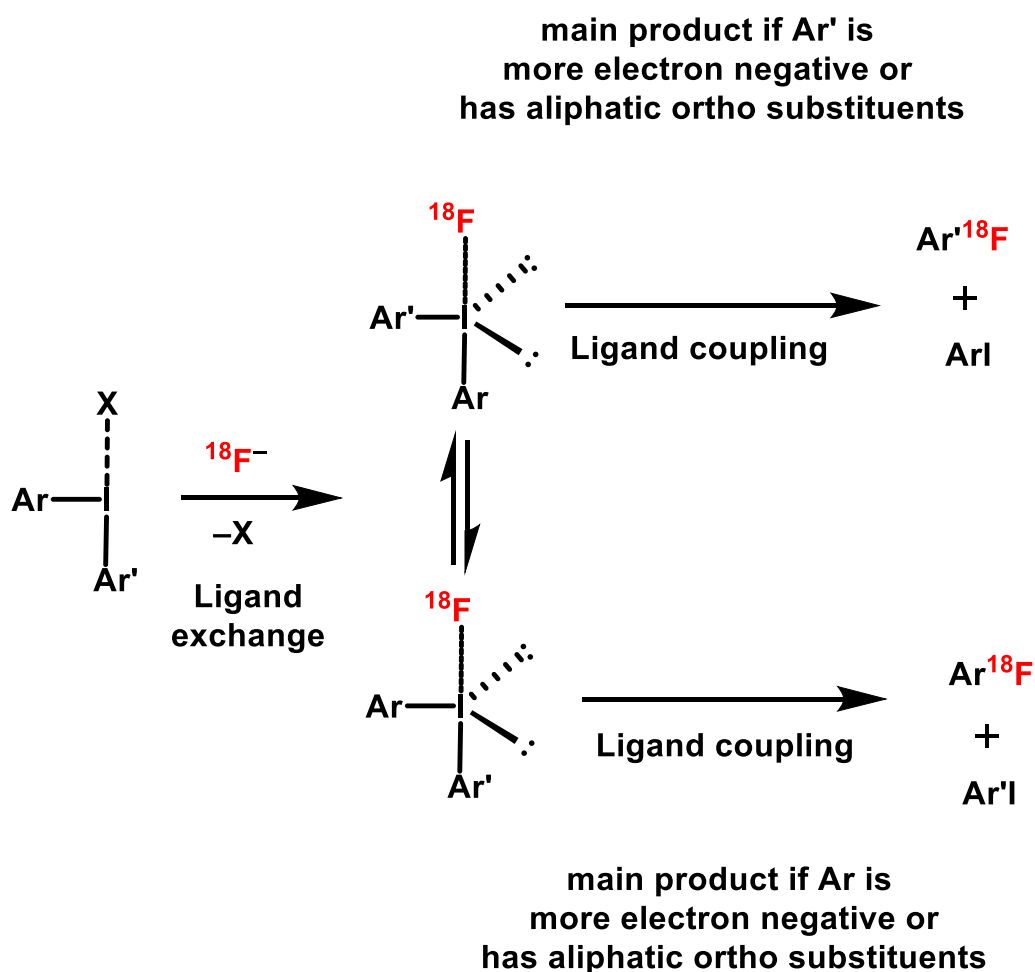


Figure 16: Mechanism of the copper-free radiofluorination of iodonium salts<sup>[19]</sup>.

In this arrangement, the equatorial ligand reacts with the axial [<sup>18</sup>F]fluoride to form the radiofluorinated product. Electron-rich ligands preferentially occupy the equatorial position, directing the radiofluorination to the other ligand. Ligands with *ortho*-methyl substituents are more susceptible to radiofluorination than those with more electronegative substituents. This ortho effect has been explained through theoretical calculations and crystal structure studies,

which suggest that it arises from differences in the energies of the transition states involved in the reaction<sup>[20,19]</sup>.

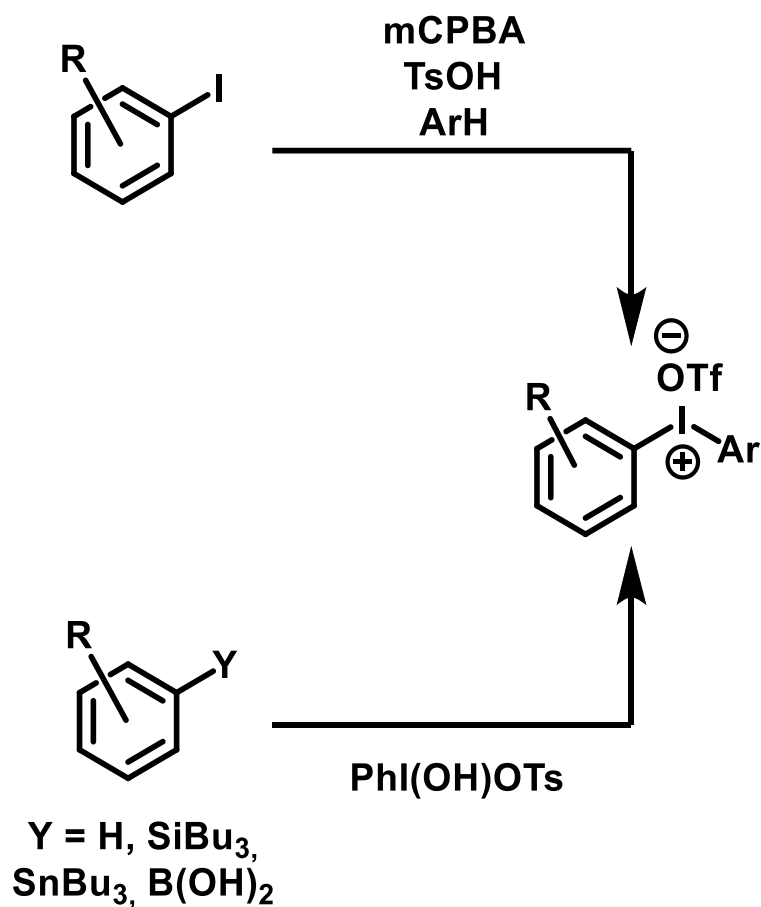


Figure 17: Selection of synthesis routes for asymmetric iodonium salts<sup>[19]</sup>.

The synthesis of asymmetric iodonium salts is a well-explored area of research<sup>[21,22a,23,24,22b]</sup> (Figure 17). The most prominent synthetic approach is the oxidation of iodine-containing compounds to the corresponding hypervalent iodane intermediate, followed by quenching with a simple spectator group<sup>[23]</sup>. Another common method involves the use of Koser's reagent<sup>[24]</sup>, which reacts with iodine compounds to efficiently produce asymmetric iodonium salts.

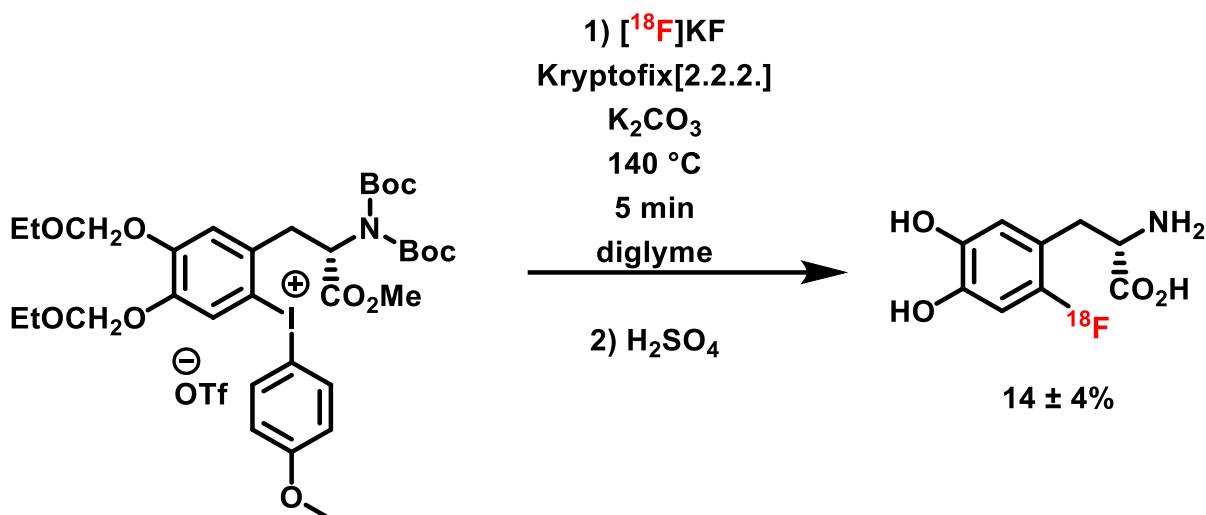


Figure 18: Synthesis of 6- $^{18}\text{F}$ FDOPA from an asymmetric iodonium salt precursor<sup>[25]</sup>.

Several radiofluorination reactions involving iodonium salts are reported in the literature. For example,  $^{18}\text{F}$ FDOPA can be synthesized by reacting a iodonium salt with kryptofix[2.2.2.] and  $^{18}\text{F}$ fluoride (Figure 18), replacing the use of electrophilic radiofluorination with  $^{18}\text{F}\text{F}_2$  by a nucleophilic radiofluorination approach.

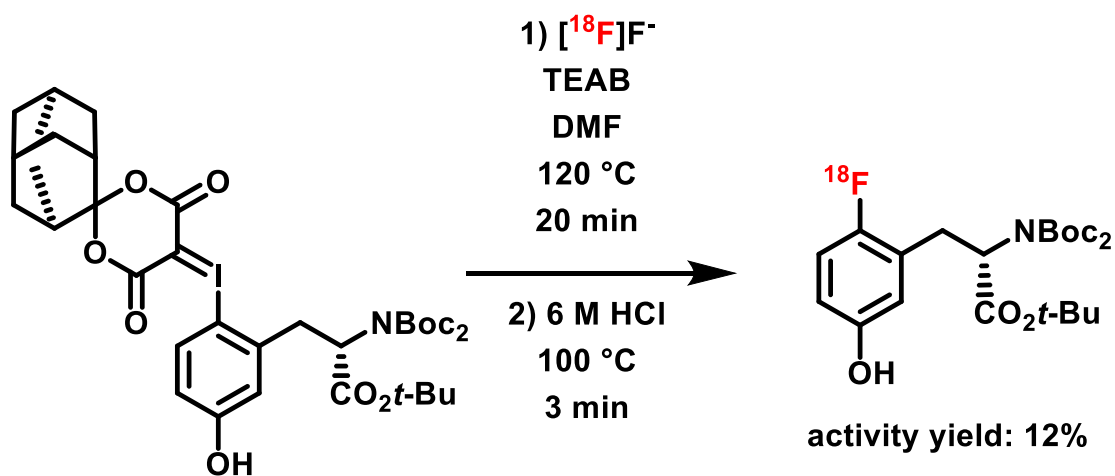


Figure 19: Radiofluorination of an ylide precursor<sup>[26]</sup>.

Apart from iodonium salts, iodonium ylides can also be utilized as precursors for nucleophilic radiofluorination. However, application of iodonium ylides could result in lower RCYs due to their instability at elevated temperatures, which can lead to precursor decomposition under radiofluorination conditions. This can be mitigated by the use of highly sterically hindered ligands like adamantane, which afford the desired products in improved RCYs. The most important advantage of iodonium substrates over ammonium or pyridinium salts consists of their suitability for the preparation of radiofluorinated electron-neutral and even moderately electron-rich (hetero)aromatics.

### 3.4.3 Sulfonium Salts

An alternative for the use in radiofluorination is the use of triarylsulfonium salts. An example for the radiofluorination of ketones with this precursor class was introduced by Sander et al who synthesized them by arylation of thioethers with iodonium salts in presence of a copper catalyst (Figure 20). The so formed triarylsulfonium salts could be employed as precursors for the following radiofluorination giving the radiofluorinated ketone in good RCCs<sup>[27]</sup>.

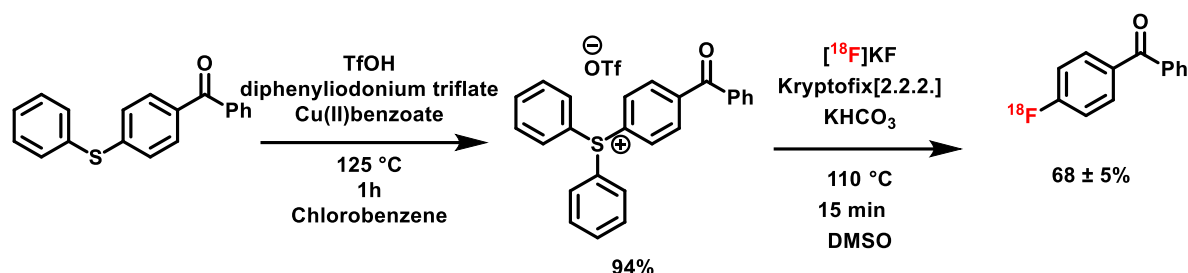


Figure 20: Synthesis and radiofluorination of a sulfonium salt precursor<sup>[27]</sup>.

Triarylsulfonium salts are also compatible precursors for ‘minimalist’ radiofluorination procedures as they are also capable of eluting the  $[^{18}\text{F}]\text{fluoride}$  from the QMA cartridge. Radiofluorination with this method provided high yields and can be performed far faster than radiofluorination methods which require the removal of water under reduced pressure (Figure 21)<sup>[13]</sup>.

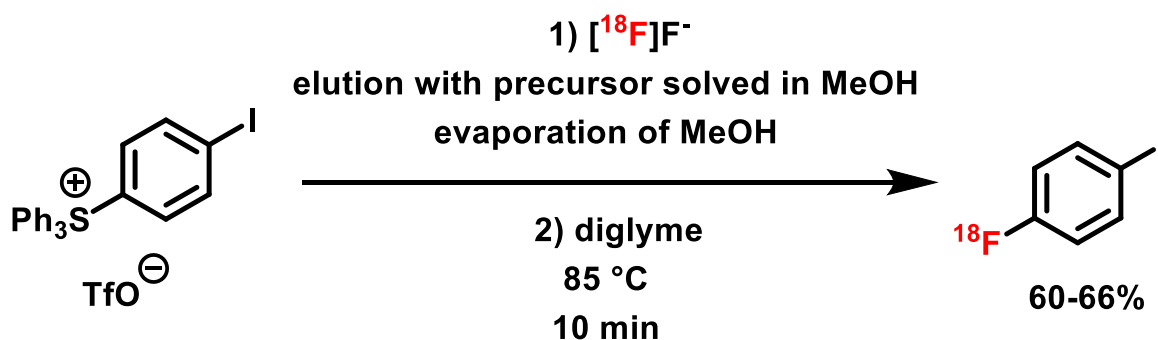


Figure 21: Radiofluorination of a triarylsulfonium salt following the minimalist protocol<sup>[13]</sup>.

A similar approach was undertaken by Ritter et al. who synthesized a dibenzothiophenium precursor by site selective C-H dibenzothiophenylation. The so attained precursors could be radiofluorinated in very good radiochemical yields (Figure 22) and the method could be applied to a wide scope of pharmacologically relevant substances<sup>[28]</sup>.

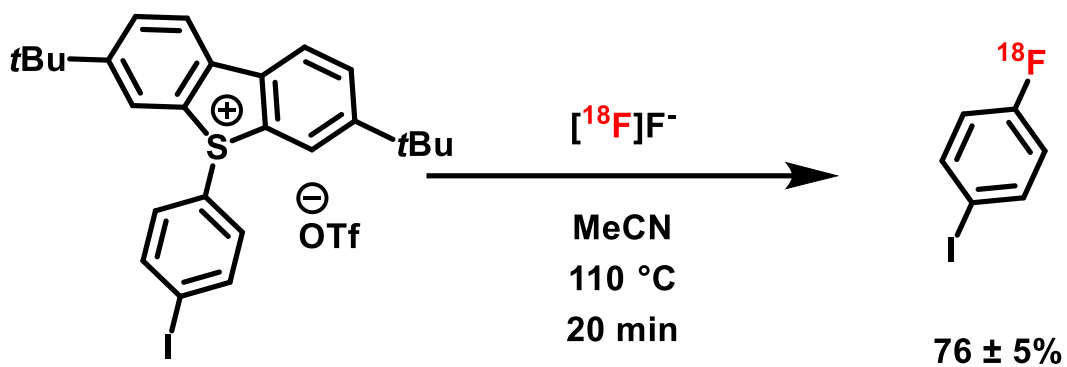


Figure 22: Radiofluorination of a dibenzothiophenium salt precursor.

All in all, triarylsulfonium salts are a class of relevant onium salt precursors which offer access to pharmacologically relevant substances and can be attained by a variety of methods including transarylation from iodonium salts and via site selective C-H activation reactions.

### 3.5 Ring Opening Radiofluorinations of Cyclic Ammonium Salts

#### 3.5.1 Azetidinium Salts

Due to their significant ring strain that confers a high reactivity, quaternary spirocyclic azetidinium salts are prime candidates for nucleophilic ring-opening reactions. However, these four-membered spirocyclic compounds are challenging to synthesize. Their ring strain is comparable to that of three-membered rings<sup>[29]</sup>, though their larger size results in less favorable reaction kinetics. Azetidinium salts are typically synthesized by introducing a leaving group onto a propyl chain, followed by heating to induce ring closure and expel the leaving group (Figure 23)<sup>[30]</sup>.

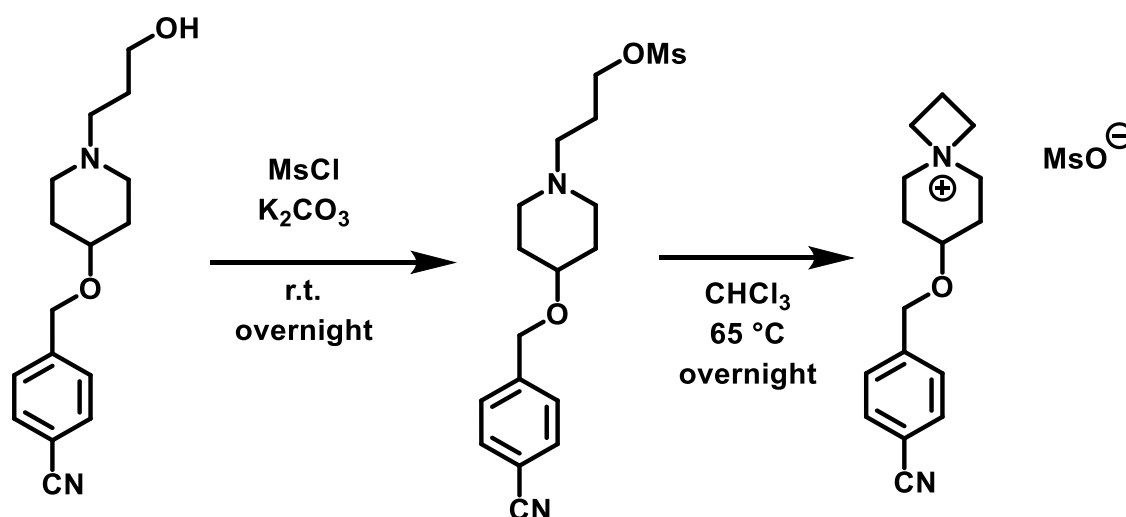
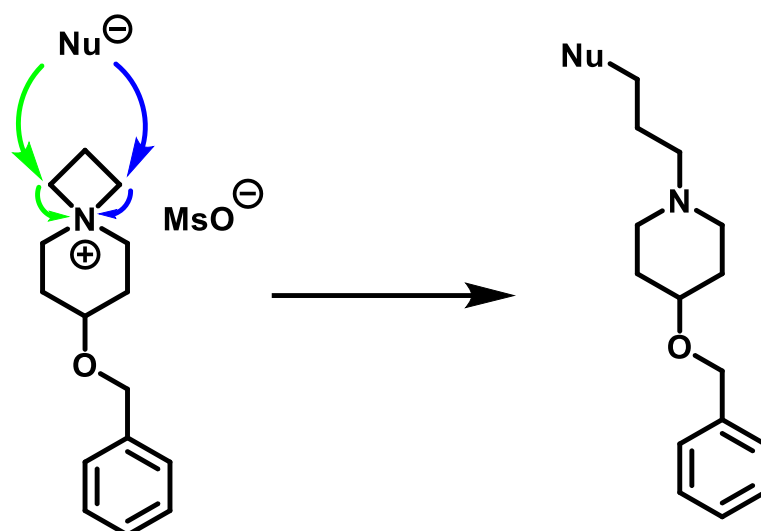
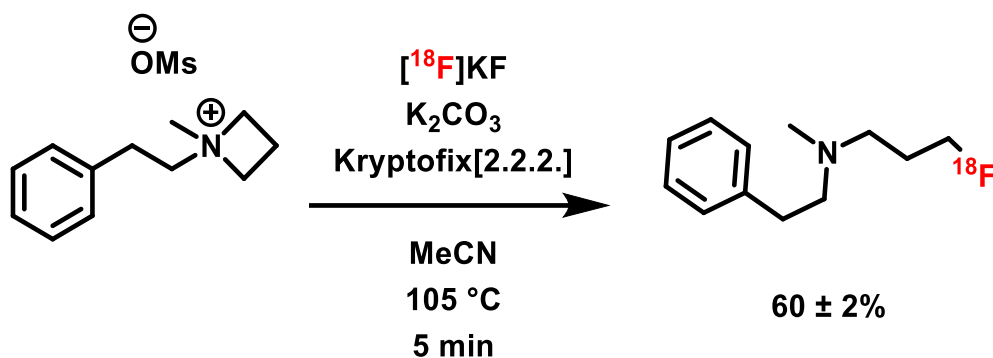


Figure 23: Synthesis of an azetidinium salt<sup>[30]</sup>.

Under nucleophilic attack, azetidinium salts undergo ring opening to form propyl-substituted tertiary amines. Due to their symmetry, nucleophilic attack at either site produces the same product (Figure 24)<sup>[31]</sup>.

Figure 24: Mechanism of the nucleophilic ring opening of azetidinium salts<sup>[31]</sup>.Figure 25: Radiofluorination of an azetidinium salt<sup>[30]</sup>.

Through a series of radiofluorination studies with different model compounds, Kiesewetter et al. demonstrated that azetidinium salts are a promising class of precursors for nucleophilic radiofluorination<sup>[30]</sup>. They screened a small collection of relevant structural analogs and found that radiofluorination of azetidinium salts proceeds in good RCYs, which could be further enhanced by adding non-radioactive carrier fluorine (Figure 25). Building on these findings, Chi et al. developed a method for the preparation of [<sup>18</sup>F]FP-CIT, a cocaine derivative used as a dopamine transporter radioligand<sup>[32]</sup>. This method involves the ring opening of an azetidinium salt precursor with [<sup>18</sup>F]fluoride at 120 °C for 10 minutes, affording the target compound in RCYs of 36 ± 5% (Figure 26).

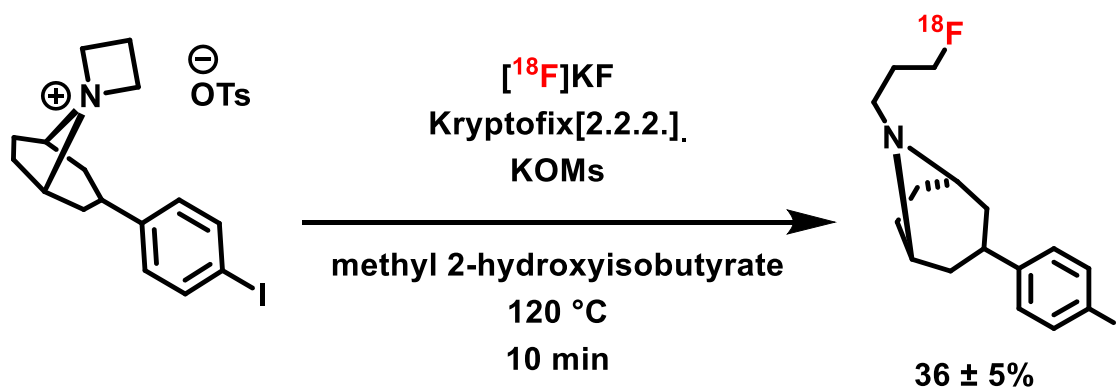


Figure 26: Preparation of  $[^{18}\text{F}]\text{FP-CIT}$  by nucleophilic radiofluorination of an azetidinium salt<sup>[32]</sup>.

In summary, azetidinium salts represent a promising class of precursors for nucleophilic radiofluorination. Among others, they provide convenient access to  $[^{18}\text{F}]$ fluoropropyl piperidines and piperazines, which are common motifs in many biologically relevant compounds.

### 3.5.2 DABCO Salts as Targets for Ring Opening Nucleophilic Attacks

As described in section 2.3.1, the DABCO motif has been utilized as a leaving group for aromatic nucleophilic radiofluorination reactions. However, the reactivity of DABCO salts can be useful for aliphatic nucleophilic radiofluorinations, since they can also undergo ring-opening reactions (Figure 27). Therefore, the outcome of nucleophilic attack on DABCO salts depends on multiple factors, including electronic activation of the DABCO motif, nucleophile type, solvent, reaction temperature, and the hybridization of the bond being cleaved. These factors collectively influence whether the radiolabeling proceeds via aromatic or aliphatic nucleophilic substitution.

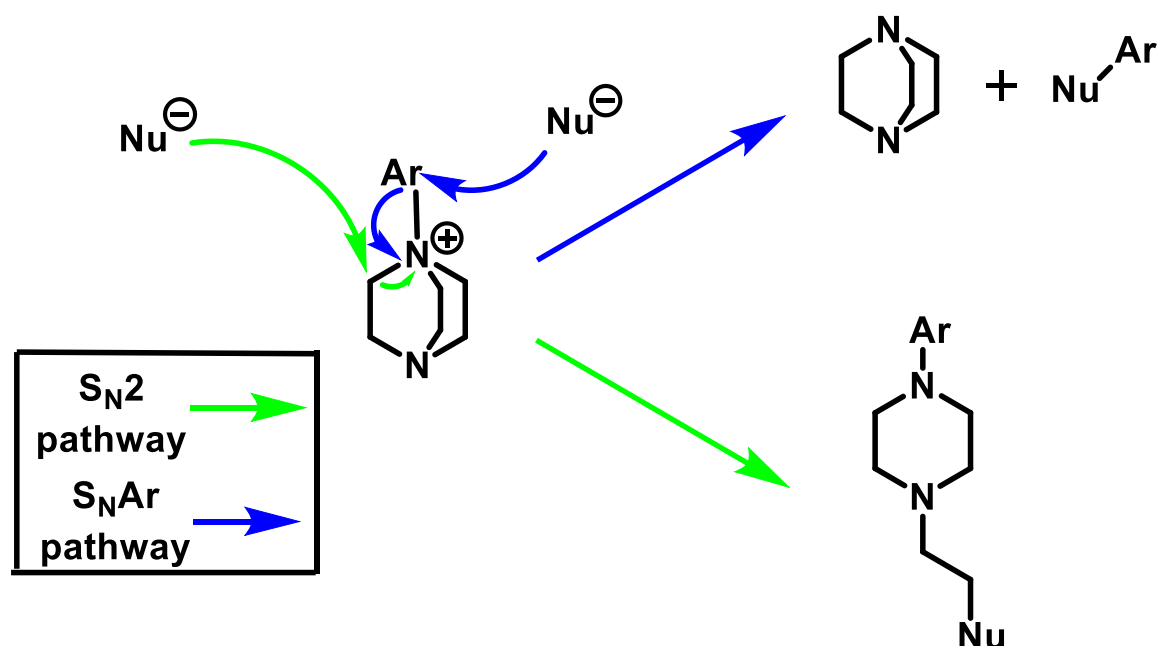


Figure 27: Pathways for the nucleophilic attack on DABCO salts.

Ross et al.<sup>[33]</sup> investigated the reaction of 1-chloro-2,4-dinitrobenzene with DABCO salts to obtain insights into the reaction mechanisms and product profiles. They found that the aromatic DABCO salt intermediate reacted so quickly that it could not be detected in the reaction mixture (Figure 28). This rapid transformation was attributed to significant resonance stabilization, favoring the formation of non-charged, thermodynamically stable products.

In addition, they observed that when DABCO was used in excess, the only isolatable product was the 2-(piperazine-1-yl)ethyl-substituted DABCO salt, while using excess 1-chloro-2,4-dinitrobenzene produced the chloroethyl piperazyl substituted product as a side product. The absence of this side product in the former case was explained by its reaction with free DABCO to yield the stable 1-aryl-4-ethyl piperazyl DABCO salt. This finding highlights the role of DABCO in driving the reaction to completion, making the 1-aryl-4-ethyl piperazyl DABCO salt the dominant product under appropriate conditions.

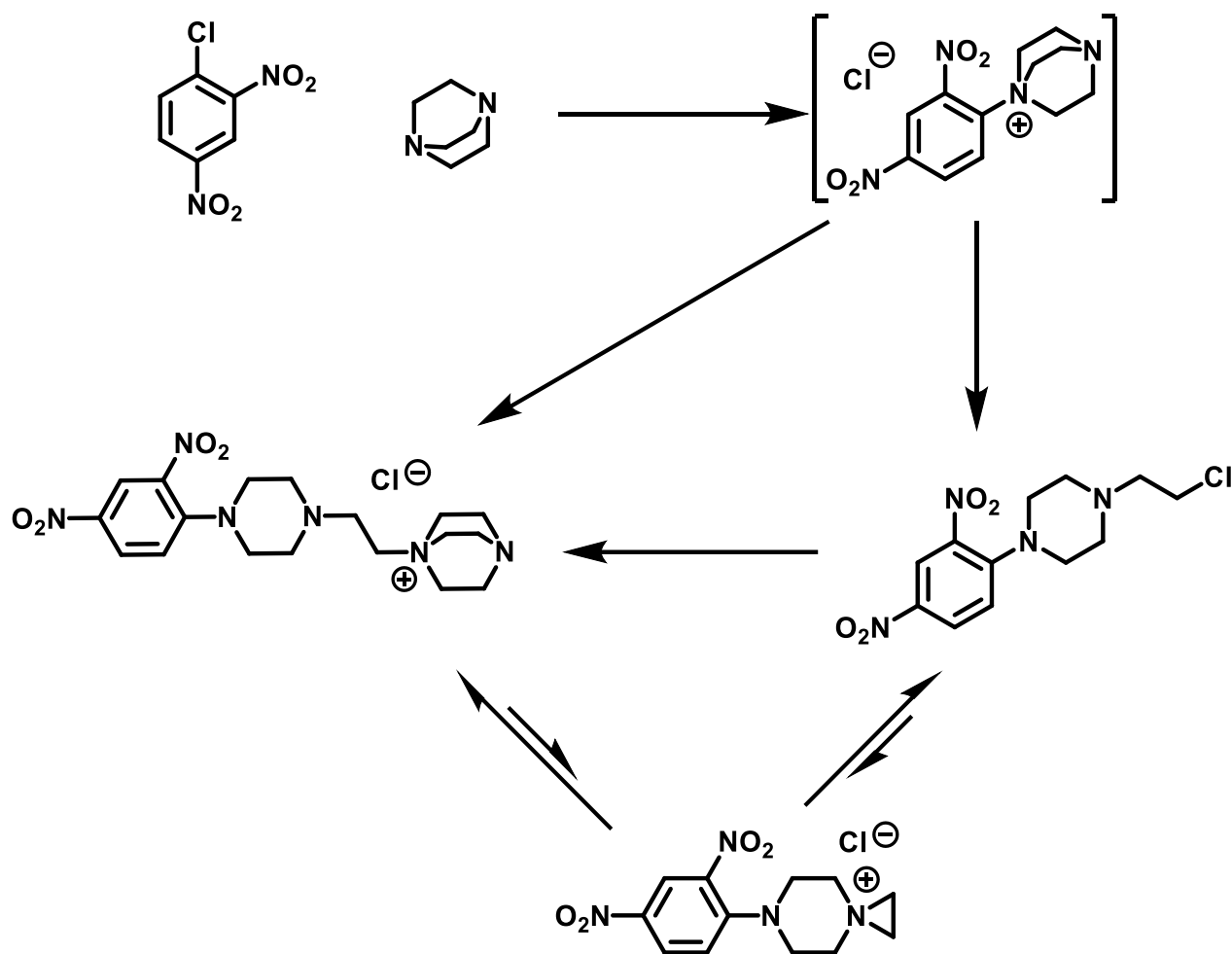


Figure 28: Reaction pathway in the ring opening of an aromatic DABCO salt<sup>[33]</sup>.

Maras et al.<sup>[34]</sup> identified aliphatic DABCO salts as suitable precursors for the preparation of disubstituted piperazines via ring-opening reactions (Figure 29). They found that nucleophilic attack of benzyl-substituted DABCO salts often results in a mixture of products, with the product distribution depending on the nature of the nucleophile. For example, phenols primarily yielded the ring-opening products, while thiols led to a nearly even split between ring-opening products and aryl benzyl ethers. In contrast, other aliphatic DABCO salts exclusively underwent ring-opening. This finding underscores the importance of the electronic environment around the DABCO motif, which is influenced by the proximity of aromatic systems and dictates the reaction pathway as well as the influence of the nucleophile.

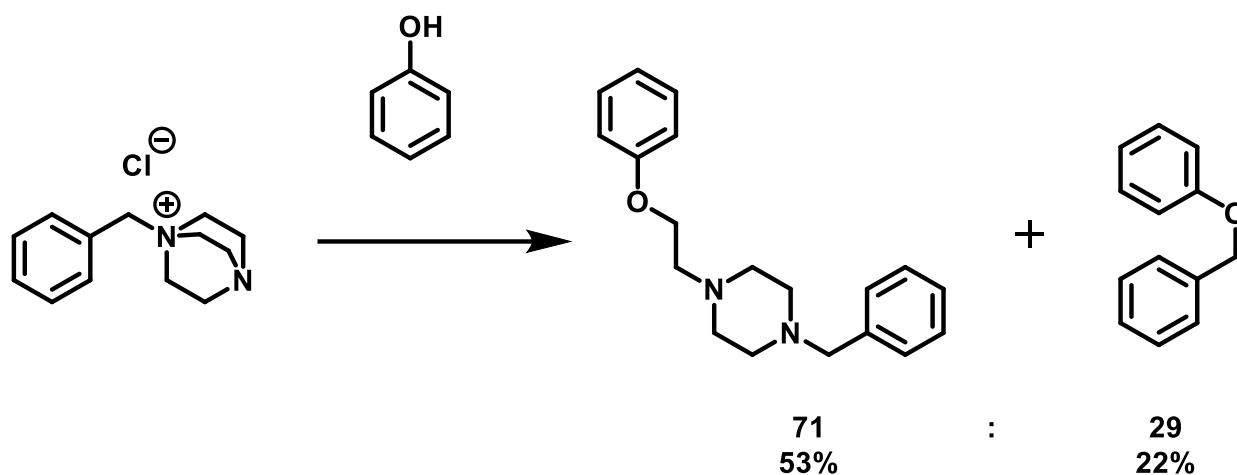


Figure 29: Ring opening of DABCO salts with nucleophiles<sup>[34]</sup>.

Another approach of using DABCO salts involves generating them *in situ* via an aryne intermediate (Figure 30). Here, an aryne generated from a suitable precursor reacts with DABCO to form the corresponding DABCO salt, which then undergoes ring-opening *in situ*. This strategy offers a one-pot route to complex structures with excellent atomic economy. However, the lack of regioselectivity can lead to regioisomer mixtures, requiring additional separation and purification steps. Despite this limitation, the method represents an efficient approach for the generation of complex structures from simple precursors.

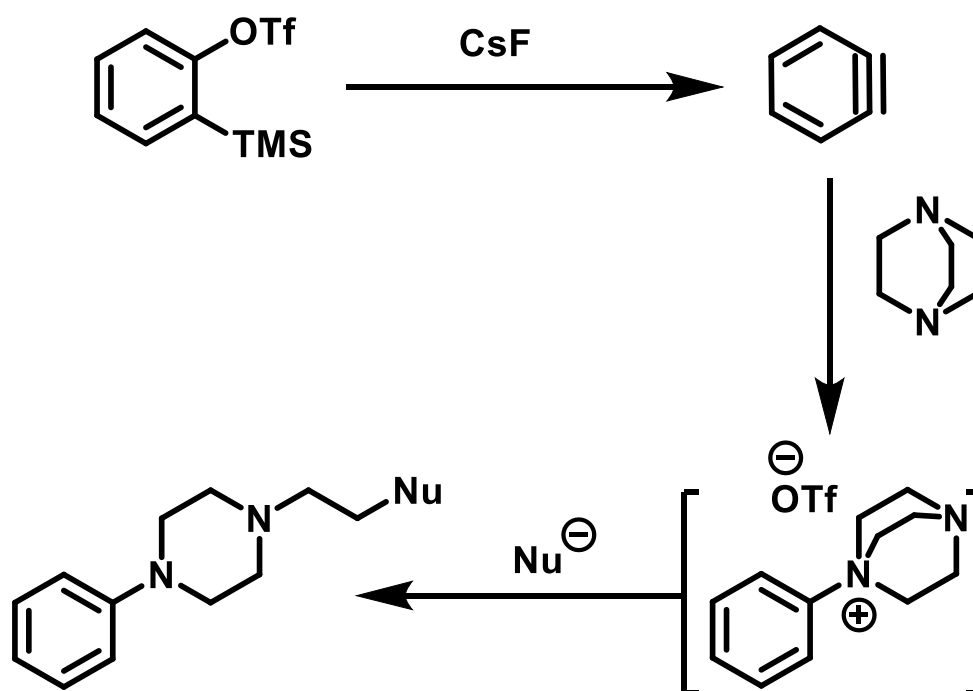


Figure 30: Scheme of the synthesis of ethyl piperazines via benzyne.

The lack of regioselectivity in aryne-based ring-opening reactions was further demonstrated by Seo et al.<sup>[35]</sup>, who reacted phthalimide with a benzyne precursor to synthesize 1-aryl-4-(2-

phthalimidylethyl)piperazines (Figure 31). While the overall yield of the reaction was satisfactory, it afforded a mixture of regioisomers, reflecting the inherent challenge of controlling the stereochemistry of aryne intermediates.

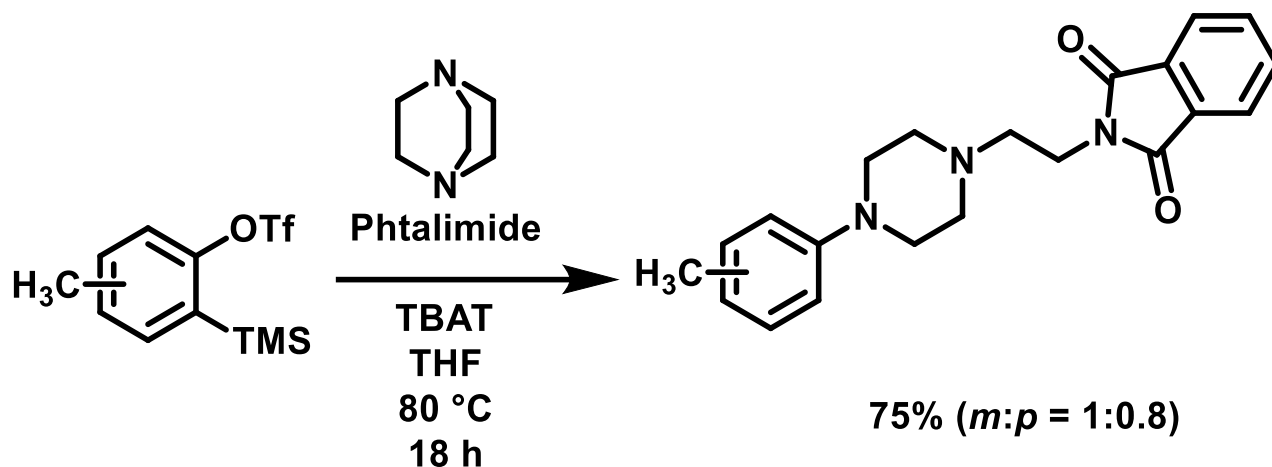


Figure 31: Example of the ring opening reaction for a in situ generated DABCO salt starting from the benzyne precursor<sup>[35]</sup>.

Overall, ring-opening reactions of DABCO salts represent a promising strategy for synthesizing pharmaceutical compounds from simple precursors. These reactions can be used to efficiently prepare complex molecular structures, though side reactions, including those where DABCO acts as a leaving group, can complicate the reaction pathway. Additionally, the synthesis of aromatic DABCO salts remains challenging, as their high reactivity and poor stability often complicates isolation. Managing these limitations is essential to fully harness the potential of DABCO salts in nucleophilic substitution and ring-opening reactions for pharmaceutical applications.

## 4 Aim of this Work

The aim of this work was to develop a novel approach to the  $S_N2$  radiofluorination via ring-opening reactions of cyclic ammonium salts using the minimalist protocol. Specifically, the study focused on two promising classes of salts for nucleophilic radiofluorination: DABCO salts and 3-hydroxyazetidinium salts.

The primary goal of this study was evaluation of the feasibility of DABCO salts ring-opening radiofluorination for the preparation of the appropriately substituted (2-[ $^{18}\text{F}$ ]fluoroethyl)piperazines.

Additionally, the applicability of ring-opening of 3-hydroxyazetidinium salts for  $^{18}\text{F}$ -labeling should also be studied.

## 5 Results and Discussion

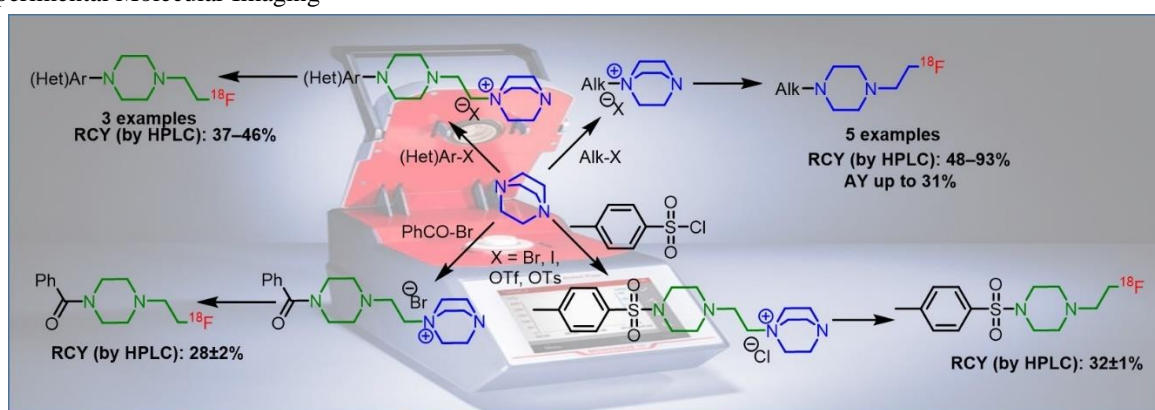
### 5.1 Manuscript Part

## Ring-opening radiofluorination of quaternary DABCO-salts using “minimalist” approach

Yannick Keuthen,<sup>1,2</sup> Bernd Neumaier,<sup>1,2\*</sup> Boris D. Zlaptopolskiy<sup>1,2</sup>

<sup>1</sup>Forschungszentrum Jülich GmbH, Institute of Neuroscience and Medicine, Nuclear Chemistry (INM-5), Wilhelm-Johnen-Straße, 52428 Jülich, Germany

<sup>2</sup>University of Cologne, Faculty of Medicine and University Hospital Cologne, Institute of Radiochemistry and Experimental Molecular Imaging



We present a novel method for the production of the [<sup>18</sup>F]fluoroethylpiperazyl-substituted tracers in an one step radiofluorination, from DABCO salts. This method uses quaternary DABCO salts to generate the [<sup>18</sup>F]fluoroethylpiperazyl motif, a structure frequently found in radiotracers via a ring opening reaction with [<sup>18</sup>F]fluoride as nucleophile. Through this approach, we successfully radiofluorinated various model compounds, including azido- and alkyne-functionalized derivatives suitable for use as prosthetic groups. Additionally, we present a method using iodonium salts as precursors for the [<sup>18</sup>F]fluoroethylpiperazyl motif by radiofluorination of in situ formed DABCO salts.

In recent years, positron emission tomography (PET) has gained considerable importance, driving the demand for a wide range of radiotracers. Among the radionuclides used for tracer development, fluorine-18 (<sup>18</sup>F) is particularly notable due to its accessibility from clinical cyclotrons<sup>[6]</sup> and its favorable imaging properties. With a half-life of approximately 110 minutes, <sup>18</sup>F is suitable for visualizing short- to medium-duration processes and enables the centralized production and distribution of tracers via the satellite concept. Additionally, its relatively low average positron energy (536 eV) results in minimal positron travel before annihilation, improving the PET image resolution. Consequently, there has been a growing demand for efficient radiofluorination protocols.

## 5 Results and Discussion

We previously introduced the simplified minimalist approach to nucleophilic  $^{18}\text{F}$ -fluorination<sup>[12][14]</sup>, in which only onium salt precursors and  $^{18}\text{F}$ fluoride are applied for the preparation of radiolabeled compounds. This approach also eliminates the need for azeotropic drying shortening the reaction time significantly. Application of the protocol to (hetero)aryl-substituted DABCO salts enabled the efficient preparation of radiofluorinated PSMA-ligands<sup>[14]</sup> as well as labeled prosthetic groups for the indirect radiofluorination<sup>[18]</sup>. Building on these findings, we now explore DABCO salts as synthons for the generation of  $^{18}\text{F}$ fluoroethylpiperazyl motif by leveraging their ring-opening reactivity.

We started with aliphatic DABCO salts, which were conveniently prepared by quaternization of DABCO with the corresponding aliphatic halides, allowing for the efficient formation of these salts in good yields. Afterwards we optimized the radiofluorination conditions to facilitate the desired ring-opening reaction.

Table 2: Influence of the reaction temperature and the heating method on the radiochemical conversions (RCCs).

1)  $^{18}\text{F}]\text{F}^-$   
elution with precursor solved in MeOH  
evaporation of solvent

2) DMF  
5 min  
T

1a  2a

entry	T/°C	Heating method	RCC
1	130	heating block	0 (n = 2)
2	140	heating block	2,5 ± 0,5% (n = 2)
3	150	heating block	5 ± 4% (n = 6)
4	150	microwave	81 ± 18% (n = 2)
5	160	microwave	88 ± 9% (n = 3)
6	110	inductive heating	17 ± 2% (n = 2)
7	120	inductive heating	30 ± 15% (n = 11)
8	130	inductive heating	55 ± 1% (n = 3)
9	140	inductive heating	64 ± 9% (n = 5)
10	150	inductive heating	96 ± 4% (n = 15)
11	160	Inductive heating	75 ± 2% (n = 2)

However, our initial experiments resulted in minimal radiochemical conversions (RCCs), prompting us to refine our heating strategy. We explored microwave and inductive heating (Anton Paar, Monowave 50), both of which significantly improved the RCCs compared to

conventional heating (Tab. 2). Due to its greater flexibility and compatibility with automated synthesis modules, inductive heating was chosen for all further experiments.

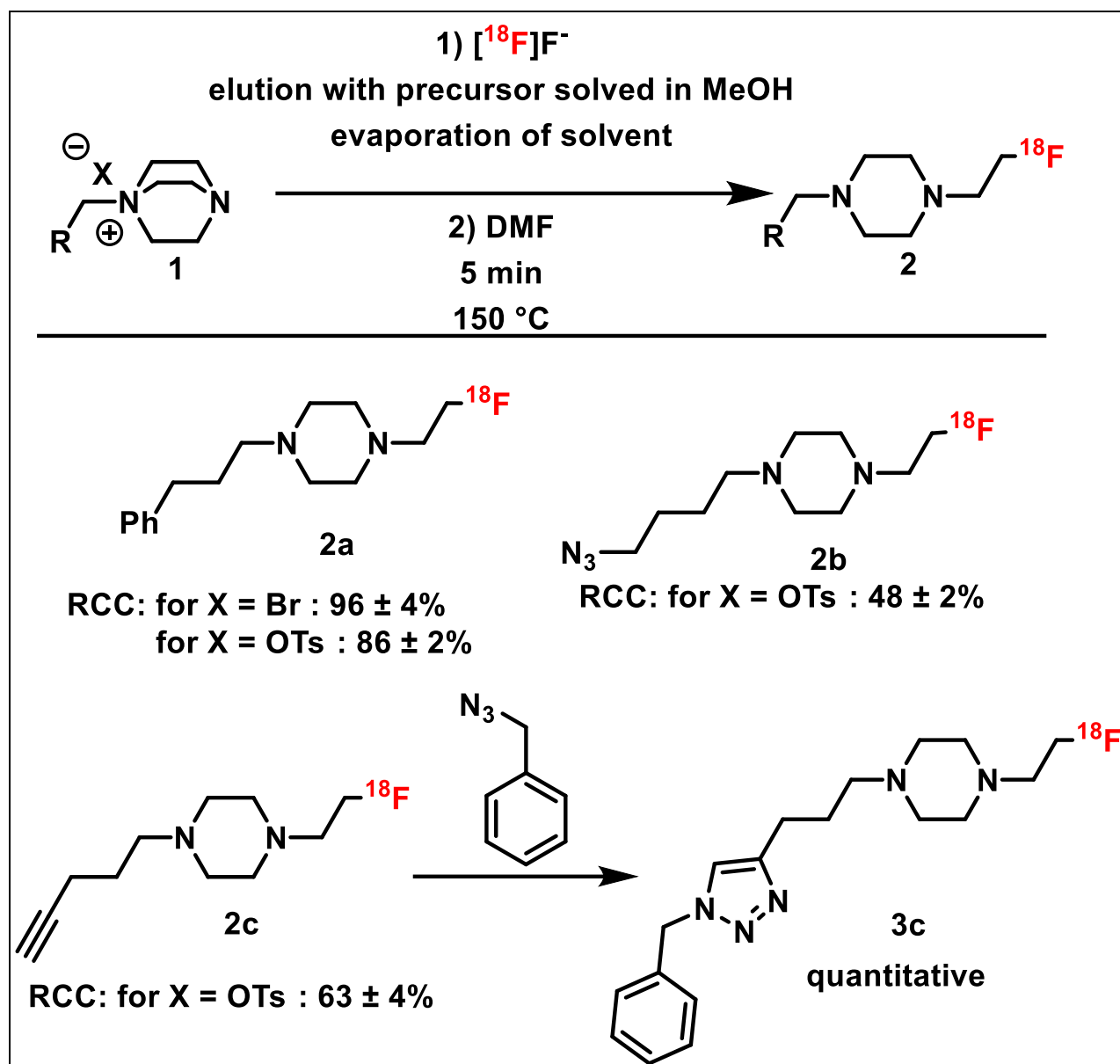


Figure 32. Radiofluorination of aliphatic DABCO-salts.

With optimized inductive heating to hand, we successfully labeled a phenylpropyl-DABCO bromide (**1a**) as model substrate, achieving a high RCC of  $96 \pm 4\%$ . In addition, azido-(**1b**) and propargyl-substituted (**1c**) DABCO salts were radiofluorinated in RCCs of  $48 \pm 2\%$  and  $63 \pm 4\%$ , respectively (Figure 32). After isolating the alkyne substrate (**2c**) by solid phase extraction, we performed a test click conjugation with benzyl azide, which proceeded quantitatively, demonstrating the potential of this approach the generation for indirect radiofluorination as well.

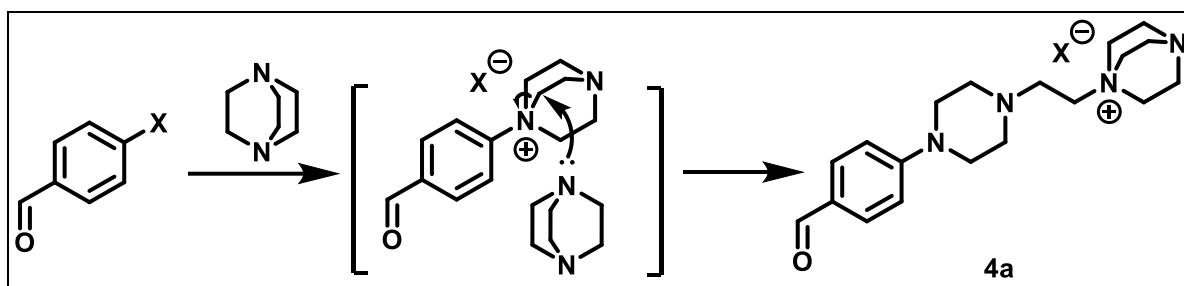


Figure 33. Proposed mechanism for the formation of ethylpiperazyl-DABCO salts.

In order to evaluate the applicability of ethylpiperazyl-DABCO salts as radiofluorination precursors, we prepared two such salts by the direct reaction of DABCO with 4-tosyloxybenzaldehyde and 2-bromo-5-iodopyridine, which resulted in exclusive formation of the corresponding ethylpiperazyl-DABCO salts **4** as single isolable products. This result aligns with previous studies on the kinetics of DABCO salt formation<sup>[33]</sup>, which indicate that they involve nucleophilic attack of DABCO on an *in situ* intermediate (Figure 33).

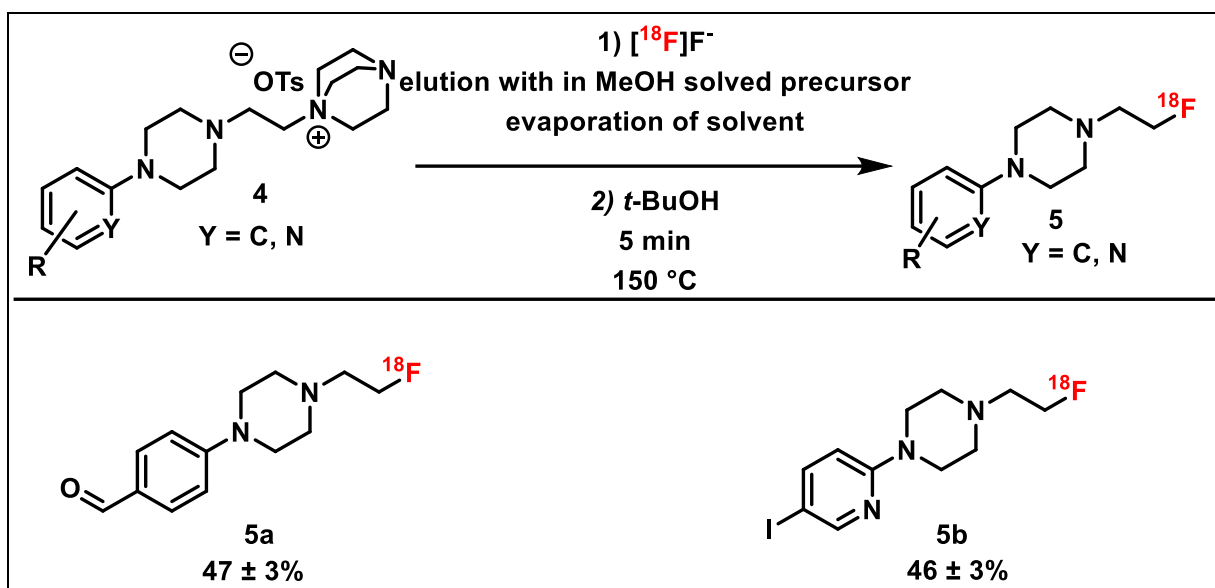


Figure 34. Radiofluorination of ethylpiperazyl DABCO salts.

We proceeded with radiofluorination of the ethylpiperazyl-DABCO salts, which revealed that the DABCO salt motif in these substrates served as effective leaving group, yielding the desired [<sup>18</sup>F]fluoroethylpiperazyl products. For the *para*-benzaldehyde substrate, the RCCs amounted to 47 ± 3%, while the iodo-pyridine derivative yielded a RCC of 46 ± 3%. These results underscore the potential of DABCO salts as effective radiofluorination precursors.

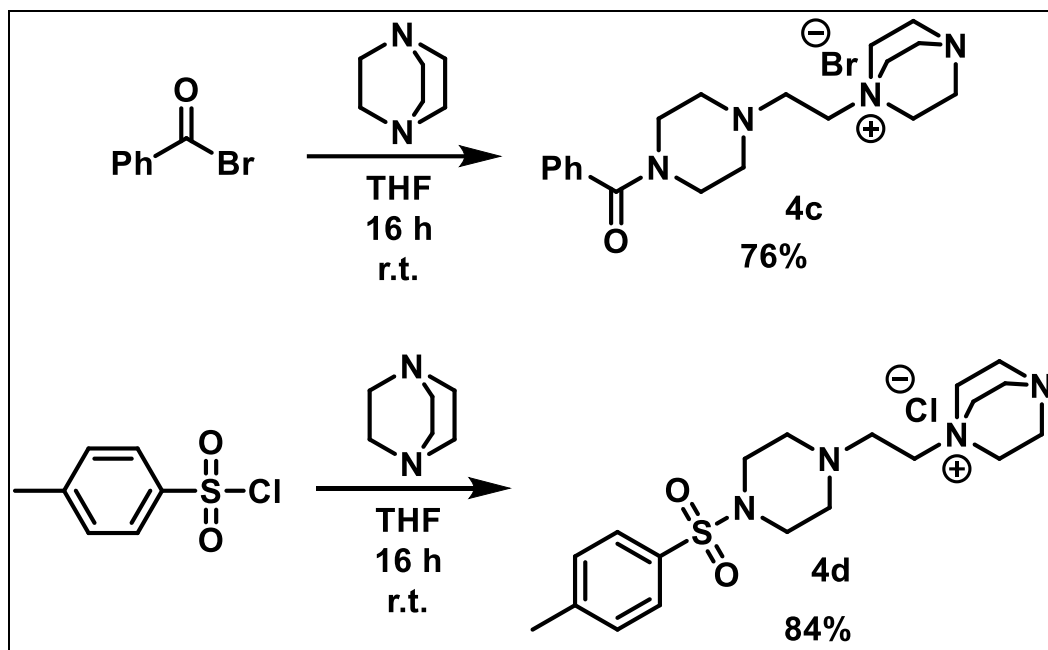


Figure 35: Synthesis of ethylpiperazyl DABCO salts starting from benzoyl bromide and tosyl chloride.

Next, we also tested the reaction of DABCO with benzoyl bromide and tosyl chloride (Figure 35). As anticipated, this reaction produced the corresponding ethylpiperazyl-DABCO salts **4c** and **4d** as only isolable products.

Subsequent radiofluorination of these substrates proceeded with reasonable RCCs of  $32 \pm 1\%$  and  $28 \pm 1\%$ , respectively, confirming that DABCO salts are effective precursors for the radiosynthesis of various products containing [ $^{18}\text{F}$ ]fluoroethylpiperazine motifs.

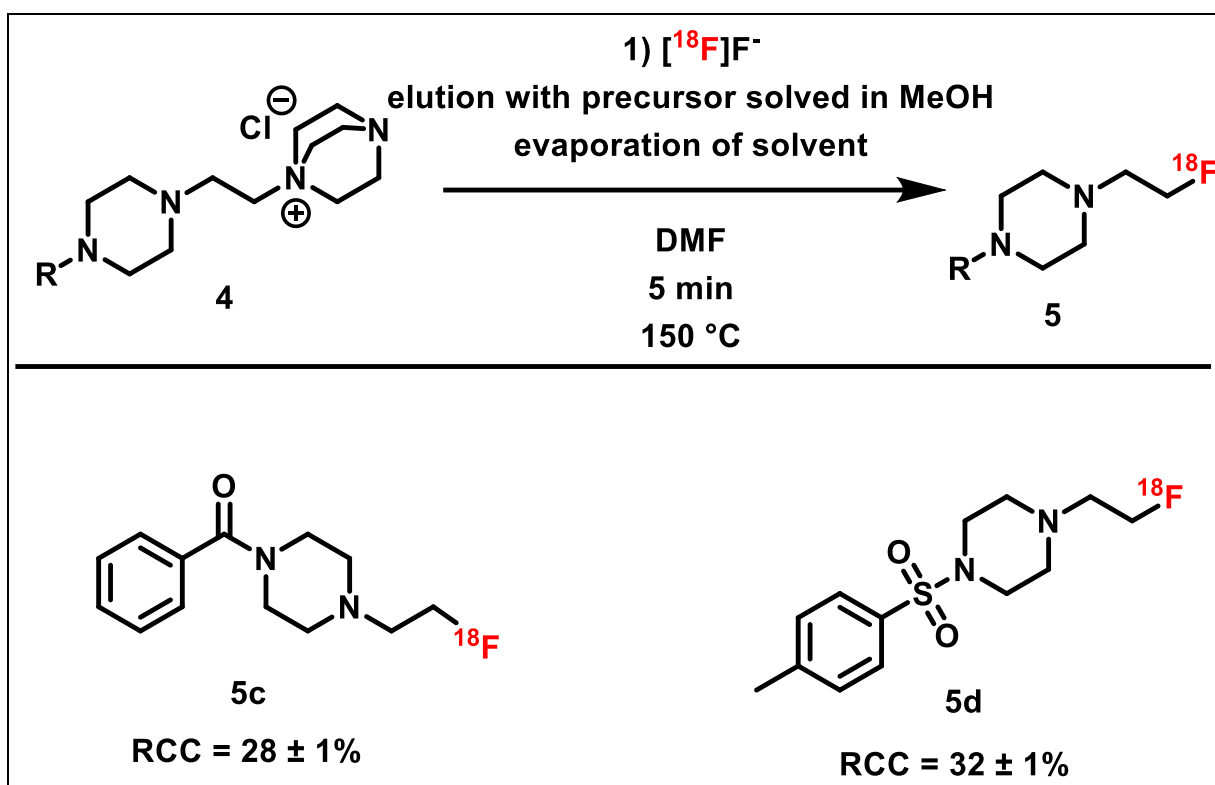


Figure 36: Radiofluorination of ethylpiperazyl-DABCO salts.

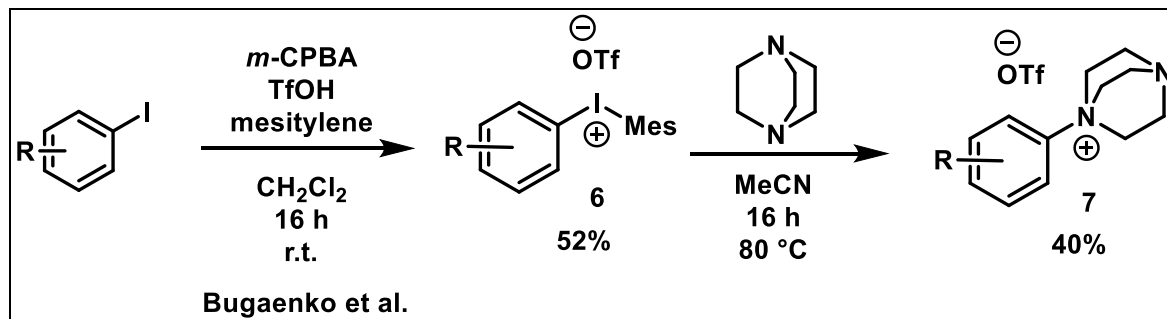
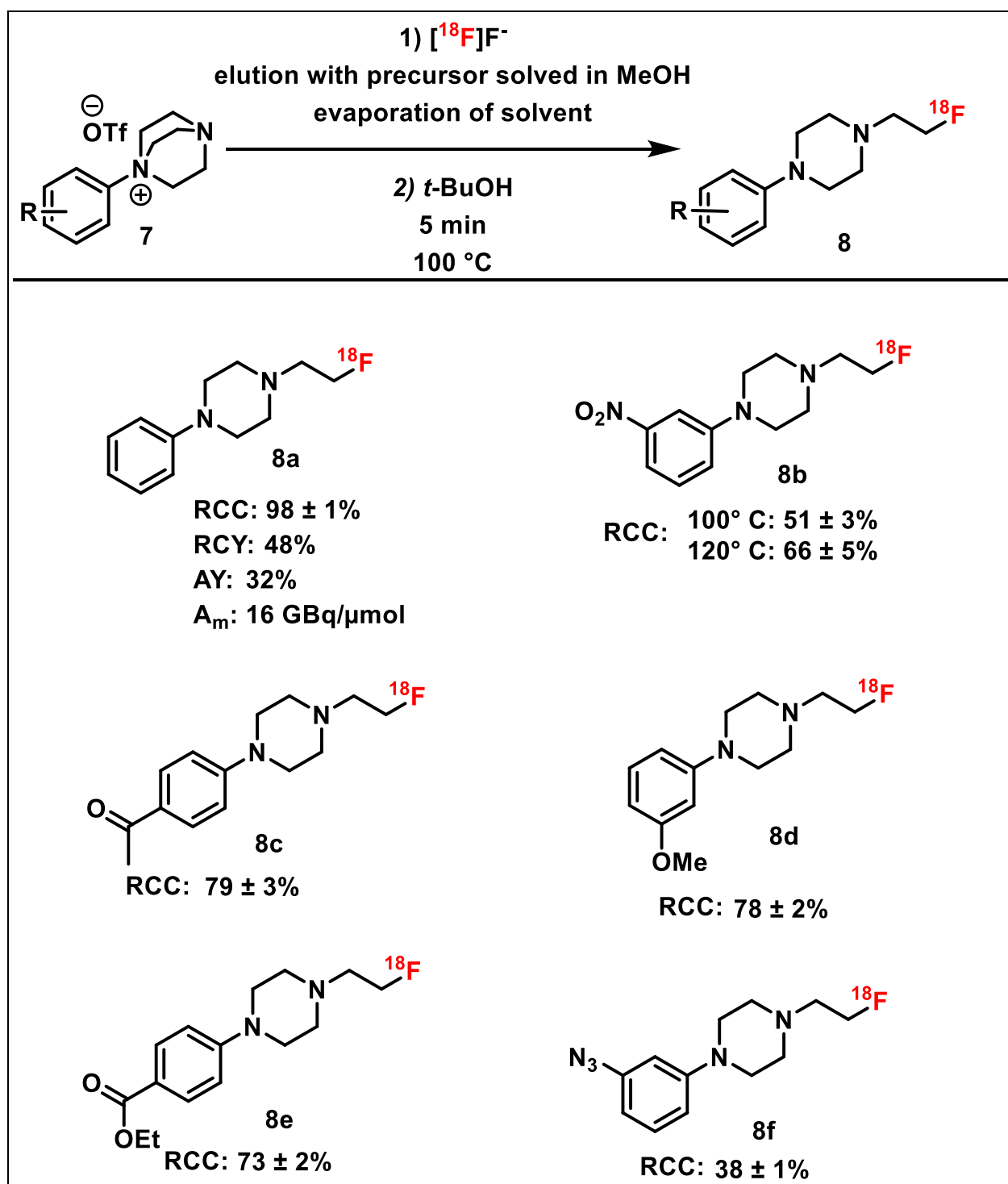


Figure 37: Synthesis of aromatic DABCO salts.

To prepare aromatic DABCO salt radiofluorination precursors, we next adapted a method developed by Bugaenko et al.<sup>[17]</sup>, which utilizes readily available diaryliodonium triflates (Figure 37).

Figure 38. Scope of aromatic [ $^{18}\text{F}$ ]fluoroethylpiperazyl substrates.

The aromatic DABCO salts (**7**) demonstrated significantly higher reactivity than their aliphatic counterparts, as evidenced by higher RCCs achieved at lower reaction temperatures (optimization is shown in SI (chapter 7.1)). However, radiofluorination of nitro (**8b**) and ethyl benzoate (**8e**) substrates, which are highly activated for  $\text{S}_{\text{N}}\text{Ar}$  substitution, in DMF resulted in considerable formation of [ $^{18}\text{F}$ ]fluoroarene side products. Formation of this side product could be suppressed by switching the reaction solvent to *tert*-butanol. A possible explanation for this

## 5 Results and Discussion

observation could be that *tert*-BuOH forms a solvate with the "naked" [<sup>18</sup>F]fluoride ion, which selectively suppresses competing S<sub>N</sub>Ar reactions by reducing its basicity while maintaining its nucleophilicity.

Regardless of the underlying mechanism, switching to *tert*-BuOH significantly improved the radiolabeling efficiency, increasing the RCC for the S<sub>N</sub>2 ring-opening reaction of the ethyl benzoate substrate (**8e**), e.g., from 17% in DMF (with a competing side reaction RCC of 22%) (more information in SI (chapter 7.1)) to 73 ± 2%, with no detectable side products. The phenyl model substrate (**8a**) yielded an almost quantitative RCC of 98 ± 1%. RCCs for the other model substrates amounted to 66–79%. Finally, azido-functionalized [<sup>18</sup>F]fluoroethylpiperazine (**8f**), which could be applied as prosthetic group for indirect click radiolabeling, was successfully prepared with an RCC of 38 ± 1%.

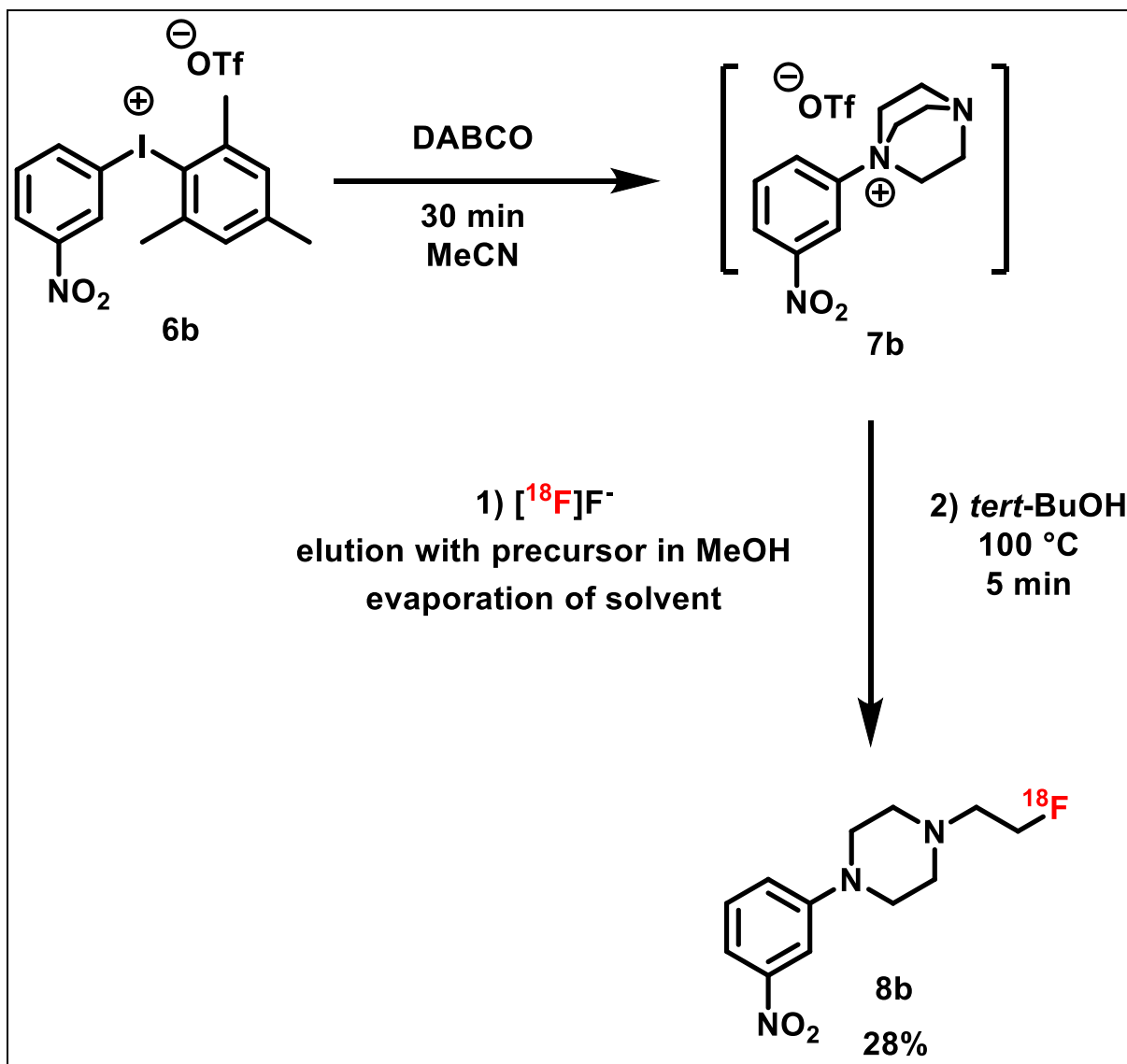


Figure 39: One-pot synthesis and radiofluorination of aromatic DABCO salts.

Finally, to streamline the preparation of aromatic  $[^{18}\text{F}]$ fluoroethylpiperazines, we aimed to develop a one-pot procedure for the synthesis and radiofluorination of aromatic precursors. To this end, we first treated iodonium salt **6b** with varying amounts of DABCO and monitored the formation of DABCO and ethylpiperazyl-DABCO salts. Our objective was to avoid residual iodonium salt precursor, which could react with  $[^{18}\text{F}]$ fluoride to produce unwanted  $[^{18}\text{F}]$ fluoroarene side products. While all reactions produced a mixture of the desired DABCO and the ethylpiperazyl-DABCO salts, radiofluorination of both salts yielded the desired product. Therefore, isolation of the pure aromatic DABCO salt was much less critical than complete conversion of the iodonium salt, which could otherwise lead to the formation of radiolabeled side products.

## 5 Results and Discussion

The optimal results were achieved using two equivalents of DABCO at 110°C for 30 minutes, which resulted in complete consumption of the iodonium salt precursor. Higher temperatures of 120°C also resulted in complete conversion of the iodonium salt, but led to increased decomposition of the *in situ* generated DABCO salts and therefore reduced the RCCs in the sequential radiofluorination step while lower reaction times led to incomplete consumption of the iodonium salt precursor. Shorter reaction times of 20 min and 25 min left unreacted iodonium salt, compromising the radiolabeling step through the formation of side products. According to the optimized procedure, the nitro-substituted iodonium salt **6b** in MeCN was treated with DABCO at 110 °C for 30 minutes, followed by removal of the solvent under reduced pressure. The residue was dissolved in MeOH and used for elution of [<sup>18</sup>F]fluoride, loaded onto a anion exchange resin, and subsequent radiofluorination according to the "minimalist" approach, which yielded the [<sup>18</sup>F]fluoroethyl product **8b** in a RCC of 28%, as compared to 66 ± 5% when starting from the isolated nitro-DABCO salt **7b**.

In conclusion, our method enables the efficient access to the diverse compounds containing diversely substituted [<sup>18</sup>F]fluoroethylpiperazine motif using quaternary DABCO salts as precursors for radiolabeling. We also successfully developed a one-pot procedure for the synthesis and radiofluorination of aromatic DABCO salts that utilize easily accessible iodonium salt precursors.

## 5.2 DABCO Salts

### 5.2.1 Optimization of Ring Opening Reaction

A new project was initiated to investigate the ring-opening reaction of DABCO salts as an alternative radiofluorination method. A model compound (**1**) was synthesized as the basis for initial optimization experiments (Figure 40).

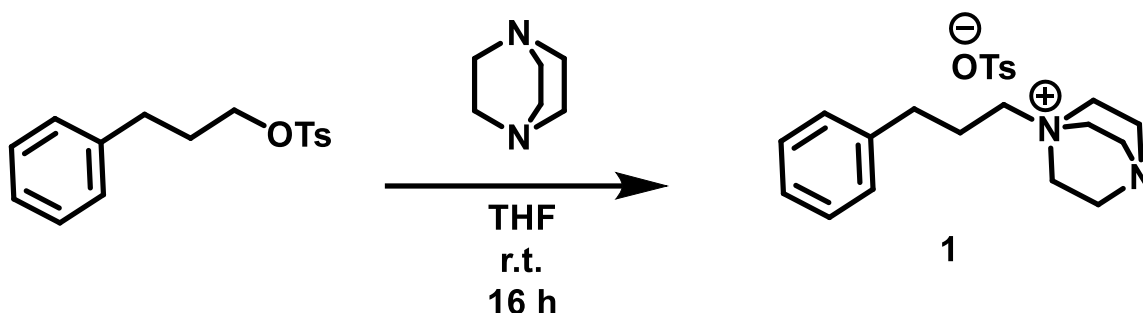


Figure 40: Synthesis of the model precursor.

The temperature dependence of the reaction was investigated first (Table 3), revealing that high temperatures are required for the ring-opening reaction. Additionally, the RCC showed a strong dependence on the heating method. Given the potential for precursor decomposition, the reaction conditions were optimized in a manner similar to those for the 3-hydroxyazetidinium salts.

Conventional heating in a heating block produced very low RCCs, with no conversion observed at or below 130 °C (entry 1) and only 2–5% conversion at higher temperatures (entries 2 and 3). As a consequence, this heating method was not further pursued.

Use of a microwave reactor significantly improved the RCCs to >80% at 150 °C (entry 4) and almost 90% at 160 °C (entry 5). However, an inductive heating reactor proved to be the most effective (entries 6–11), reaching almost quantitative RCCs at 150 °C (entry 10). The superior performance of inductive heating is possibly resulting from rapid cooling, which minimizes precursor decomposition. Thus, in the inductive heating reactor, cooling after the reaction is achieved by a stream of air, while the microwave reactor cools only passively. The lower RCC observed at 160 °C (entry 11), which suggests that decomposition increases at higher temperatures supports this idea. Inductive heating was therefore selected as the preferred method for all subsequent experiments.

## 5 Results and Discussion

Table 3: Optimization of reaction temperature and heating method.

entry	T/°C	Heating method	RCC
1	130	heating block	0 (n = 2)
2	140	heating block	2,5 ± 0,5% (n = 2)
3	150	heating block	5 ± 4% (n = 6)
4	150	microwave	81 ± 18% (n = 2)
5	160	microwave	88 ± 9% (n = 3)
6	110	inductive heating	17 ± 2% (n = 2)
7	120	inductive heating	30 ± 15% (n = 11)
8	130	inductive heating	55 ± 1% (n = 3)
9	140	inductive heating	64 ± 9% (n = 5)
10	150	inductive heating	96 ± 4% (n = 15)
11	160	Inductive heating	75 ± 2% (n = 2)

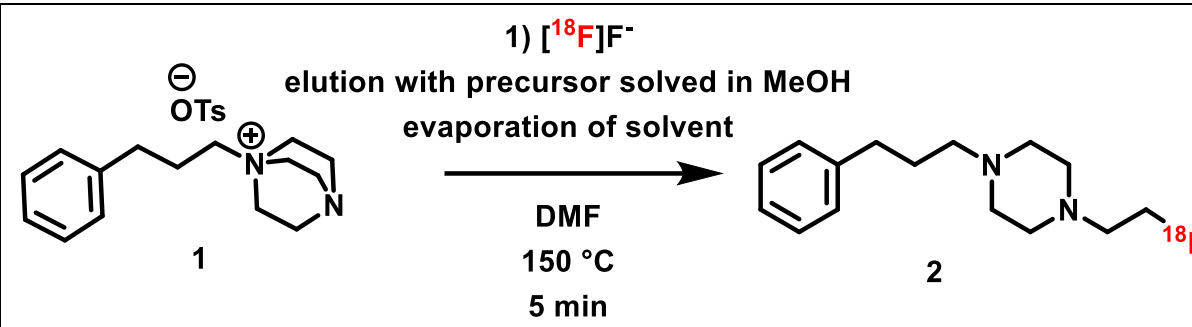
As the temperature optimization suggested the occurrence of decomposition, the effects of silanization and the addition of a stirring bar were also investigated. To this end, twelve reactions were carried out across different heating methods, with and without stirring bars, and in silanized versus non-silanized reactors (Table 4). Consistent with the results described above, the heating method proved to have the most significant impact: RCCs were very low with conventional heating (0–8%), while microwave heating yielded RCCs between 45% and 87%. In microwave heated reactions performed with silanized reactors, stirring improved the RCCs compared to non-stirred reactions, likely due to improved reaction kinetics. However, in non-silanized reactors, stirring resulted in lower RCCs, possibly due to increased adsorption of [<sup>18</sup>F]fluoride on the unprotected reactor walls.

In the inductive heating reactor, reactions without stirring bar performed very well, with RCCs of 96% and 97%, regardless of silanization.

Based on these findings, all subsequent reactions were conducted in non-silanized reactors without stirring to streamline the procedure.

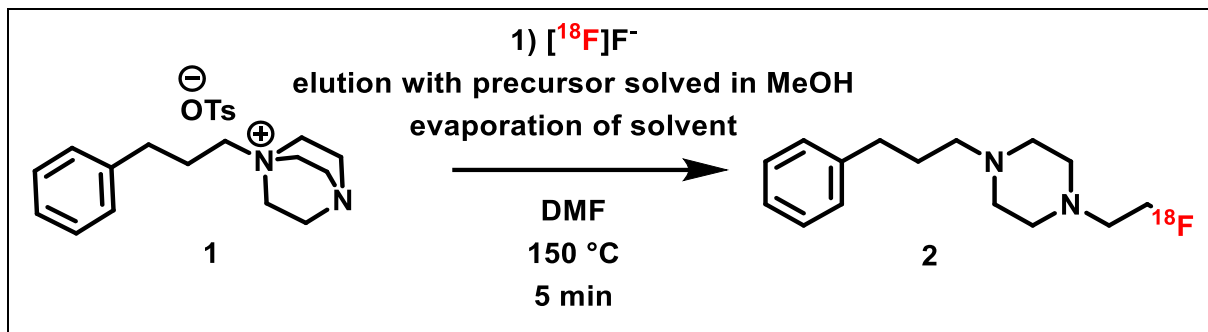
## 5 Results and Discussion

Table 4: Example reactions to investigate the influence of silanization and presence of a stirring bar on the RCC.

				
entry	stirring bar	silanisation	heating method	RCC
1	No	no	Heating block	5
2	No	yes	Heating block	3
3	Yes	no	Heating block	0
4	yes	yes	Heating block	8
5	No	no	microwave	87
6	No	yes	microwave	45
7	Yes	no	microwave	58
8	yes	yes	microwave	69
9	No	no	inductive heating	96
10	No	yes	inductive heating	97
11	Yes	no	inductive heating	21
12	yes	yes	inductive heating	15

Finally, the effect of precursor loading was investigated by determination of the RCCs obtained with precursor amounts ranging from 37.5  $\mu\text{mol}$  to 1.25  $\mu\text{mol}$  (Table 5). Near-quantitative RCCs were obtained with precursor amounts down to 7.5  $\mu\text{mol}$ , while a further decrease in precursor loading led to a slight reduction at 5  $\mu\text{mol}$ , and a sharp reduction at 2.5  $\mu\text{mol}$  and below. Therefore, 7.5  $\mu\text{mol}$  was selected as the optimal precursor loading.

Table 5: Determination of optimal precursor amount.



Entry	Precursor loading / $\mu\text{mol}$	RCC / %
1	37.5	100
2	25	100
3	12.5	100
4	7.5	97
5	5	87
6	2.5	53
7	1.25	3

### 5.2.2 Influence of Solvent on Ring Opening Ratio

After optimization of the conditions for radiofluorination of an aliphatic model compound, a iodopyridyl-substituted DABCO salt (**3**) which was developed in our group as a  $S_NAr$  precursor<sup>[18]</sup> was tested to investigate the feasibility of  $S_N2$  vs.  $S_NAr$  pathway in the case DABCO salts with electron-poor (hetero)aryl substituents.

In **3**, the ring-opening reaction competes with an  $S_NAr$  reaction, where the DABCO salt motif acts as a leaving group to form 2-[<sup>18</sup>F]fluoro-5-iodopyridine **5**. To assess whether this side reaction can be controlled, various reaction solvents were tested (Table 6). While the  $S_NAr$  reaction was favored in all solvents, solvent choice significantly influenced the product distribution (Table 6).

Aprotic solvents efficiently suppressed the formation of the ring-opening product. Isopropanol afforded the desired substituted 2-[<sup>18</sup>F]fluoroethylpiperazine in a RCC of 32% together with 2-[<sup>18</sup>F]fluoro-5-iodopyridine in 46% RCC. RCCs of **4** in all other tested solvents were much lower.

## 5 Results and Discussion

Table 6: Influence of solvents on the ratio of ring opening and aromatic substitution reaction.

1) [<sup>18</sup>F]F<sup>-</sup>  
 elution with in MeOH solved precursor  
 evaporation of solvent  
 solvent  
 150 °C  
 5 min

entry	solvent	RCC A	RCC B
1	<i>tert</i> -BuOH	18	69
2	EtOH	4	6
3	MTBE	0	3
4	<i>iso</i> -PrOH	32	46
5	<i>tert</i> -BuNH <sub>2</sub>	3	23
6	<i>n</i> -BuOH	1	5
7	acetone	4	58
8	THF	6	90
9	<i>tert</i> -AmylOH	0	58
10	<i>Alpha</i> -Me-THF	1-3	71
11	dioxane	1	62
12	toluene	0	8
13	benzene	0	21

Accordingly, further work with iodopyridine DABCO triflate was discontinued and the preparation of DABCO salts, which could serve as radiolabeling precursors for potential PET-tracers was investigated.

### 5.2.3 Attempts to Prepare DABCO Salts Containing Pharmacophores

After investigation of the reaction with model compounds, we try to prepare pharmacophores-containing DABCO salts.

Initially, we focused on the synthesis of amine and carboxyl reactive DABCO salts. First, DABCO salt **7**, which contains a carboxylic group was prepared via acidic hydrolysis of the corresponding ethyl ester (Figure 41).

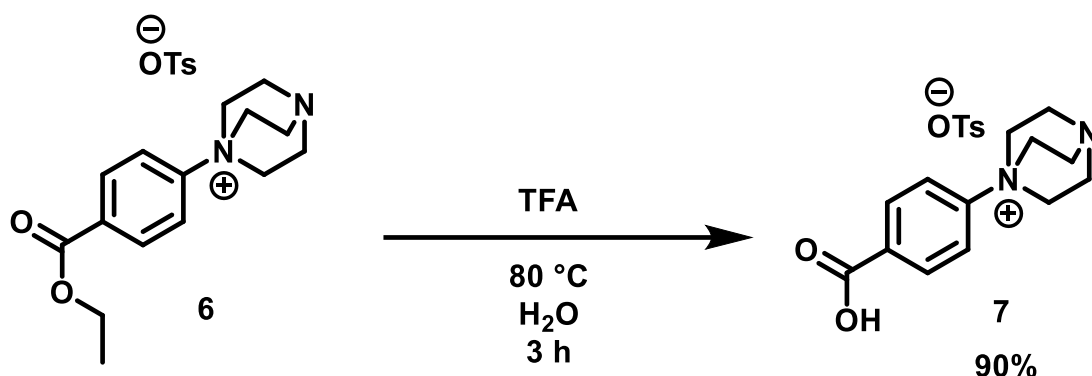


Figure 41: Synthesis of the free acid starting from the ethyl ester.

Unfortunately, acid **7** displayed extremely poor solubility in aprotic solvents, and was well soluble only in H<sub>2</sub>O and MeOH. All attempts to apply prepared amides from **7** using carbodiimide activation, formation of active esters and chloroanhydride as well as reaction with isocyanates were unsuccessful. This rendered the CO<sub>2</sub>H-bearing DABCO salt **7** impractical for conjugation reactions.

Next, we synthesized an amine-substituted DABCO salt (**11**) by reducing the nitro-substituted precursor **9** (Figure 42). Initially, the reduction was attempted by hydrogenation with palladium on charcoal, reaction control with mass spectroscopy showed the hydroxylamine intermediate **10** as only formed product. Repeating the reaction with fresh catalyst and prolonged hydrogen exposure similarly failed to produce the desired amine **11**.

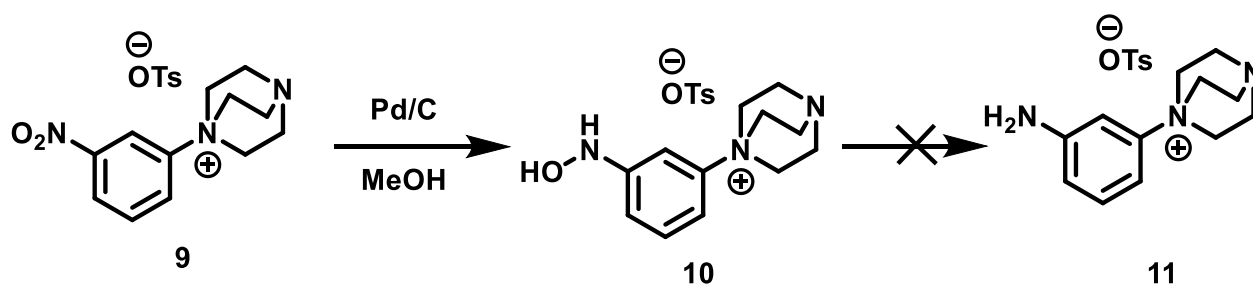


Figure 42: Synthesis of amine bearing DABCO salt by reduction with hydrogen.

Reduction with Zn and NH<sub>4</sub>Cl instead of hydrogen also stalled at the hydroxylamine intermediate **10** or yielded only decomposition products after an extended reaction time of 16 hours (Figure 43).

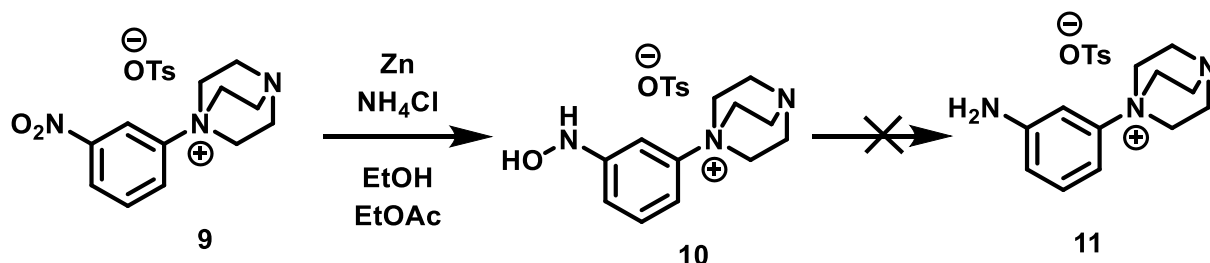


Figure 43: Reduction of the nitro bearing DABCO salt with zinc and ammoniumchloride.

Likewise, reduction with tin and hydrochloric acid, which generates nascent hydrogen that should be more reactive than hydrogen gas, did not afford the desired product (Figure 44).

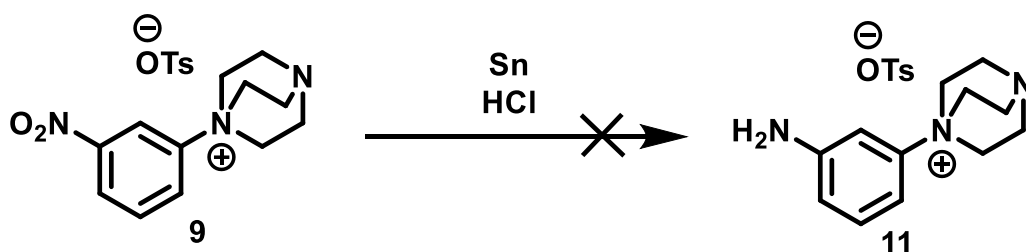


Figure 44: Reduction of the nitro bearing DABCO salt with tin and hydrogenchloride.

Finally, reduction with iron and acetic acid produced the desired amine in very good yields, with complete consumption of the starting material. The product was easily isolated by lowering the pH of the reaction mixture and removing the iron oxide side product by filtration (Figure 45).

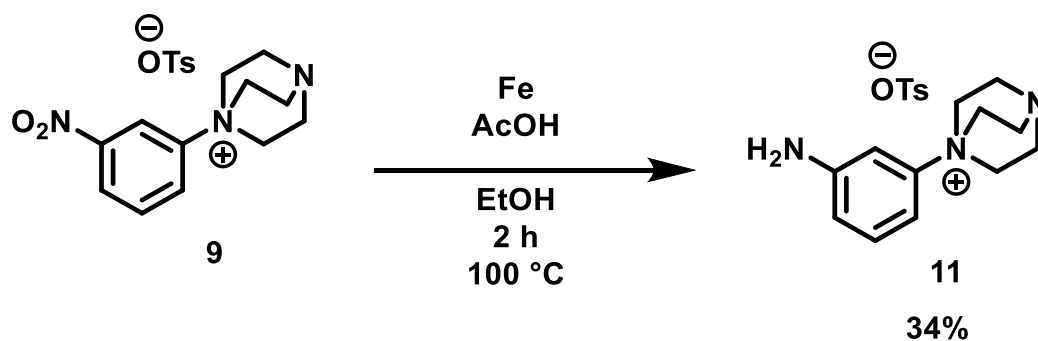


Figure 45: Reduction of the nitro bearing DABCO salt with iron and acetic acid.

Next, several conjugation methods were tested by treating the amine-bearing DABCO salt **11** with appropriate model compounds. Full consumption of the starting material was essential

due to challenges in separating the DABCO amine from the desired products. First, the amine was reacted with an acid chloride to evaluate its suitability for acid chloride coupling (Figure 46, pathway A). Although the conjugation was successful, a significant amount of the starting material did not react. Even with excess acid chloride, increased temperature, or extended reaction time, the reaction remained incomplete. As an alternative conjugation method, we also tested the reaction with tetrafluorophenyl (TFP) esters, which are easily synthesized, sufficiently stable for isolation and identification, and highly reactive towards amines even in the absence of bases and at room temperature. (Figure 46, pathway B). However, despite addition of base and extended heating, only traces of the desired product were observed and the DABCO amine remained the main component in the reaction mixture. This lack of reaction may stem from the electron-withdrawing properties of the DABCO group, which likely hinders conjugation.

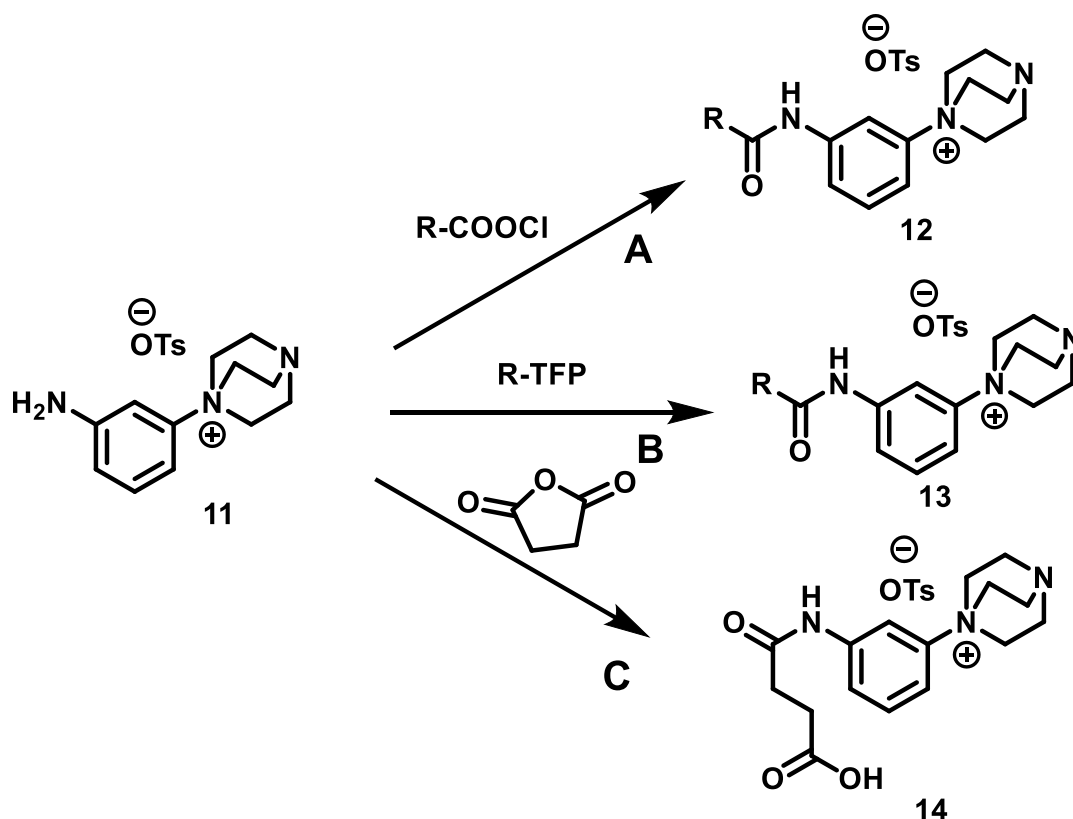


Figure 46: Conjugation of the amine DABCO salt with model compounds.

Finally, conjugation with cyclic diacid anhydrides was tested by reacting the DABCO amine with succinic anhydride (Figure 46, pathway C). This reaction fully consumed the starting material and produced the desired product, confirming its suitability for further conjugation studies. As a next step, Boc-protected glutaric anhydride was used as a more complex cyclic anhydride.

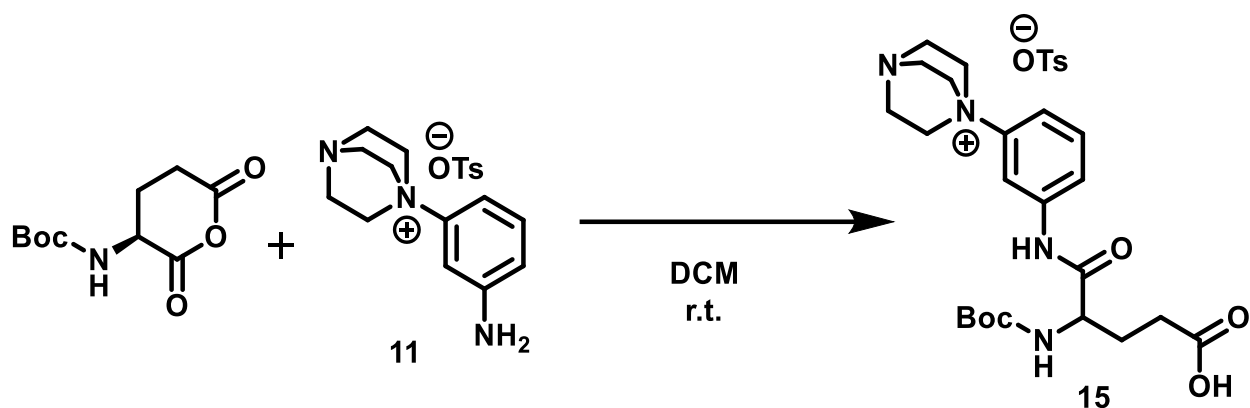


Figure 47: Conjugation of the amine DABCO salt with boc-glutaric anhydride.

However, conjugation of DABCO amine with this substrate resulted in an incomplete reaction with unreacted starting material in the reaction mixture, rendering this approach unfeasible due to the difficulty of separating the two DABCO salts.

Given these challenges, we pursued a different strategy based on ribose as a readily available prosthetic group that can be conjugated with aminoxy-modified peptides<sup>[36]</sup> (Figure 48).

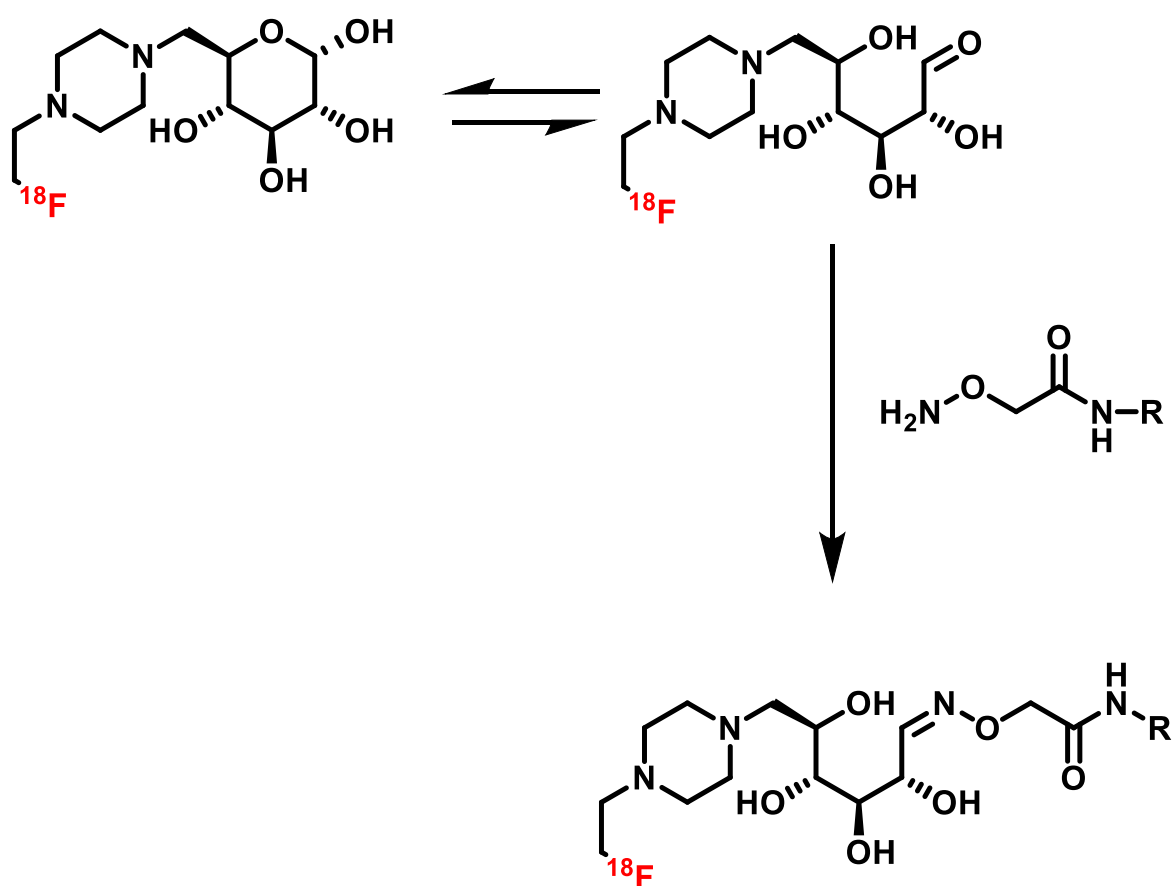


Figure 48: Mechanism of the conjugation of the target molecule with an aminoxy peptide.

## 5 Results and Discussion

To this end, 1-*O*-Methyl-D-ribose was treated with tosyl chloride and the tosylated intermediate reacted with DABCO in THF to form the corresponding ribose-DABCO salt **18** in excellent yields (Figure 49).

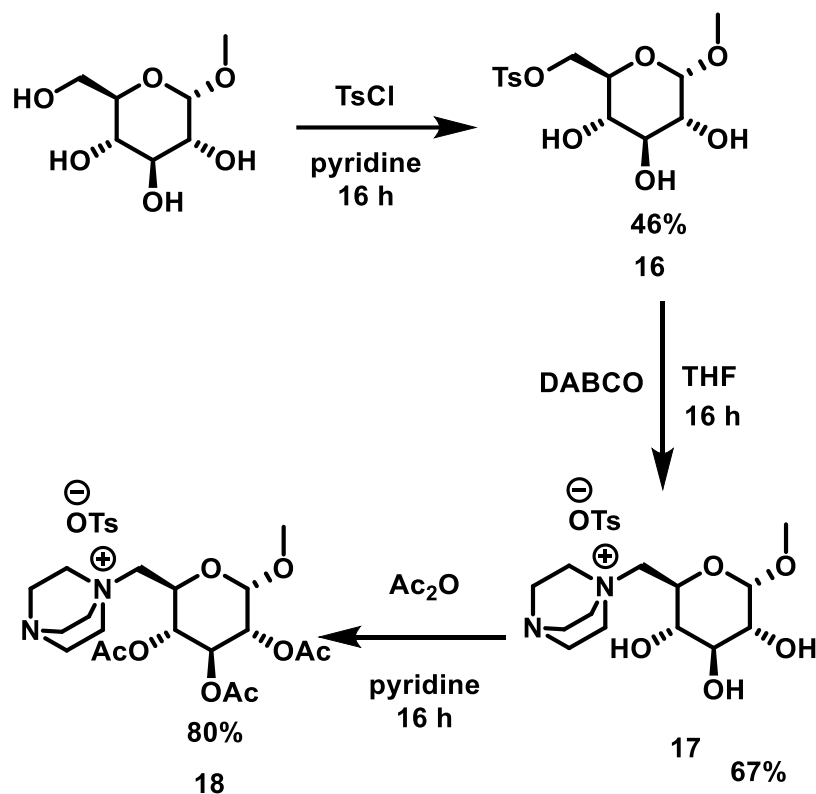


Figure 49: Synthesis of a ribose DABCO salt.

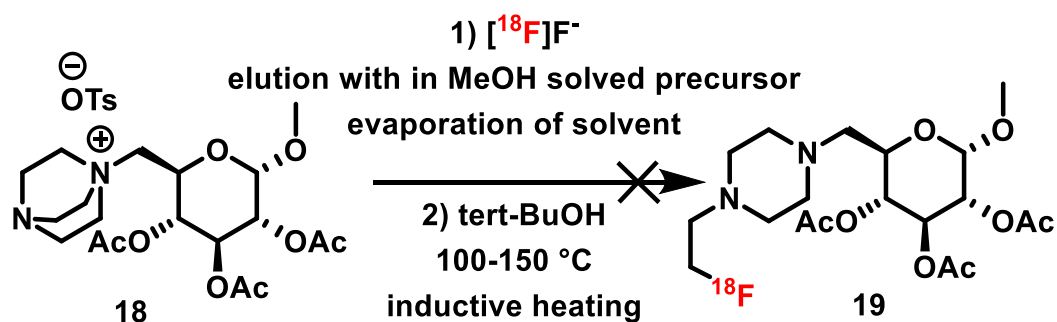


Figure 50: Radiofluorination attempt of the ribose DABCO salt.

However, subsequent radiofluorination of the ribose-DABCO salt did not yield the radiofluorinated product (Figure 50). This likely resulted from the temperature sensitivity of the precursor, as the radiofluorination required heating to 150 °C, a temperature incompatible with the thermal stability of ribose.

## 5 Results and Discussion

Subsequently, a precursor for a prostate-specific membrane antigen (PSMA) radioligand was prepared by coupling bromo-butanoic acid with the lysine residue of a urea-based PSMA inhibitor, followed by reaction with DABCO in THF (Figure 51).

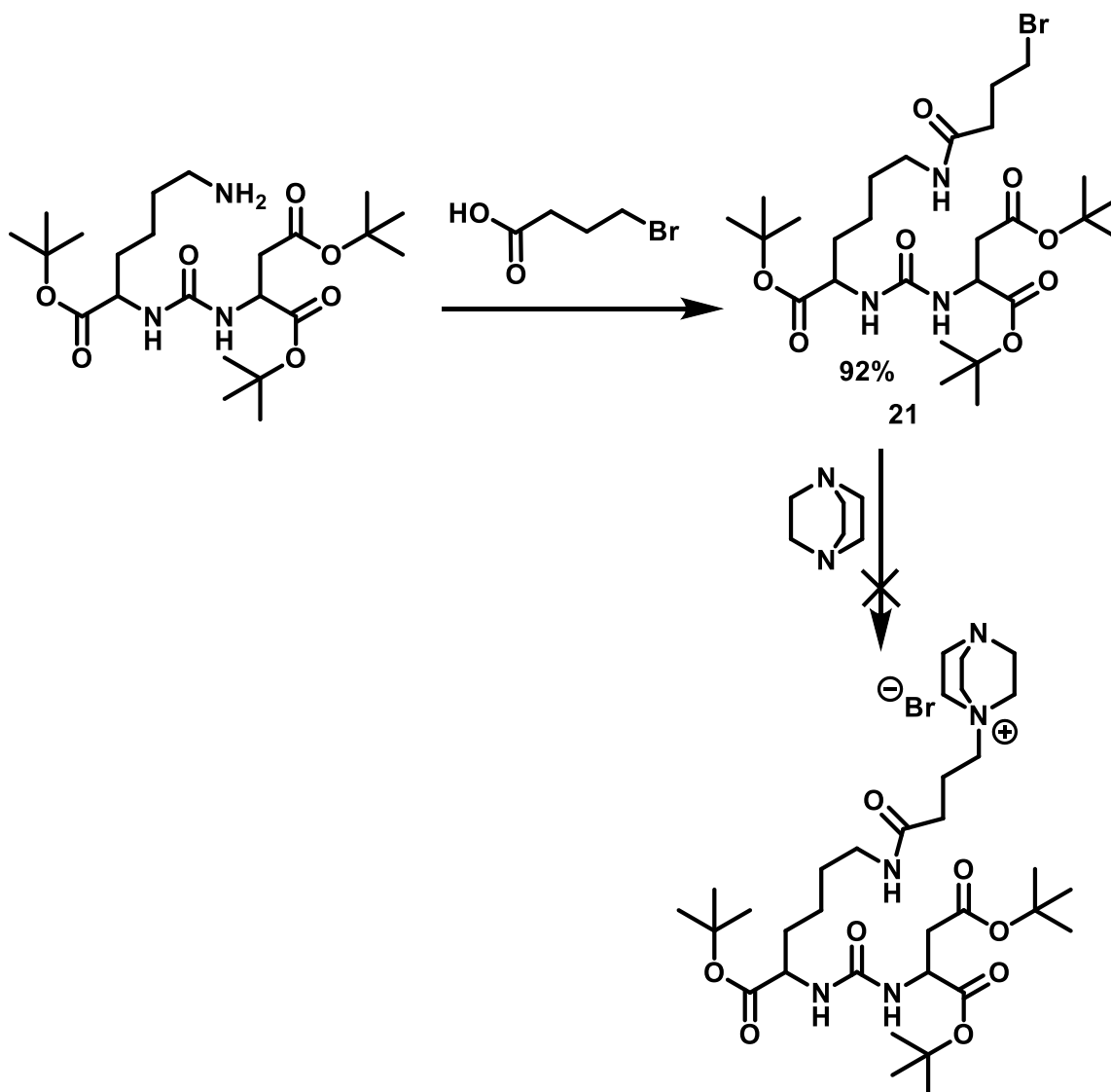


Figure 51: Synthesis of DABCO-substituted PSMA ligand.

Unfortunately, the desired DABCO salt could not be isolated, presumably because it underwent ring closure with either DABCO or bromine acting as a leaving group. Since the compound with bromine as counter ion could be isolated in acceptable yields, it is more likely that the ring closure reaction proceeded with DABCO as the leaving group (Figure 52).

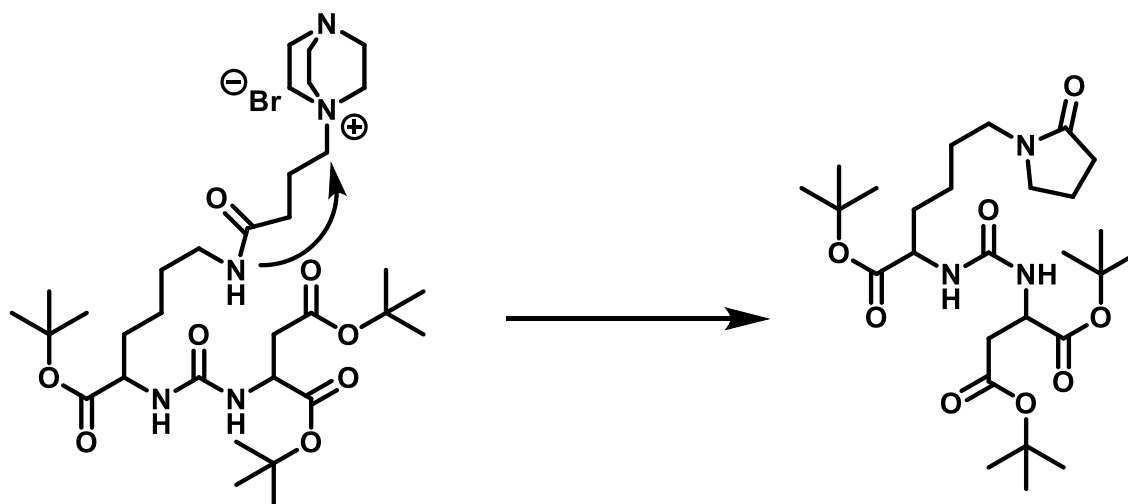


Figure 52: Proposed side reaction preventing isolation of the DABCO-substituted PSMA ligand.

To mitigate this potential side reaction, several DABCO-bearing active esters were prepared by coupling bromo-butanoic acid with the corresponding active ester precursor using HATU as the coupling reagent. The resulting compounds were then treated with DABCO to form the respective DABCO active esters (Figure 53). Unfortunately, only the succinimide ester **23c** could be successfully synthesized.

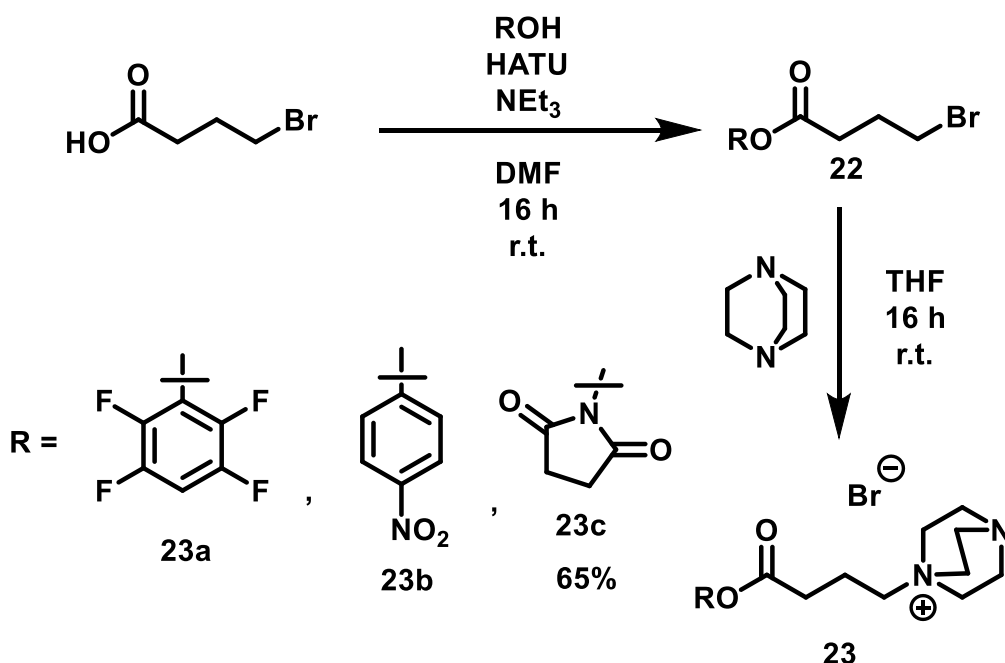


Figure 53: Synthesis of DABCO bearing active esters.

However, this active ester did not undergo conjugation with model amines or with the lysine residue of the PSMA inhibitor. It is likely that ring closure reactions prevented the formation of the conjugated product, as the active ester was consumed, and only minor formation of the free acid could be observed.

## 5 Results and Discussion

Additionally, the active ester proved to be insufficiently stable for radiofluorination, which did not afford radiolabeled products, likely due to the high temperatures required for the reaction.

To prevent ring closure, DABCO salts attached to an aromatic scaffold were also tested, as steric hindrance was expected to inhibit this side reaction. To this end, an iodonium salt of the active ester was synthesized and a coupling with the PSMA inhibitor was tested. However, only trace amounts of the coupled iodonium salt **26** could be observed (Figure 54).

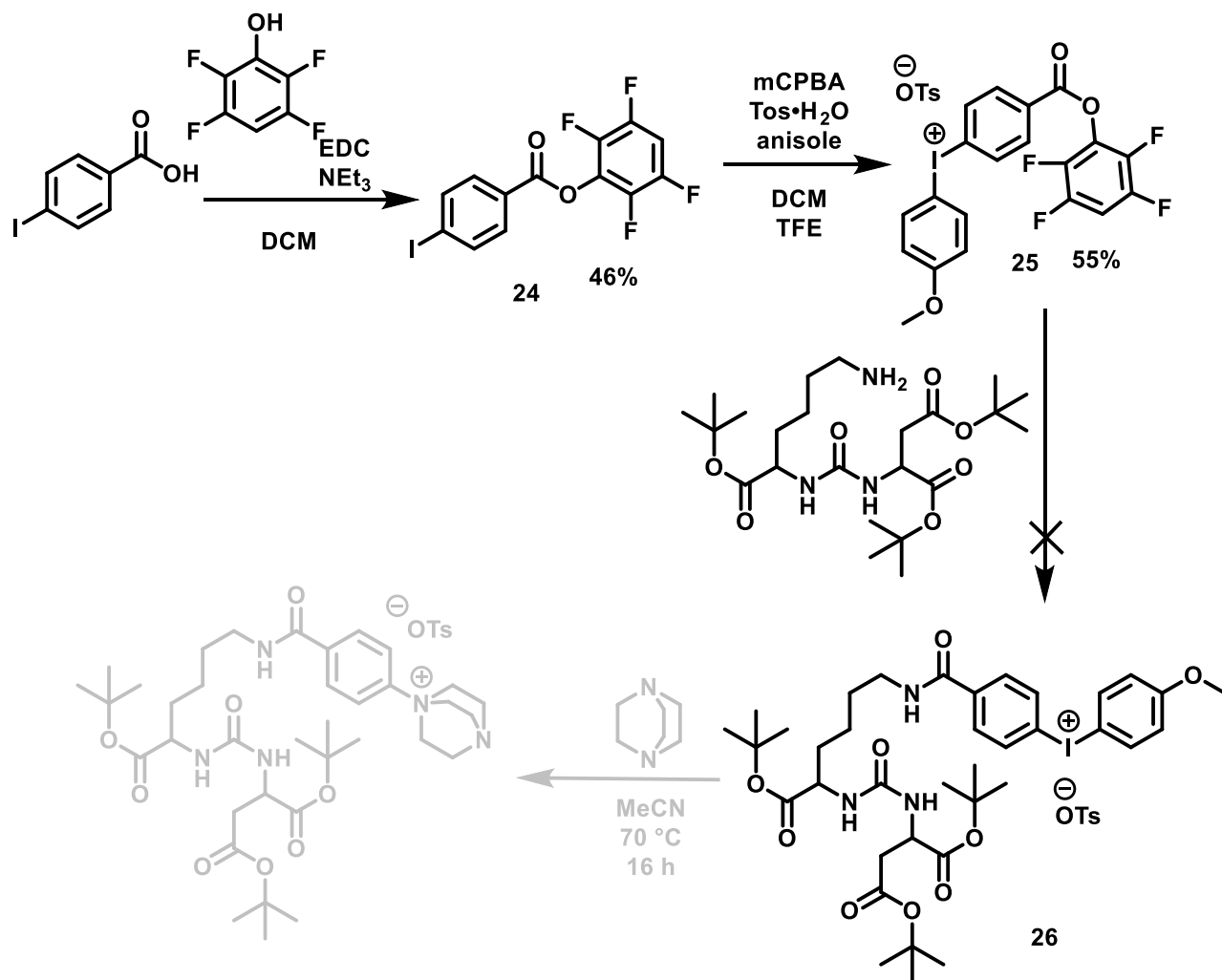


Figure 54: Synthesis of a DABCO salt bearing PSMA precursor.

To investigate this phenomenon further, a tyrosine iodonium salt (**28**) was synthesized by converting Boc- and *tert*-butyl-protected iodo-tyrosine into the corresponding trimethylstannane (**27**), which was then treated with Koser's reagent to obtain the iodonium salt (Figure 55). The subsequent reaction was carried out under standard conditions for transarylation to DABCO salts.

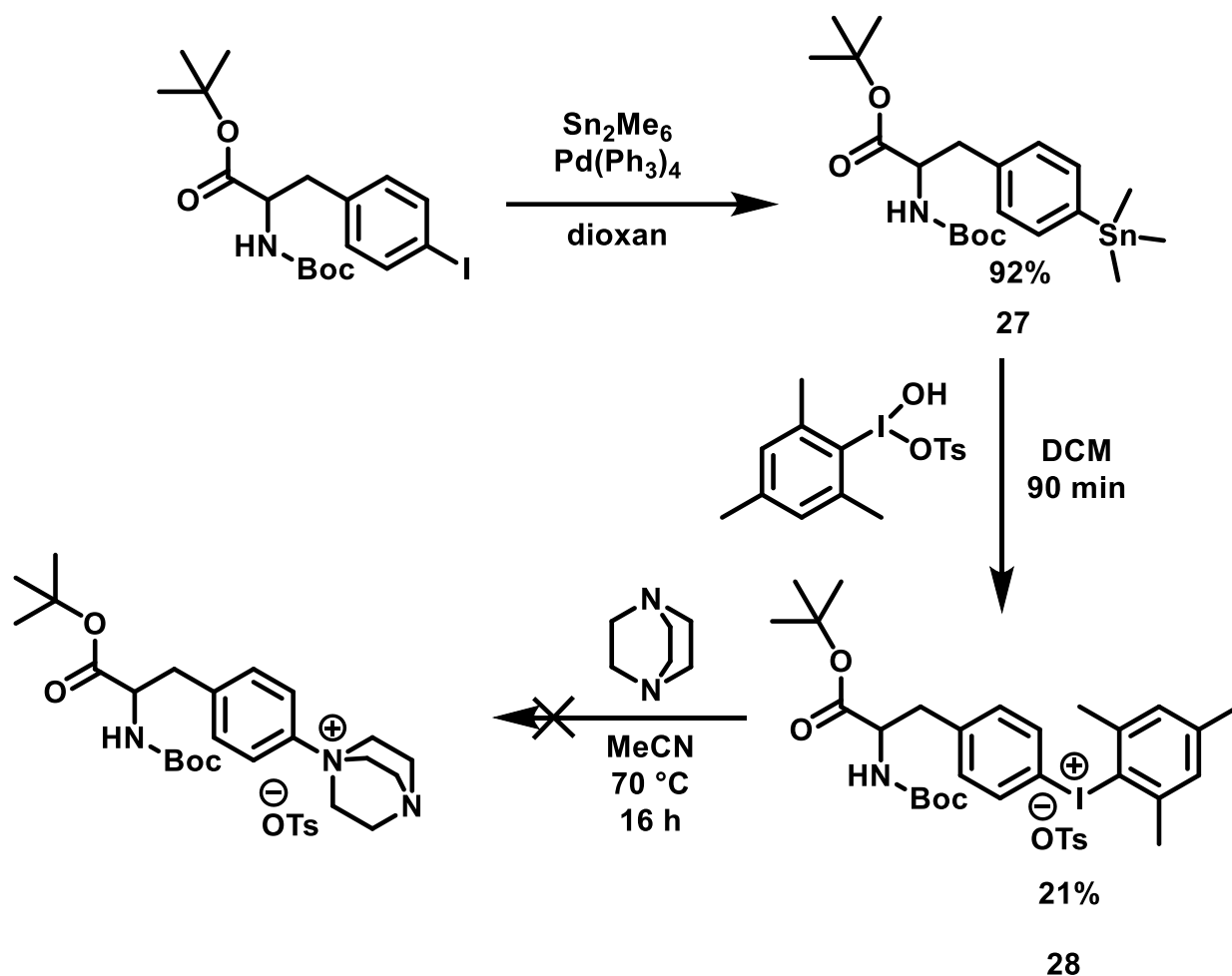


Figure 55: Synthesis of a tyrosine DABCO salt via a tyrosine iodonium salt.

Although the stannylation and oxidation reactions proceeded with acceptable yields, the DABCO transfer was unsuccessful. This suggests that the transfer of DABCO to iodonium salts is limited to small model compounds. A potential reason for this could be the electronic structure of the tyrosine iodonium salt. The more electron-deficient aromatic ring might enhance the reactivity of the iodonium salt, making successful DABCO salt formation less favorable. To overcome the inability of the unmodified tyrosine aromatic ring to undergo DABCO salt formation, the use of a linker-modified tyrosine analog was explored (Figure 56). Specifically, 2-(bromomethyl)-2-(hydroxymethyl)-1,3-propanediol was first transformed into a cyclic acetal to protect the two hydroxyl groups, leaving one hydroxyl group unprotected. The unprotected hydroxyl group was then tosylated, and subsequent nucleophilic substitution on the tyrosine derivative afforded the desired product. Finally, a  $\text{S}_{\text{N}}2$  substitution with DABCO should yield the targeted product.

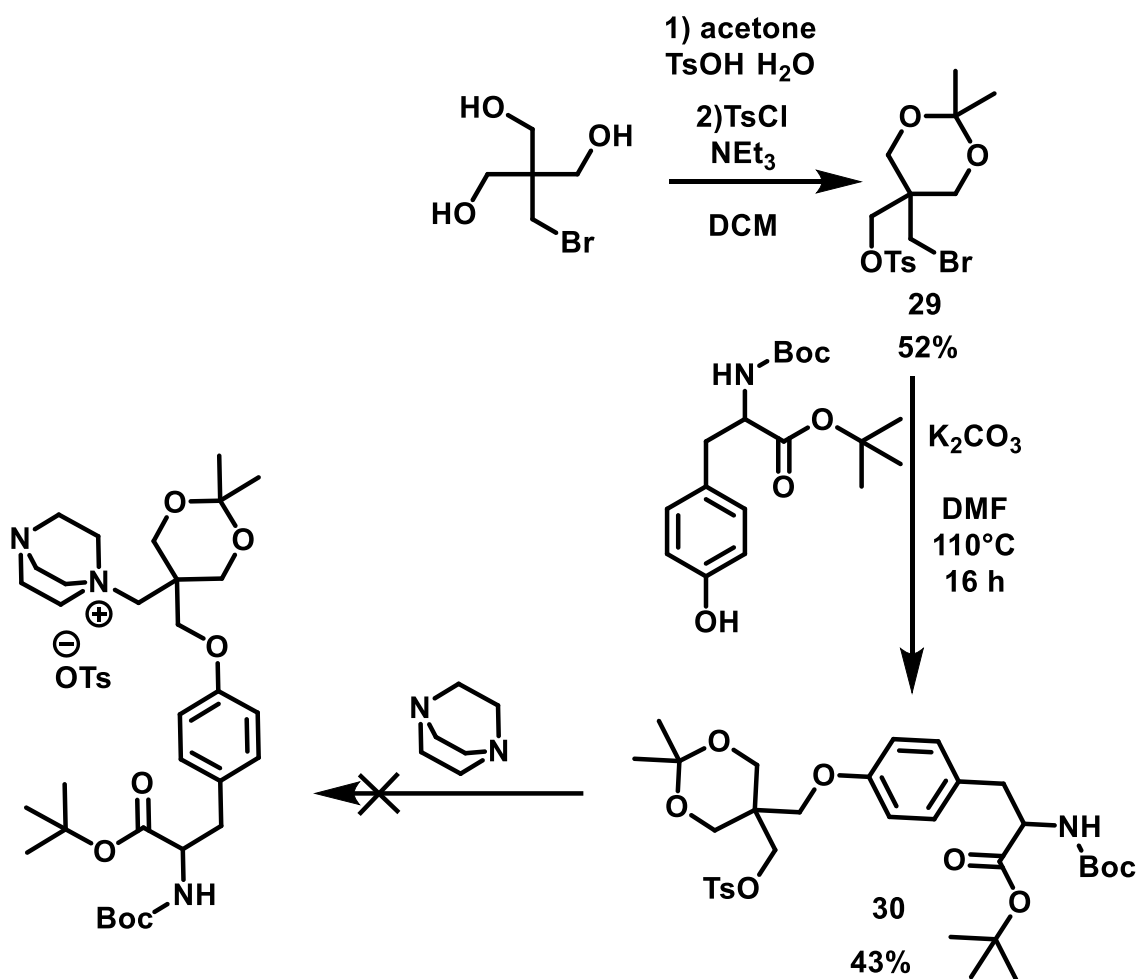


Figure 56: Synthesis of a tyrosine DABCO salt with a linker.

Regrettably, the substitution with DABCO did not proceed as expected. Steric hindrance is likely the key issue, as the nucleophilic attack on the carbon bearing the tosylate leaving group proves to be quite challenging. Attempts to mitigate this by transforming the tosylate (**29**) into an iodine—thereby reducing the steric demands of the reaction—also failed to yield the desired DABCO salt. In subsequent experiments, the linker (**29**) was treated with DABCO prior to coupling onto the tyrosine, but this did not result in the formation of a DABCO-substituted linker. This led to the conclusion that this particular linker is not compatible with DABCO substitution.

In summary, the ring-opening reaction of DABCO salts shows significant promise, as demonstrated by the successful radiofluorination of a broad range of substrates with high radiochemical conversions. However, conjugating DABCO salts to pharmacologically relevant structures remains a major challenge. While the preparation of aromatic DABCO salts bearing pharmacophores is hampered by the poor reactivity of iodonium salt precursors, the synthesis of aliphatic DABCO salts is more feasible. Unfortunately, the high temperatures required for

## 5 Results and Discussion

radiofluorination of aliphatic DABCO salts severely limit the scope of compatible pharmacophores. This challenge in synthesizing pharmacophores bearing a DABCO salt motif remains a significant hurdle for further applications and will be a key focus of future research.

### 5.3 3-Hydroxyazetidinium Salts

Based on a method developed in our group<sup>[37]</sup>, the objective of this sub-project was to establish and optimize a ring-opening reaction that uses 3-hydroxyazetidinium salts as precursors for the radiosynthesis of 1-(4-benzylpiperidin-1-yl)-3-([<sup>18</sup>F]fluoro)propan-2-amine. Apart from the common approach to prepare azetidinium salts by heating a propylamine fitted with a suitable leaving group, 3-hydroxyazetidinium salts are easily accessible from the corresponding piperidine and epichlorohydrin<sup>[38]</sup>. The counterion is subsequently exchanged using silver triflate in an anion metathesis reaction, which enhances the reactivity and elution efficiency by introducing the less-coordinating triflate anion (Figure 57).

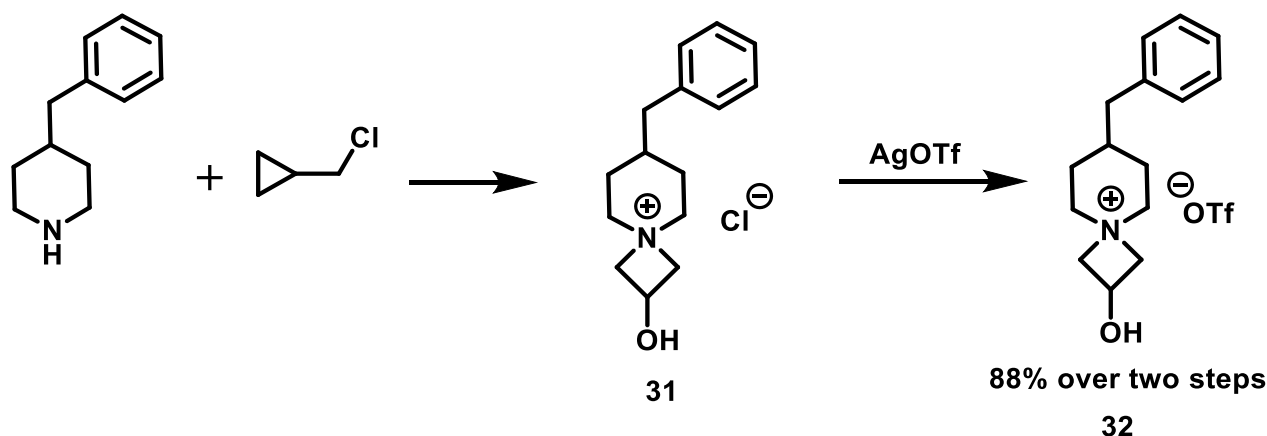


Figure 57: Synthesis scheme of 7-benzyl-2-hydroxy-4-azaspiro[3.5]nonan-4-ium tosylate.

#### 5.3.1 Optimization of Reaction Conditions

Radiofluorination of the model 3-hydroxyazetidinium salt was performed using the "minimalist" approach, where the precursor is used to elute [<sup>18</sup>F]fluoride from an anion exchange cartridge. In preliminary experiments conducted under the reaction conditions summarized in Table 7, the reaction demonstrated low radiochemical conversion (RCCs). In addition, significant variability in the RCCs obtained under identical conditions suggested possible decomposition of either the precursor or the product during the reaction. To address this issue, a systematic evaluation of the reaction parameters was conducted to assess the influence of precursor loading, solvent volume, reactor setup, temperature, stirring method, and anion type.

## 5 Results and Discussion

Table 7: Preliminary experiments for the determination of RCC.

1) [<sup>18</sup>F]F<sup>-</sup>  
elution with precursor solved in MeOH  
evaporation of solvent  
110 °C  
5 min  
DMF

No.	m /mg	T /°C	t /min	solvent	V /mL	RCC /%
1	5	110	5	DMF	1	10
2	5	110	5	DMF	1	11
3	5	110	5	DMF	1	6
4	5	110	5	DMF	1	37

First, different precursor loadings were tested to determine whether increasing the amount of precursor could improve RCCs. In these experiments, the influence of solvent volume was also investigated, as it is a critical parameter in preventing substrate decomposition during heating.

Table 8: Determination of the effect of precursor loading and solvent volume on radiochemical conversion.

1) [<sup>18</sup>F]F<sup>-</sup>  
elution with precursor solved in MeOH  
evaporation of solvent  
110 °C  
5 min  
DMF

No.	Precursor loading /mg	Solvent volume /mL	RCC
1	5	1	16 ± 12% (n = 4)
2	15	1	23 ± 3% (n = 3)
3	15	0,5	26 ± 9% (n = 4)

These experiments revealed that 0.5 mL of solvent and a higher precursor loading of 36 μmol yielded the highest RCCs. However, the RCCs remained lower than desired, with a relatively

## 5 Results and Discussion

high standard deviation. To identify the reasons for the high standard deviation, additional reaction parameters were evaluated, including the presence of a stirring bar, the roughness of the reactor surface, and reactor conditioning.

First, the reactors were silanized by treatment of the reactor walls with trimethylchlorosilane to create a uniform, highly apolar surface and improve the comparability between reactors by minimizing the influence of small scratches on the reactor walls. This is achieved through the reaction of free silanol groups on the surface with trimethylchlorosilane, resulting in the formation of a trimethylsilane-substituted surface (Figure 58).

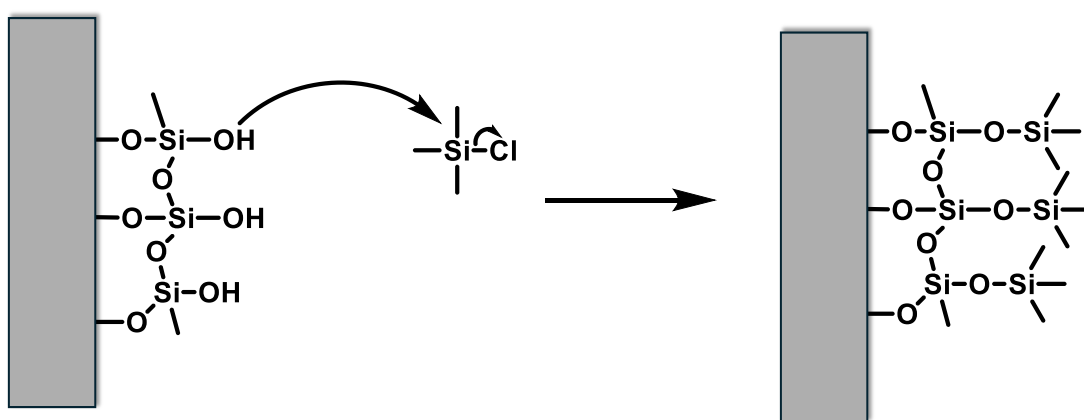


Figure 58: Schematic depiction of the silanization of a reactor wall.

Table 9: Optimization of non-stirred 3-hydroxyazetidinium salt radiofluorinations.

No.	Anion	Reactor	RCC
1	OTs	non-silanized reactor	36 ± 20% (n = 5)
2	OTs	silanized reactor	30 ± 5% (n = 6)
3	OTs	freshly silanized reactor	47 ± 8% (n = 7)
4	ClO <sub>4</sub>	freshly silanized reactor	32 ± 10% (n = 3)

As illustrated in Table 9, reactions performed in silanized and non-silanized reactors afforded similar RCCs, but silanization resulted in more consistent results. Specifically, the standard deviation of RCCs obtained in silanized reactors ranged from 5–10%, while the non-silanized reactor exhibited a standard deviation of 20%, indicating a lower reproducibility. This was most likely due to increased interactions between the thermally unstable precursor and the unprotected reactor walls in non-silanized reactors. Such interactions result in a longer residence time of the precursor on the reactor wall, leading to increased decomposition at the hot surface. The unpredictability of this residence time likely contributed to the observed

## 5 Results and Discussion

variability. Consequently, for all subsequent optimization experiments, the reactors were silanized on the day of the reaction.

To further reduce potential decomposition of the precursor at the reactor walls, the heating method was changed to microwave irradiation. Microwave heating creates an inverted temperature profile, with the hottest region in the center and the coldest at the walls, which should minimize precursor decomposition at the reactor walls.

Table 10: Investigation of microwave heating on the reaction.

No	t/min	m /mg	RCC
1	2	15	65 ± 22% (n = 3)
2	3	15	49 ± 7% (n = 2)
3	4	15	65 ± 17% (n = 14)

**1) [<sup>18</sup>F]F<sup>-</sup>**  
 elution with precursor solved in MeOH  
 evaporation of solvent  
**2) 110°C**  
 microwave irradiation <sup>18</sup>F  
 DMF

The results (Table 10) showed that microwave heating improves the RCCs compared to conventional heating in a metal block. However, for entries 1 and 3, the high variability persisted, suggesting that decomposition effects still occurred. It is likely that the decomposition primarily took place on the reactor walls, although it may also have occurred in solution. Nevertheless, the RCCs were generally much higher than those observed with conventional heating. This improvement may be attributed to the more uniform and rapid heating provided by microwave irradiation, as well as the colder reactor walls resulting from the inverted temperature profile.

Interestingly, a 3-minute microwave irradiation resulted in a significantly lower RCC (entry 2). This could be due to statistical effects in this highly variable reaction, as only two repetitions were performed.

Since microwave heating did not lead to the desired reduction in standard deviation, further experiments were conducted in an inductive heating reactor. In this system, the reactor is

uniformly heated by a heating mantle that is powered by an inductive coil. In addition, both temperature and pressure within the reactor are continuously monitored, allowing for the detection of any leaks in the reactor's septum.

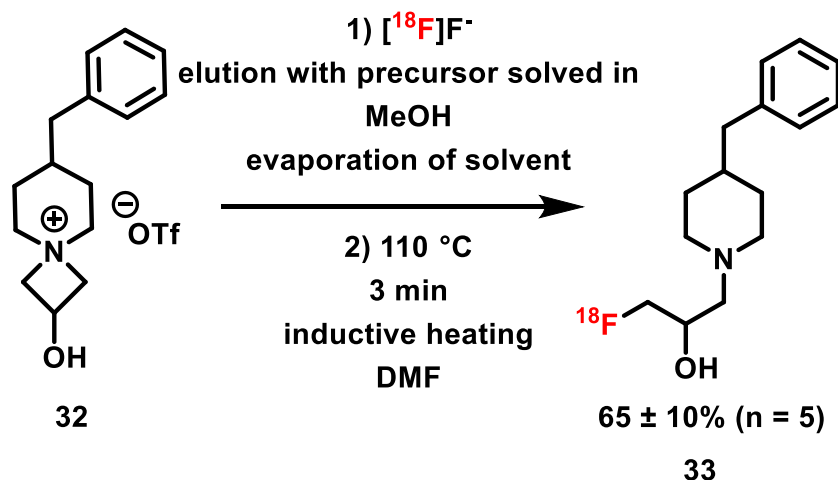


Figure 59: Results of the radiofluorination with an inductive heater.

As illustrated in Figure 59, inductive heating afforded RCCs similar to those obtained with microwave irradiation but with much lower standard deviation, making this method the most effective for ensuring high yields and reproducibility.

In summary, the optimal conditions for radiofluorination of 3-hydroxyazetidinium salts were as follows: heating in an inductive heater using a freshly silanized reactor for 3 minutes at 110 °C, resulting in a mean RCC of 65% with a standard deviation of 10%.

### 5.3.2 Preparation of Radiolabeled Prosthetic Groups for Click Labeling

Having established optimized reaction conditions for radiofluorination of the model compound, two precursors containing alkyne and azide functional groups were tested under these conditions to explore the feasibility of applying this method to radiopharmaceutical syntheses. These functional groups facilitate incorporation of the piperidine scaffold into pharmacophores via click chemistry, allowing for two different radiolabeling approaches – use of  $^{18}\text{F}$ -labeled 3-hydroxyazetidinium salts as a prosthetic group by performing the click reaction after radiofluorination, or synthesis of pharmacophore-bearing precursors by performing the click reaction prior to the radiofluorination.

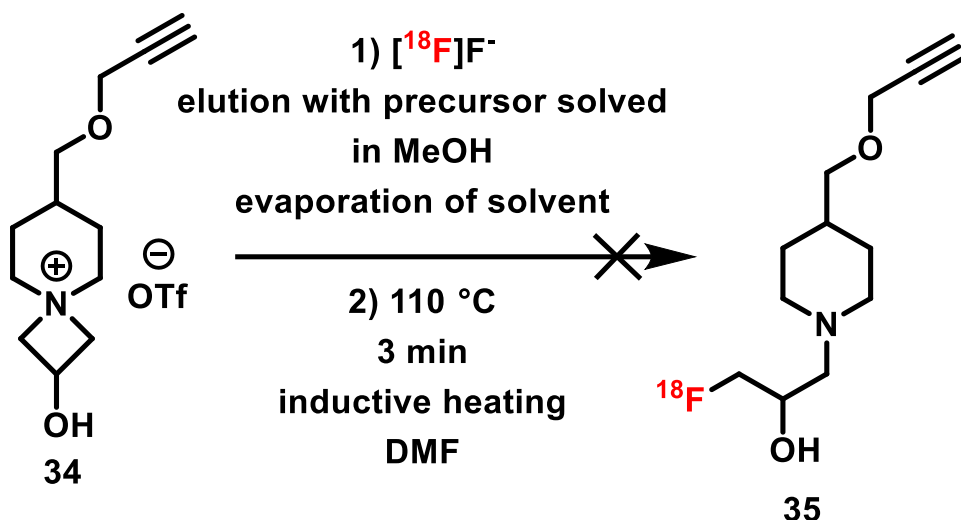


Figure 60: Radiofluorination attempt of alkyne-substituted 3-hydroxyazetidinium salt.

Radiofluorination of the alkyne-substituted 3-hydroxyazetidinium salt under optimized conditions yielded no radioactive product, suggesting insufficient stability of the precursor for the ring-opening reaction.

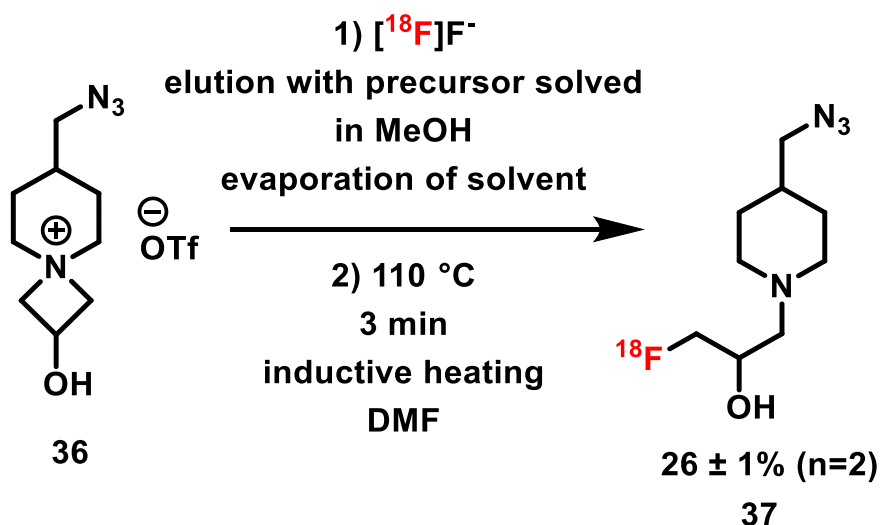


Figure 61: Radiofluorination of azide-substituted 3-hydroxyazetidinium salt.

In contrast, the azide-substituted 3-hydroxyazetidinium salt was successfully radiofluorinated with an RCC of 26%, thus confirming the feasibility of the method. However, the low conversion highlights a key disadvantage of 3-hydroxyazetidinium salts – their inherent instability under the harsh reaction conditions. This instability is likely to be exacerbated in more complex substrates with additional reactive sites, posing a significant challenge for their use as precursors in radiopharmaceutical applications. Due to these stability issues and the insufficient robustness of the reaction, this sub-project was not pursued further.

## 6 Summary and Outlook

This study explored cyclic ammonium salts as precursors for nucleophilic radiofluorination using the minimalist protocol. Specifically, DABCO and 3-hydroxyazetidinium salts were synthesized and evaluated as potential radiolabeling precursors.

The radiofluorination of aliphatic and aromatic DABCO salts under optimized conditions afforded good to very good radiochemical conversions. Likewise, model compounds incorporating an ethyl piperazine DABCO motif could be  $^{18}\text{F}$ -labeled with good to fair radiochemical conversions. However, translating these findings into practical applications proved challenging. Thus, although various strategies – including conjugation reactions, amino acid synthesis, and the incorporation of clickable groups – were investigated, none of these approaches led to the desired reactivity or efficient conjugation.

Direct radiofluorination of DABCO-bearing amino acids was unsuccessful, while radiofluorination of clickable model compounds was achieved. Unfortunately, subsequent click reactions did not proceed effectively for the aromatic DABCO-salt. Efforts to synthesize a DABCO-bearing PSMA ligand, DABCO-modified amino acids or linkers for amino acid conjugation were still unsuccessful.

The model 3-hydroxyazetidinium salt **32**, was successfully prepared. However, radiofluorination of this model compound yielded inconsistent radiochemical conversions. To overcome this issue, several reaction parameters—such as temperature, solvent, precursor loading, and heating method—were optimized. Especially under inductive heating conditions the desired radiofluorinated product was successfully prepared in RCCs up to  $65 \pm 10\%$ . Despite these efforts, radiofluorination of the alkyne-functionalized precursor was unsuccessful, while the azide-functionalized radiofluorinated product was successfully prepared in moderate yields of 26%. These suboptimal results led to discontinuation of the studies on 3-hydroxyazetidinium salts.

For the successful application of the developed radiofluorination method, efficient procedures for the preparation of highly substituted DABCO salts are to be developed. This would open the possibility for one step access to [ $^{18}\text{F}$ ]ethyl piperazyl substituted radiopharmaceuticals. Accordingly, the development of this synthetic procedure would present a promising direction for overcoming the limitations of this method and should therefore be an aim in future studies.

## 7 Experimental Part

### 7.1 Supporting Information of the Manuscript

#### Organic Synthesis Procedures

##### General Procedure A for the Synthesis of Aliphatic DABCO Salts

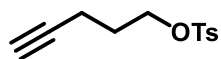
The corresponding bromide (1 equiv.) was treated with DABCO (1 equiv.) in THF and stirred at room temperature for 16 h. Afterwards the formed colorless precipitate was filtered off and washed with THF and Et<sub>2</sub>O to give the corresponding DABCO salts as colorless solids.

##### General Procedure B for the Synthesis of Iodonium Salts

The iodoarene is dissolved in DCM and the oxidation agent and the acid are added. Afterwards, the dummy ligand is added to the reaction mixture. The reaction mixture is stirred for 16 h. After the stirring time Et<sub>2</sub>O is added to the reaction. The resulting colorless precipitate is filtered off and washed with Et<sub>2</sub>O to give the analytically pure iodonium salts as colorless solids.

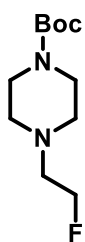
##### General Procedure C for the Synthesis of Aromatic DABCO Salts

Aromatic DABCO salts are synthesized according to a procedure from Bugaenko et al.<sup>[17]</sup> The corresponding iodonium salt (2 equiv.) is dissolved in acetonitrile (0.5 M). To the stirred solution DABCO (1 equiv.) is added in one portion and the reaction mixture is heated to 80 °C for 16 h. The solvent is removed under reduced pressure and the residue is stirred for 15 min with a mixture of Et<sub>2</sub>O and acetone (95:5). The formed solid is filtered off on a precooled frit and washed with cool Et<sub>2</sub>O. Afterwards the residue is washed under rapid stirring with a spatula with ice water (3x10 mL). The filtrate is then evaporated and dried by evaporation with toluene (2x15 mL) to give the target compound as colorless solid.

**Pent-4-yn-1-yl 4-methylbenzenesulfonate**

Pent-4-yn-1-yl 4-methylbenzenesulfonate was synthesized starting from pent-4-yn-1-ol (6 mmol, 0.5 g, 1 equiv.). Treatment with tosyl chloride (7.2 mmol, 1.36 g, 1.2 equiv.) and  $\text{NEt}_3$  (18 mmol, 1.8 g, 3 equiv.) in DCM (10 mL) gave the crude title compound after stirring for 16 h. The reaction mixture was washed with water and brine (2x15 mL) and dried with  $\text{Na}_2\text{SO}_4$ . The solvent was removed under reduced pressure and the resulting oil was used for later steps without further purification (4.41 mmol, 0.973 g, 69%). The analytical data are in accordance with the publicized data<sup>[39]</sup>.

$^1\text{H}$  NMR (400 MHz,  $\text{CDCl}_3$ )  $\delta$  = 7.81 – 7.76 (m, 2H), 7.34 (dd,  $J$  = 8.5, 0.6 Hz, 2H), 4.13 (t,  $J$  = 6.1 Hz, 2H), 2.44 (s, 3H), 2.25 (td,  $J$  = 6.9, 2.7 Hz, 2H), 1.89 – 1.81 (m, 3H).

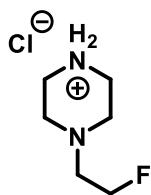
***tert*-Butyl 4-(2-fluoroethyl)piperazine-1-carboxylate**

*tert*-Butyl 4-(2-fluoroethyl)piperazine-1-carboxylate was synthesized starting from *tert*-butyl piperazine-1-carboxylate (1.6 mmol, 0.3 g, 1 equiv.). The start material was dissolved in MeCN (6 mL) and treated with 1-fluoro-2-iodoethane (1.92 mmol, 0.334 g, 1.2 equiv.) and  $\text{K}_2\text{CO}_3$  (2.4 mmol, 0.334 g, 1.5 equiv.) the mixture was stirred at 75 C for 16 h. The solid was filtered off and the solvent removed under reduced pressure giving the title product as a colorless solid (0.290 g, 78%). The analytical data are in accordance with the publicized data<sup>[40]</sup>.

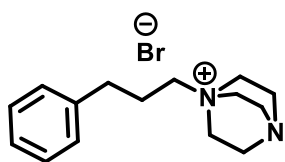
$^1\text{H}$  NMR (400 MHz,  $\text{CDCl}_3$ )  $\delta$  = 4.67 – 4.47 (m, 2H), 3.52 – 3.40 (m, 4H), 2.82 – 2.63 (m, 2H), 2.54 – 2.44 (m, 4H), 1.45 (s, 9H).

$^{13}\text{C}$  NMR (101 MHz,  $\text{CDCl}_3$ )  $\delta$  = 154.69, 81.80 (d,  $J$  = 167.8 Hz), 79.69, 77.36, 77.04, 76.73, 58.23 (d,  $J$  = 19.8 Hz), 53.26, 28.41.

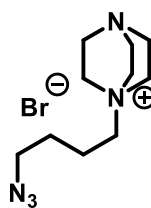
$^{19}\text{F}$  NMR (376 MHz,  $\text{CDCl}_3$ )  $\delta$  = -218.18.

**1-(2-Fluoroethyl)piperazin-1-ium chloride**

1-(2-Fluoroethyl)piperazin-1-ium chloride was synthesized by treating *tert*-butyl 4-(2-fluoroethyl)piperazine-1-carboxylate (0.43 mmol, 100 mg, 1 equiv.) with 1 M HCl in dioxan. After stirring for 2 h the formed precipitate was filtered off and used without further purification (0.41 mmol, 70 mg, 96%). The compound is already described<sup>[41]</sup>. The analytical data are in accordance with the published data.

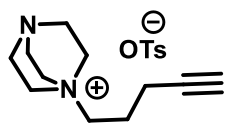
**1-(3-Phenylpropyl)-1,4-diazabicyclo[2.2.2]octan-1-ium 4-methylbenzenesulfonate (1a)**

1-(3-Phenylpropyl)-1,4-diazabicyclo[2.2.2]octan-1-ium 4-methylbenzenesulfonate was synthesized by treatment of (3-bromopropyl)benzene (2.5 mmol, 0.500 g, 1 equiv.) with DABCO (2.5 mmol, 0.281 g, 1 equiv.) in THF. After stirring for 16 h the formed colorless precipitate was filtered off and washed with THF (5 mL) and Et<sub>2</sub>O (5 mL) to give the title compound as colorless solid (1.9 mmol, 0.764 g, 76%). The compound is already described in the literature<sup>[34]</sup>. The analytical data are in accordance with the published data.

**1-(4-Azidobutyl)-1,4-diazabicyclo[2.2.2]octan-1-ium bromide (1b)**

To synthesize 1-(4-azidobutyl)-1,4-diazabicyclo[2.2.2]octan-1-ium bromide, 1,4-dibromobutane (2.3 mmol, 0.500 g, 1 equiv.) was treated with sodium azide (2.3 mmol, 151 mg, 1 equiv.) in MeCN (10 mL). The resulting reaction mixture was stirred at room temperature for 3 h. DCM (10 mL) was added to the reaction mixture and the mixture was washed with water (20 mL). The organic phase was dried with Na<sub>2</sub>SO<sub>4</sub> and the solvent removed under reduced pressure. The resulting oil was given to DABCO (2.3 mmol, 259 mg, 1 equiv.) in THF (10 mL) and stirred at room temperature for 48 h. The formed colorless precipitate was filtered off and washed with THF (5 mL) and Et<sub>2</sub>O (5 mL) to give the title compound as colorless solid (1.25 mmol, 363 mg, 54%) which was used without further purification. The compound is already described in the literature<sup>[43]</sup>. The analytical data are in accordance with the published data.

**1-(Pent-4-yn-1-yl)-1,4-diazabicyclo[2.2.2]octan-1-ium 4-methylbenzenesulfonate (1c)**



1-(Pent-4-yn-1-yl)-1,4-diazabicyclo[2.2.2]octan-1-ium

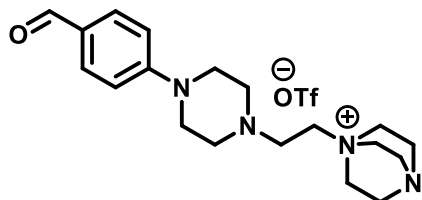
4-

methylbenzenesulfonate was synthesized by treatment of pent-4-yn-1-yl 4-methylbenzenesulfonate (3.8 mmol, 0.900 g, 1 equiv.) with DABCO (3.8 mmol, 0.423 g, 1 equiv.) in THF (10 mL). After stirring the reaction for 36 h the formed colorless solid is filtered off and washed with THF (5 mL) and Et<sub>2</sub>O (5 mL) to give the title compound as colorless solid (2.8 mmol, 987 mg, 74%).

<sup>1</sup>H NMR (400 MHz, CD<sub>3</sub>OD)  $\delta$  = 7.78 – 7.63 (m, 2H), 7.26 (dd,  $J$  = 8.5, 0.6 Hz, 2H), 3.43 – 3.34 (m, 8H), 3.21 (t,  $J$  = 3.8 Hz, 6H), 2.44 (t,  $J$  = 2.7 Hz, 1H), 2.36 (td,  $J$  = 6.8, 2.7 Hz, 2H), 2.00 (dt,  $J$  = 18.8, 6.9 Hz, 2H).

<sup>13</sup>C NMR (101 MHz, CD<sub>3</sub>OD)  $\delta$  = 124.31, 118.80, 84.27, 82.97, 68.88, 54.34, 53.30, 52.07, 51.16, 44.66.

**1-(2-(4-(4-Formylphenyl)piperazin-1-yl)ethyl)-1,4-diazabicyclo[2.2.2]octan-1-ium trifluoromethanesulfonate (4a)**



1-(2-(4-(4-Formylphenyl)piperazin-1-yl)ethyl)-1,4-

diazabicyclo[2.2.2]octan-1-ium trifluoromethanesulfonate

was synthesized starting from 4-formylphenyl triflate (1 mmol, 0.254 g, 1 equiv.). It was heated in THF (2 mL) with DABCO (1 mmol, 112 mg, 1 equiv.) in an inductive heater for 16 h at 120 °C. The resulting reaction mixture was filtered and the solid was washed with THF (5 mL) and Et<sub>2</sub>O (10 mL). The solid was taken into MeOH (1 mL) and recrystallized with Et<sub>2</sub>O (5 mL) to give the title compound as a colorless solid (0.7 mmol, 0.343 g, 44%).

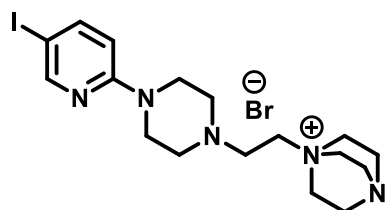
<sup>1</sup>H NMR (400 MHz, CD<sub>3</sub>OD)  $\delta$  = 9.72 (s, 1H), 7.87 – 7.73 (m, 2H), 7.13 – 6.91 (m, 2H), 3.54 (dd,  $J$  = 13.1, 5.2 Hz, 6H), 3.51 – 3.46 (m, 6H), 3.26 – 3.20 (m, 6H), 2.92 (t,  $J$  = 5.8 Hz, 2H), 2.75 – 2.66 (m, 4H).

<sup>13</sup>C NMR (101 MHz, CD<sub>3</sub>OD)  $\delta$  = 191.09, 155.41, 131.64, 126.85, 113.28, 60.26, 54.80, 52.75, 50.68, 46.41, 44.69.

<sup>19</sup>F NMR (376 MHz, CD<sub>3</sub>OD)  $\delta$  = -80.10.

HRMS ( $m/z$ ): [M]<sup>+</sup> calcd. for C<sub>19</sub>H<sub>29</sub>N<sub>4</sub>O, 329.23359; found, 329.23360.

**1-(2-(4-(5-Iodopyridin-2-yl)piperazin-1-yl)ethyl)-1,4-diazabicyclo[2.2.2]octan-1-ium bromide (4b)**



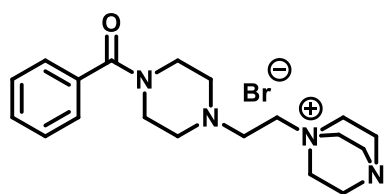
1-(2-(4-(5-Iodopyridin-2-yl)piperazin-1-yl)ethyl)-1,4-diazabicyclo[2.2.2]octan-1-ium bromide was synthesized from 2-bromo-5-iodopyridine (1 mmol, 0.284 g, 1 equiv.). The start material was treated with DABCO (2 mmol, 0.224 g, 2 equiv.) in THF (2 mL) and heated inductively for 12 h at 120 °C. The formed solid was filtered off and the residue washed with THF (5 mL) to give the title compound as colorless solid. (0.79 mmol, 0.400 g, 79%)

$^1\text{H}$  NMR (400 MHz,  $\text{CD}_3\text{OD}$ )  $\delta$  = 8.26 (dd,  $J$  = 2.3, 0.6 Hz, 1H), 7.77 (dd,  $J$  = 9.0, 2.4 Hz, 1H), 6.71 (d,  $J$  = 0.5 Hz, 1H), 3.60 – 3.51 (m, 10H), 3.47 (dd,  $J$  = 15.4, 9.4 Hz, 2H), 3.27 – 3.18 (m, 6H), 2.90 (t,  $J$  = 5.8 Hz, 2H), 2.71 – 2.62 (m, 4H).

$^{13}\text{C}$  NMR (101 MHz,  $\text{CD}_3\text{OD}$ )  $\delta$  = 151.93, 151.36, 142.39, 121.91, 114.14, 58.68, 51.43, 51.38, 49.14, 44.11, 43.72.

HRMS ( $m/z$ ):  $[\text{M}]^+$  calcd. for  $\text{C}_{17}\text{H}_{27}\text{N}_5\text{I}$ , 428.13057; found, 428.13073.

**1-(2-(4-Benzoylpiperazin-1-yl)ethyl)-1,4-diazabicyclo[2.2.2]octan-1-ium bromide (4c)**



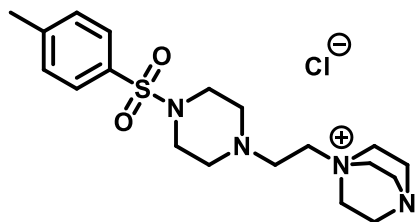
1-(2-(4-Benzoylpiperazin-1-yl)ethyl)-1,4-diazabicyclo[2.2.2]octan-1-ium bromide was synthesized by treating benzoyl bromide (3.5 mmol, 0.650 g, 1 equiv.) with DABCO (3.5 mmol, 0.394 g, 1 equiv.) in THF (3 mL) in an inductive heater at 120 °C for 16 h. The colorless precipitate was filtered off and washed with THF (5 mL) and  $\text{Et}_2\text{O}$  (5 mL) to give the title compound as colorless solid (1.5 mmol, 0.617 g, 43%).

$^1\text{H}$  NMR (400 MHz,  $\text{CD}_3\text{OD}$ )  $\delta$  = 7.54 – 7.41 (m, 5H), 3.78 (d,  $J$  = 28.8 Hz, 2H), 3.63 – 3.54 (m, 6H), 3.54 – 3.48 (m, 3H), 3.33 (dt,  $J$  = 3.3, 1.6 Hz, 2H), 3.21 (d,  $J$  = 8.4 Hz, 6H), 2.92 (t,  $J$  = 5.6 Hz, 2H), 2.62 (d,  $J$  = 44.5 Hz, 4H).

$^{13}\text{C}$  NMR (101 MHz,  $\text{CD}_3\text{OD}$ )  $\delta$  171.05, 135.35, 129.80, 128.40, 126.64, 60.24, 52.78, 52.15, 50.59, 44.73, 44.21.

HRMS ( $m/z$ ):  $[\text{M}]^+$  calcd. for  $\text{C}_{19}\text{H}_{29}\text{N}_4\text{O}$ , 329.23359; found, 329.23342.

**1-(2-(4-Tosylpiperazin-1-yl)ethyl)-1,4-diazabicyclo[2.2.2]octan-1-ium chloride (4d)**



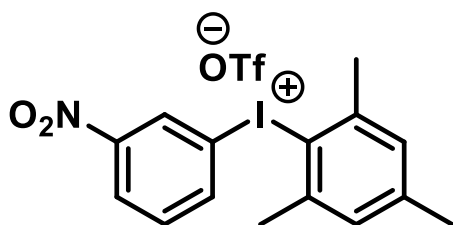
1-(2-(4-Tosylpiperazin-1-yl)ethyl)-1,4-diazabicyclo[2.2.2]octan-1-ium chloride was synthesized from 4-toluenesulfonyl chloride (1.5 mmol, 0.284 g, 1 equiv.). The start material was treated with DABCO (3 mmol, 0.224 g, 2 equiv.) in THF (2 mL) and heated inductively for 12 h at 120 °C. The formed solid was filtered off and the residue washed with THF to give the title compound as colorless solid. (1.2 mmol, 0.400 g, 79%)

$^1\text{H}$  NMR (400 MHz,  $(\text{CD}_3)_2\text{SO}$ )  $\delta$  = 7.64 (d,  $J$  = 8.2 Hz, 2H), 7.48 (dd,  $J$  = 7.8, 5.3 Hz, 2H), 3.32 (dd,  $J$  = 15.2, 5.8 Hz, 6H), 2.96 (dd,  $J$  = 15.5, 8.4 Hz, 6H), 2.89 (s, 4H), 2.71 (dd,  $J$  = 14.7, 9.1 Hz, 2H), 2.57 – 2.48 (m, 6H), 2.42 (s, 3H).

$^{13}\text{C}$  NMR (101 MHz,  $(\text{CD}_3)_2\text{SO}$ )  $\delta$  = 144.19, 132.61, 130.39, 128.06, 59.88, 52.39, 51.85, 50.24, 46.16, 45.13, 44.41.

m/z:  $[\text{M}^+]$  calcd. for  $\text{C}_{19}\text{H}_{31}\text{N}_4\text{O}_2\text{S}$ , 379.22; found, 379.26.

**Mesityl(3-nitrophenyl)iodonium trifluoromethanesulfonate (6b)**

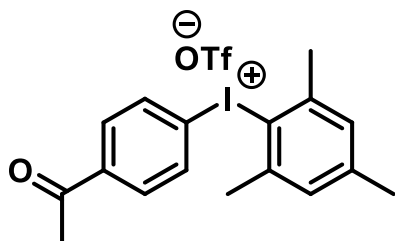


Mesityl(3-nitrophenyl)iodonium trifluoromethanesulfonate was synthesized according to General Procedure **B** from 1-iodo-3-nitrobenzene (16 mmol, 4 g, 1 equiv.), Oxone<sup>®</sup> (64 mmol, 9.779 g, 4 equiv.), mesitylene (19.2 mmol, 2.317 g, 1.2 equiv.) and trifluoromethanesulfonic acid (37 mmol, 5.545 g, 2.3 equiv.) giving the target compound as a yellow solid (7 mmol, 3.65 g, 44%). The compound is already described in the literature<sup>[17]</sup>.

$^1\text{H}$  NMR (400 MHz,  $\text{CD}_3\text{OD}$ )  $\delta$  = 8.77 (t,  $J$  = 1.9 Hz, 1H), 8.49 (ddd,  $J$  = 8.3, 2.1, 0.9 Hz, 1H), 8.19 (ddd,  $J$  = 8.1, 1.8, 0.9 Hz, 1H), 7.77 (t,  $J$  = 8.2 Hz, 1H), 7.31 (d,  $J$  = 0.5 Hz, 2H), 2.70 (s, 6H), 2.40 (s, 3H).

$^{13}\text{C}$  NMR (101 MHz,  $\text{CD}_3\text{OD}$ )  $\delta$  = 145.12, 142.34, 138.88, 132.76, 130.20, 128.31, 126.42, 121.08, 112.24, 25.68, 19.67.

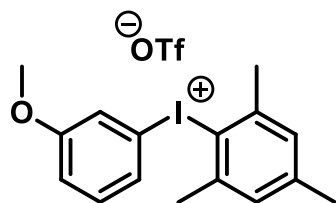
$^{19}\text{F}$  NMR (376 MHz,  $\text{CD}_3\text{OD}$ )  $\delta$  = -80.04.

**(4-Acetylphenyl)(mesityl)iodonium trifluoromethanesulfonate (6c)**

(4-Acetylphenyl)(mesityl)iodonium trifluoromethanesulfonate was synthesized according to General Procedure **B** from 1-(4-iodophenyl)ethan-1-one (8.1 mmol, 2 g, 1 equiv.), Oxone<sup>®</sup> (32.3 mmol, 4.948 g, 4 equiv.), mesitylene (9.8 mmol, 1.17 g, 1.2 equiv.) and trifluoromethanesulfonic acid (18.7 mmol, 2.806 g, 2.3 equiv.) giving the target compound as a colorless solid (3.9 mmol, 2 g, 48%). The compound is already described in the literature<sup>[42]</sup>.

<sup>1</sup>H NMR (400 MHz, CD<sub>3</sub>OD)  $\delta$  = 8.46 (t,  $J$  = 1.7 Hz, 1H), 8.26 – 8.22 (m, 1H), 8.07 (ddd,  $J$  = 8.1, 1.9, 0.9 Hz, 1H), 7.66 (t,  $J$  = 8.0 Hz, 1H), 7.28 (s, 2H), 2.69 (s, 6H), 2.62 (s, 3H), 2.39 (s, 3H).

<sup>19</sup>F NMR (376 MHz, CD<sub>3</sub>OD)  $\delta$  = -79.96.

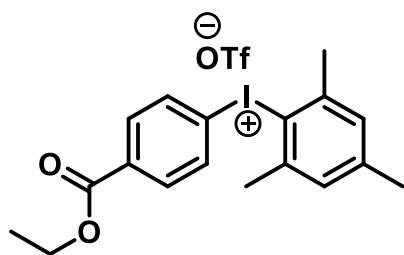
**Mesityl(3-methoxyphenyl)iodonium trifluoromethanesulfonate (6d)**

Mesityl(3-methoxyphenyl)iodonium trifluoromethanesulfonate was synthesized according to General Procedure **B** from 1-iodo-3-methoxybenzene (8.55 mmol, 2 g, 1 equiv.), Oxone<sup>®</sup> (34 mmol, 5.205 g, 4 equiv.), mesitylene (10.2 mmol, 1.233 g, 1.2 equiv.) and trifluoromethanesulfonic acid (34 mmol, 5.198 g, 4 equiv.) giving the target compound as a colorless solid (6.1 mmol, 3.049 g, 71%). The compound is already described in the literature<sup>[17]</sup>.

<sup>1</sup>H NMR (400 MHz, CD<sub>3</sub>OD)  $\delta$  = 7.46 – 7.35 (m, 3H), 7.31 – 7.16 (m, 3H), 3.83 (s, 3H), 2.68 (s, 6H), 2.39 (s, 3H).

<sup>13</sup>C NMR (101 MHz, CD<sub>3</sub>OD)  $\delta$  = 161.61, 144.57, 142.19, 132.52, 129.95, 125.21, 120.74, 119.20, 117.42, 112.35, 55.06, 25.66, 19.64.

<sup>19</sup>F NMR (376 MHz, CD<sub>3</sub>OD)  $\delta$  = -80.00.

**(4-(Ethoxycarbonyl)phenyl)(mesityl)iodonium trifluoromethanesulfonate****(6e)**

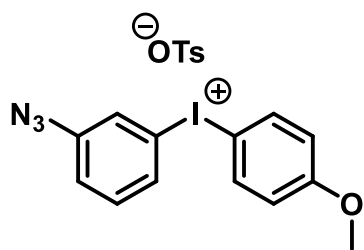
(4-(Ethoxycarbonyl)phenyl)(mesityl)iodonium

trifluoromethanesulfonate was synthesized according to General Procedure **B** from ethyl 4-iodobenzoate (7.2 mmol, 2 g, 1 equiv.), mesitylene (8.6 mmol, 1.045 g, 1.2 equiv.) and trifluoromethanesulfonic acid (16.4 mmol, 2.5 g, 2.3 equiv.)

giving the target compound as a colorless solid (4.5 mmol, 2.452 g, 63%). The compound is already described in the literature<sup>[17]</sup>.

<sup>1</sup>H NMR (400 MHz, CD<sub>3</sub>OD)  $\delta$  = 8.05 (dd,  $J$  = 33.4, 8.4 Hz, 4H), 7.29 (s, 2H), 4.05 – 3.92 (m, 2H), 3.47 – 3.24 (m, 3H), 2.68 (s, 6H), 2.39 (s, 3H).

<sup>13</sup>C NMR (101 MHz, CD<sub>3</sub>OD)  $\delta$  = 144.81, 142.26, 133.83, 133.43, 132.27, 131.29, 130.09, 121.40, 117.23, 51.82, 45.22, 25.67, 19.65.

**(3-Azidophenyl)(4-methoxyphenyl)iodonium 4-methylbenzenesulfonate****(6f)**

(3-Azidophenyl)(4-methoxyphenyl)iodonium

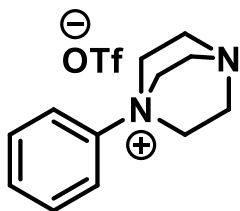
4-

methylbenzenesulfonate was synthesized according to General Procedure **B** from 3-azido iodobenzene (7.2 mmol, 0.768 g, 1 equiv.), *m*-CPBA (7.92 mmol, 0.595 g, 1.1 equiv.), anisole (36 mmol, 3.888 g, 5 equiv., 1.7 mL) and *p*-

toluenesulfonic acid (7.9 mmol, 0.414 mg, 1.1 equiv.) giving the target compound as a colorless solid (2.9 mmol, 0.678 g, 41%). The compound is already described in the literature<sup>[21]</sup>.

<sup>1</sup>H NMR (400 MHz, CD<sub>3</sub>OD)  $\delta$  = 8.12 (d,  $J$  = 9.2 Hz, 2H), 7.87 (d,  $J$  = 7.9 Hz, 2H), 7.70 (d,  $J$  = 8.2 Hz, 2H), 7.51 (t,  $J$  = 8.0 Hz, 1H), 7.36 (d,  $J$  = 5.2 Hz, 1H), 7.23 (d,  $J$  = 8.5 Hz, 2H), 7.08 (d,  $J$  = 9.2 Hz, 2H), 3.86 (s, 3H), 2.38 (s, 3H).

<sup>13</sup>C NMR (101 MHz, CD<sub>3</sub>OD)  $\delta$  = 163.24, 143.25, 140.24, 137.34, 132.58, 130.47, 128.40, 125.56, 124.79, 122.49, 117.51, 115.36, 103.20, 54.98, 19.91.

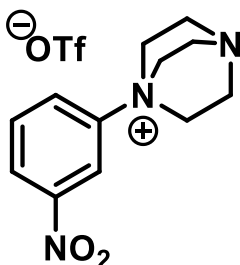
**1-Phenyl-1,4-diazabicyclo[2.2.2]octan-1-ium trifluoromethanesulfonate****(7a)**

1-Phenyl-1,4-diazabicyclo[2.2.2]octan-1-ium trifluoromethanesulfonate was synthesized according to General Procedure **C** from diphenyliodonium trifluoromethanesulfonate (4 mmol, 1.3 g, 2 equiv.) and DABCO (2 mmol, 0.229 g, 1 equiv.) in MeCN (20 mL) to give the title compound as colorless solid (1.26 mmol, 435 mg, 63%). The compound is already described in the literature<sup>[17]</sup>.

<sup>1</sup>H NMR (400 MHz, CD<sub>3</sub>OD)  $\delta$  = 7.93 – 7.83 (m, 2H), 7.73 – 7.61 (m, 3H), 3.99 – 3.87 (m, 6H), 3.39 (dd,  $J$  = 12.5, 5.1 Hz, 6H).

<sup>13</sup>C NMR (101 MHz, CD<sub>3</sub>OD)  $\delta$  = 130.41, 120.66, 55.57, 45.26.

<sup>19</sup>F NMR (376 MHz, CD<sub>3</sub>OD)  $\delta$  = -80.10.

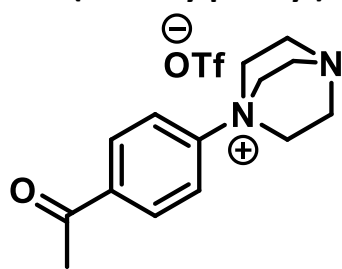
**1-(3-Nitrophenyl)-1,4-diazabicyclo[2.2.2]octan-1-ium****trifluoromethanesulfonate (7b)**

1-(3-Nitrophenyl)-1,4-diazabicyclo[2.2.2]octan-1-ium trifluoromethanesulfonate was synthesized according to General Procedure **C** from mesityl(3-nitrophenyl)iodonium trifluoromethanesulfonate (2.3 mmol, 1.2 g, 2 equiv.) and DABCO (1.15 mmol, 130 mg, 1 equiv.) in MeCN (12 mL) to give the title compound as yellow solid (0.45 mmol, 173 mg, 39%). The compound is already described in the literature<sup>[17]</sup>.

<sup>1</sup>H NMR (400 MHz, CD<sub>3</sub>OD)  $\delta$  = 8.78 (s, 1H), 8.51 (d,  $J$  = 8.1 Hz, 1H), 8.35 (dd,  $J$  = 8.5, 2.5 Hz, 1H), 7.98 (t,  $J$  = 8.4 Hz, 1H), 4.08 – 3.99 (m, 6H), 3.48 – 3.39 (m, 6H).

<sup>13</sup>C NMR (101 MHz, CD<sub>3</sub>OD)  $\delta$  = 131.86, 127.19, 125.20, 116.99, 55.92, 45.21.

<sup>19</sup>F NMR (376 MHz, CD<sub>3</sub>OD)  $\delta$  = -80.06.

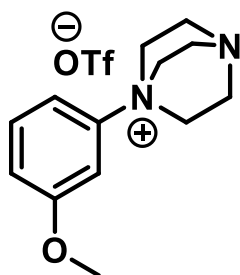
**1-(4-Acetylphenyl)-1,4-diazabicyclo[2.2.2]octan-1-ium****trifluoromethanesulfonate (7c)**

1-(4-Acetylphenyl)-1,4-diazabicyclo[2.2.2]octan-1-ium trifluoromethanesulfonate was synthesized according to General Procedure C from (4-acetylphenyl)(mesityl)iodonium trifluoromethanesulfonate (2 mmol, 1 g, 2 equiv.) and DABCO (1 mmol, 109 mg, 1 equiv.) in MeCN (10 mL) to give the title compound as colorless solid (0.43 mmol, 159 mg, 43%).

$^1\text{H}$  NMR (400 MHz,  $\text{CD}_3\text{OD}$ )  $\delta$  = 8.40 (dd,  $J$  = 2.7, 1.3 Hz, 1H), 8.27 – 8.23 (m, 1H), 8.14 (ddd,  $J$  = 8.5, 2.8, 0.7 Hz, 1H), 7.87 – 7.82 (m, 1H), 4.03 – 3.95 (m, 6H), 3.50 – 3.38 (m, 6H), 2.71 (s, 3H).

$^{13}\text{C}$  NMR (101 MHz,  $\text{CD}_3\text{OD}$ )  $\delta$  196.76, 131.05, 130.30, 125.09, 120.27, 55.66, 45.25, 25.49.

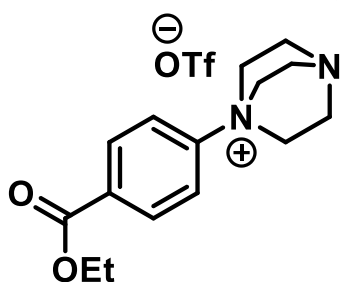
$^{19}\text{F}$  NMR (376 MHz,  $\text{CD}_3\text{OD}$ )  $\delta$  = -80.02.

**1-(3-Methoxyphenyl)-1,4-diazabicyclo[2.2.2]octan-1-ium****trifluoromethanesulfonate (7d)**

1-(3-Methoxyphenyl)-1,4-diazabicyclo[2.2.2]octan-1-ium trifluoromethanesulfonate was synthesized according to General Procedure C from mesityl(3-methoxyphenyl)iodonium trifluoromethanesulfonate (2.4 mmol, 1.3 g, 2 equiv.) and DABCO (1.2 mmol, 145 mg, 1 equiv.) in MeCN (12 mL) to give the title compound as colorless solid (0.6 mmol, 243 mg, 51%). The compound is already described in the literature<sup>[17]</sup>.

$^1\text{H}$  NMR (400 MHz,  $\text{CD}_3\text{OD}$ )  $\delta$  = 7.63 – 7.54 (m, 1H), 7.44 – 7.35 (m, 2H), 7.25 – 7.16 (m, 1H), 3.96 – 3.84 (m, 9H), 3.42 – 3.35 (m, 6H).

$^{19}\text{F}$  NMR (376 MHz,  $\text{CD}_3\text{OD}$ )  $\delta$  = -80.10.

**1-(4-(Ethoxycarbonyl)phenyl)-1,4-diazabicyclo[2.2.2]octan-1-ium****trifluoromethanesulfonate (7e)**

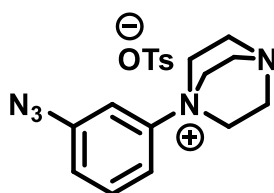
1-(4-(Ethoxycarbonyl)phenyl)-1,4-diazabicyclo[2.2.2]octan-1-ium trifluoromethanesulfonate was synthesized according to General Procedure C from (4-(ethoxycarbonyl)phenyl)(mesityl)iodonium

trifluoromethanesulfonate (2.8 mmol, 1.5 g, 2 equiv.) and DABCO (1.4 mmol, 154 mg, 1 equiv.) in MeCN (14 mL) to give the title compound as colorless solid (0.47 mmol, 187 mg, 33%). The compound is already described in the literature<sup>[17]</sup>.

<sup>1</sup>H NMR (400 MHz, CD<sub>3</sub>OD)  $\delta$  = 8.32 – 8.26 (m, 2H), 8.04 – 7.99 (m, 2H), 4.44 (q,  $J$  = 7.1 Hz, 2H), 4.00 – 3.93 (m, 6H), 3.44 – 3.38 (m, 6H), 1.43 (t,  $J$  = 7.1 Hz, 3H).

<sup>13</sup>C NMR (101 MHz, CD<sub>3</sub>OD)  $\delta$  = 131.24, 121.32, 61.53, 55.68, 45.23, 13.09.

<sup>19</sup>F NMR (376 MHz, CD<sub>3</sub>OD)  $\delta$  = -80.09.

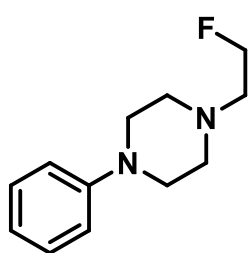
**1-(3-Azidophenyl)-1,4-diazabicyclo[2.2.2]octan-1-ium 4-****methylbenzenesulfonate (7f)**

1-(3-Azidophenyl)-1,4-diazabicyclo[2.2.2]octan-1-ium 4-methylbenzenesulfonate was synthesized according to General

Procedure C from ((3-azidophenyl)(4-methoxyphenyl)iodonium 4-methylbenzenesulfonate (1 mmol, 600 mg, 2 equiv.) and DABCO (0.5 mmol 1 equiv., 64 mg) in MeCN (5 mL) and giving a the title compound as a colorless solid (0.1 mmol, 46 mg, 20%).

<sup>1</sup>H NMR (400 MHz, CD<sub>3</sub>OD)  $\delta$  = 7.51 – 6.93 (m, 5H), 3.40 – 3.34 (m, 6H), 3.30 – 3.25 (m, 2H), 3.23 – 3.16 (m, 6H), 2.74 (t,  $J$  = 7.5 Hz, 2H), 2.13 (ddd,  $J$  = 15.9, 11.7, 5.4 Hz, 2H).

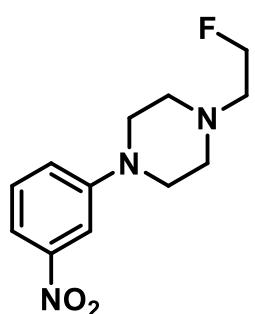
<sup>13</sup>C NMR (101 MHz, CD<sub>3</sub>OD)  $\delta$  = 140.31, 131.68, 128.43, 125.55, 120.68, 116.82, 112.30, 55.67, 44.20, 19.89.

**1-(2-Fluoroethyl)-4-phenylpiperazine (8a)**

1-(2-Fluoroethyl)-4-phenylpiperazine was synthesized by treatment of phenylpiperazine (0.54 mmol, 100 mg, 1 equiv.) with 1-fluoro-2-iodoethane (0.64 mmol, 112 mg, 1.2 equiv.) and  $K_2CO_3$  (0.8 mmol, 110 mg, 1.5 equiv.) in MeCN (3 mL). The reaction mixture was stirred for 16 h at room temperature. After completion the mixture was diluted with DCM and filtered. The solvent was removed under reduced pressure to give the crude product which was purified by column chromatography (30:70 cyclohexane:EtOAc to 30:70 MeOH:DCM) to give the title compound as colorless oil (0.26 mmol, 54 mg, 48%). The compound is already described in the literature<sup>[44]</sup>.

$^1H$  NMR (400 MHz,  $CD_3OD$ )  $\delta$  = 7.29 – 7.22 (m, 2H), 7.00 – 6.96 (m, 2H), 6.86 (t,  $J$  = 7.3 Hz, 1H), 4.73 – 4.68 (m, 1H), 4.61 – 4.56 (m, 1H), 3.25 – 3.20 (m, 4H), 2.89 – 2.84 (m, 1H), 2.82 – 2.77 (m, 5H).

$^{13}C$  NMR (101 MHz,  $CD_3OD$ )  $\delta$  = 151.26, 128.66, 119.80, 116.10, 81.18 (d,  $J$  = 166.4 Hz), 57.86 (d,  $J$  = 19.7 Hz), 53.17, 48.79.

**1-(2-Fluoroethyl)-4-(3-nitrophenyl)piperazine (8b)**

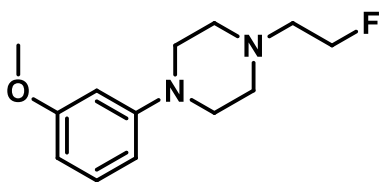
1-(2-Fluoroethyl)-4-(3-nitrophenyl)piperazine was synthesized by treatment of 3-fluoronitrobenzene (2.3 mmol, 322 mg, 1 equiv.) with fluoroethylpiperazine (2.3 mmol, 375 mg, 1 equiv.) in DMSO (2 mL) with  $K_2CO_3$  (8.9 mmol, 946 mg, 3 equiv.) as a base. The reaction mixture was stirred for 12 h at 110 °C in an Anton Parr Monowave 50 inductive heater. Afterwards, the mixture was extracted with DCM the organic phase separated and dried with  $Na_2SO_4$ . The solvent was removed under reduced pressure and the crude product purified by column chromatography (30:70 cyclohexane:EtOAc to 30:70 MeOH:DCM) to give the title compound as colorless oil (0.43 mmol, 110 mg, 19%).

$^1H$  NMR (400 MHz,  $CD_3OD$ )  $\delta$  = 7.76 (t,  $J$  = 2.3 Hz, 1H), 7.66 (ddd,  $J$  = 8.0, 2.1, 0.9 Hz, 1H), 7.51 – 7.42 (m, 1H), 7.36 (ddd,  $J$  = 8.4, 2.5, 0.8 Hz, 1H), 4.74 – 4.67 (m, 1H), 4.62 – 4.56 (m, 1H), 3.37 – 3.33 (m, 4H), 2.84 (dd,  $J$  = 12.0, 7.2 Hz, 1H), 2.80 – 2.74 (m, 5H).

$^{13}C$  NMR (101 MHz,  $CD_3OD$ )  $\delta$  151.95, 129.58, 121.08, 113.10, 108.95, 81.81(d,  $J$  = 166.4 Hz), 57.79 (d,  $J$  = 19.7 Hz), 52.88, 47.65.

$^{19}F$  NMR (376 MHz,  $CD_3OD$ )  $\delta$  = -220.24.

HRMS (m/z):  $[M+H]^+$  calcd. for  $C_{12}H_{16}N_3O_2F$ , 253.12211; found, 253.1219.

**1-(2-Fluoroethyl)-4-(3-methoxyphenyl)piperazine (8c)**

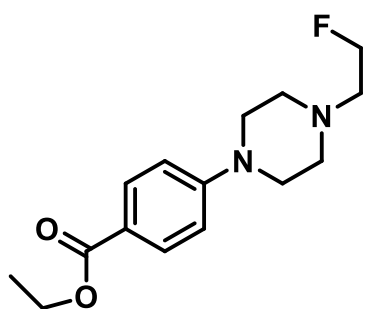
1-(2-Fluoroethyl)-4-(3-methoxyphenyl)piperazine was synthesized by treatment of 1-(3-methoxyphenyl)piperazine (0.6 mmol, 84 mg, 1 equiv.) with 1-fluoro-2-iodo-ethane (0.6 mmol., 100 mg, 1 equiv.) and  $K_2CO_3$  (1.7 mmol, 0.230 g, 3 equiv.) in MeCN (3 mL). The reaction mixture was stirred for 16 h at room temperature. After completion the mixture was diluted with DCM (5 mL) and filtered. The solvent was removed under reduced pressure to give the crude product which was purified by column chromatography (30:70 cyclohexane:EtOAc to 30:70 MeOH:DCM) to give the title compound as colorless oil (0.2 mmol, 52 mg, 36%).

$^1H$  NMR (400 MHz,  $CD_3OD$ )  $\delta$  = 7.15 (t,  $J$  = 8.2 Hz, 1H), 6.63 – 6.54 (m, 1H), 6.51 (t,  $J$  = 2.3 Hz, 1H), 6.47 – 6.42 (m, 1H), 4.76 – 4.63 (m, 1H), 4.60 – 4.51 (m, 1H), 3.26 – 3.15 (m, 4H), 2.83 – 2.79 (m, 1H), 2.72 (dd,  $J$  = 10.0, 5.3 Hz, 5H).

$^{13}C$  NMR (101 MHz,  $CD_3OD$ )  $\delta$  = 152.60, 129.36, 108.70, 104.73, 102.32, 81.19 (d,  $J$  = 166.4 Hz), 57.86 (d,  $J$  = 19.7 Hz), 54.17, 53.15, 48.65.

$^{19}F$  NMR (376 MHz,  $CD_3OD$ )  $\delta$  = -220.08.

HRMS (m/z):  $[M+H]^+$  calcd. for  $C_{13}H_{19}N_2OF$ , 238.14759; found, 238.1474.

**Ethyl 4-(4-(2-fluoroethyl)piperazin-1-yl)benzoate (8d)**

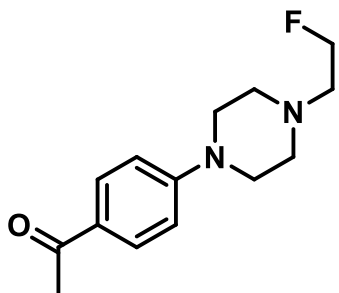
Ethyl 4-(4-(2-fluoroethyl)piperazin-1-yl)benzoate was synthesized by treatment of ethyl 4-fluorobenzoate (0.6 mmol, 100 mg, 1 equiv.) with 1-(2-fluoroethyl)piperazine (0.6 mmol, 100 mg, 1 equiv.) in DMSO (5 mL) with  $K_2CO_3$  (1.8 mmol, 0.250 g, 3 equiv.) as a base. The reaction mixture was stirred for 12 h at 110 °C in an Anton Parr Monowave 50 inductive heater. Afterwards, the mixture was extracted with DCM (5 mL) the organic phase separated and dried with  $Na_2SO_4$ . The solvent was removed under reduced pressure and the crude product purified by column chromatography (30:70 cyclohexane:EtOAc to 30:70 MeOH:DCM) to give the title compound as colorless oil (0.08 mmol, 43 mg, 13%).

$^1H$  NMR (400 MHz,  $CD_3OD$ )  $\delta$  = 7.93 – 7.84 (m, 2H), 7.01 – 6.94 (m, 2H), 4.77 – 4.62 (m, 1H), 4.62 – 4.53 (m, 1H), 4.32 (q,  $J$  = 7.1 Hz, 2H), 3.42 – 3.37 (m, 4H), 2.83 – 2.80 (m, 1H), 2.77 – 2.71 (m, 5H), 1.38 (t,  $J$  = 7.1 Hz, 3H).

$^{13}C$  NMR (101 MHz,  $CD_3OD$ )  $\delta$  = 167.09, 154.40, 130.70, 119.45, 113.40, 81.23 (d,  $J$  = 166.4 Hz), 60.14, 57.84 (d,  $J$  = 19.7 Hz), 52.91, 46.79, 13.28.

$^{19}F$  NMR (376 MHz,  $CD_3OD$ )  $\delta$  = -220.19.

HRMS ( $m/z$ ):  $[M+H]^+$  calcd. for  $C_{15}H_{21}N_2O_2F$ , 280.15816; found, 280.1579.

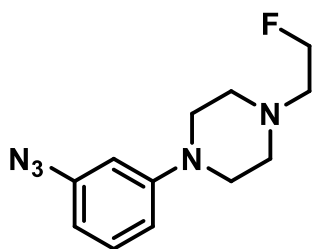
**1-(4-(4-(2-Fluoroethyl)piperazin-1-yl)phenyl)ethan-1-one (8e)**

1-(4-(4-(2-Fluoroethyl)piperazin-1-yl)phenyl)ethan-1-one was synthesized by treatment of 4-fluoro-phenylacetone (0.6 mmol, 84 mg, 1 equiv.) with 1-(2-fluoroethyl)piperazine (0.6 mmol, 100 mg, 1 equiv) in DMSO (3 mL) with  $K_2CO_3$  (1.8 mmol, 0.230 g, 3 equiv.) as a base. The reaction mixture was stirred for 12 h at 110 °C in an Anton Parr Monowave 50 inductive heater. Afterwards, the mixture was extracted with DCM (10 mL) the organic phase separated and dried with  $Na_2SO_4$ . The solvent was removed under reduced pressure and the crude product purified by column chromatography (30:70 cyclohexane:EtOAc to 30:70 MeOH:DCM) to give the title compound as colorless oil (0.17 mmol, 41 mg, 28%). The compound is already described in the literature<sup>[45]</sup>.

$^1H$  NMR (400 MHz,  $CD_3OD$ )  $\delta$  = 7.93 – 7.88 (m, 2H), 7.02 – 6.96 (m, 2H), 4.74 – 4.53 (m, 2H), 3.47 – 3.40 (m, 4H), 2.84 – 2.81 (m, 1H), 2.78 – 2.70 (m, 5H), 2.53 (s, 3H).

$^{13}C$  NMR (101 MHz  $CD_3OD$ )  $\delta$  = 185.72, 154.55, 130.24, 129.95, 113.10, 81.23 (d,  $J$  = 166.4 Hz), 57.83 (d,  $J$  = 19.7 Hz), 52.87, 46.54, 24.68.

$^{19}F$  NMR (376 MHz,  $CD_3OD$ )  $\delta$  = -220.21.

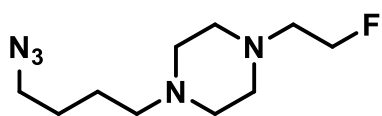
**1-(3-Azidophenyl)-4-(2-fluoroethyl)piperazine (8f)**

1-(3-Azidophenyl)-4-(2-fluoroethyl)piperazine was synthesized starting from 1-(2-fluoroethyl)-4-(3-nitrophenyl)piperazine (0.2 mmol, 50 mg, 1 equiv.). The start material was dissolved in MeOH (2 mL) and hydrogen gas was led through the solution for 2 h in the presence of 30% Pd/C (5 mg, 10 mass%). Afterwards, the suspension was filtered through cotton and the solvent was removed under reduced pressure. Without further purification the residue was taken up in water, cooled to 0°C, acidified with TFA (0.5 mL) and treated with NaNO<sub>2</sub> (0.22 mmol, 15 mg, 1.1 equiv.). After stirring the solution for 1 h at 0 °C, NaN<sub>3</sub> (0.22 mmol, 14 mg, 1.1 equiv) was added slowly. The reaction was stirred for 2 h at room temperature and extracted with DCM (5 mL). The organic phase was separated and dried with Na<sub>2</sub>SO<sub>4</sub>. Removal of the solvent under reduced pressure gave the analytically pure product as a colorless oil (0.04 mmol, 10 mg, 19%).

<sup>1</sup>H NMR (400 MHz, (CD<sub>3</sub>)<sub>2</sub>SO) δ = 7.65 (t, *J* = 2.3 Hz, 1H), 7.58 (ddd, *J* = 7.9, 2.1, 0.9 Hz, 1H), 7.52 – 7.39 (m, 2H), 4.67 – 4.62 (m, 1H), 4.56 – 4.49 (m, 1H), 3.28 (dd, *J* = 5.8, 4.3 Hz, 4H), 2.75 – 2.57 (m, 6H).

<sup>13</sup>C NMR (101 MHz, (CD<sub>3</sub>)<sub>2</sub>SO) δ = 152.05, 130.62, 121.77, 113.13, 108.75, 82.34 (d, *J* = 166.4 Hz), 57.91 (d, *J* = 19.7 Hz), 53.05, 47.90.

<sup>19</sup>F NMR (376 MHz, (CD<sub>3</sub>)<sub>2</sub>SO) δ = -217.04.

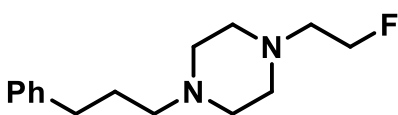
**1-(4-Azidobutyl)-4-(2-fluoroethyl)piperazine (8g)**

1-(4-Azidobutyl)-4-(2-fluoroethyl)piperazine was synthesized by treatment of 4-azidobutan-1-ol (0.6 mmol, 91 mg, 1 equiv.) with 1-(2-fluoroethyl)piperazine (0.6 mmol, 100 mg, 1 equiv.) and  $K_2CO_3$  (1.8 mmol, 0.230 g, 3 equiv.) in MeCN (3 mL). The reaction mixture was stirred for 16 h at room temperature. After completion the mixture was diluted with DCM (10 mL) and filtered. The solvent was removed under reduced pressure to give the crude product which was purified by column chromatography (30:70 cyclohexane:EtOAc to 30:70 MeOH:DCM) to give the title compound as colorless oil (0.17 mmol, 35 mg, 28%).

$^1H$  NMR (400 MHz,  $CD_3OD$ )  $\delta$  = 4.74 – 4.56 (m, 1H), 4.60 – 4.48 (m, 1H), 3.45 – 3.21 (m, 3H), 2.86 – 2.53 (m, 9H), 2.52 – 2.41 (m, 2H), 1.70 – 1.57 (m, 4H).

$^{13}C$  NMR (101 MHz,  $CD_3OD$ )  $\delta$  = 81.13 (d,  $J$  = 166.4 Hz), 57.74 (d,  $J$  = 19.7 Hz), 57.53, 52.61, 52.27, 50.86, 26.48, 23.21.

$^{19}F$  NMR (376 MHz,  $CD_3OD$ )  $\delta$  = -220.25.

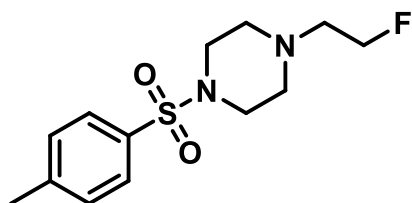
**1-(2-Fluoroethyl)-4-(3-phenylpropyl)piperazine (8h)**

1-(2-Fluoroethyl)-4-(3-phenylpropyl)piperazine was synthesized by treatment of (3-bromopropyl)benzene (0.6 mmol, 47 mg, 1 equiv.) with 1-(2-fluoroethyl)piperazine (0.6 mmol, 100 mg, 1 equiv.) and  $K_2CO_3$  (1.8 mmol, 3 equiv., 0.230 g) in MeCN (3 mL). The reaction mixture was stirred for 16 h at room temperature. After completion the mixture was diluted with DCM (10 mL) and filtered. The solvent was removed under reduced pressure to give the crude product which was purified by column chromatography (30:70 cyclohexane:EtOAc to 30:70 MeOH:DCM) to give the title compound as colorless oil (0.31 mmol, 72 mg, 52%).

$^1H$  NMR (400 MHz,  $CD_3OD$ )  $\delta$  = 7.32 – 7.13 (m, 5H), 4.64 (t,  $J$  = 4.7 Hz, 1H), 4.52 (t,  $J$  = 4.7 Hz, 1H), 2.86 – 2.34 (m, 14H), 1.94 – 1.77 (m, 2H).

$^{13}C$  NMR (101 MHz,  $CD_3OD$ )  $\delta$  = 141.64, 128.03, 128.01, 125.55, 81.15 (d,  $J$  = 166.4 Hz), 57.70 (d,  $J$  = 19.7 Hz), 57.50, 52.46, 52.27, 33.16, 27.75.

HRMS (m/z):  $[M+H]^+$  calcd. for  $C_{15}H_{24}N_2F$ , 251.19180; found, 251.1915.

**1-(2-Fluoroethyl)-4-tosylpiperazine (8i)**

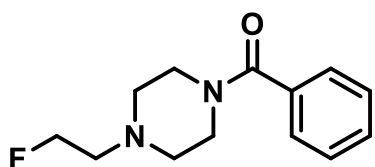
1-(2-Fluoroethyl)-4-tosylpiperazine was synthesized by treatment of *p*-toluenesulfonyl chloride (0.6 mmol, 105 mg, 1 equiv.) with 1-(2-fluoroethyl)piperazine (0.6 mmol, 100 mg, 1 equiv.) and  $K_2CO_3$  (1.8 mmol, 0.230 g, 3 equiv.) in MeCN (3 mL). The reaction mixture was stirred for 16 h at room temperature. After completion the mixture was diluted with DCM (10 mL) and filtered. The solvent was removed under reduced pressure to give the crude product which was purified by column chromatography (30:70 cyclohexane:EtOAc to 30:70 MeOH:DCM) to give the title compound as colorless oil (0.34 mmol, 90 mg, 57%).

$^1H$  NMR (400 MHz,  $CD_3OD$ )  $\delta$  = 7.68 (d,  $J$  = 8.3 Hz, 2H), 7.45 (d,  $J$  = 8.0 Hz, 2H), 4.60 – 4.56 (m, 1H), 4.48 – 4.44 (m, 1H), 3.05 – 2.99 (m, 4H), 2.75 – 2.70 (m, 1H), 2.68 – 2.58 (m, 5H), 2.47 (s, 3H).

$^{13}C$  NMR (101 MHz,  $CD_3OD$ )  $\delta$  = 144.09, 132.39, 129.45, 127.62, 81.27 (d,  $J$  = 166.4 Hz), 57.34 (d,  $J$  = 19.7 Hz), 52.22, 45.68, 20.07.

$^{19}F$  NMR (376 MHz,  $CD_3OD$ )  $\delta$  = -220.25.

HRMS ( $m/z$ ):  $[M+H]^+$  calcd. for  $C_{13}H_{19}FN_2O_2^{32}S$ , 286.11458; calcd. for  $C_{13}H_{19}FN_2O_2^{32}S$ , 288.11037; found, 286.1141, 288.1098.

**(4-(2-Fluoroethyl)piperazin-1-yl)(phenyl)methanone (8j)**

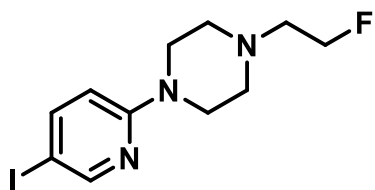
(4-(2-Fluoroethyl)piperazin-1-yl)(phenyl)methanone was synthesized by treatment of benzoyl chloride (0.6 mmol, 78 mg, 1 equiv.) with 1-(2-fluoroethyl)piperazine (0.6 mmol, 100 mg, 1 equiv.) and  $K_2CO_3$  (1.8 mmol, 3 equiv., 0.230 g) in MeCN (3 mL). The reaction mixture was stirred for 16 h at room temperature. After completion the mixture was diluted with DCM (10 mL) and filtered. The solvent was removed under reduced pressure to give the crude product which was purified by column chromatography (30:70 cyclohexane:EtOAc to 30:70 MeOH:DCM) to give the title compound as colorless oil (0.4 mmol, 84 mg, 65%).

$^1H$  NMR (400 MHz,  $CD_3OD$ )  $\delta$  = 7.53 – 7.39 (m, 5H), 4.68 – 4.63 (m, 1H), 4.56 – 4.51 (m, 1H), 3.81 (s, 2H), 3.49 (s, 2H), 2.82 – 2.77 (m, 1H), 2.76 – 2.71 (m, 1H), 2.60 (d,  $J$  = 48.4 Hz, 4H).

$^{13}C$  NMR (101 MHz,  $CD_3OD$ )  $\delta$  = 171.03, 135.33, 129.76, 128.36, 126.64, 81.25 (d,  $J$  = 166.4 Hz), 57.63 (d,  $J$  = 19.7 Hz), 52.95, 41.65.

$^{19}F$  NMR (376 MHz,  $CD_3OD$ )  $\delta$  = -220.20.

HRMS ( $m/z$ ):  $[M+H]^+$  calcd. for  $C_{13}H_{17}N_2OF$ , 236.13194; found, 236.1319.

**1-(2-Fluoroethyl)-4-(5-iodopyridin-2-yl)piperazine (8k)**

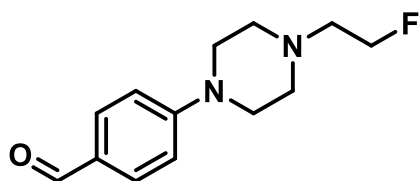
1-(2-Fluoroethyl)-4-(5-iodopyridin-2-yl)piperazine was synthesized by treatment of 2-fluoro-5-iodopyridine (0.6 mmol, 136 mg, 1 equiv.) with 1-(2-fluoroethyl)piperazine (1 equiv, 100 mg) in DMSO (3 mL) with  $K_2CO_3$  (1.8 mmol, 230 mg, 3 equiv.) as a base. The reaction mixture was stirred for 12 h at 110 °C in an Anton Parr Monowave 50 inductive heater. Afterwards, the mixture was extracted with DCM (10 mL) the organic phase separated and dried with  $Na_2SO_4$ . The solvent was removed under reduced pressure and the crude product purified by column chromatography (30:70 cyclohexane:EtOAc to 30:70 MeOH:DCM) to give the title compound as colorless oil (0.14 mmol, 48 mg, 24%).

$^1H$  NMR (400 MHz,  $CD_3OD$ )  $\delta$  = 8.26 (d,  $J$  = 2.8 Hz, 1H), 7.76 (dd,  $J$  = 9.0, 2.4 Hz, 1H), 6.70 (d,  $J$  = 8.6 Hz, 1H), 4.72 – 4.68 (m, 1H), 4.63 – 4.48 (m, 1H), 3.65 – 3.44 (m, 4H), 2.84 – 2.78 (m, 1H), 2.77 – 2.71 (m, 1H), 2.71 – 2.63 (m, 4H).

$^{13}C$  NMR (101 MHz,  $CD_3OD$ )  $\delta$  = 158.23, 152.98, 145.14, 109.57, 81.16 (d,  $J$  = 166.4 Hz), 76.61, 57.86 (d,  $J$  = 19.7 Hz), 52.78, 44.35.

$^{19}F$  NMR (376 MHz,  $CD_3OD$ )  $\delta$  = -220.18.

HRMS (m/z):  $[M]^+$  calcd. for  $C_{11}H_{15}N_3OF^{127}I$ , 335.02892; found, 335.0282.

**4-(4-(2-Fluoroethyl)piperazin-1-yl)benzaldehyde (8I)**

4-(4-(2-Fluoroethyl)piperazin-1-yl)benzaldehyde was synthesized by treatment of 4-fluoro-phenylacetone (0.6 mmol, 77 mg, 1 equiv.) with 1-(2-fluoroethyl)piperazin (0.6 mmol, 100 mg, 1 equiv) in DMSO (4 mL) with  $K_2CO_3$  (1.8 mmol, 230 mg, 3 equiv.) as a base. The reaction mixture was stirred for 12 h at 110 °C in an Anton Parr Monowave 50 inductive heater. Afterwards, the mixture was extracted with DCM the organic phase separated and dried with  $Na_2SO_4$ . The solvent was removed under reduced pressure and the crude product purified by column chromatography (30:70 cyclohexane:EtOAc to 30:70 MeOH:DCM) to give the title compound as colorless oil (0.17 mmol, 41 mg, 29%).

$^1H$  NMR (400 MHz,  $CD_3OD$ )  $\delta$  = 9.71 (s, 1H), 7.78 (d,  $J$  = 9.0 Hz, 2H), 7.05 (d,  $J$  = 9.0 Hz, 2H), 4.72 – 4.68 (m, 1H), 4.60 – 4.55 (m, 1H), 3.51 – 3.46 (m, 4H), 2.92 – 2.80 (m, 1H), 2.78 – 2.70 (m, 5H).

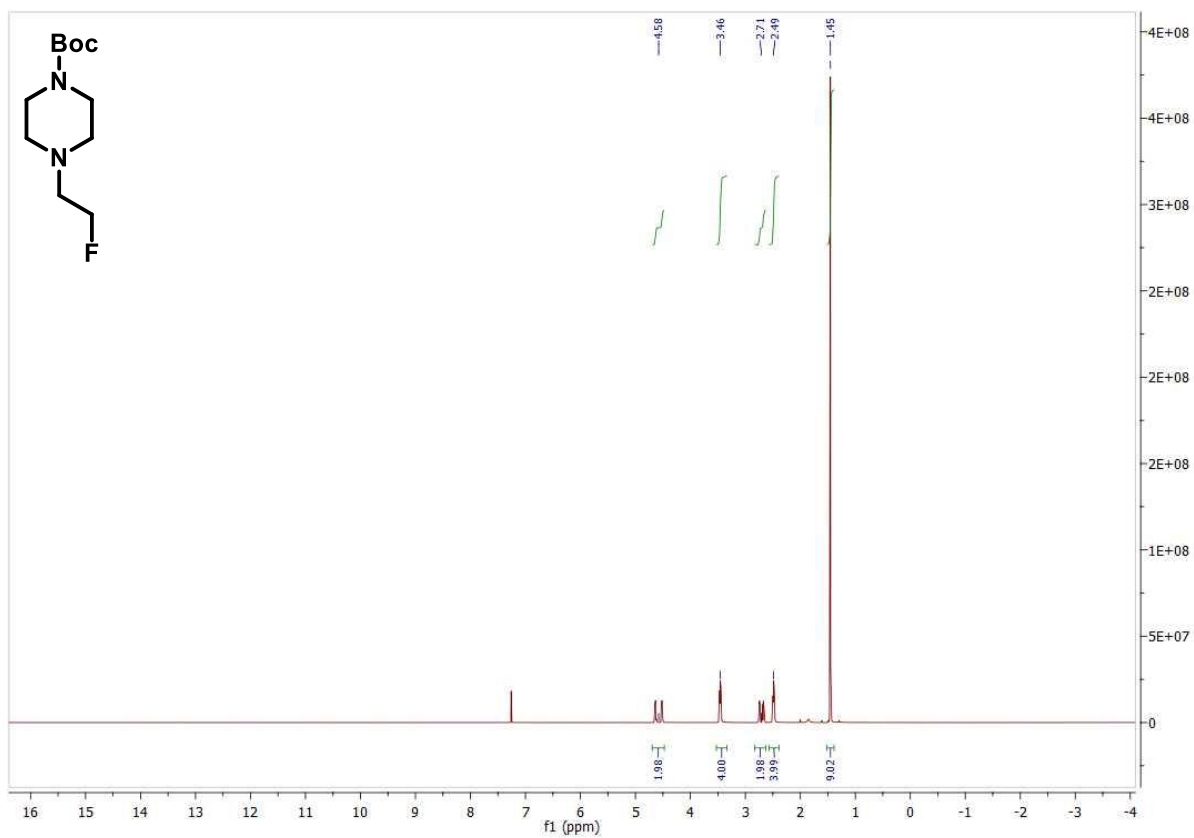
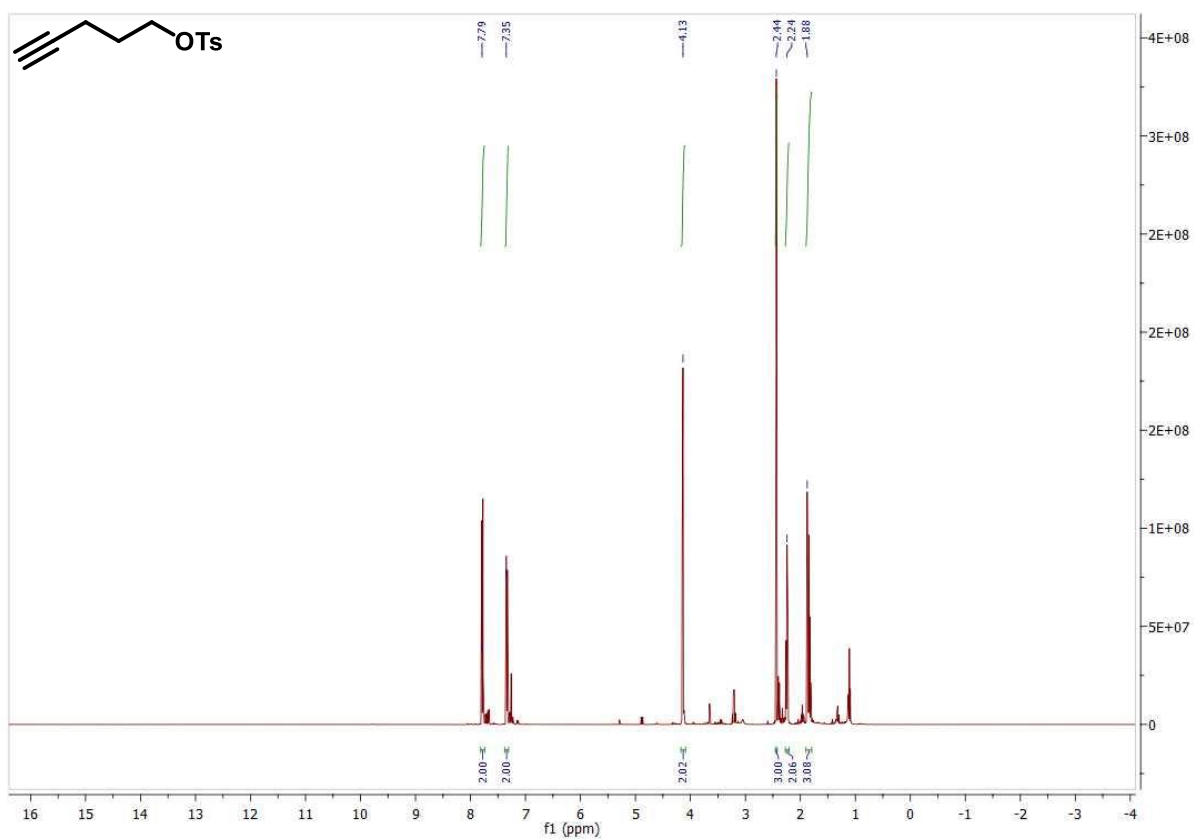
$^{13}C$  NMR (101 MHz,  $CD_3OD$ )  $\delta$  = 191.12, 155.41, 131.62, 126.88, 113.30, 81.24 (d,  $J$  = 166.4 Hz), 57.80 (d,  $J$  = 19.7 Hz), 52.83, 46.35.

$^{19}F$  NMR (376 MHz,  $CD_3OD$ )  $\delta$  = -220.14.

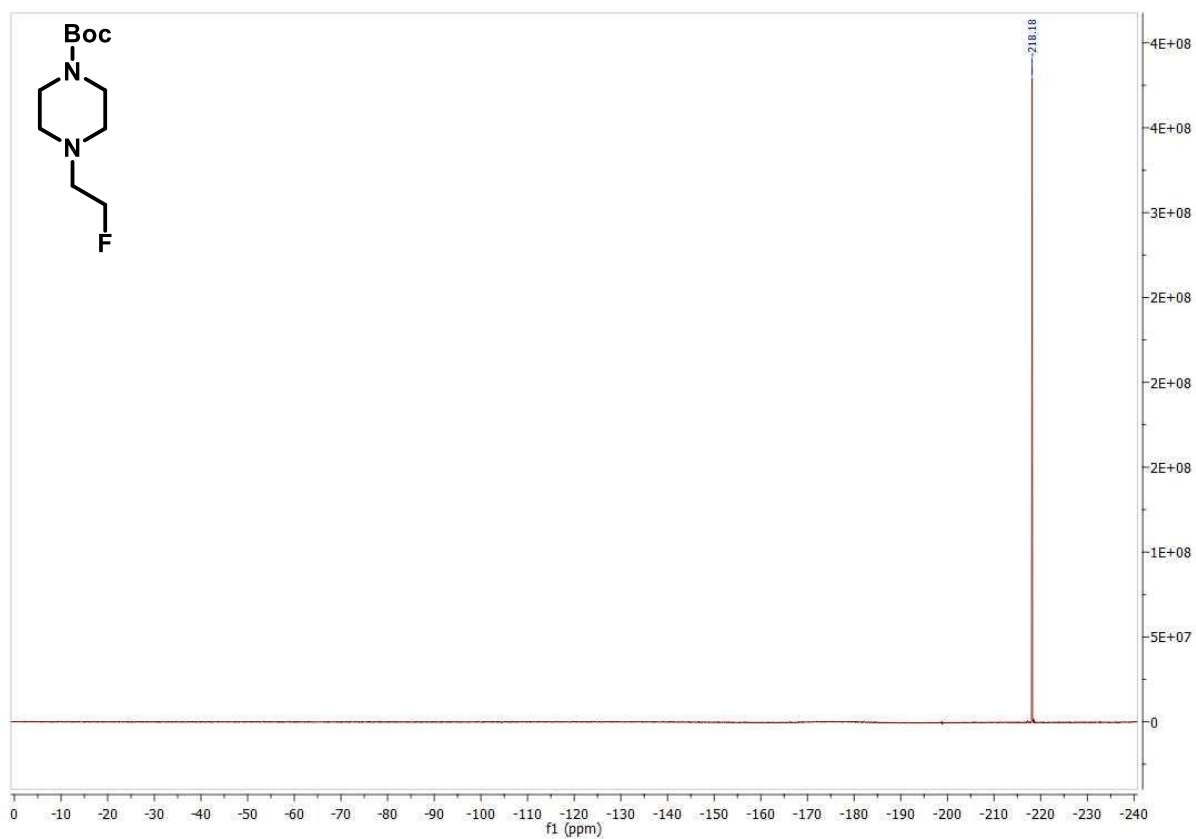
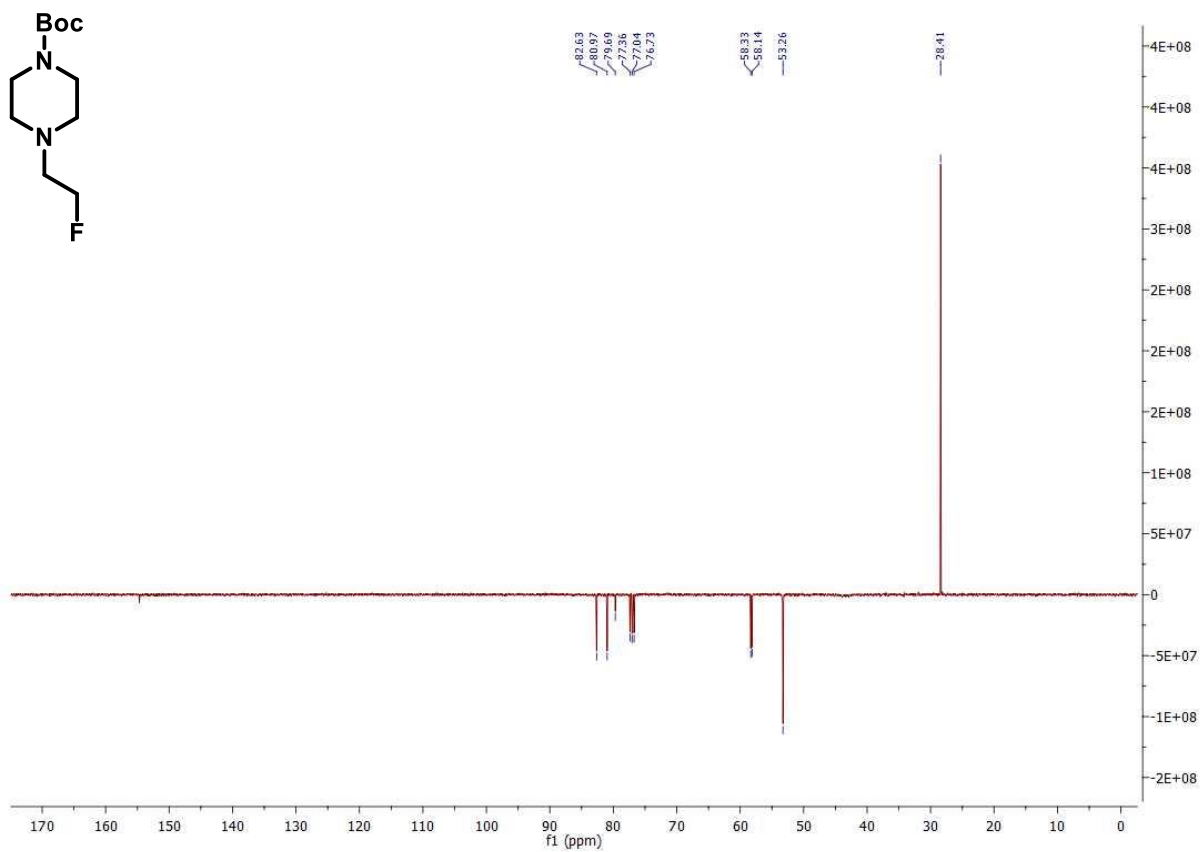
HRMS (m/z):  $[M]^+$  calcd. for  $C_{13}H_{17}N_2OF$ , 236.13194; found, 236.1316

## 7 Experimental Part

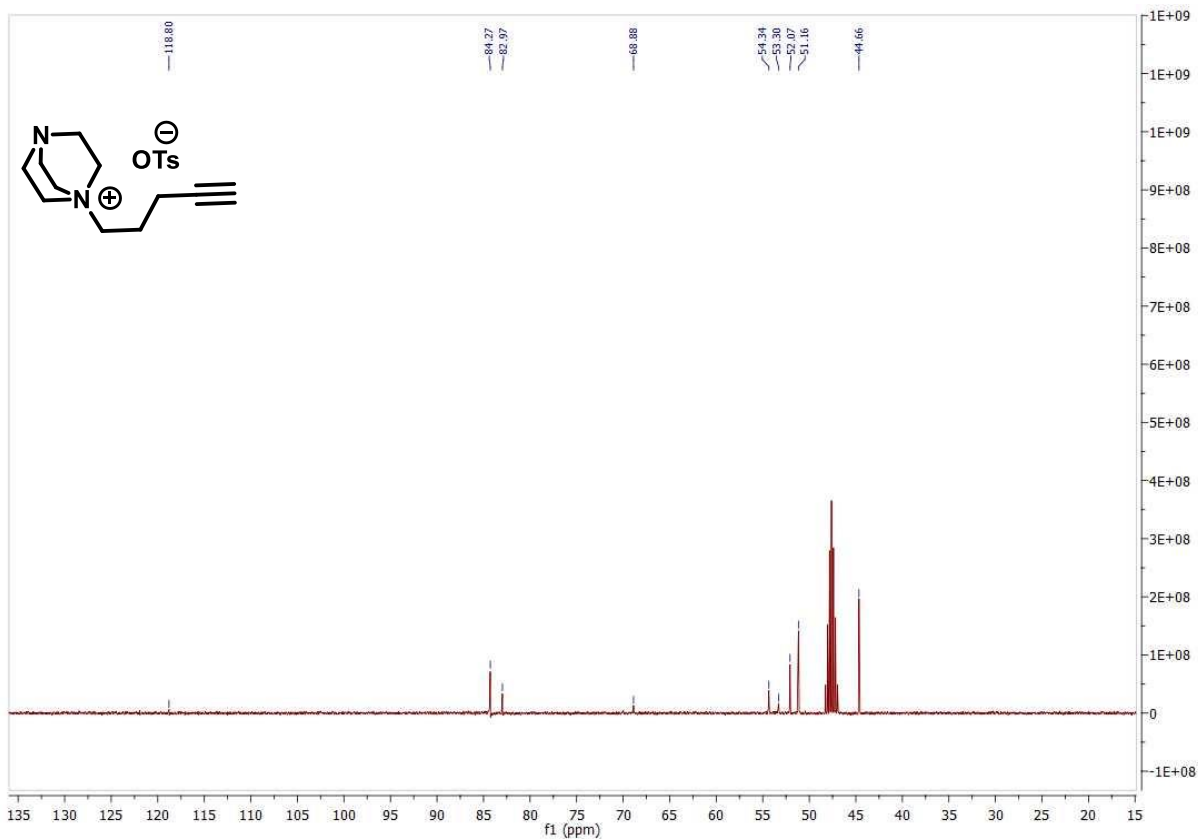
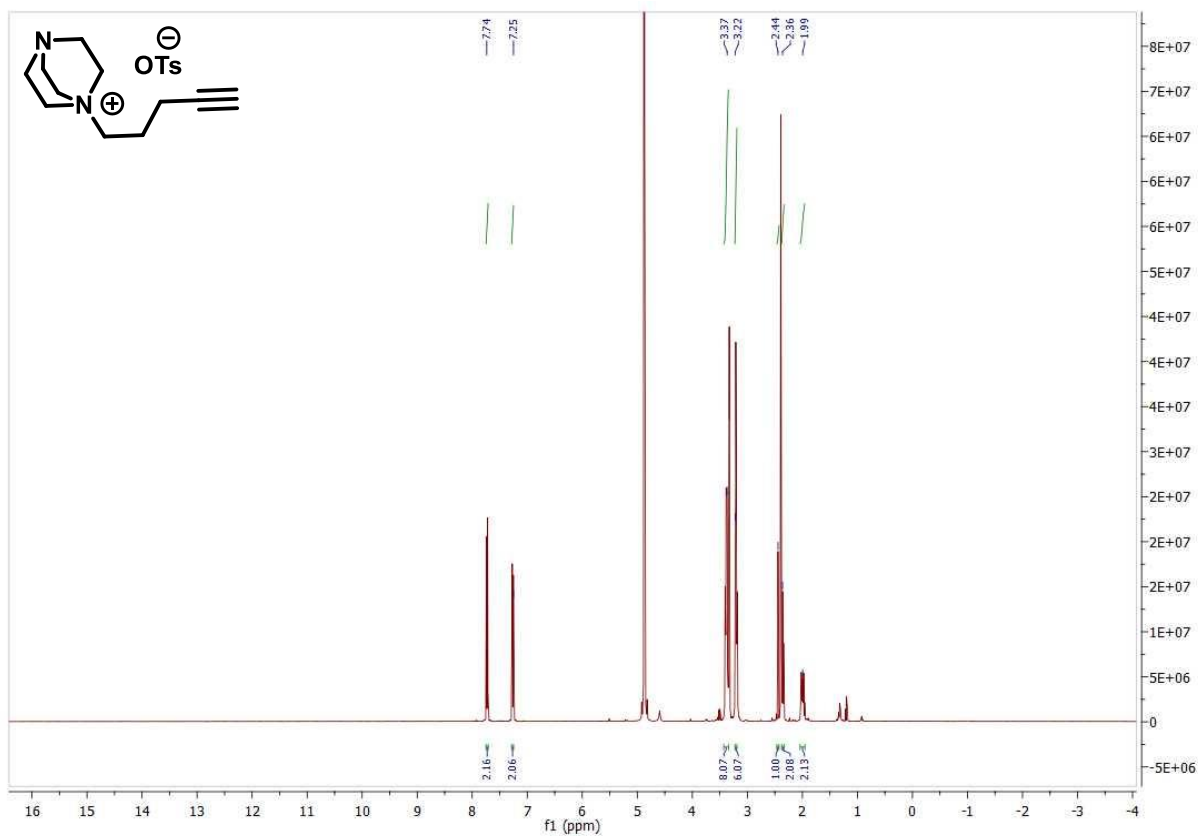
### NMR-Spectra



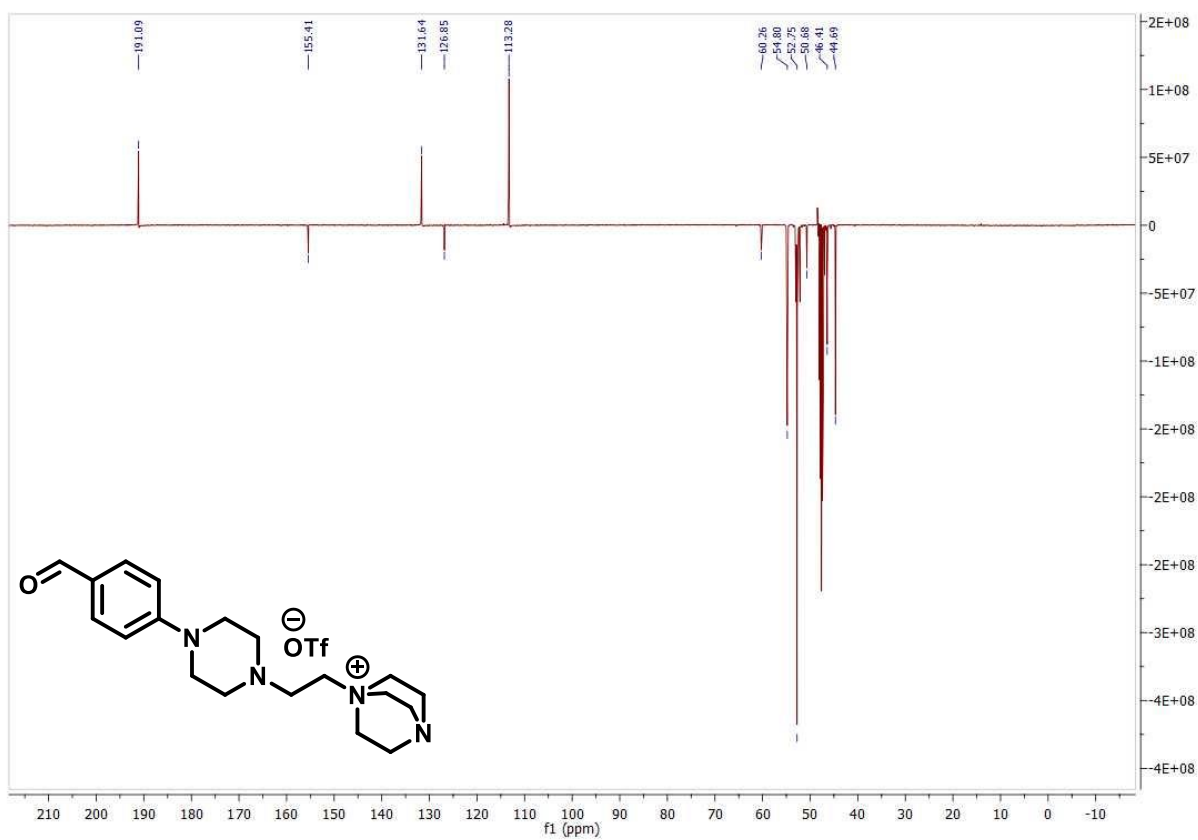
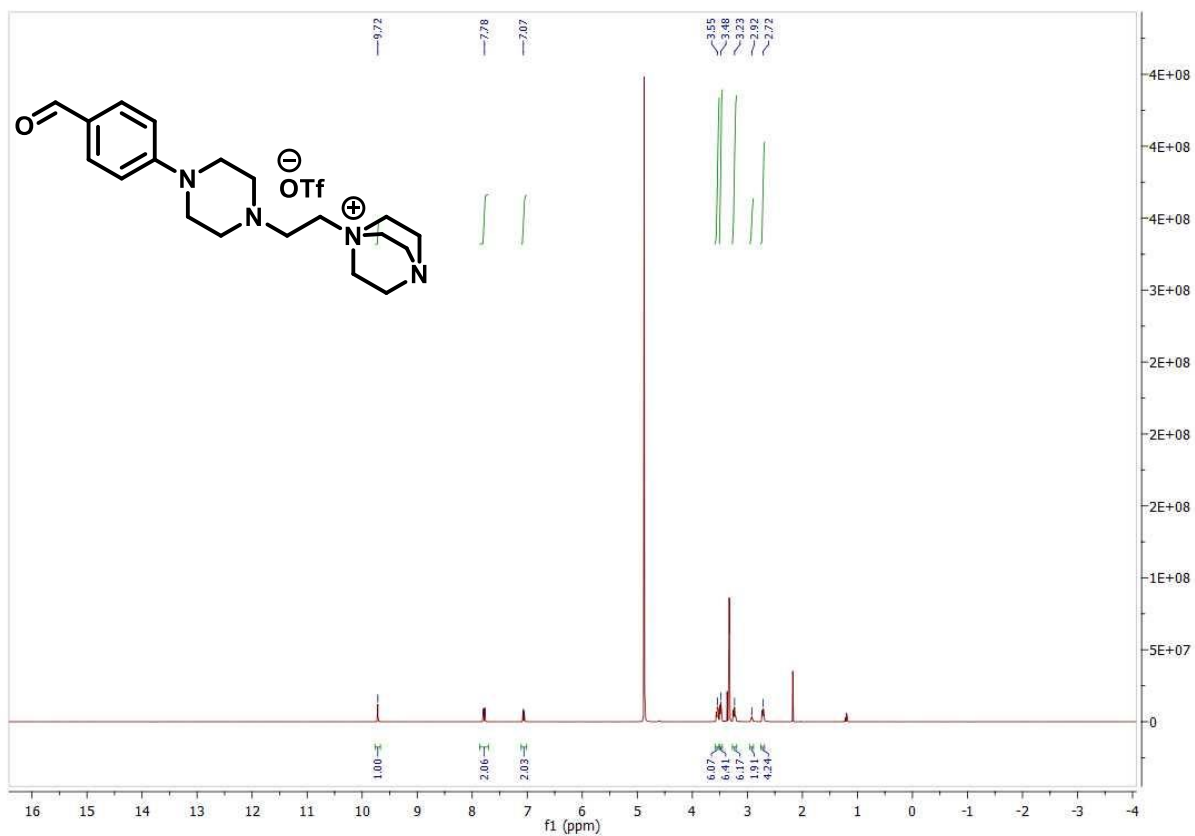
## 7 Experimental Part



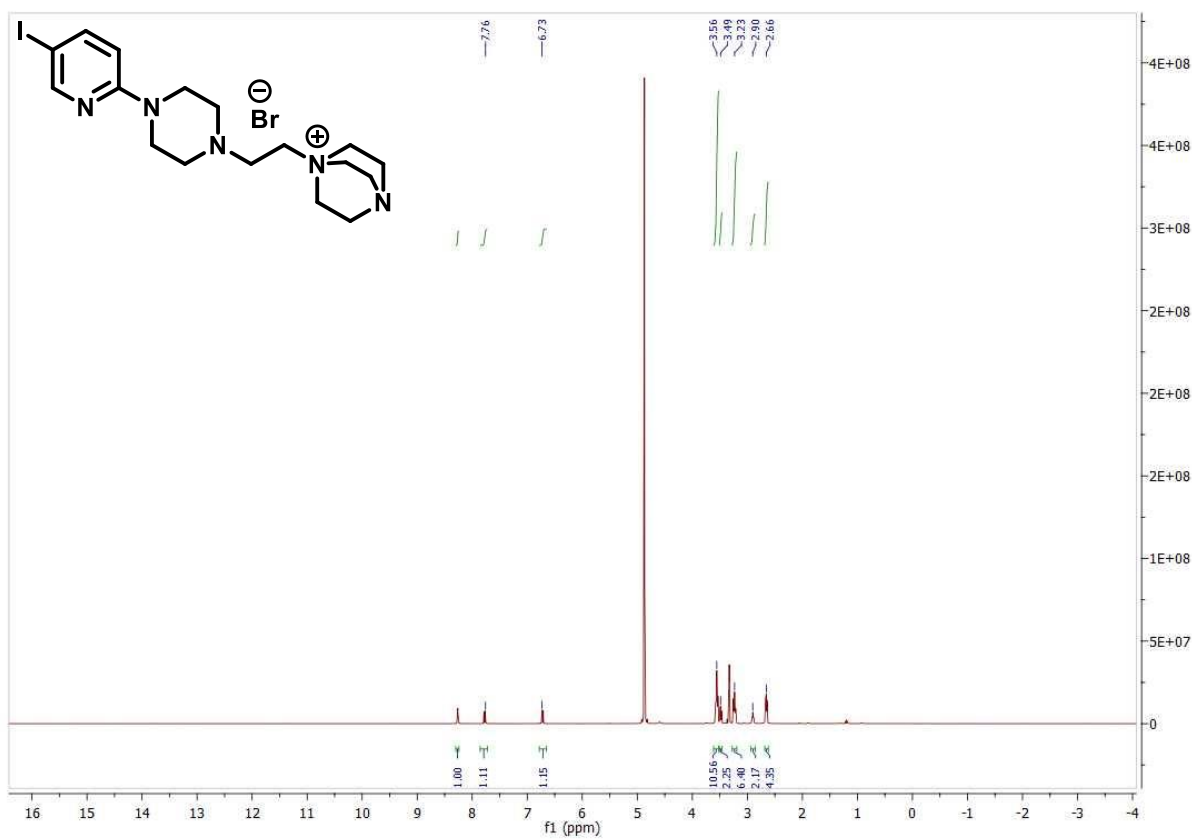
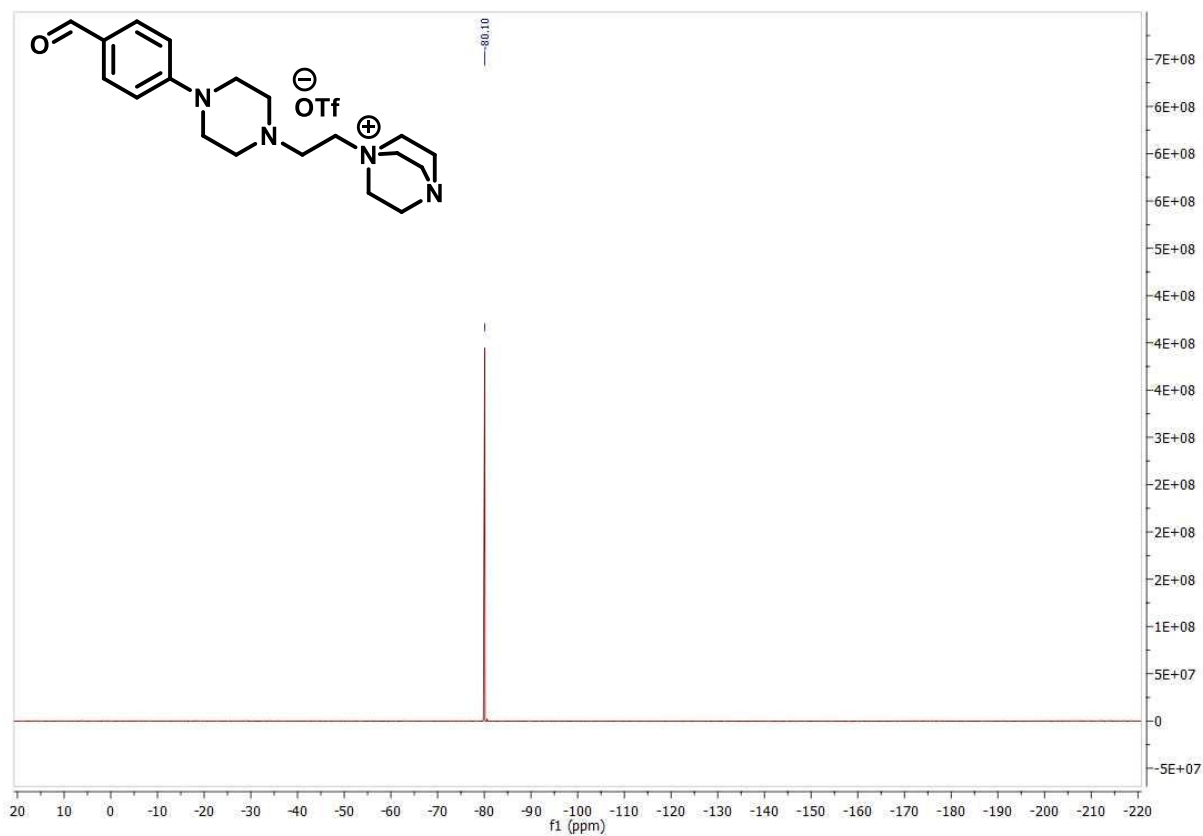
## 7 Experimental Part



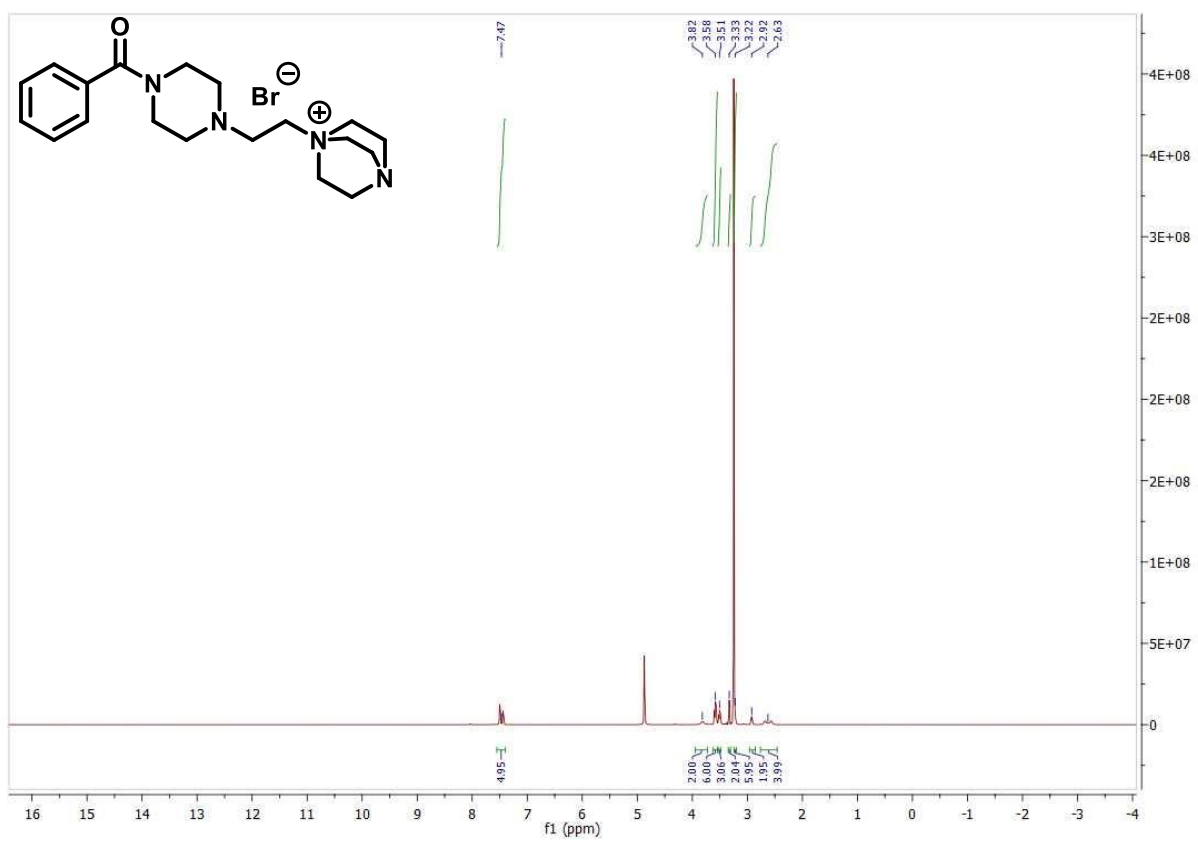
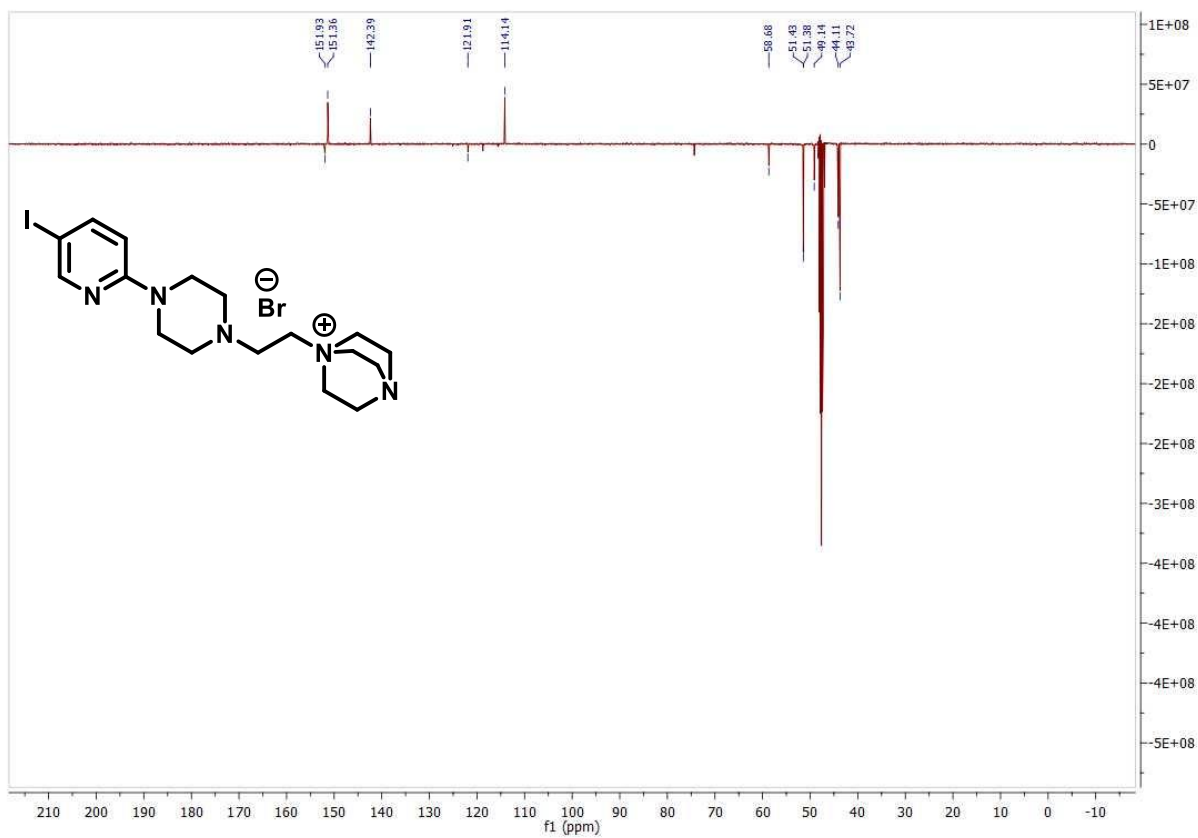
## 7 Experimental Part



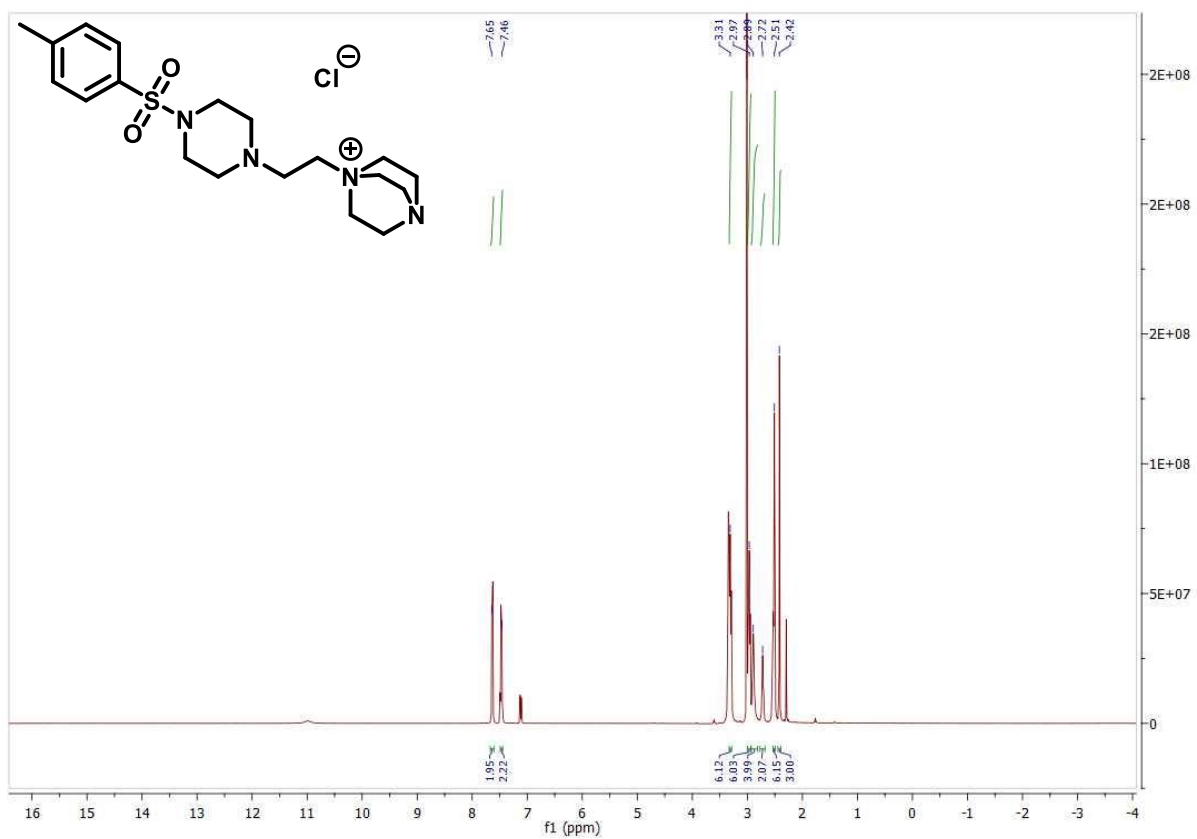
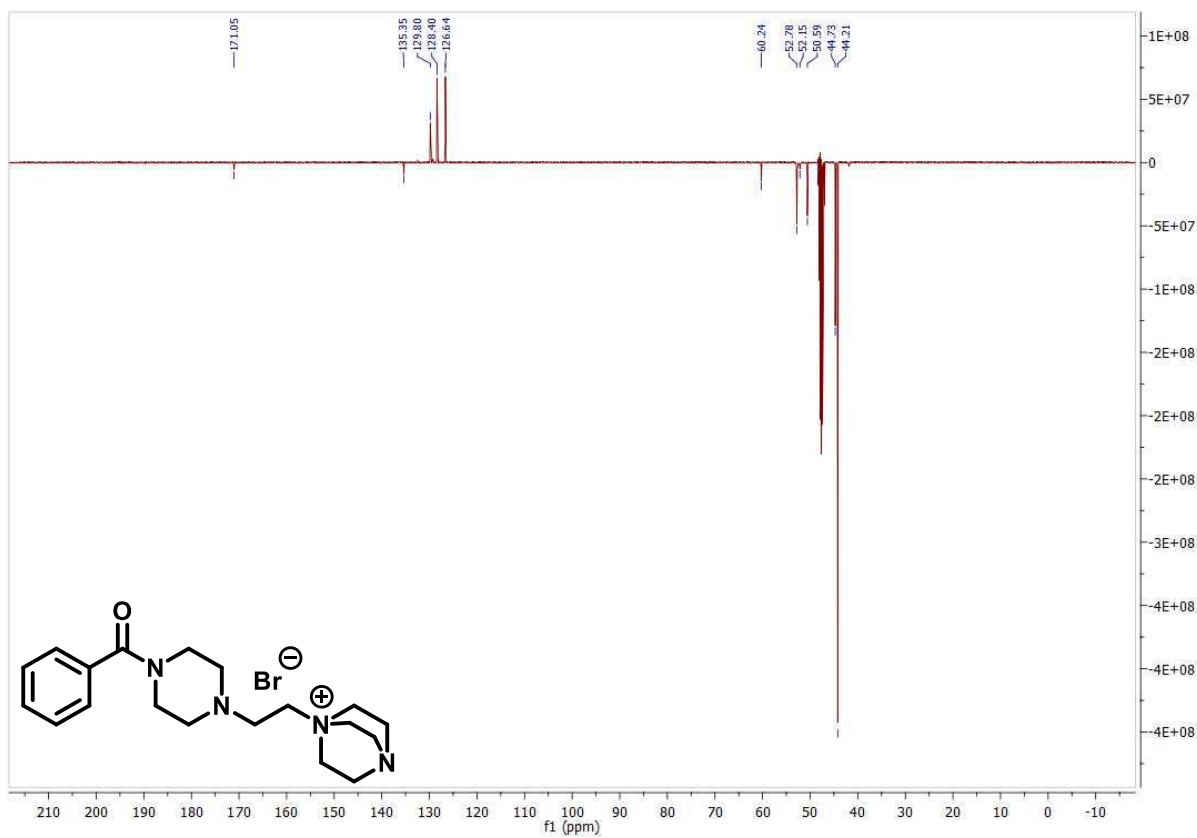
## 7 Experimental Part



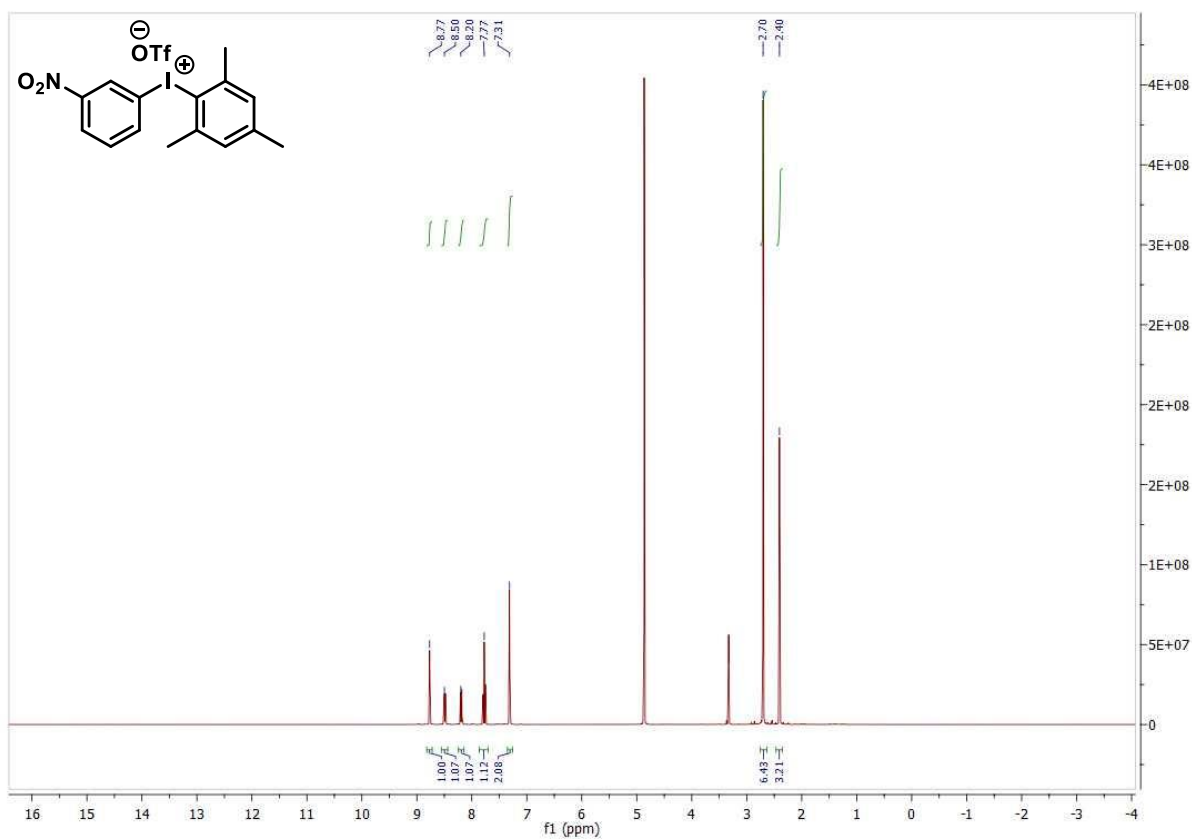
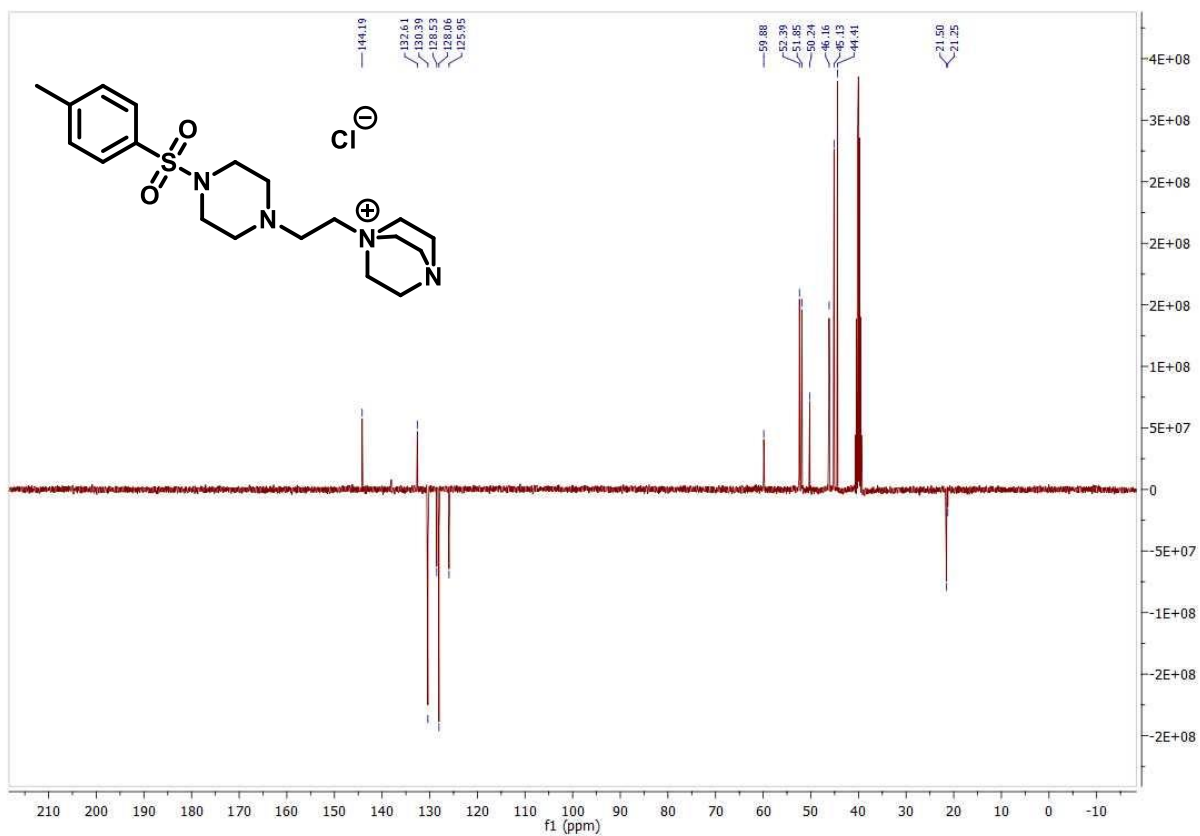
## 7 Experimental Part



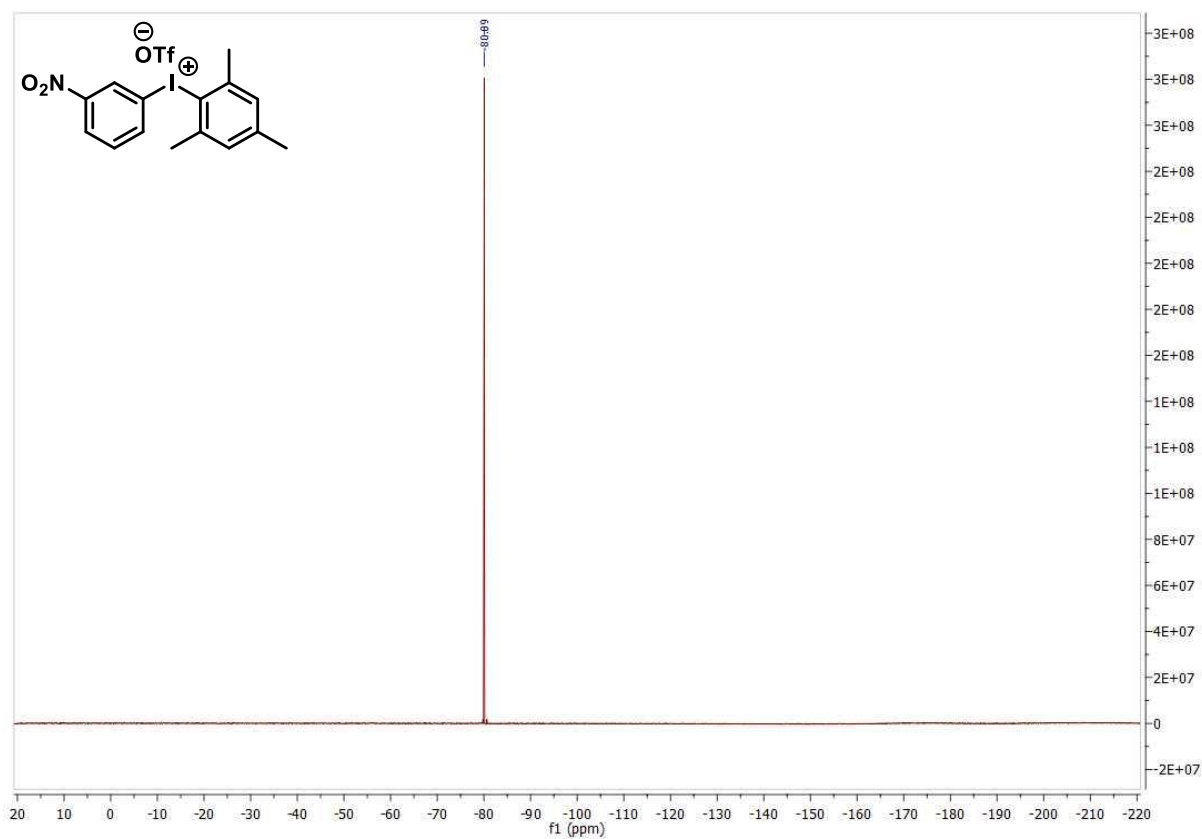
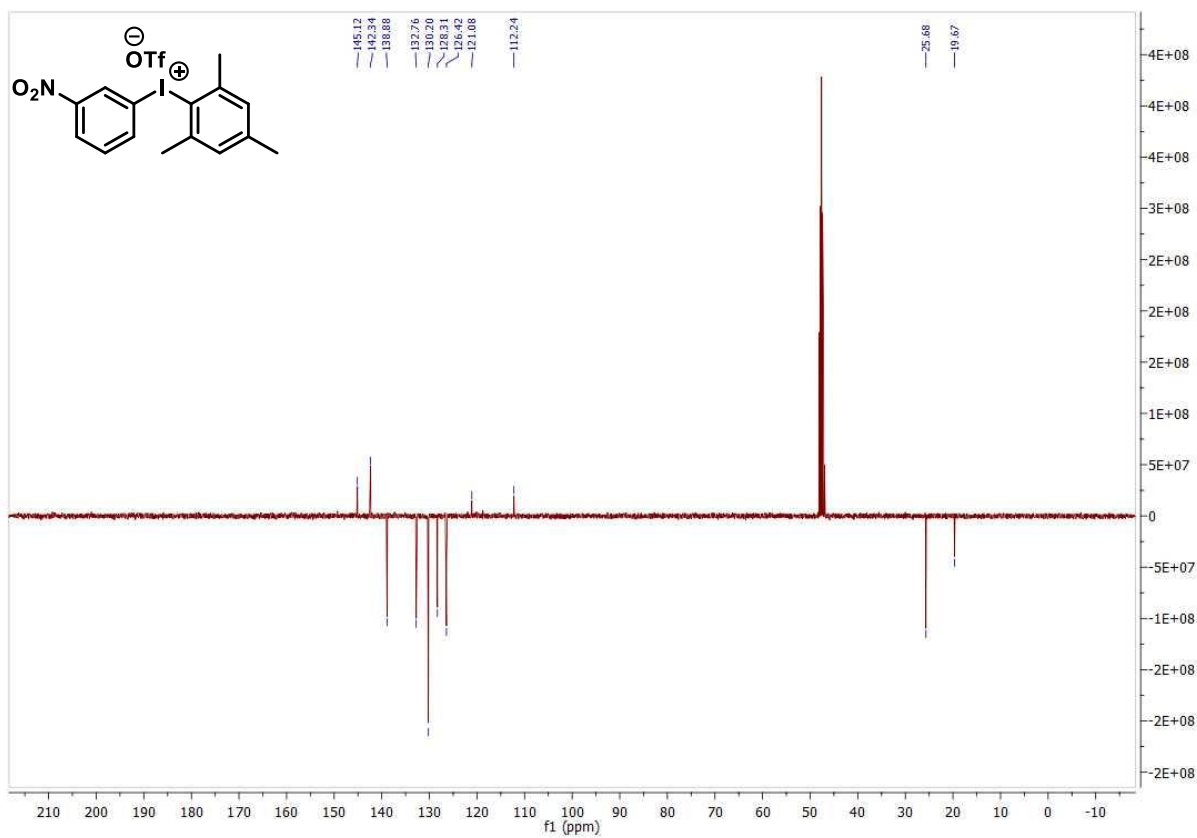
## 7 Experimental Part



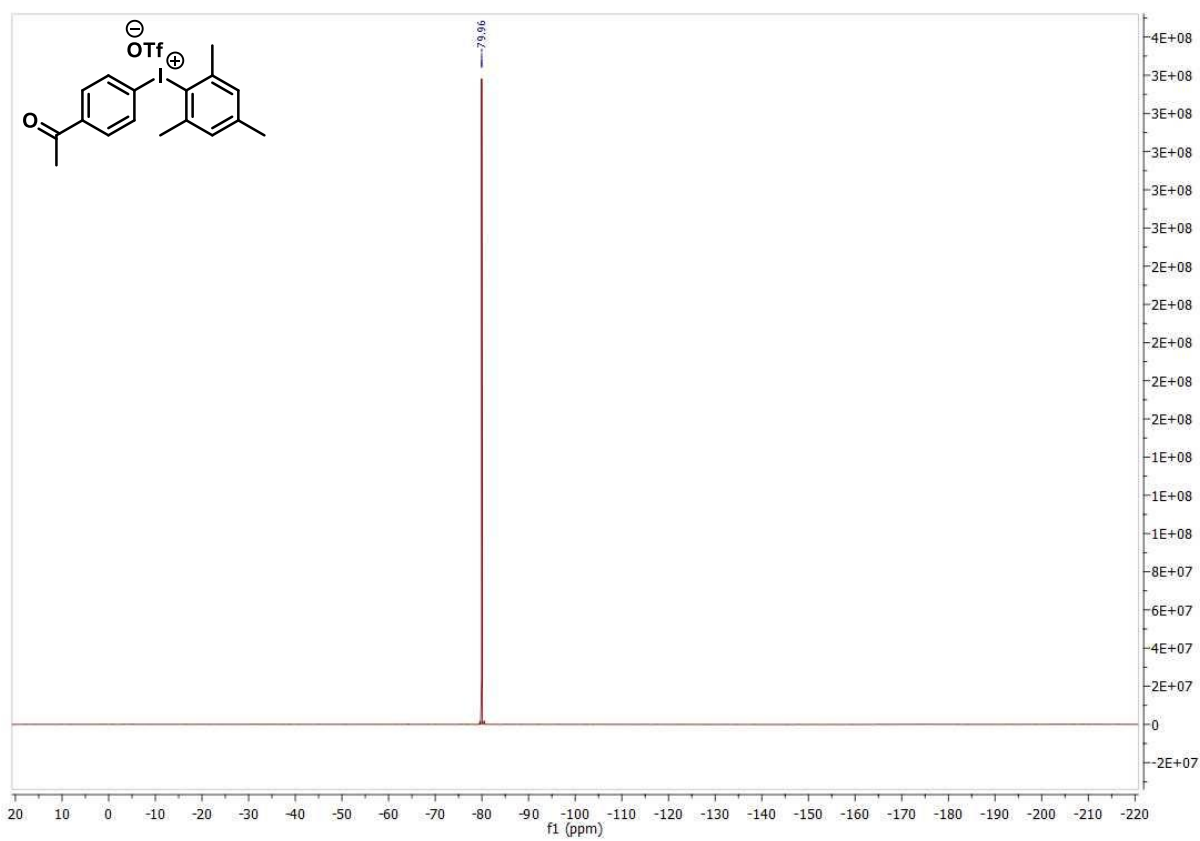
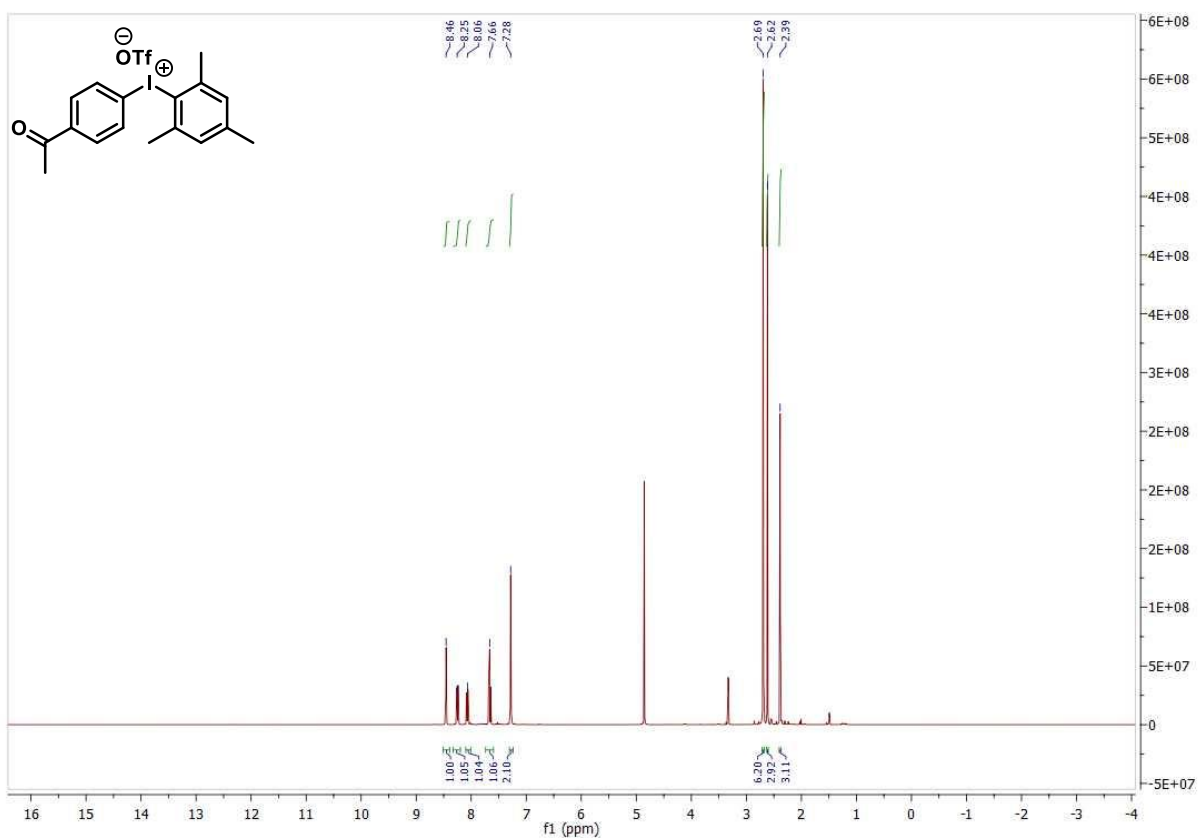
## 7 Experimental Part



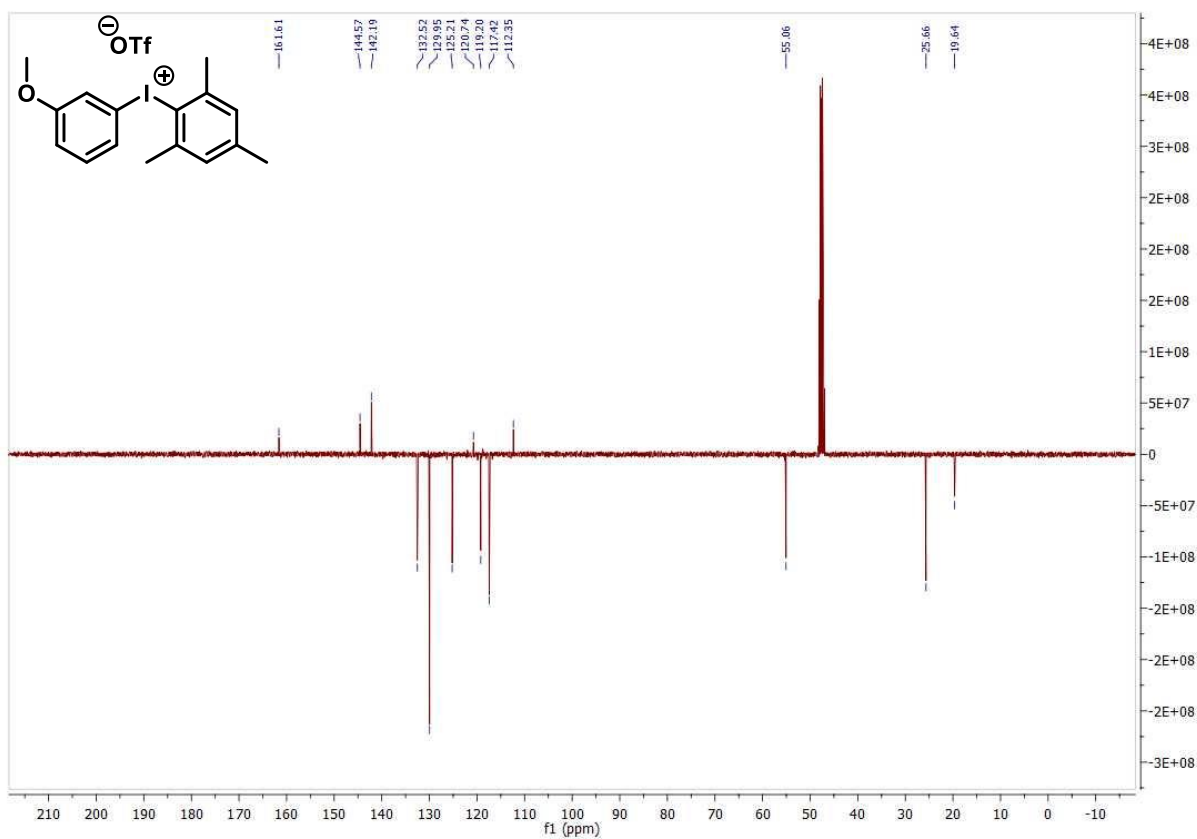
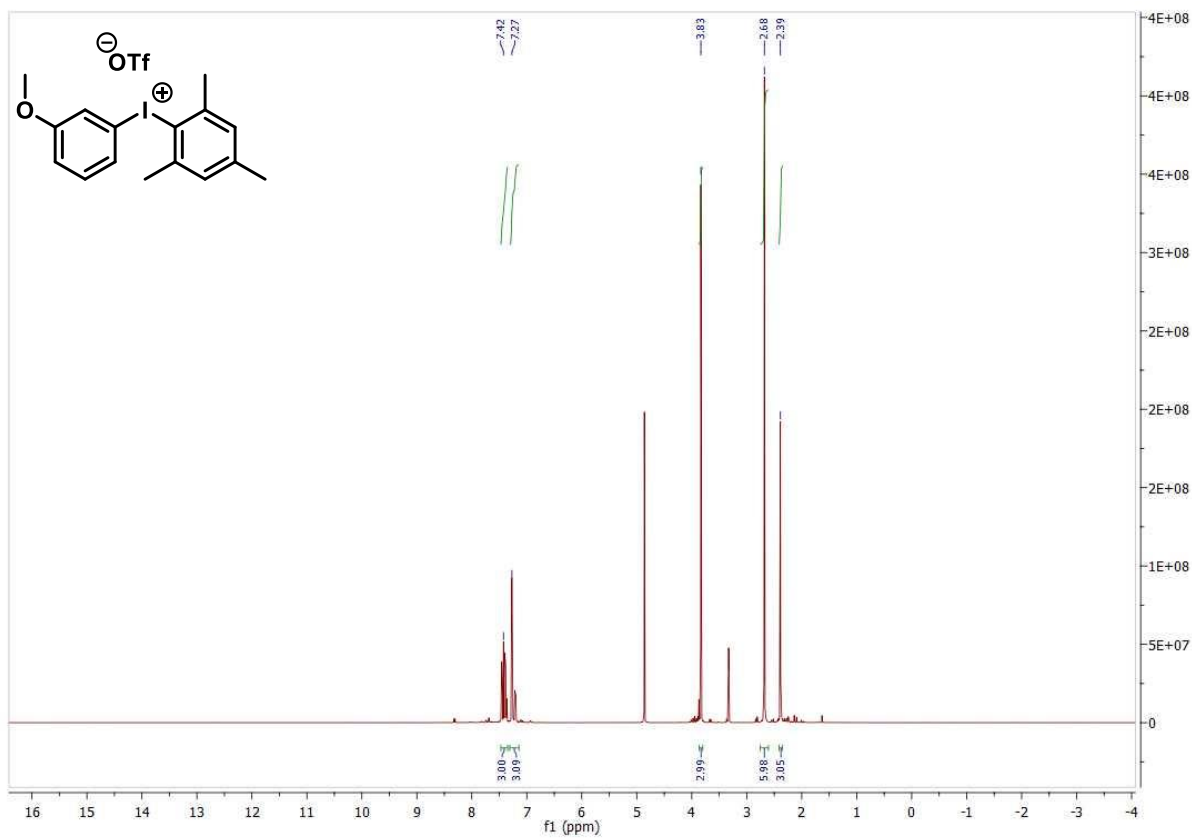
## 7 Experimental Part



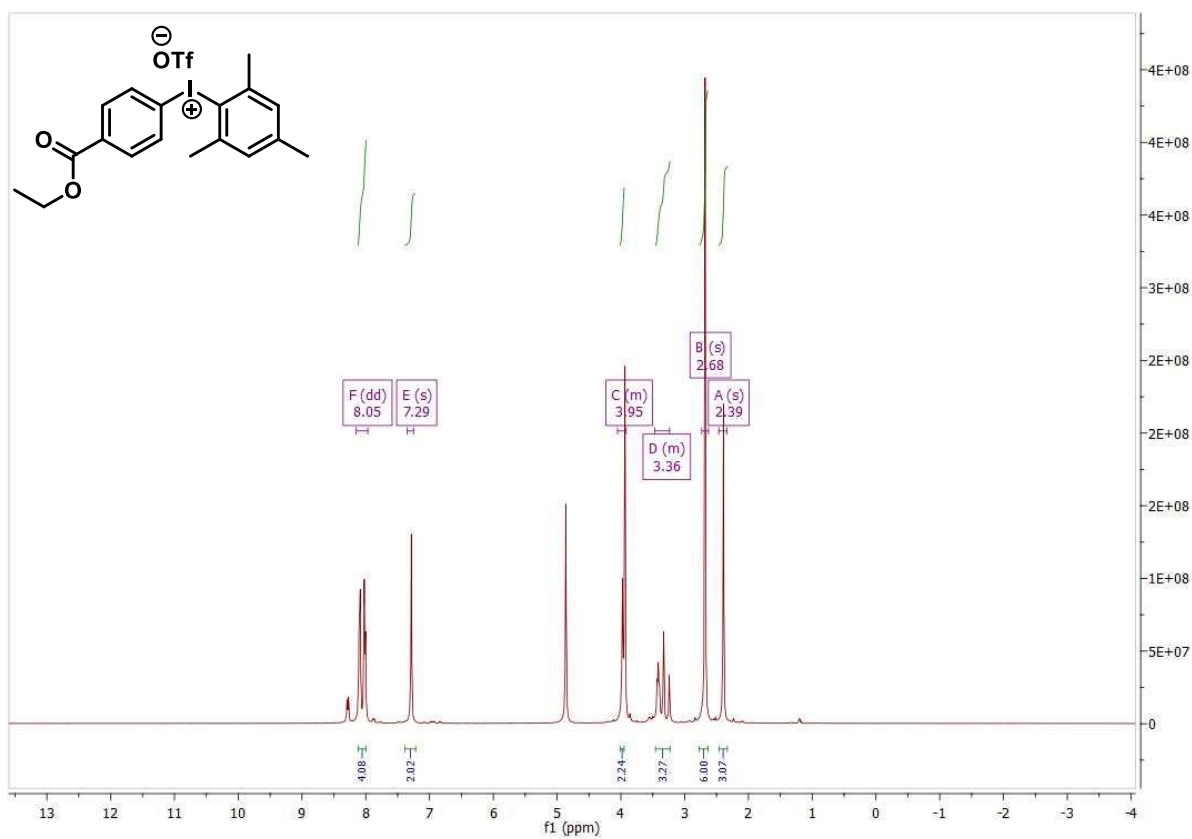
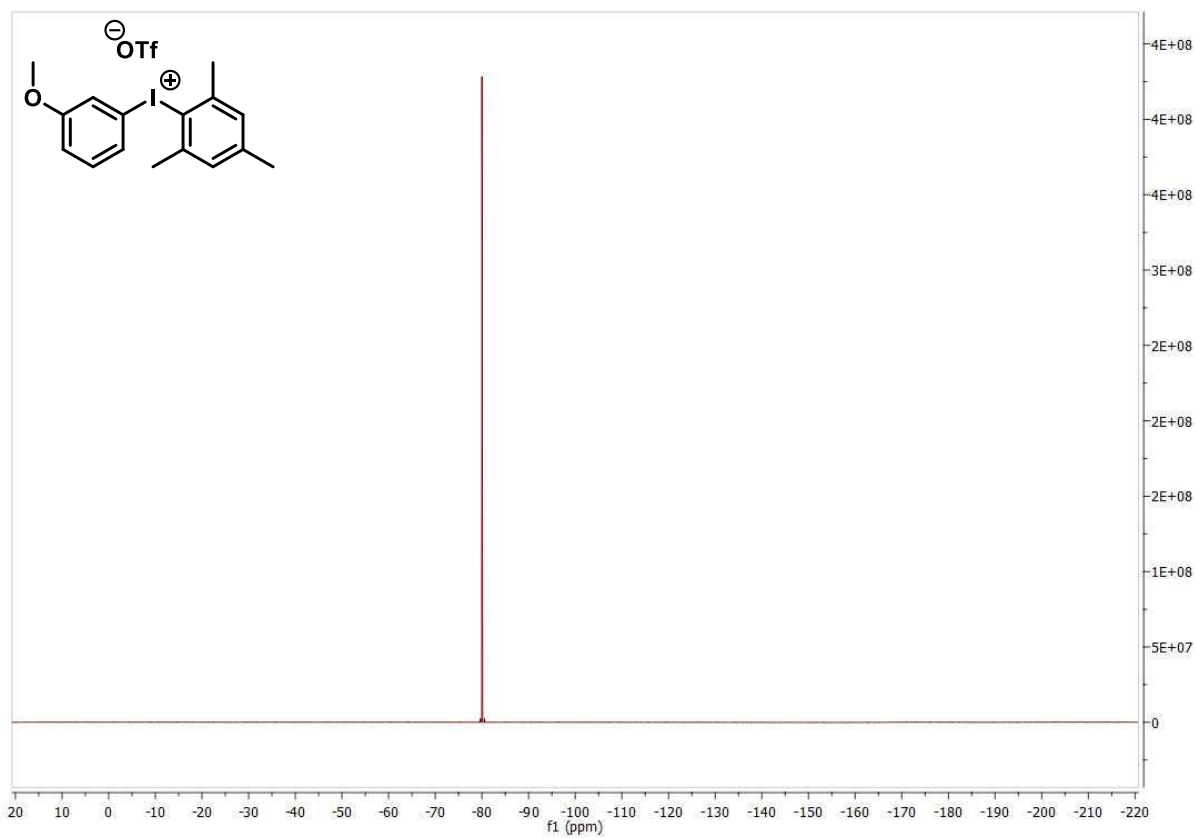
## 7 Experimental Part



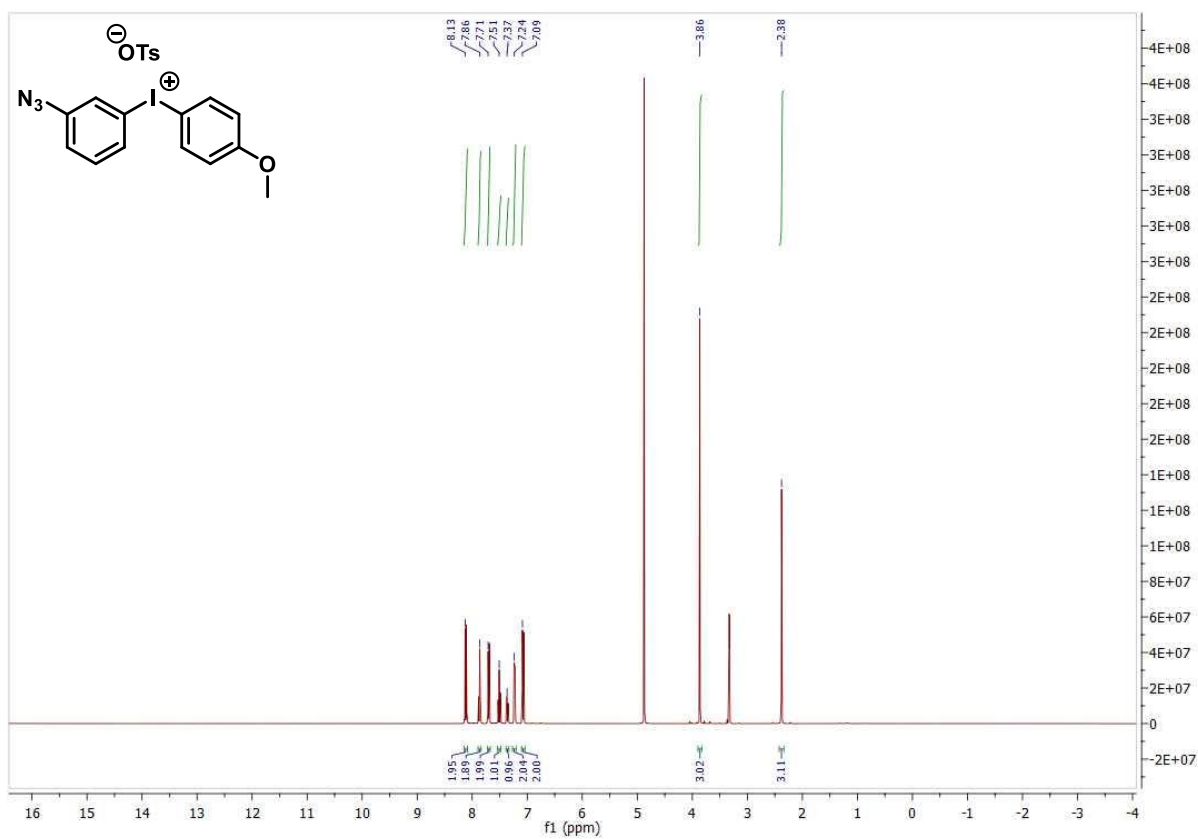
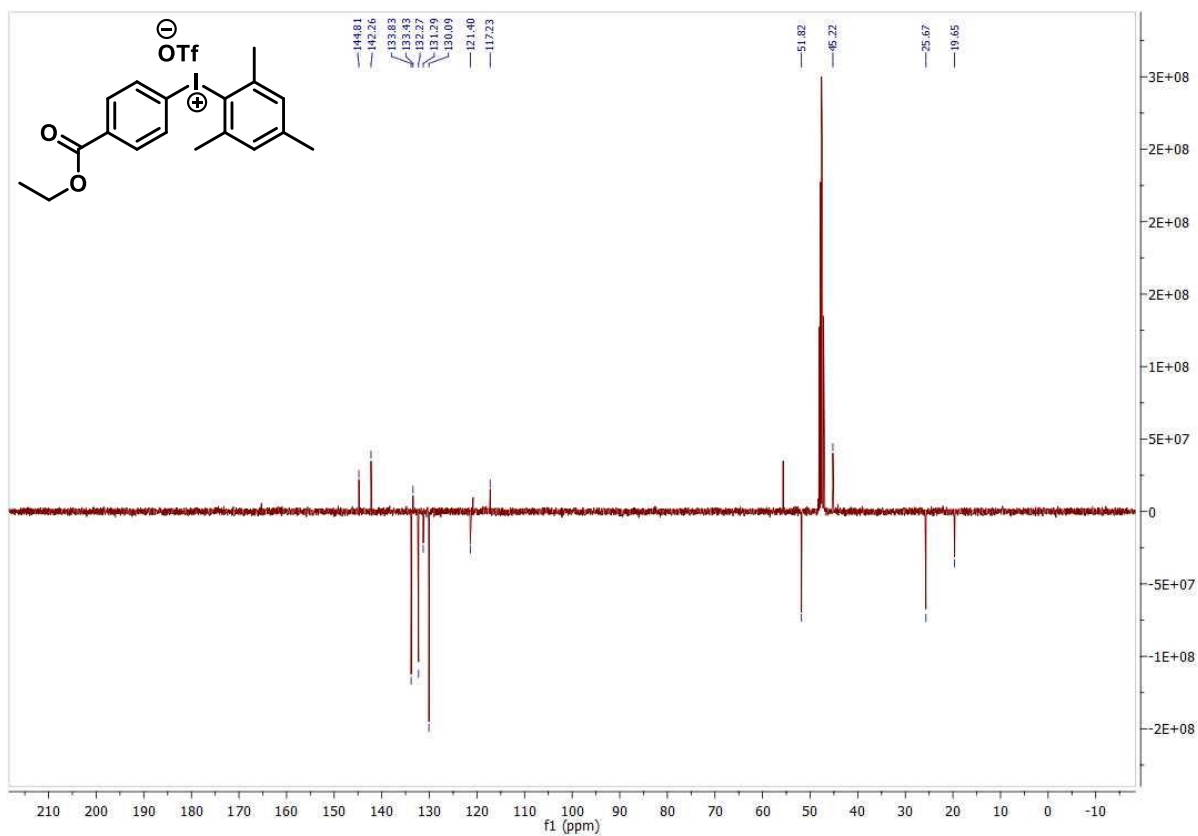
## 7 Experimental Part



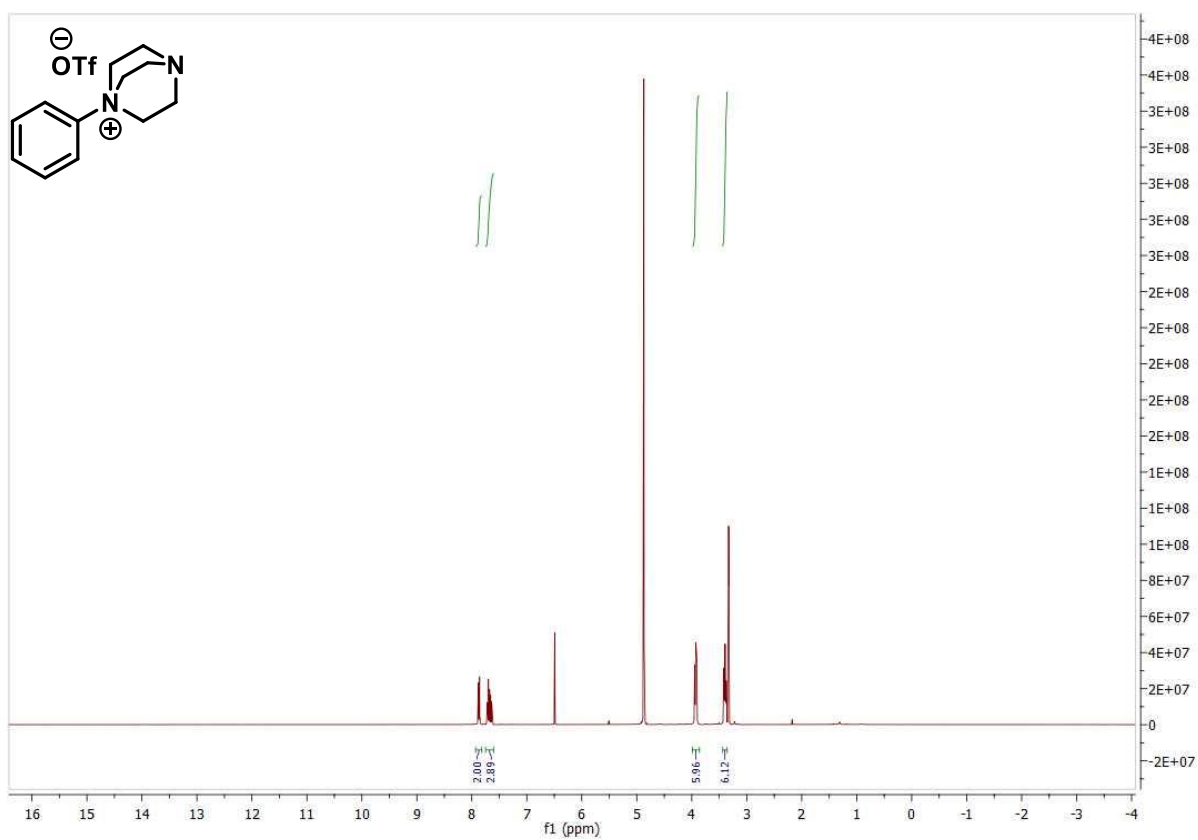
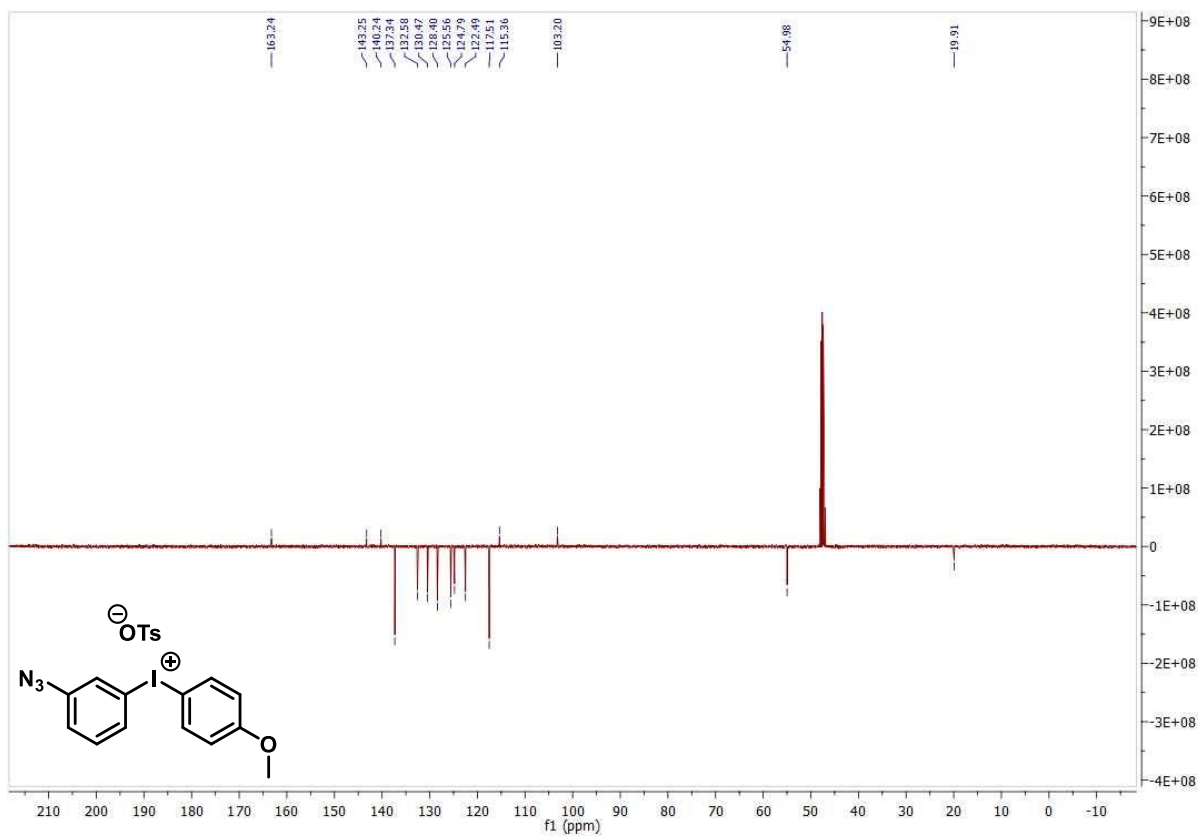
## 7 Experimental Part



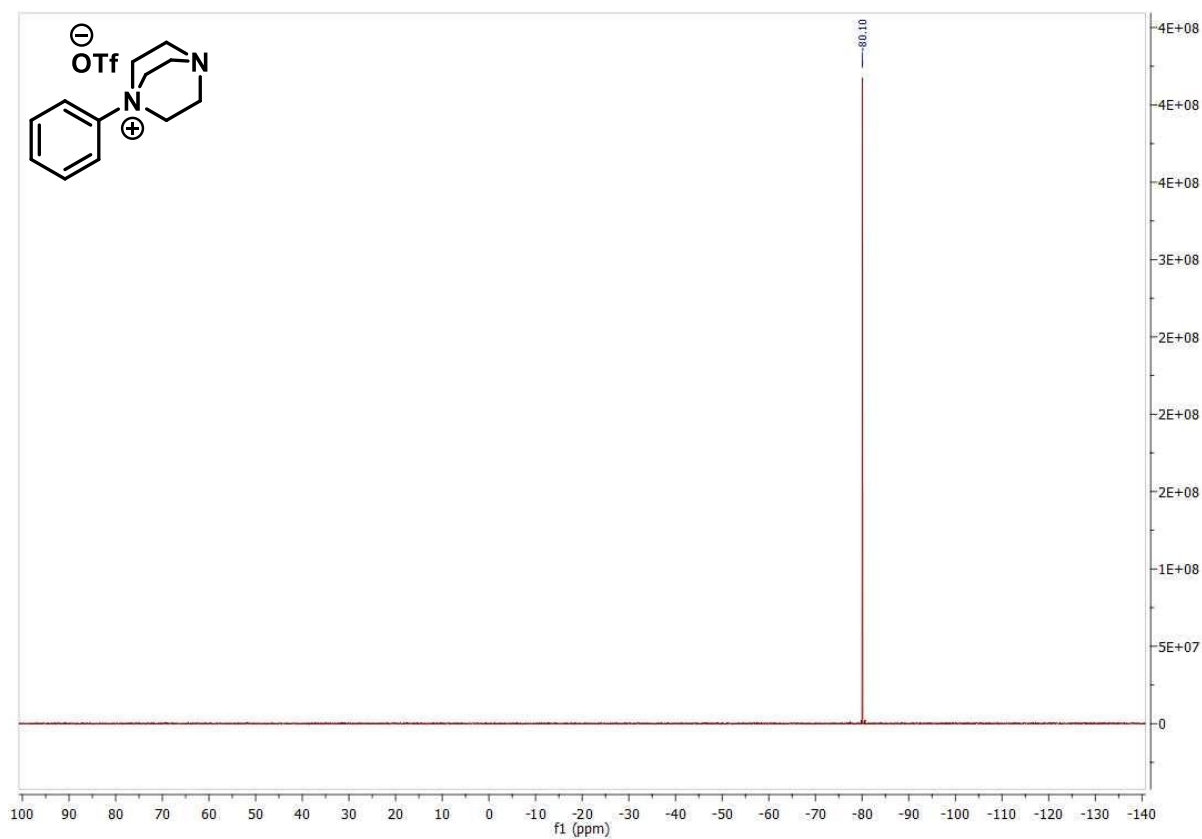
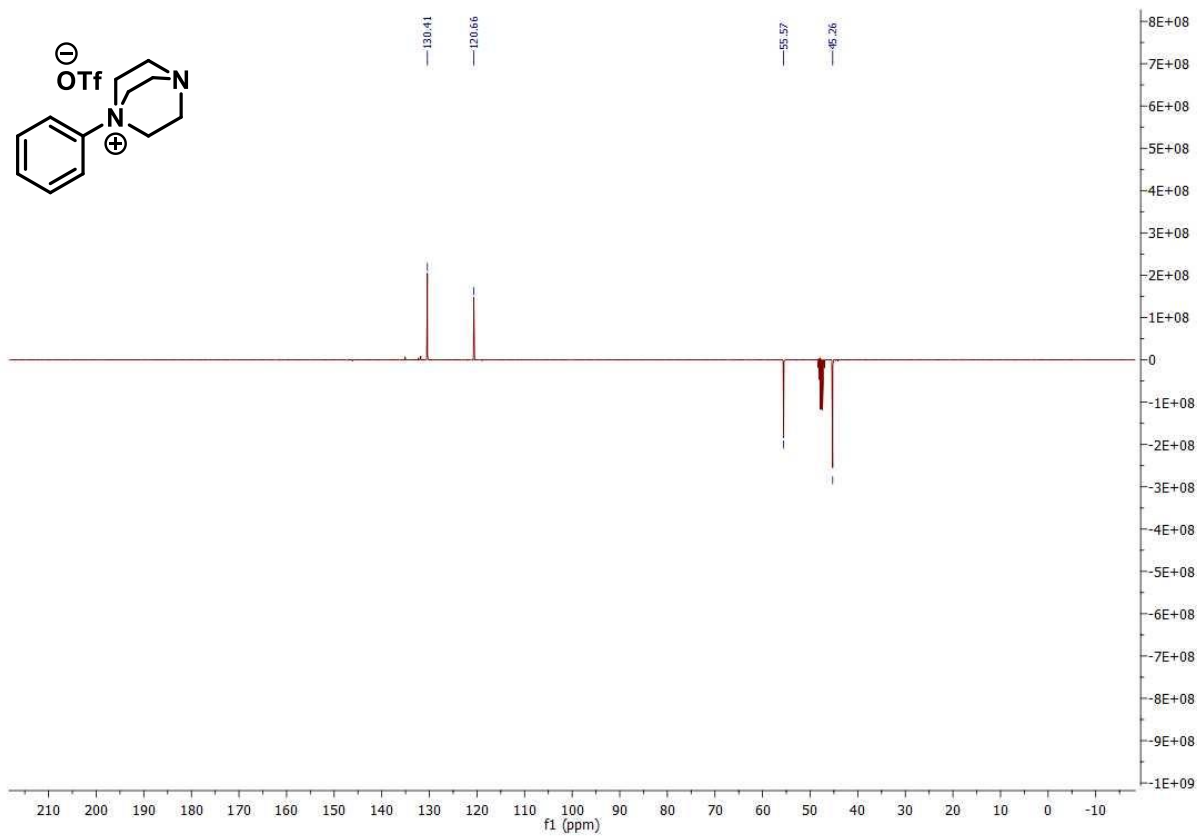
## 7 Experimental Part



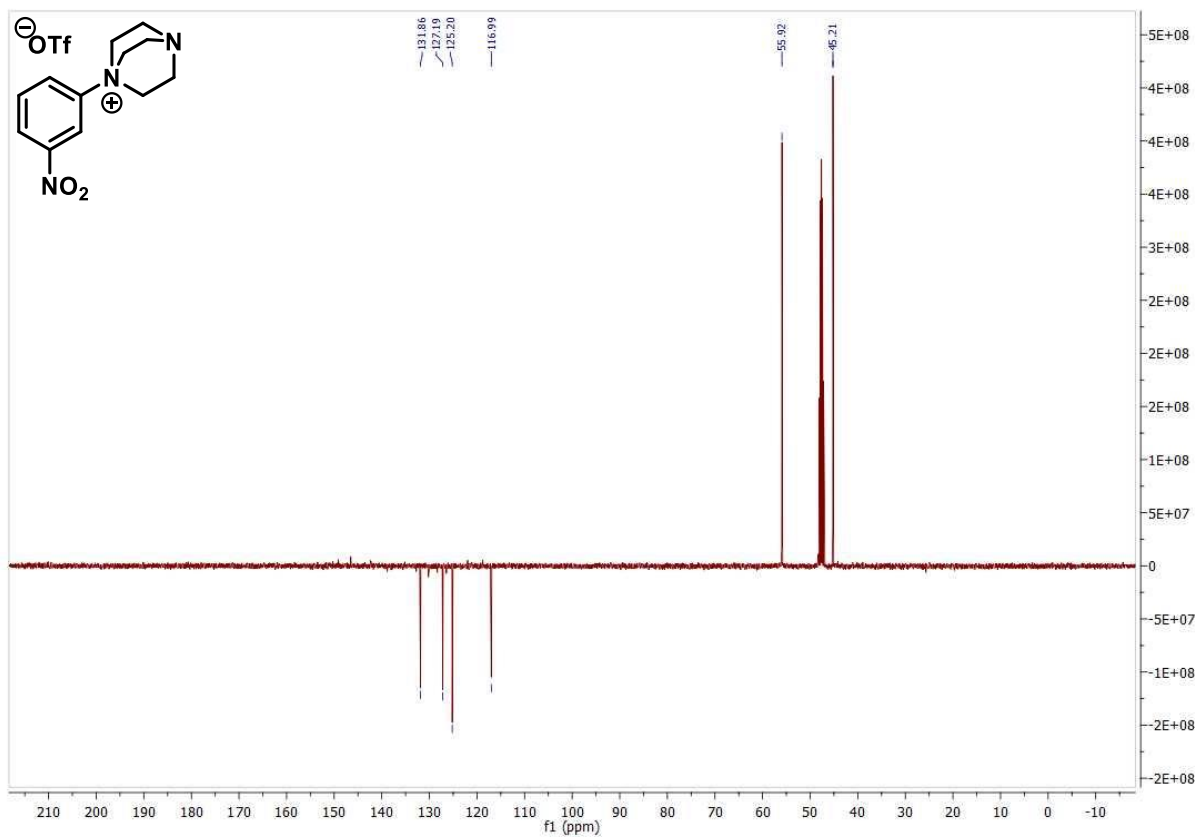
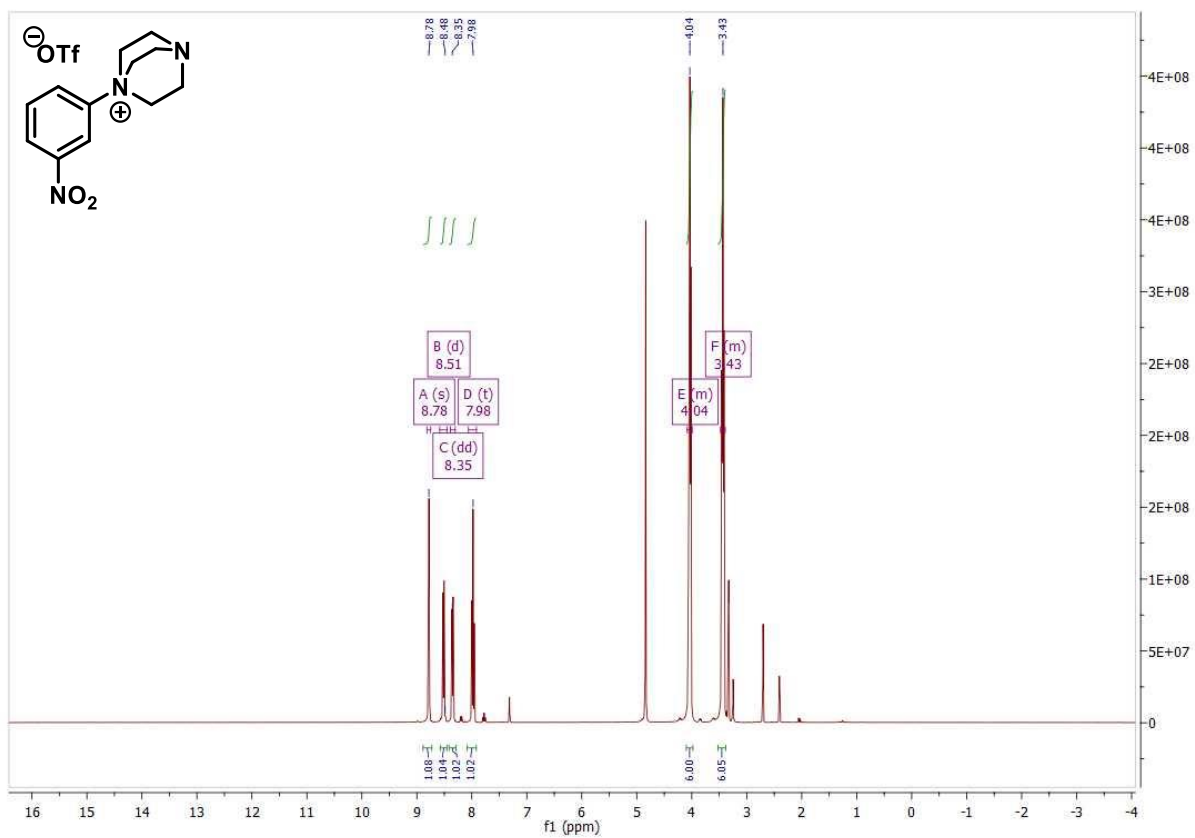
## 7 Experimental Part



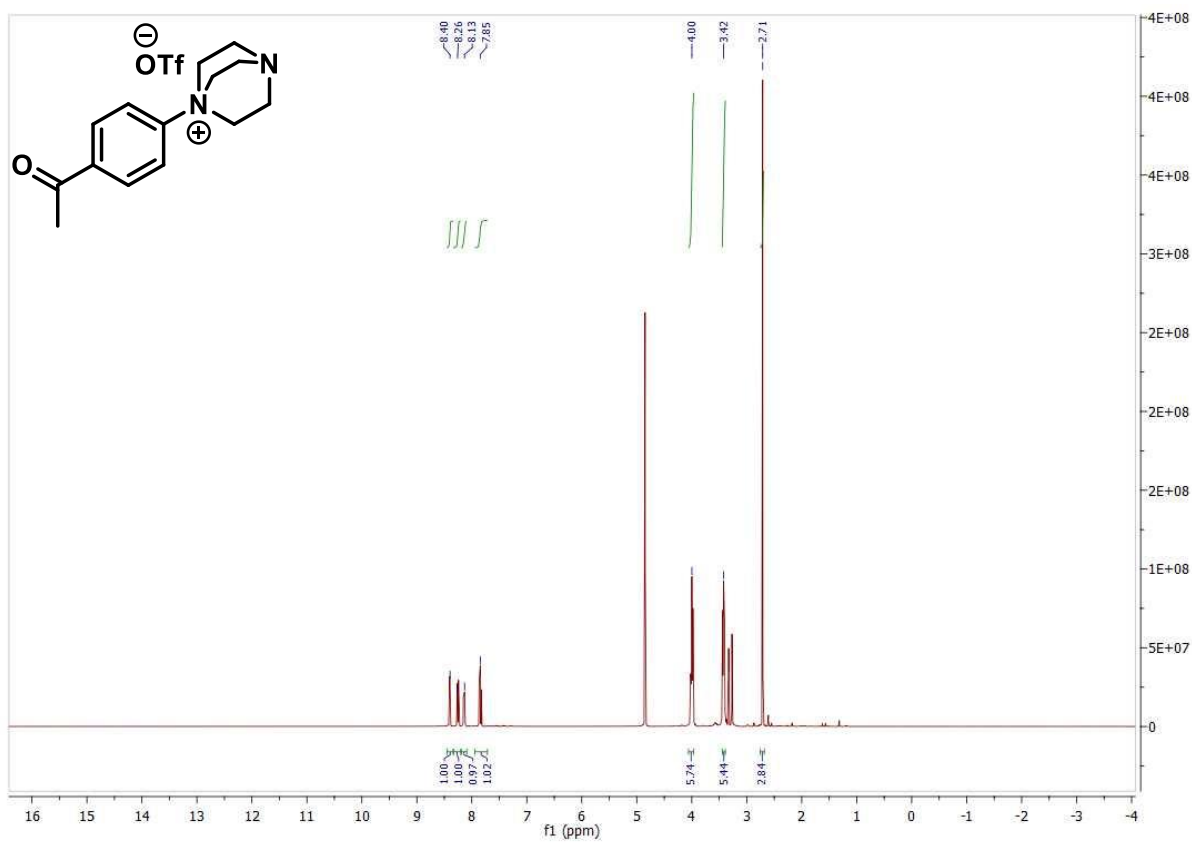
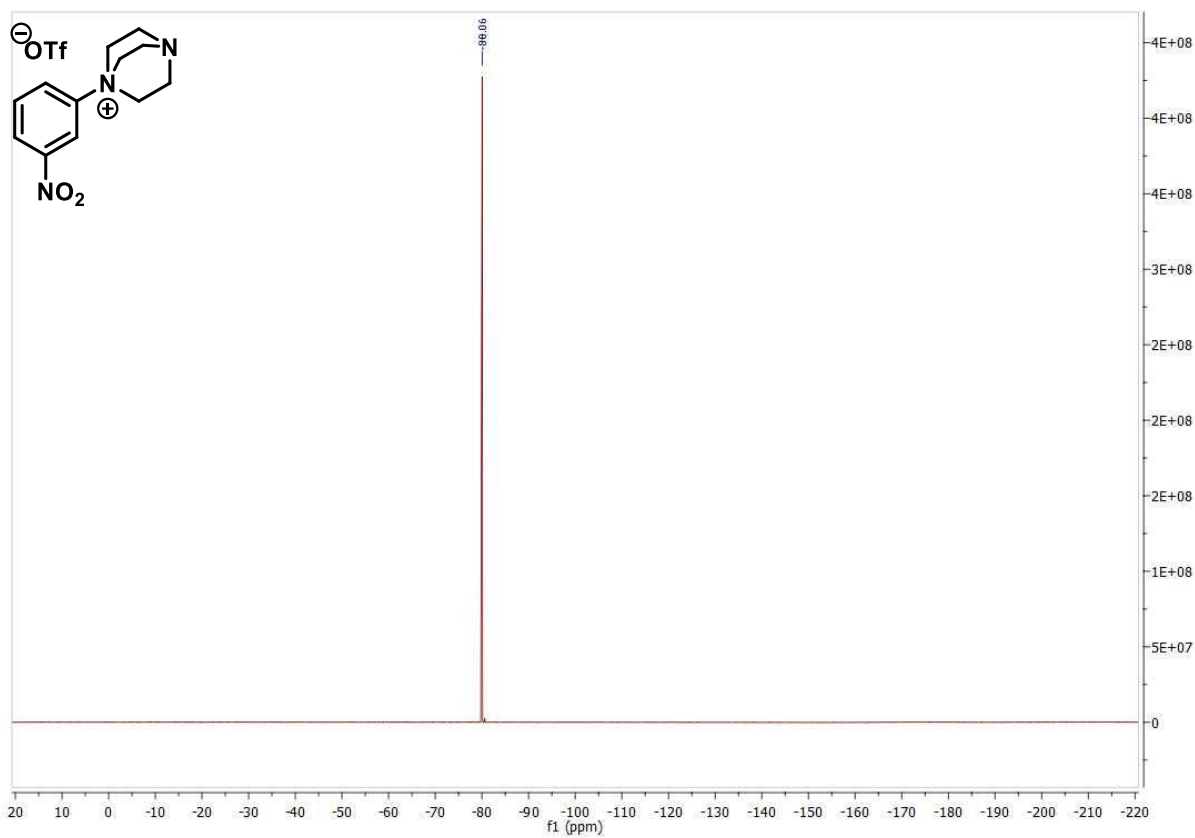
## 7 Experimental Part



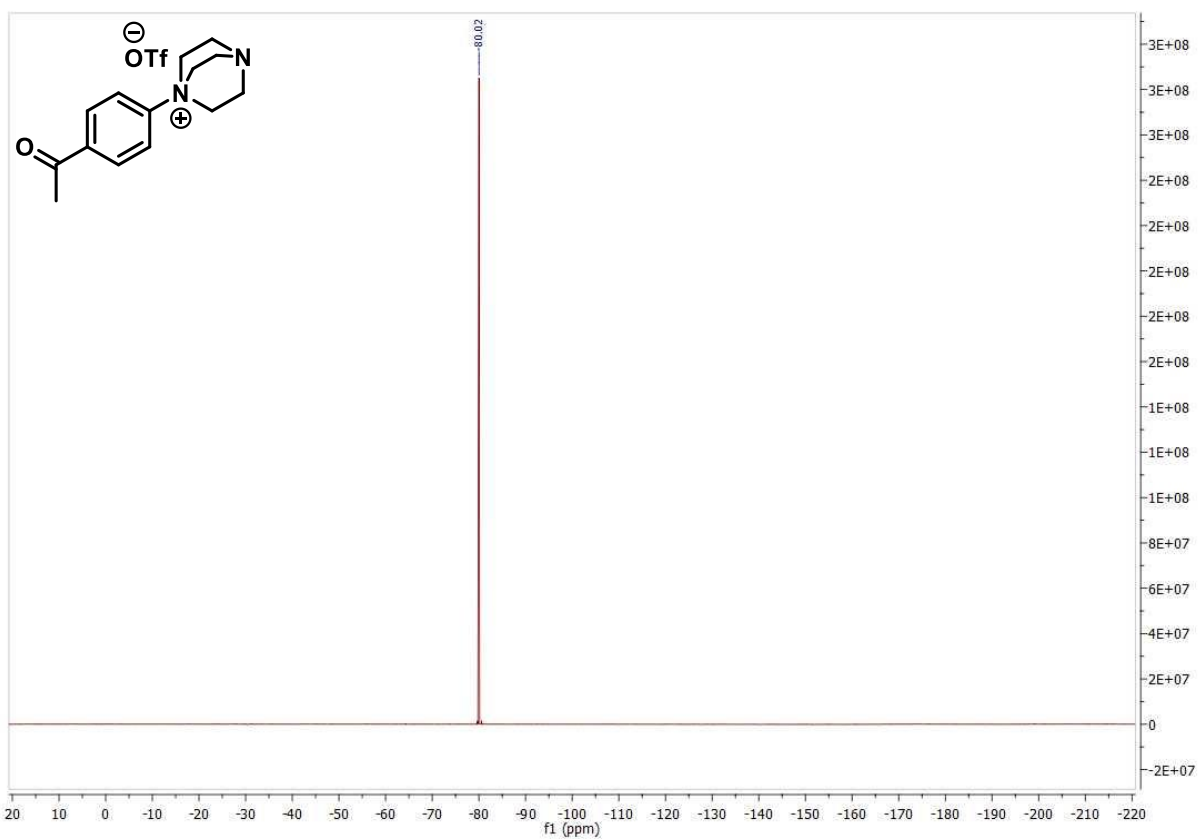
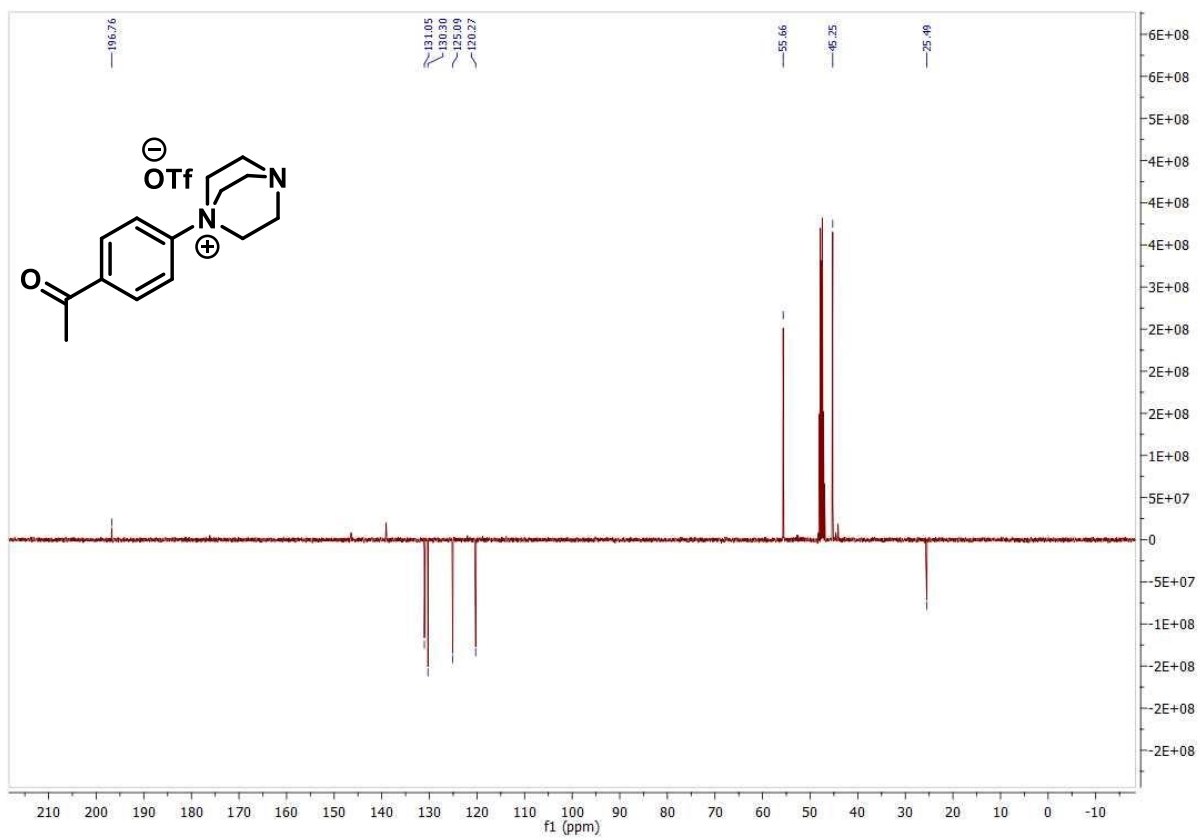
## 7 Experimental Part



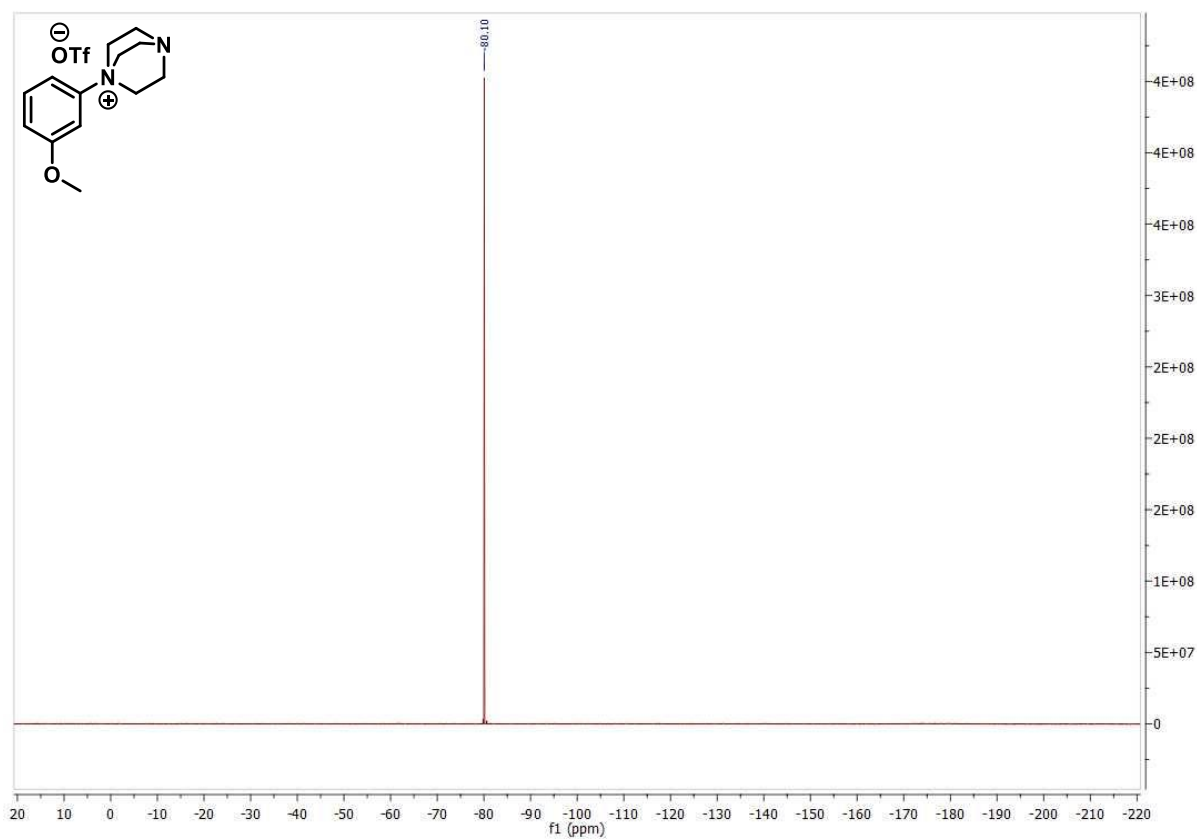
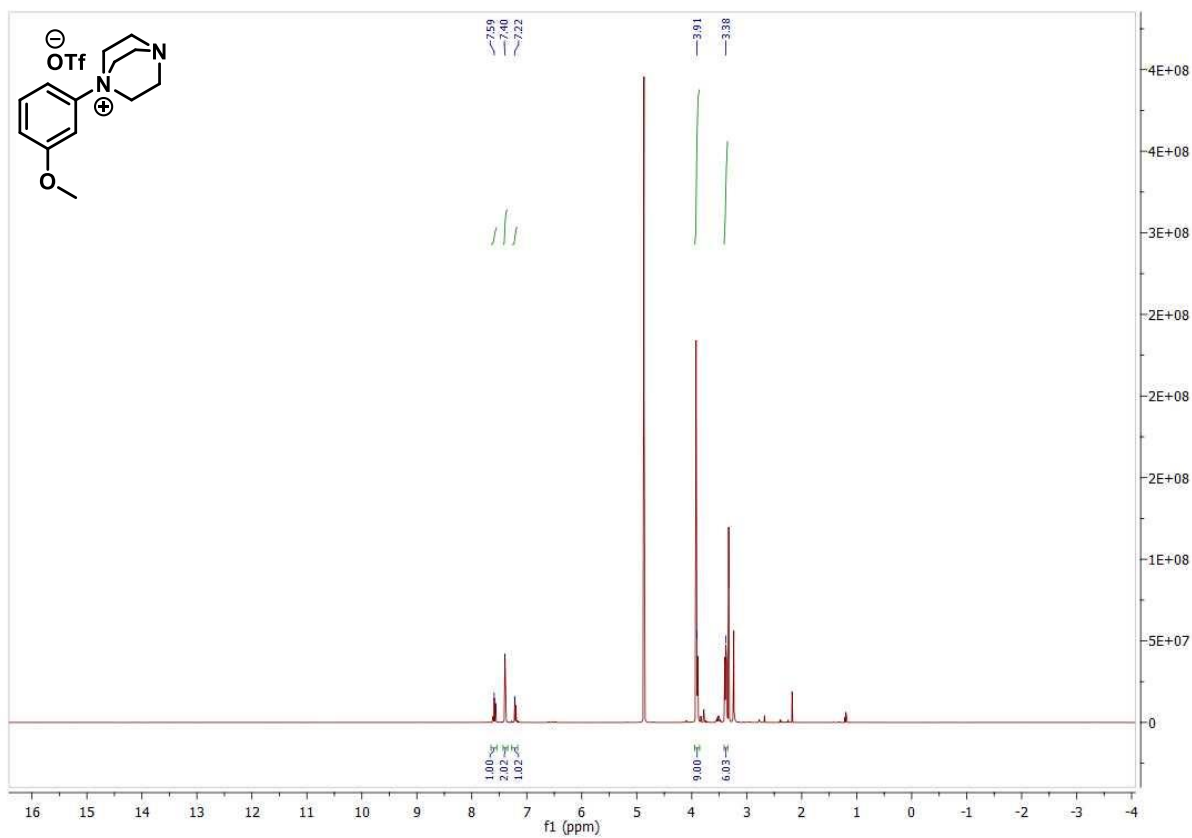
## 7 Experimental Part



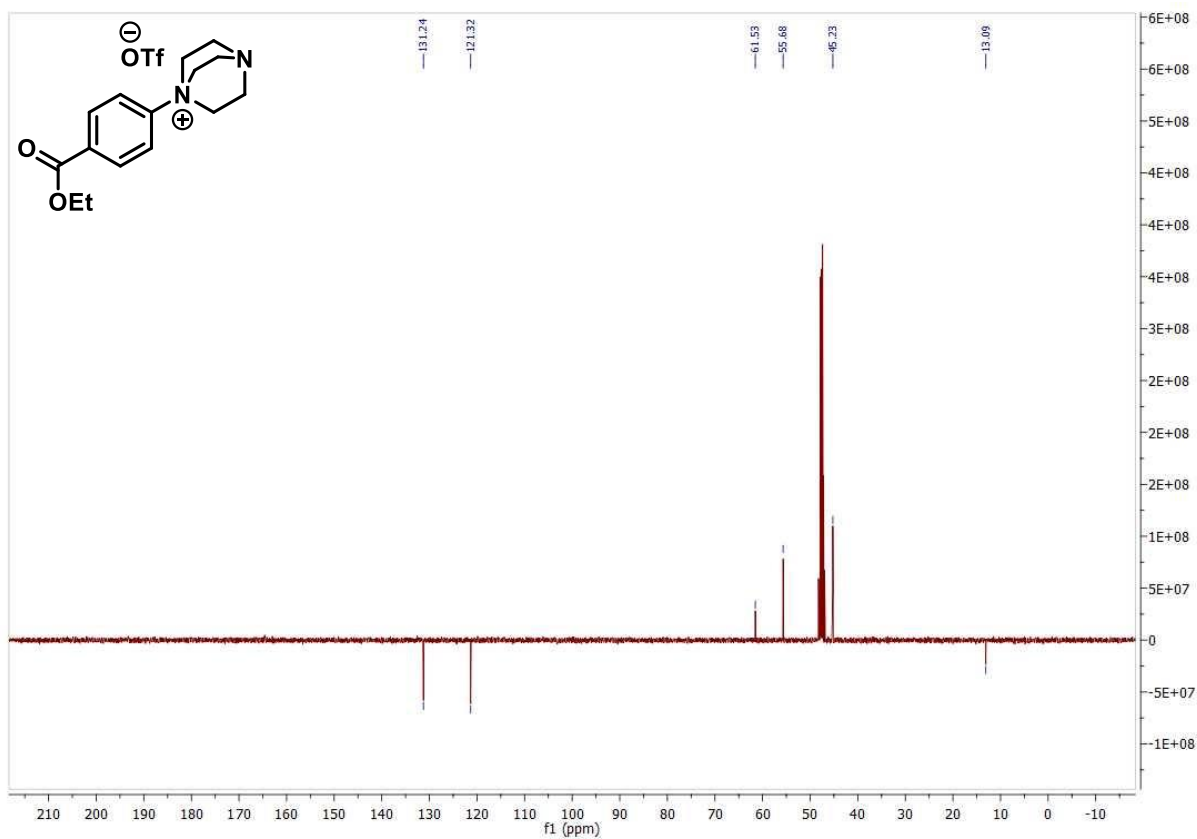
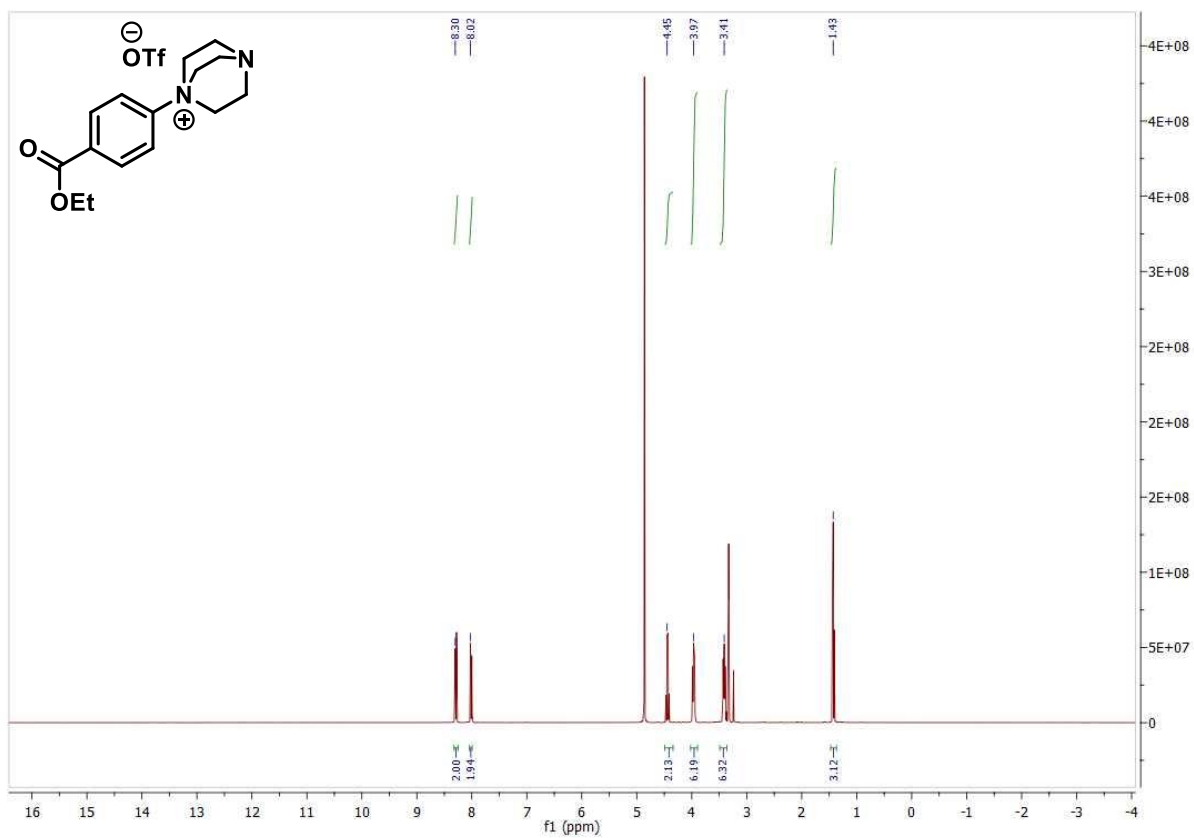
## 7 Experimental Part



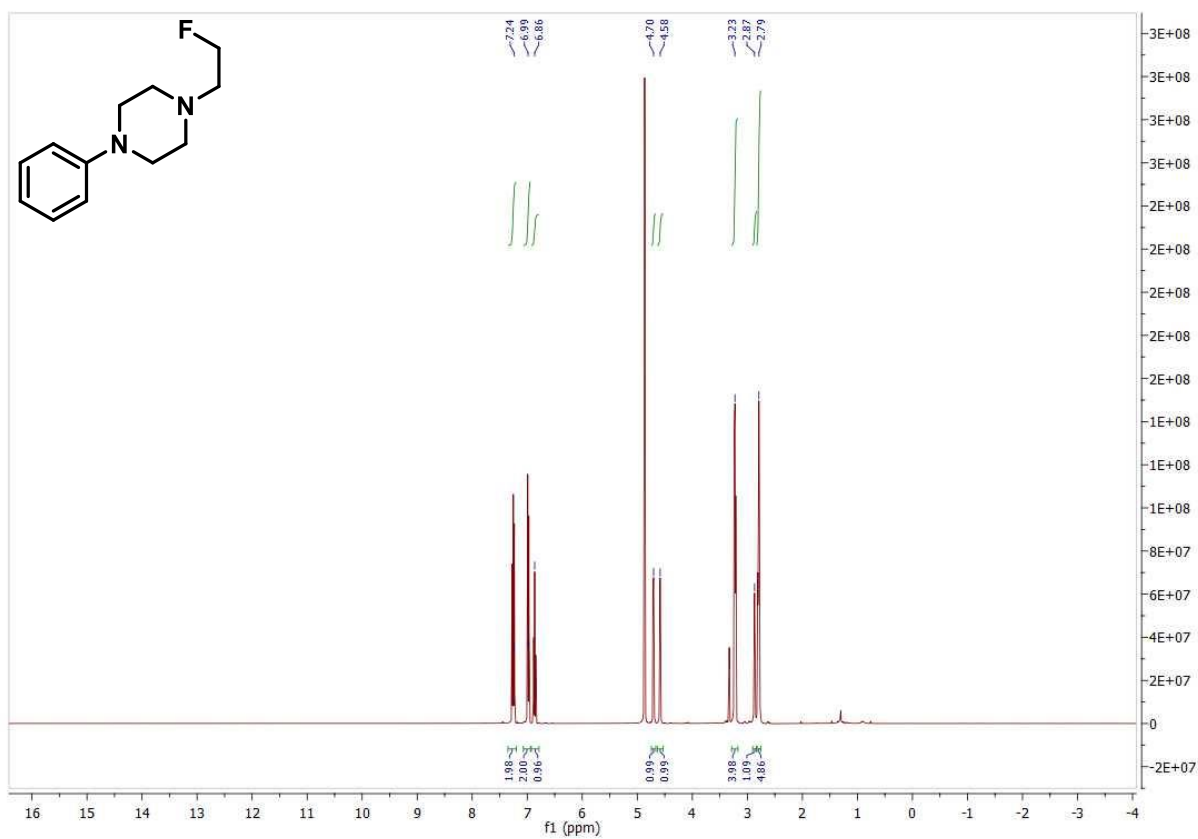
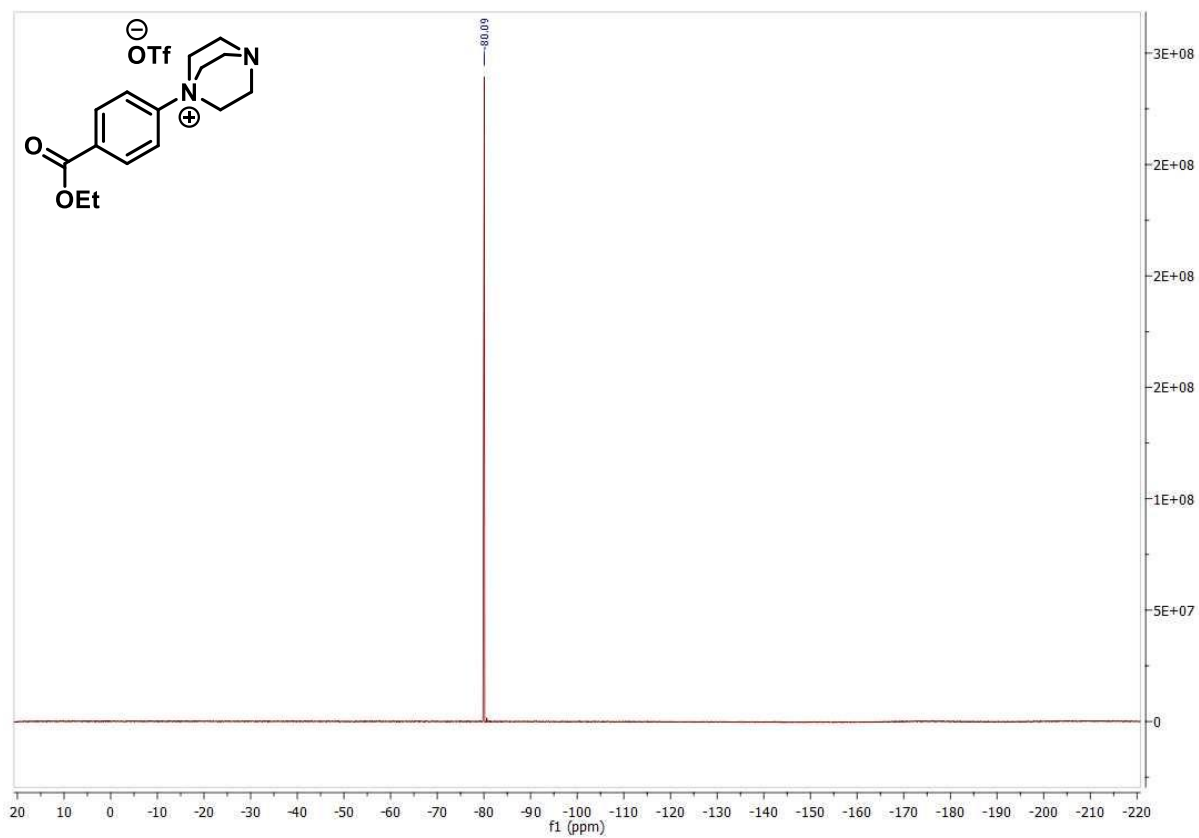
## 7 Experimental Part



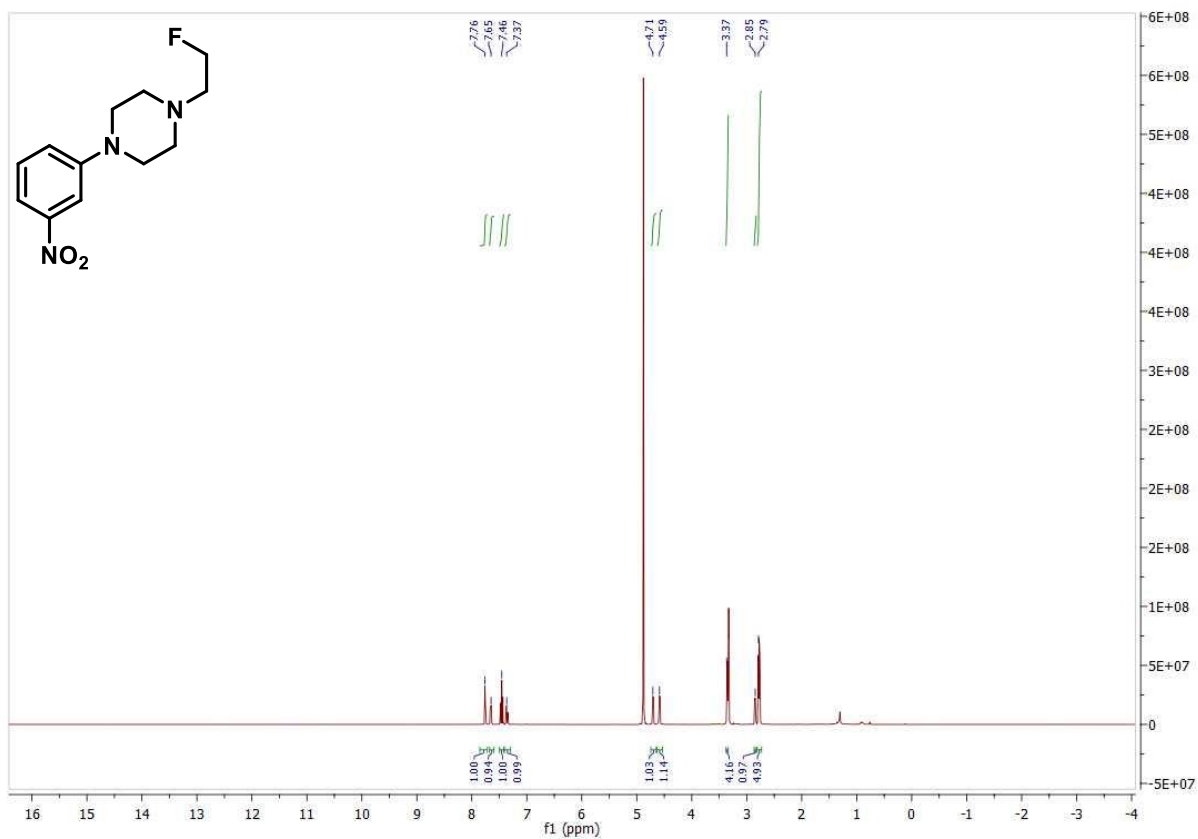
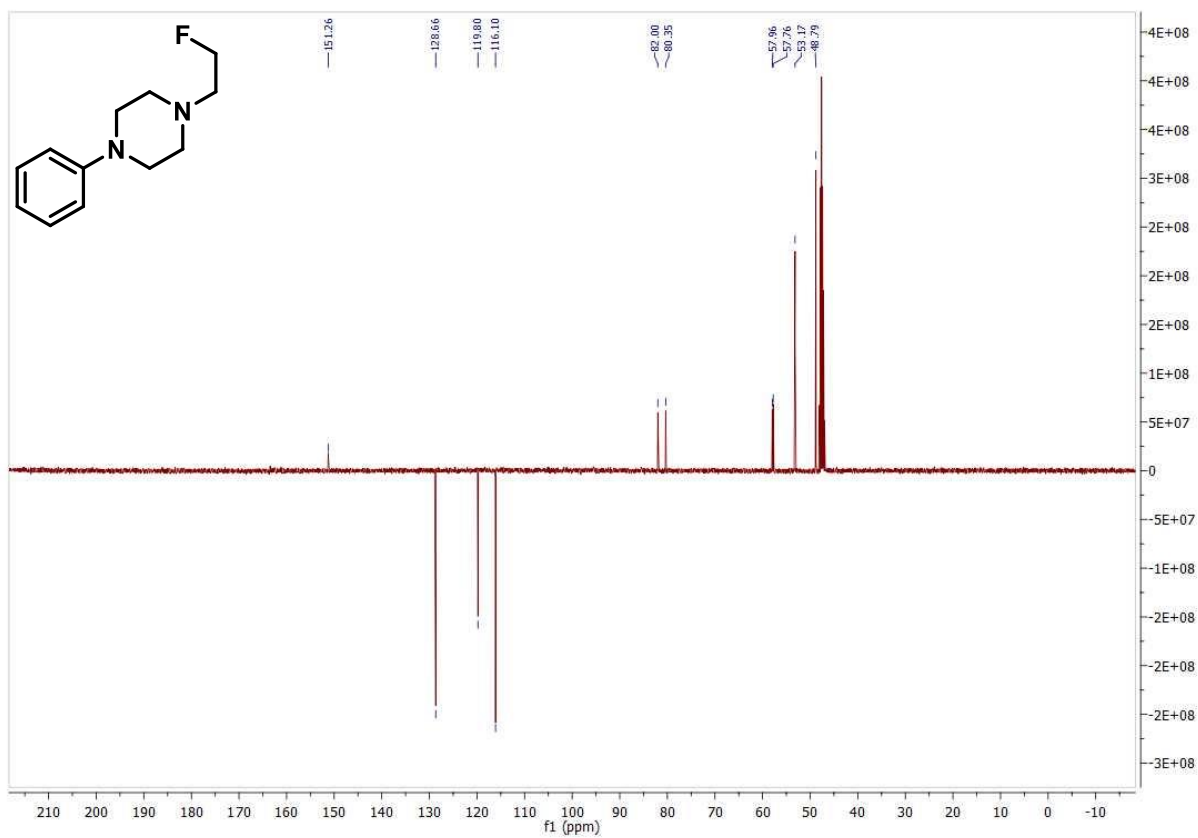
## 7 Experimental Part



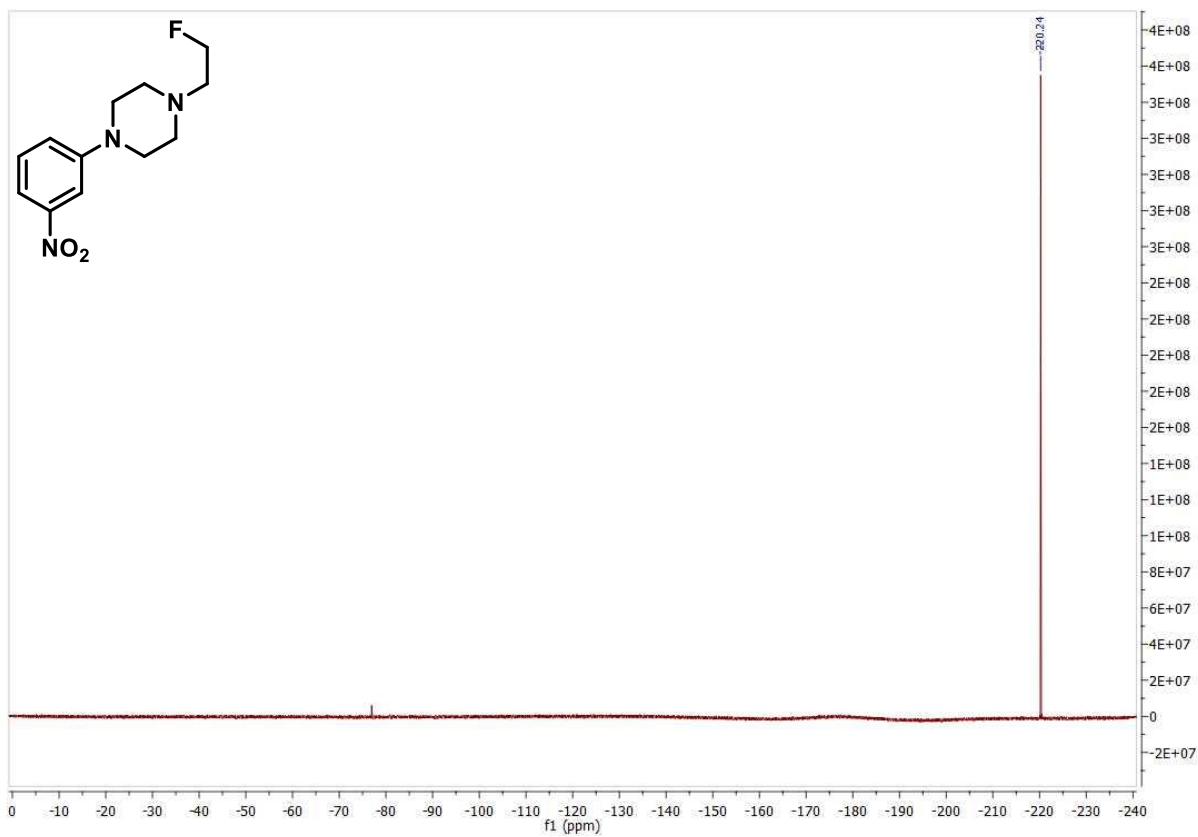
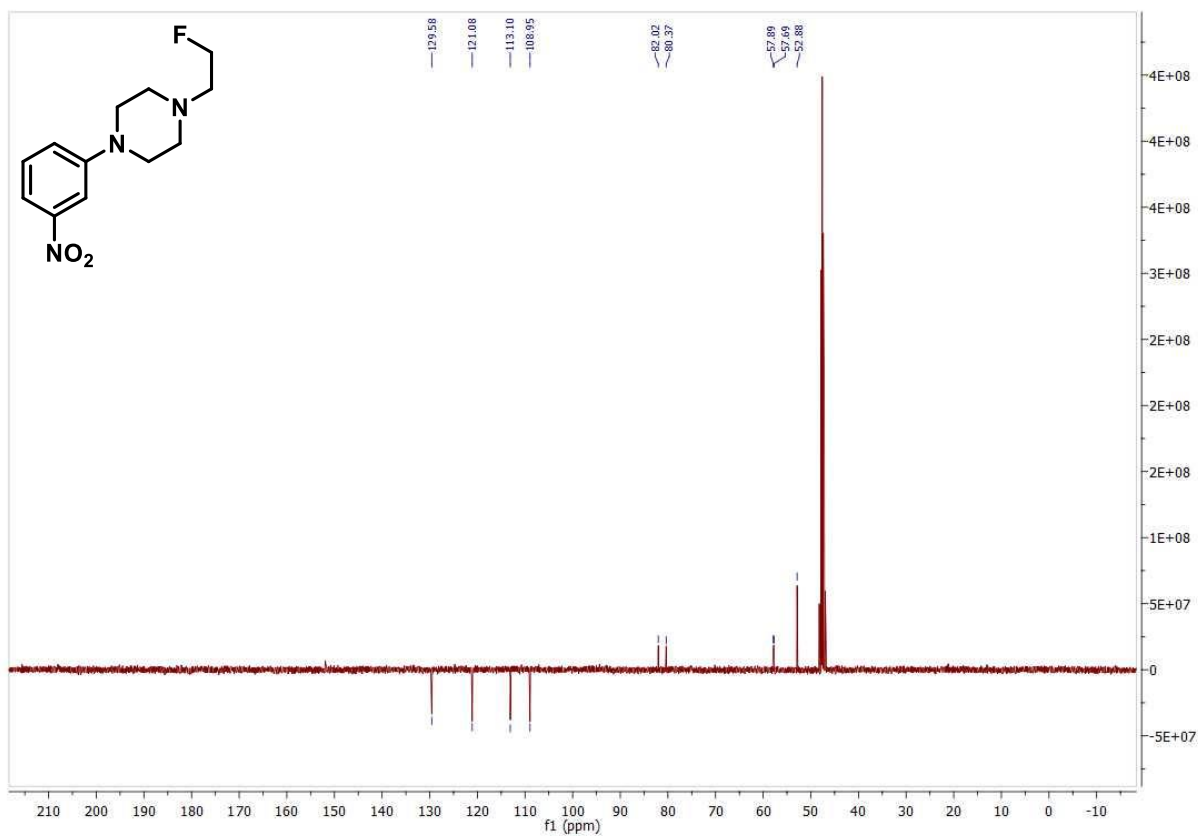
## 7 Experimental Part



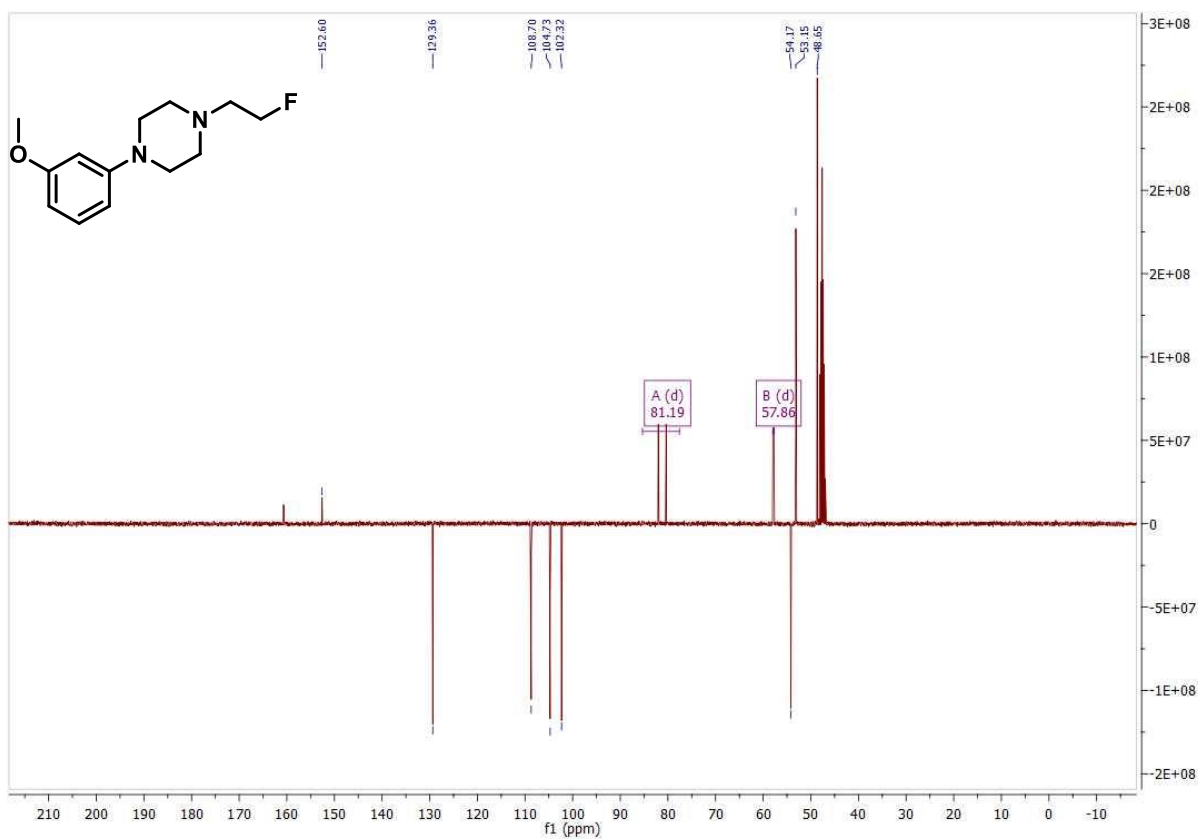
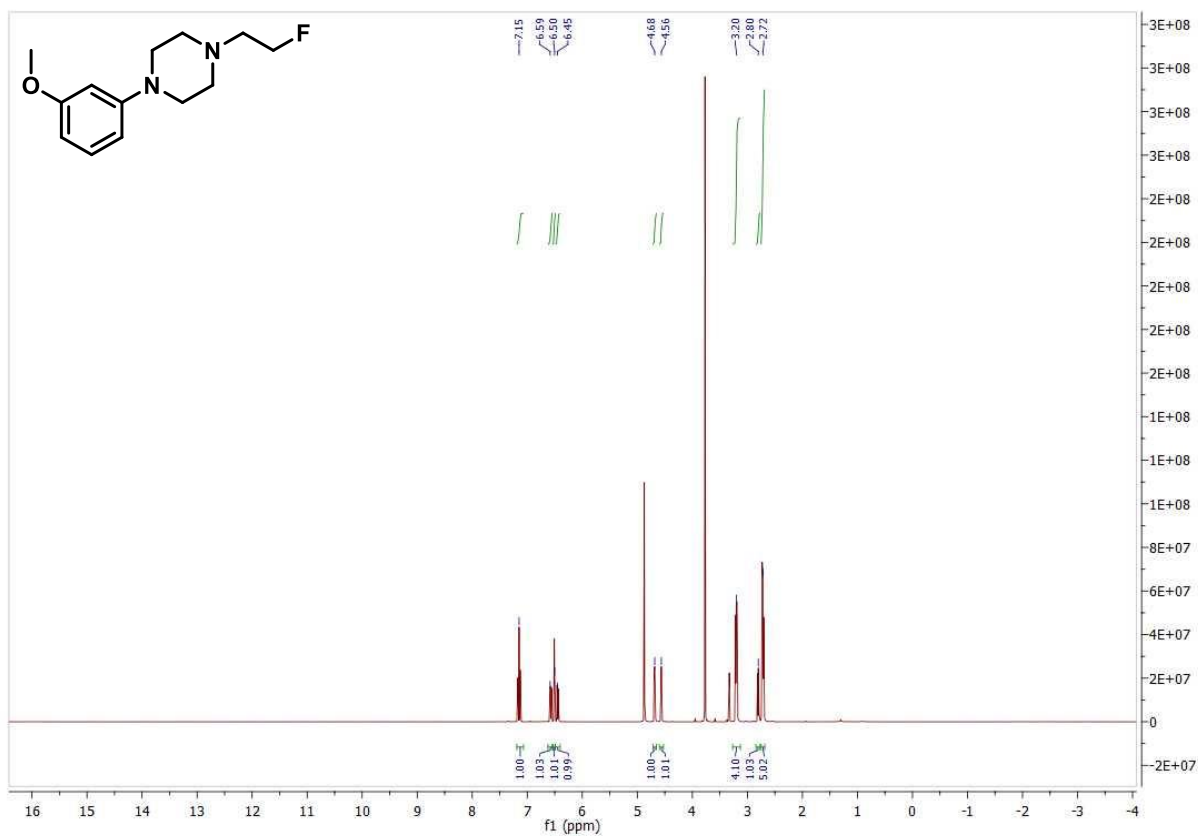
## 7 Experimental Part



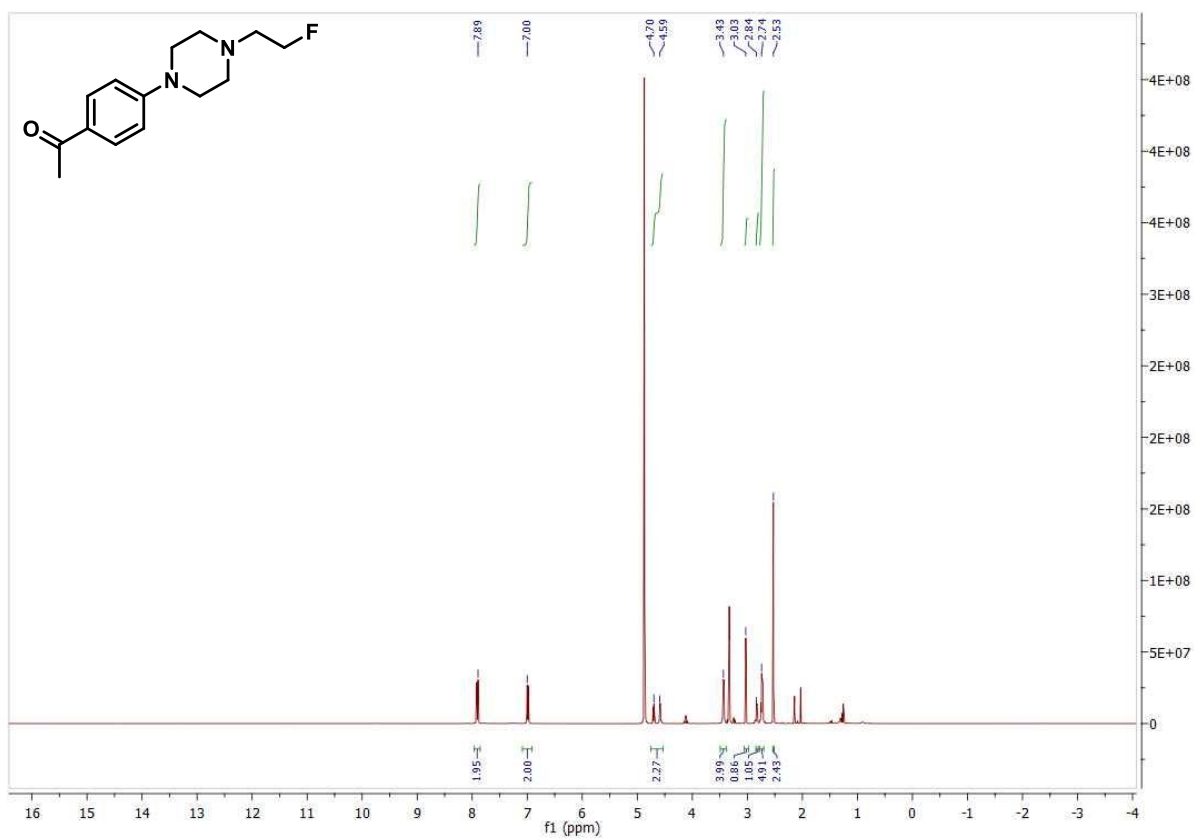
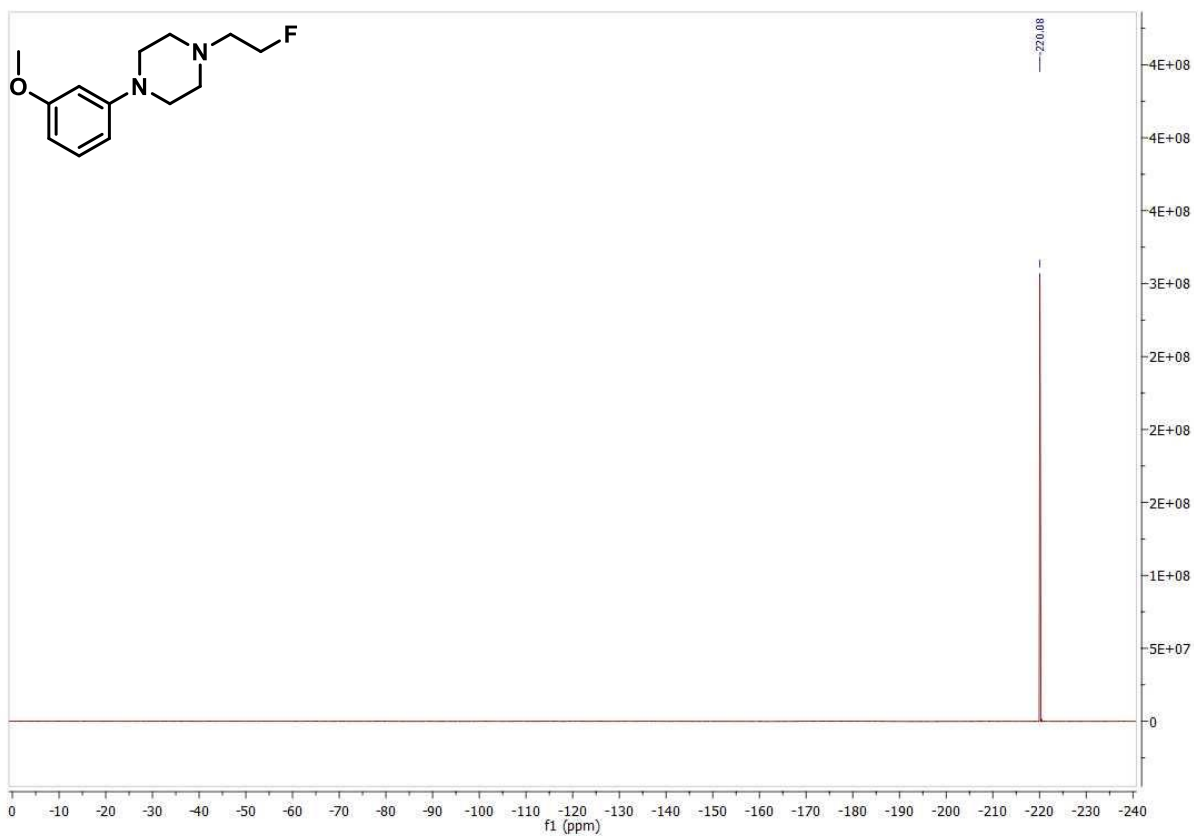
## 7 Experimental Part



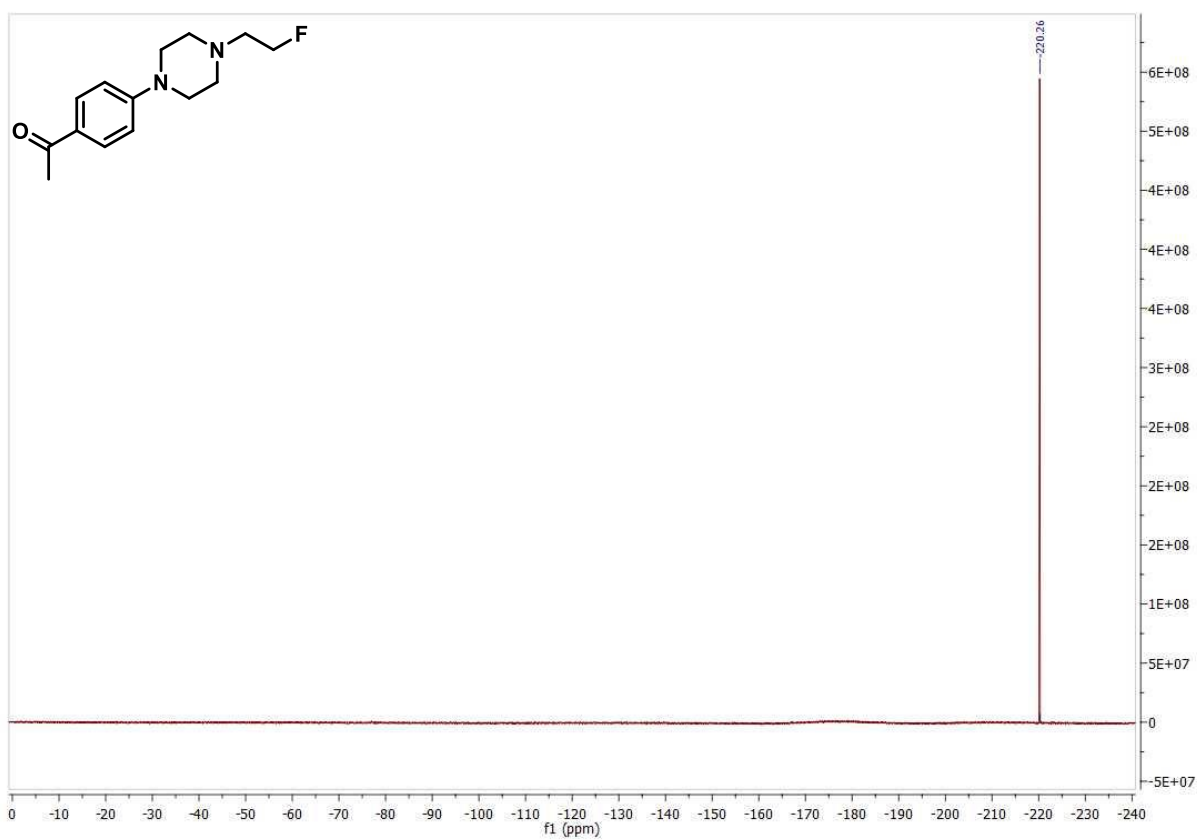
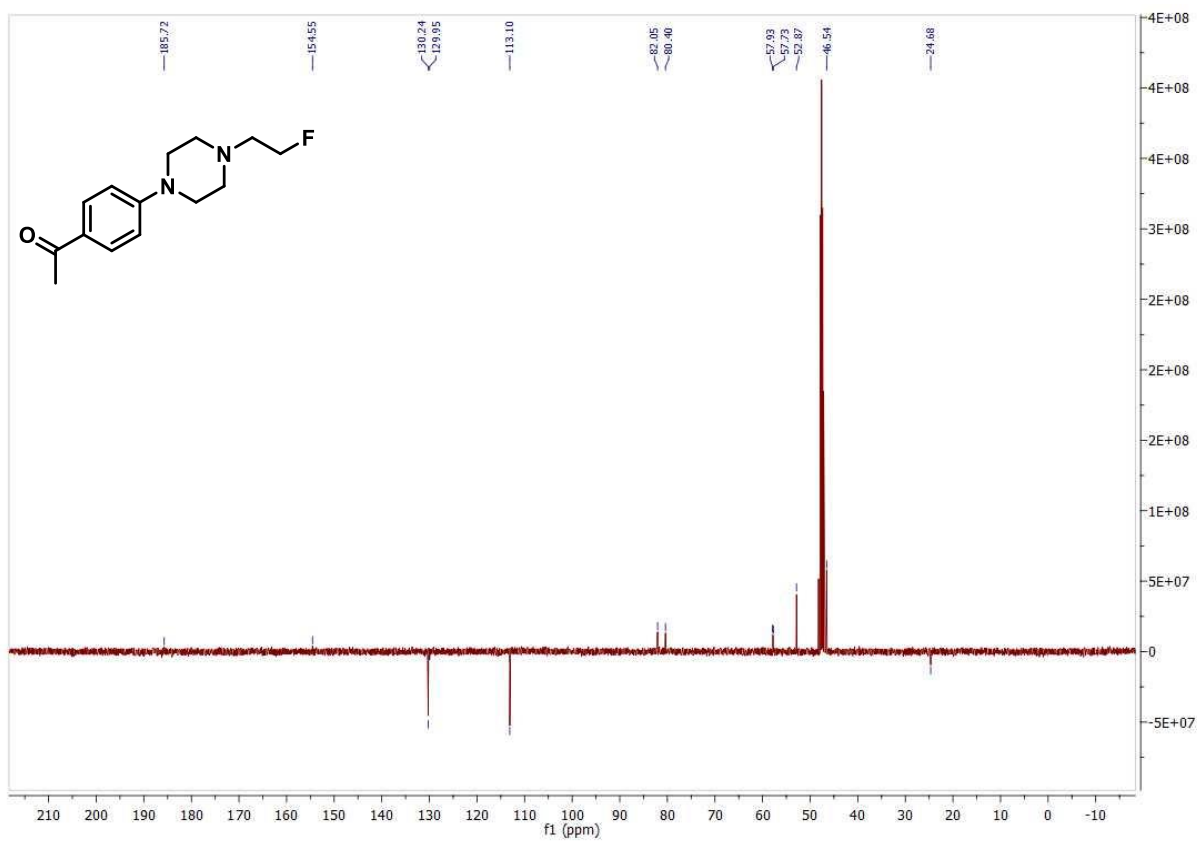
## 7 Experimental Part



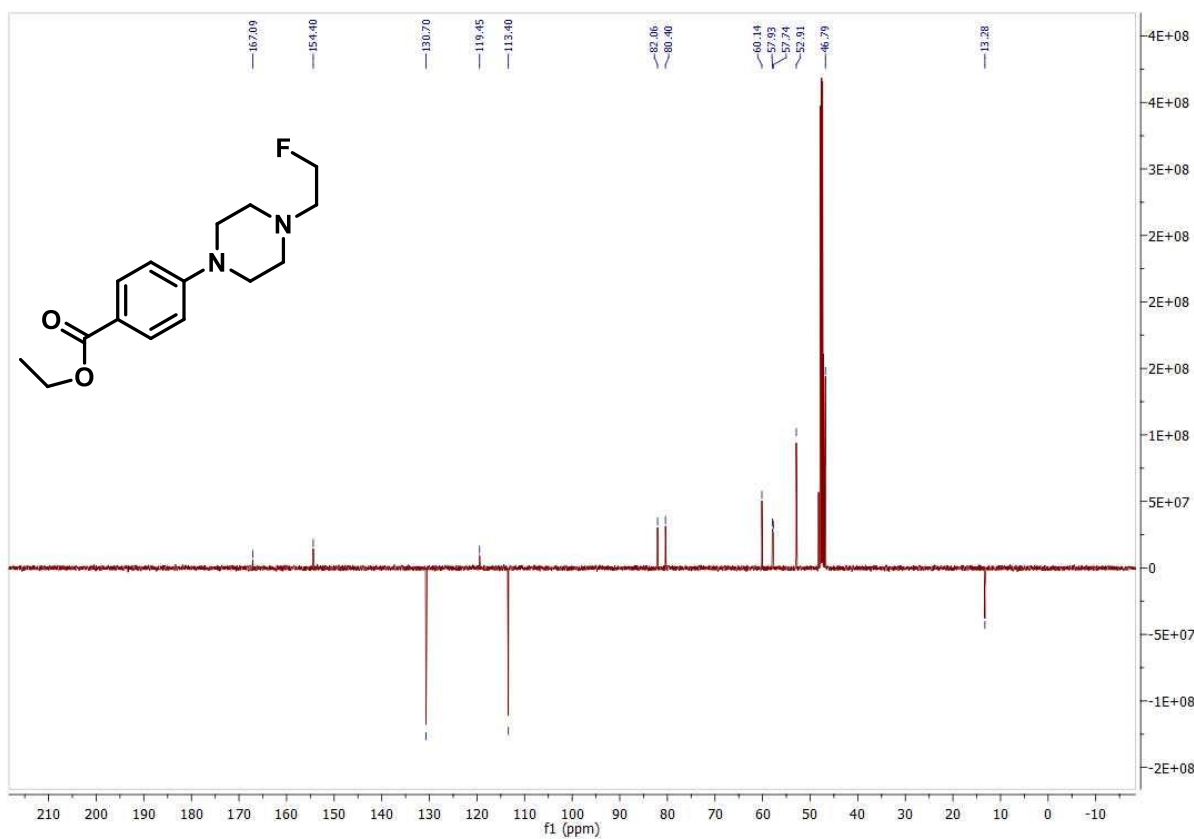
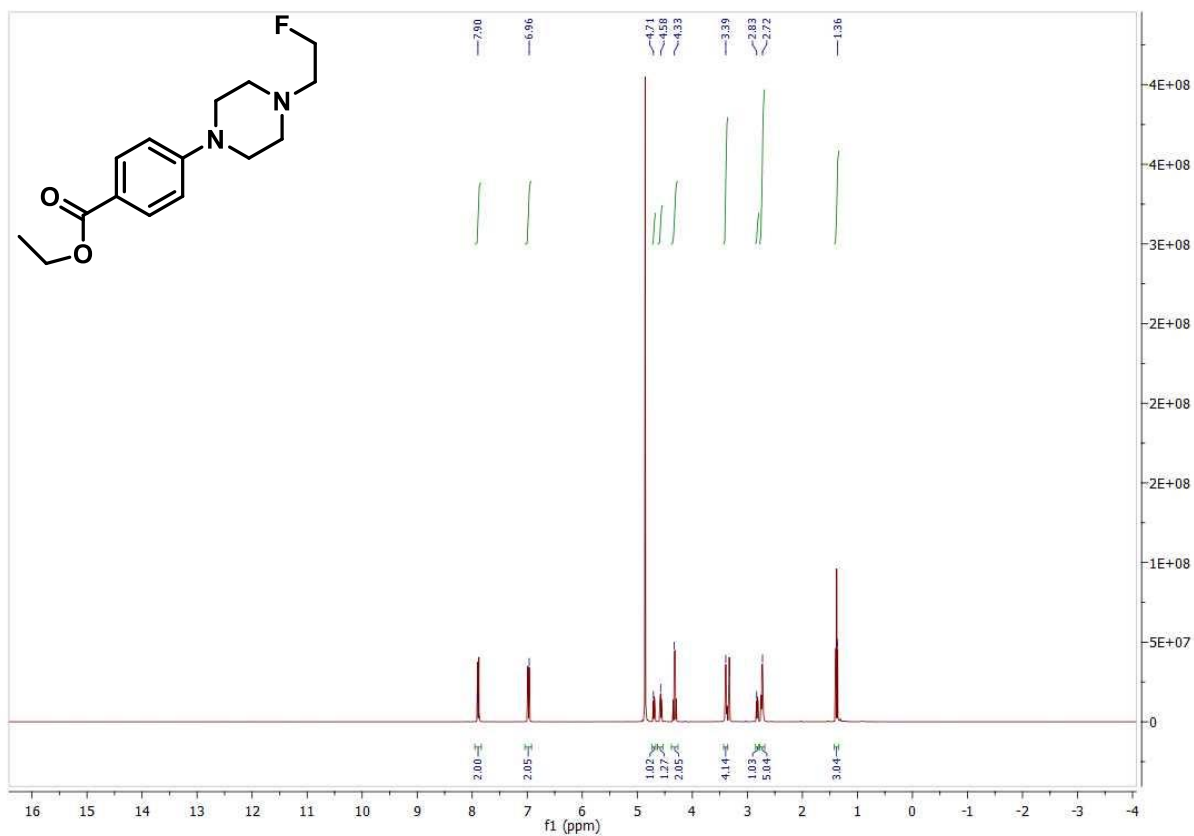
## 7 Experimental Part



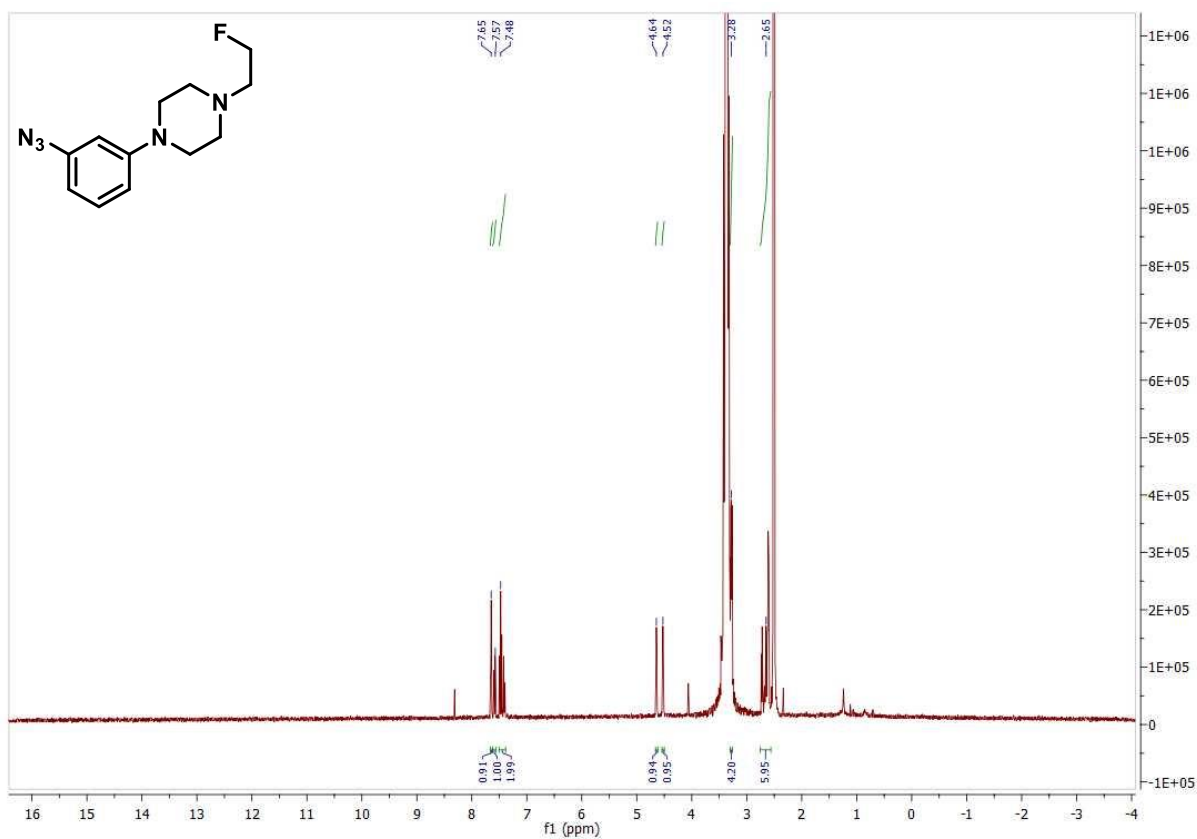
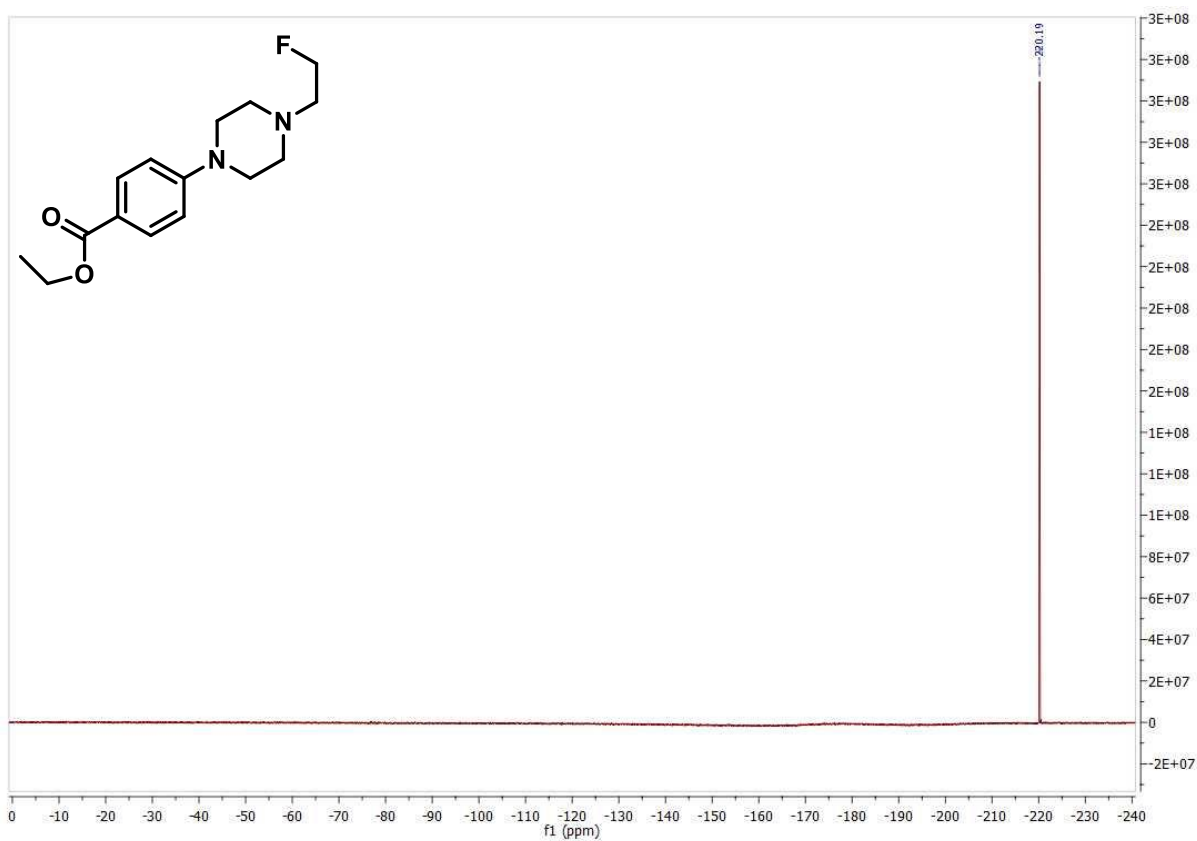
## 7 Experimental Part



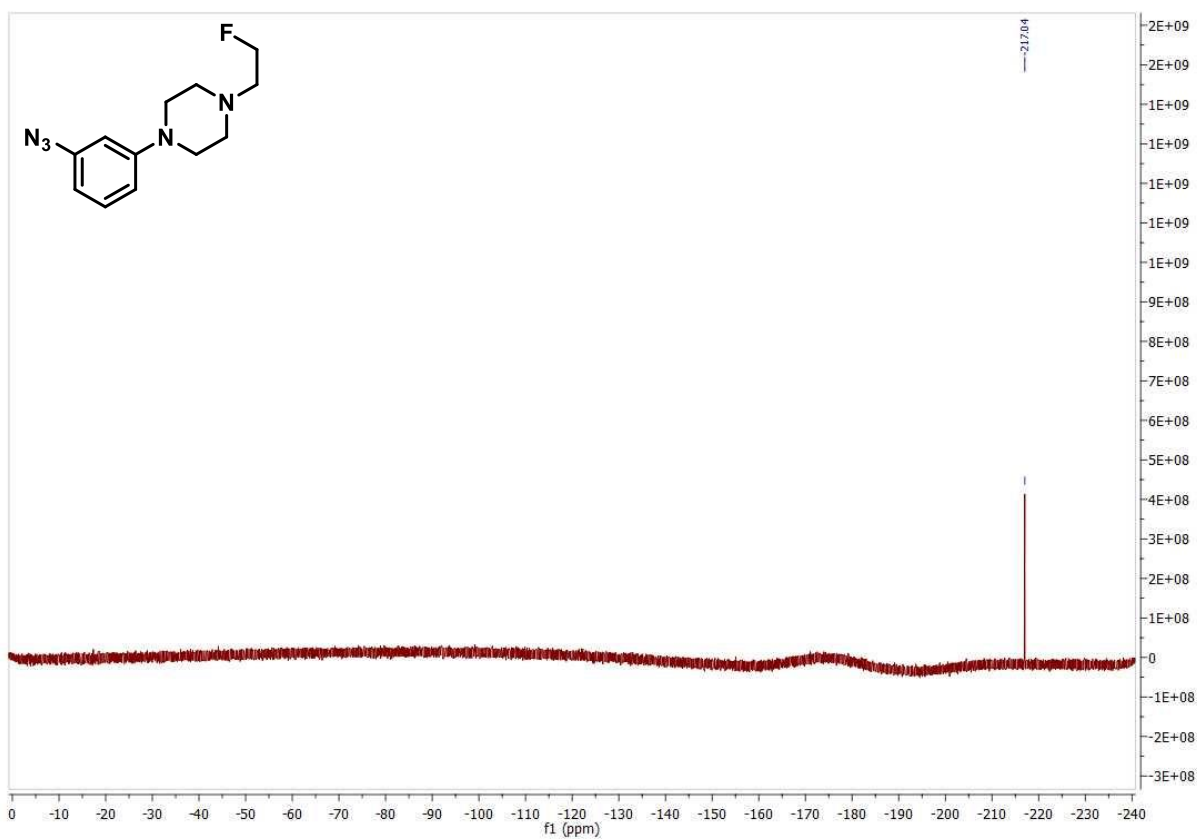
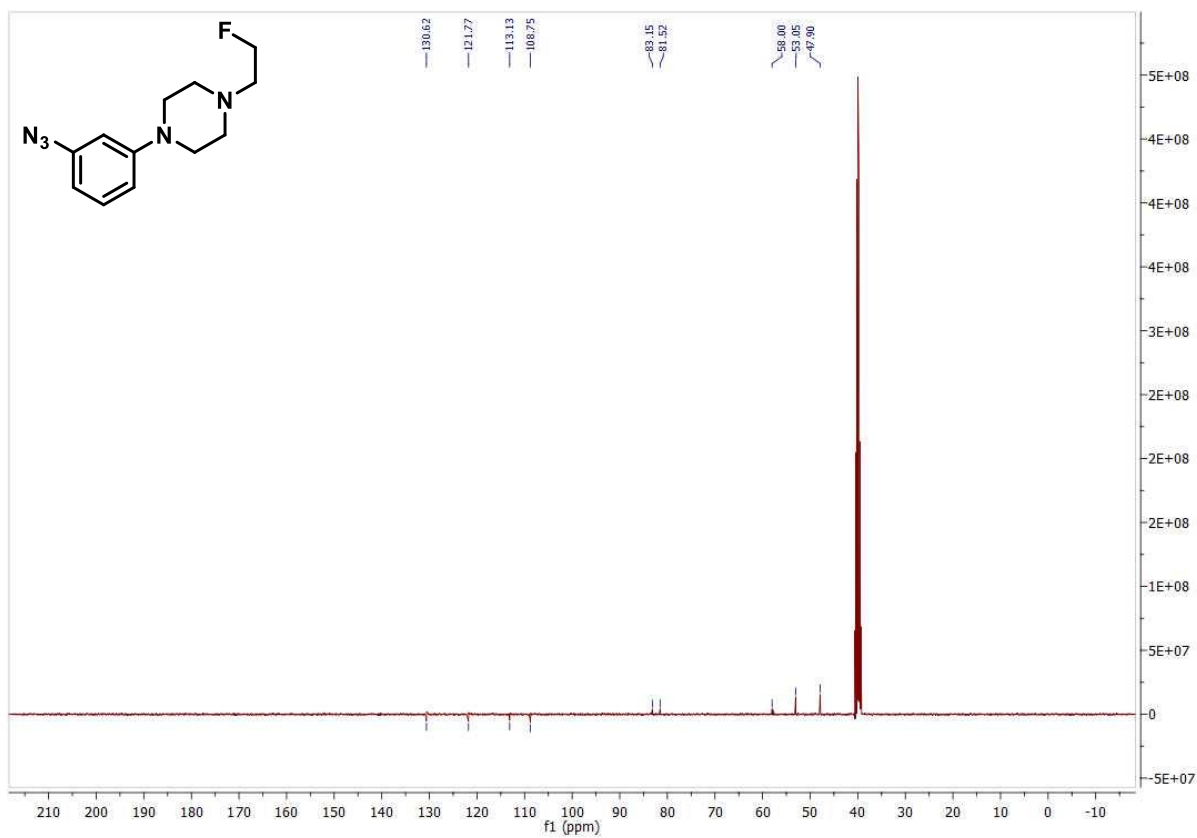
## 7 Experimental Part



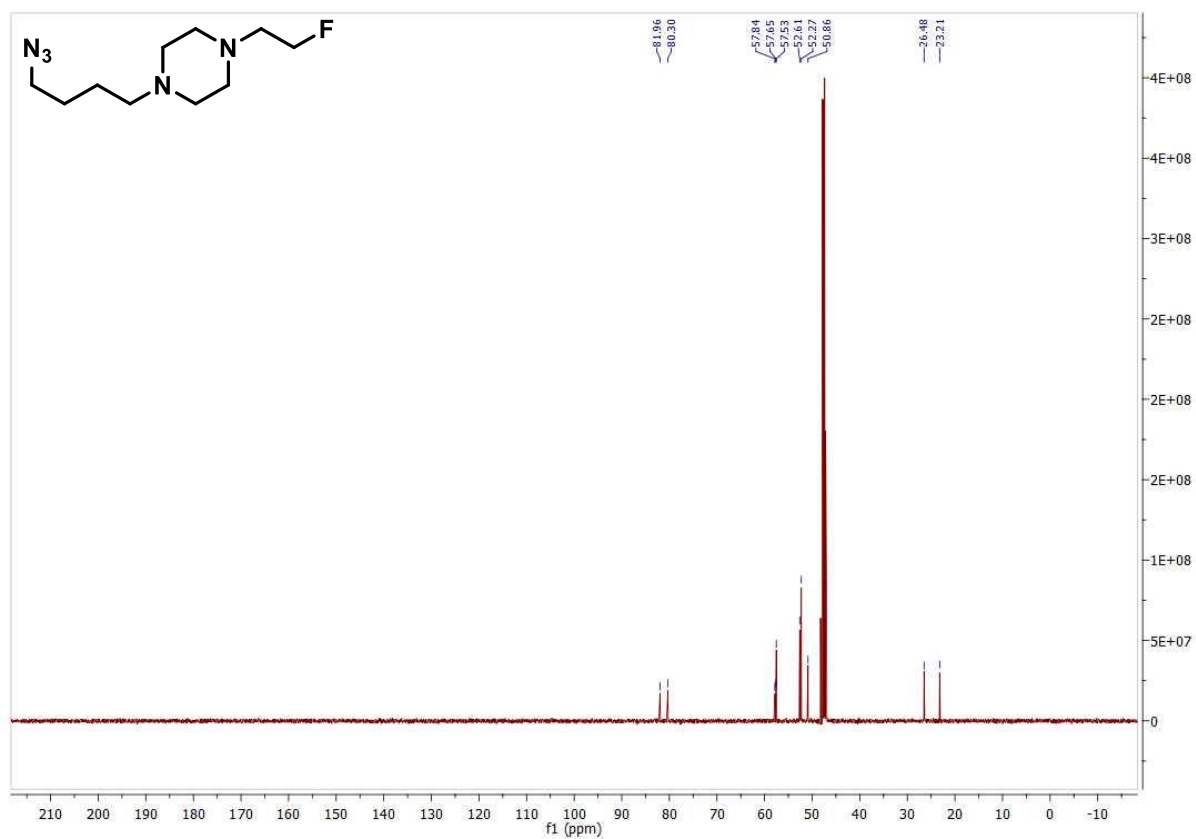
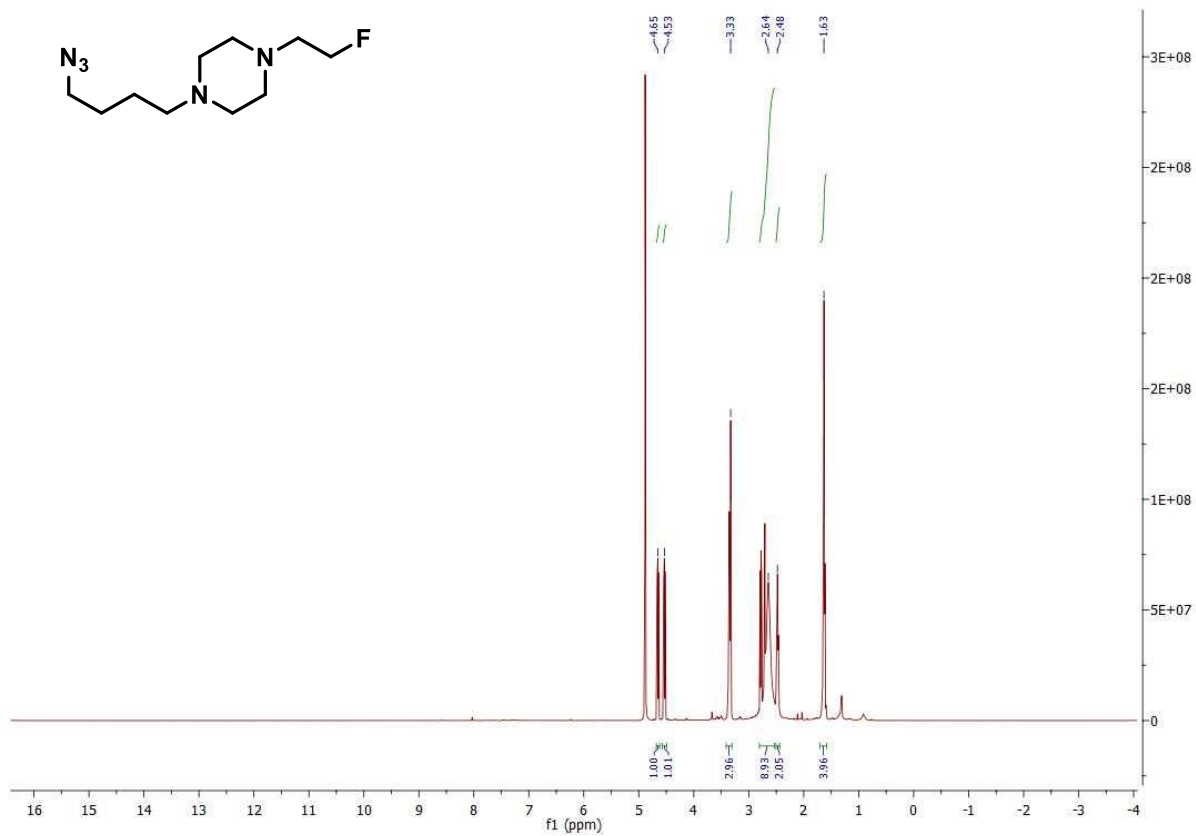
## 7 Experimental Part



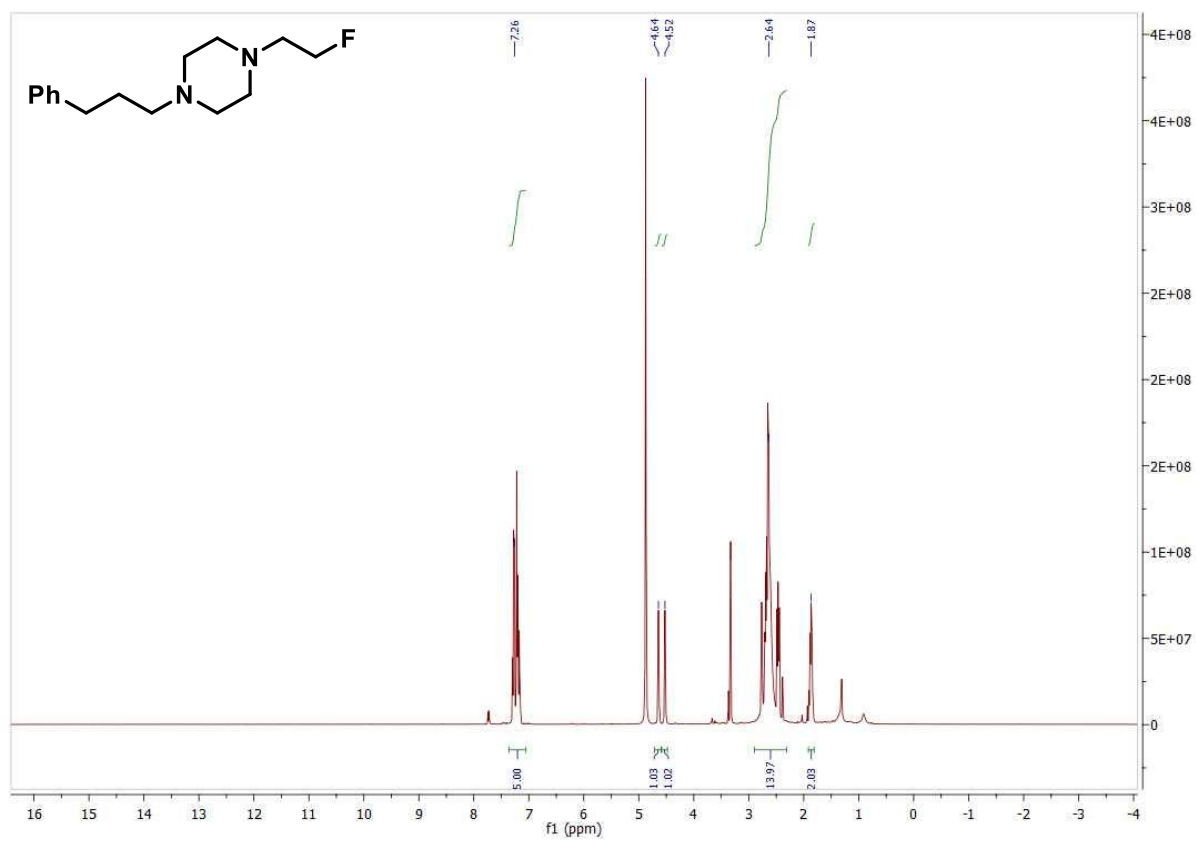
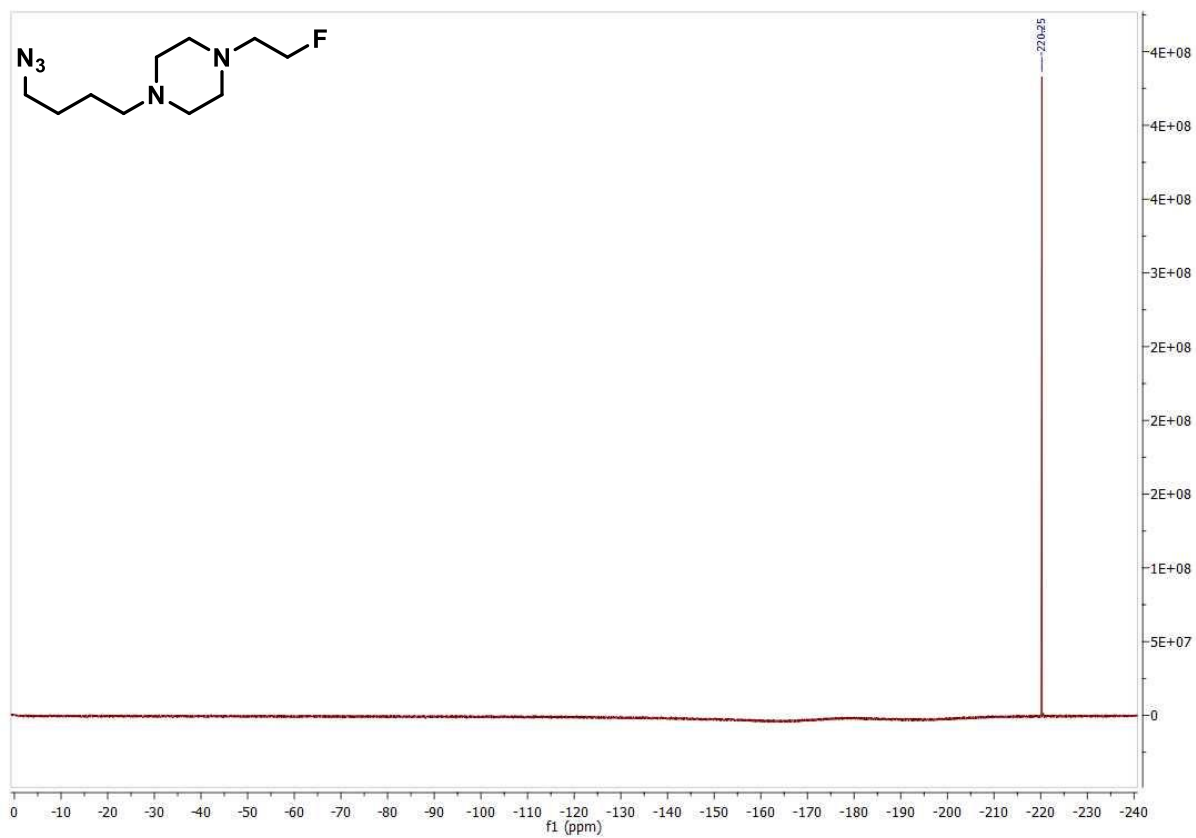
## 7 Experimental Part



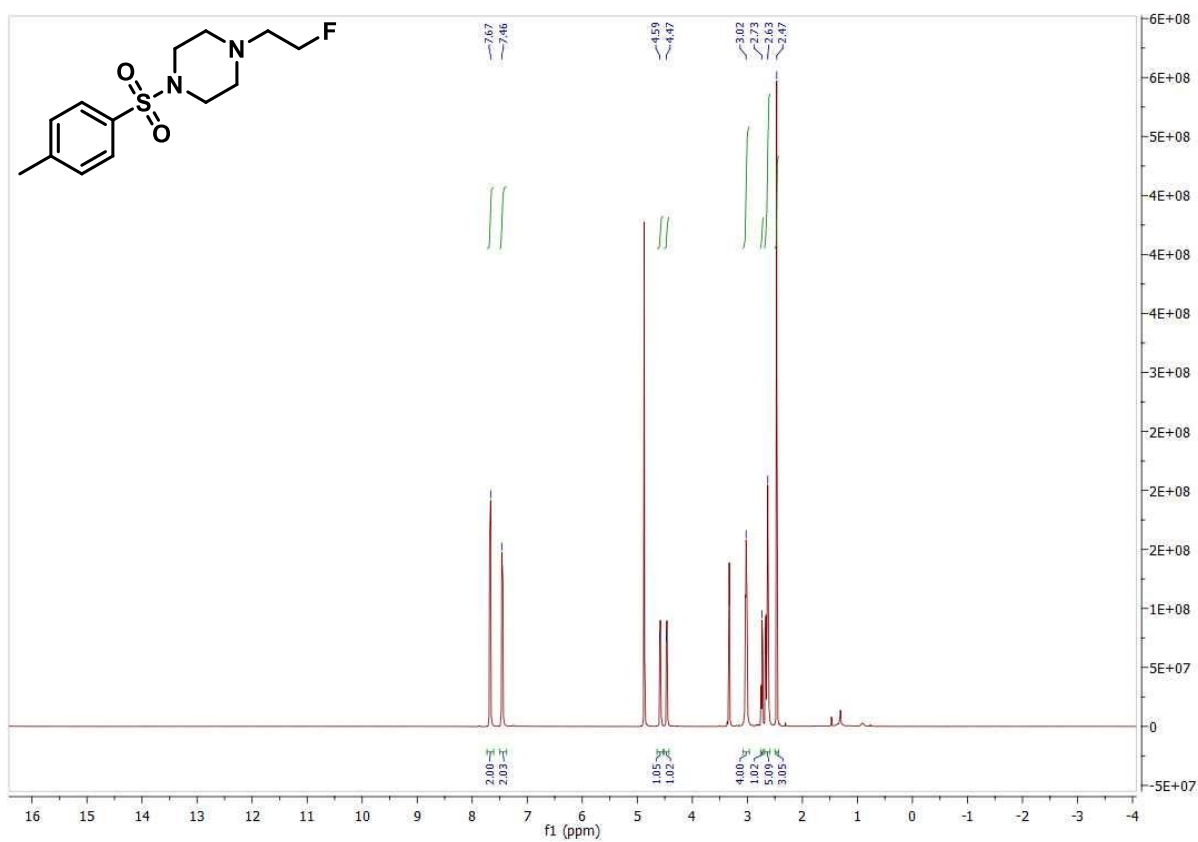
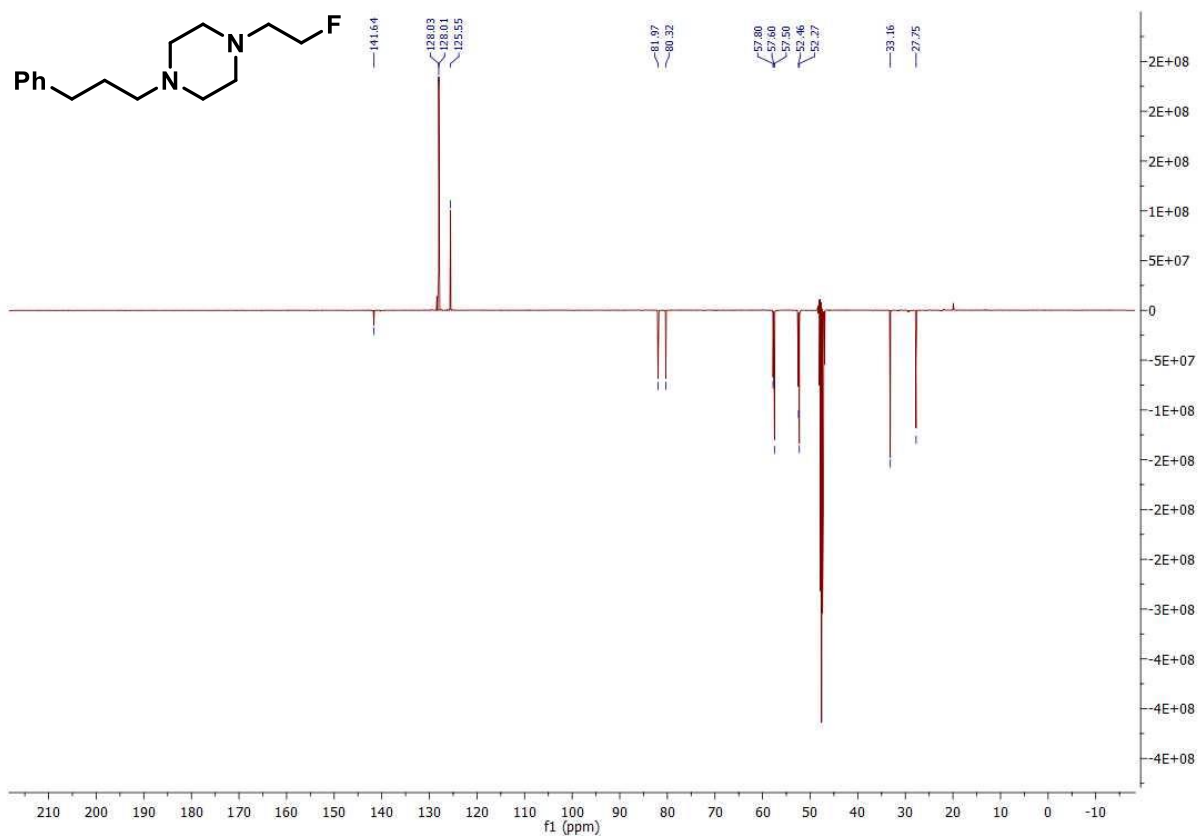
## 7 Experimental Part



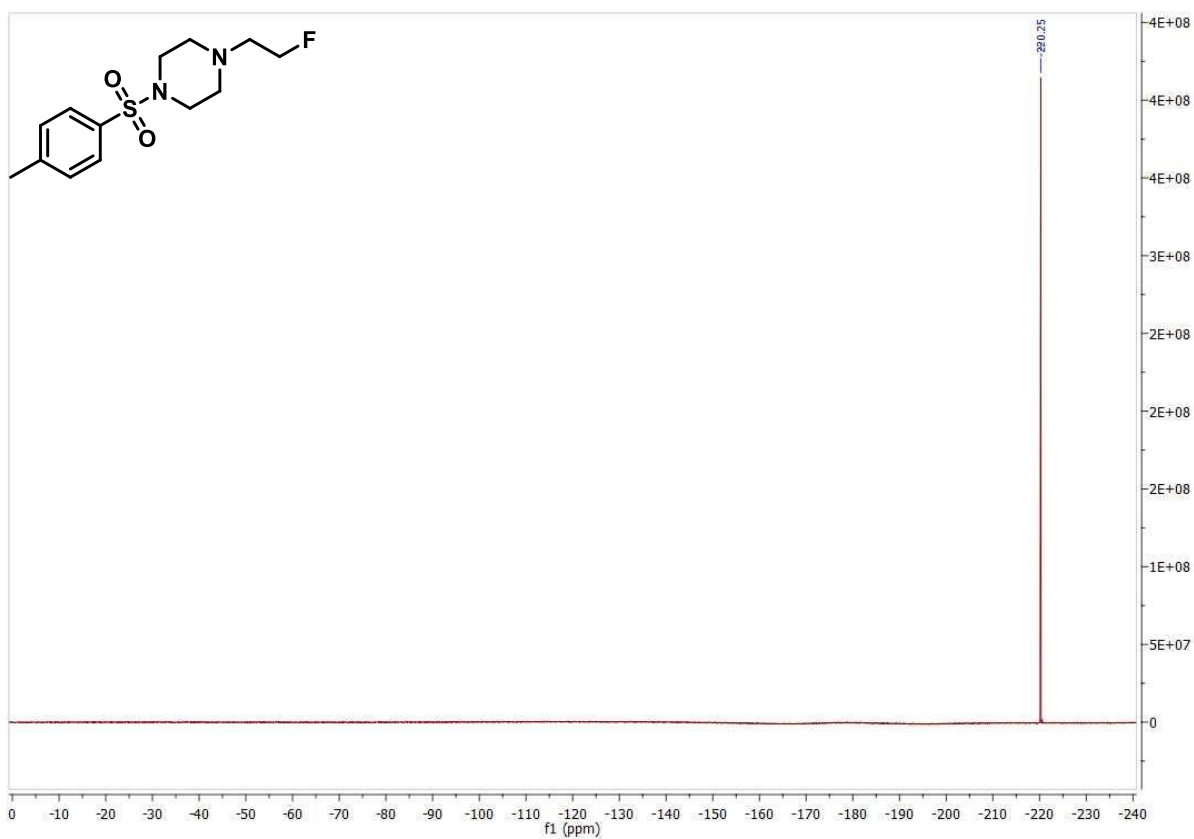
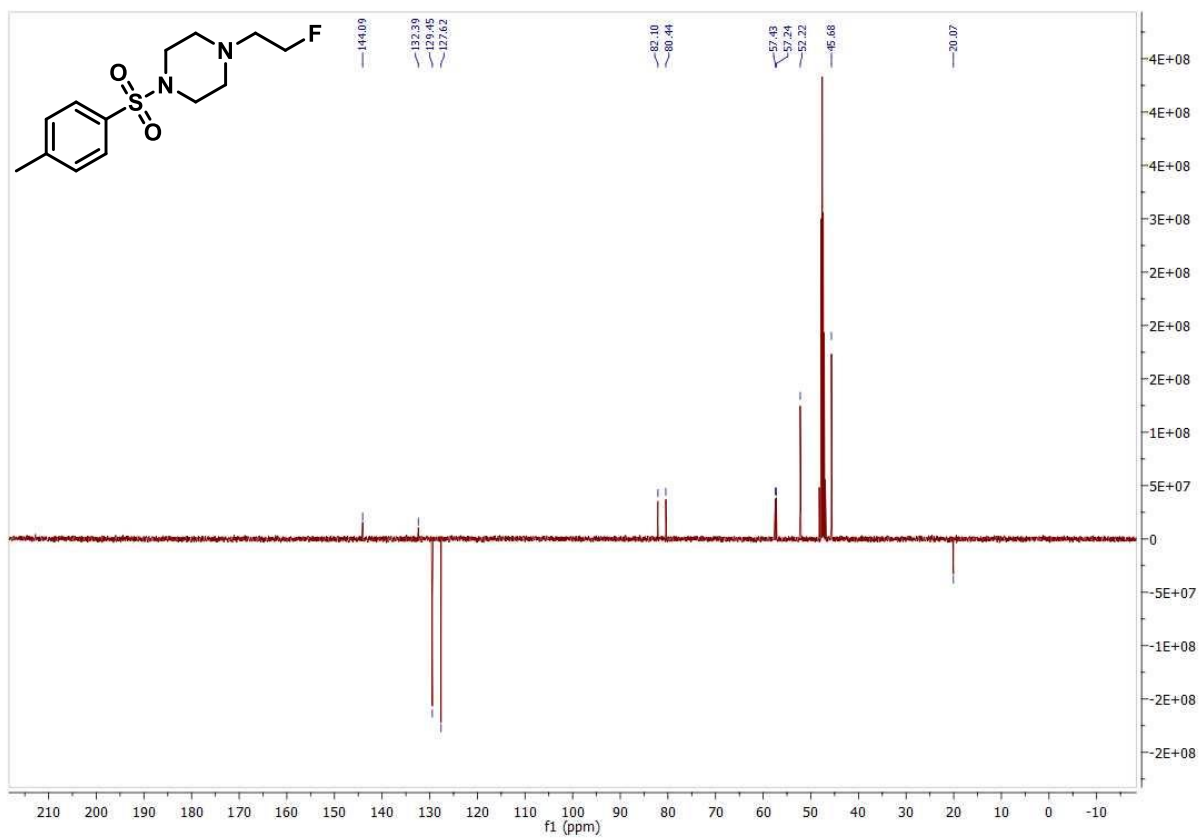
## 7 Experimental Part



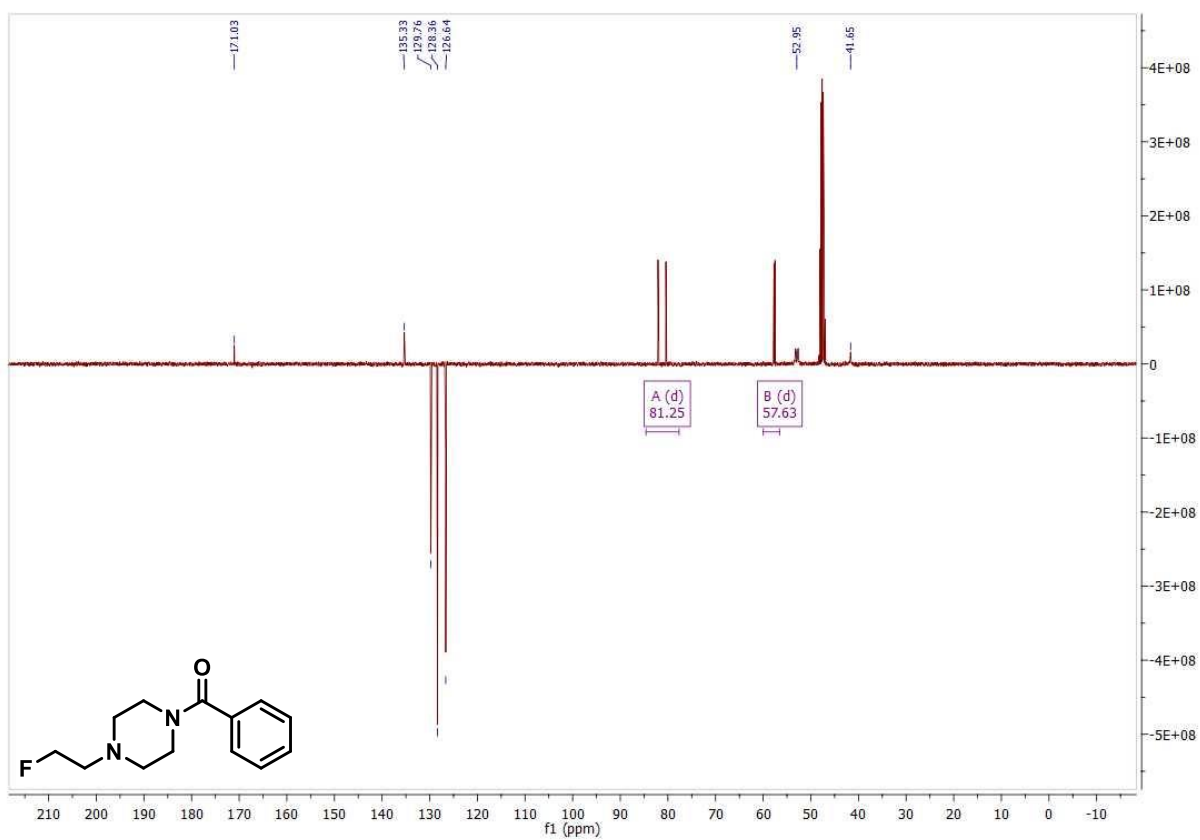
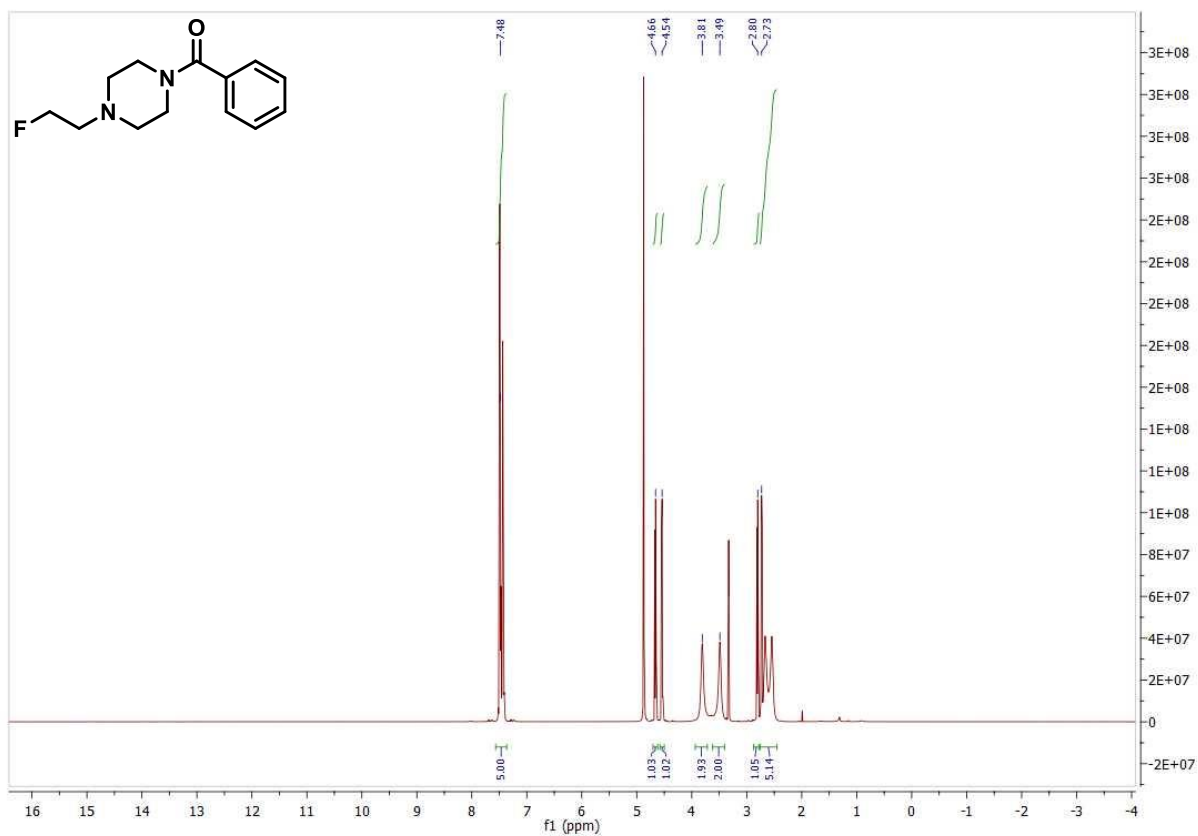
## 7 Experimental Part



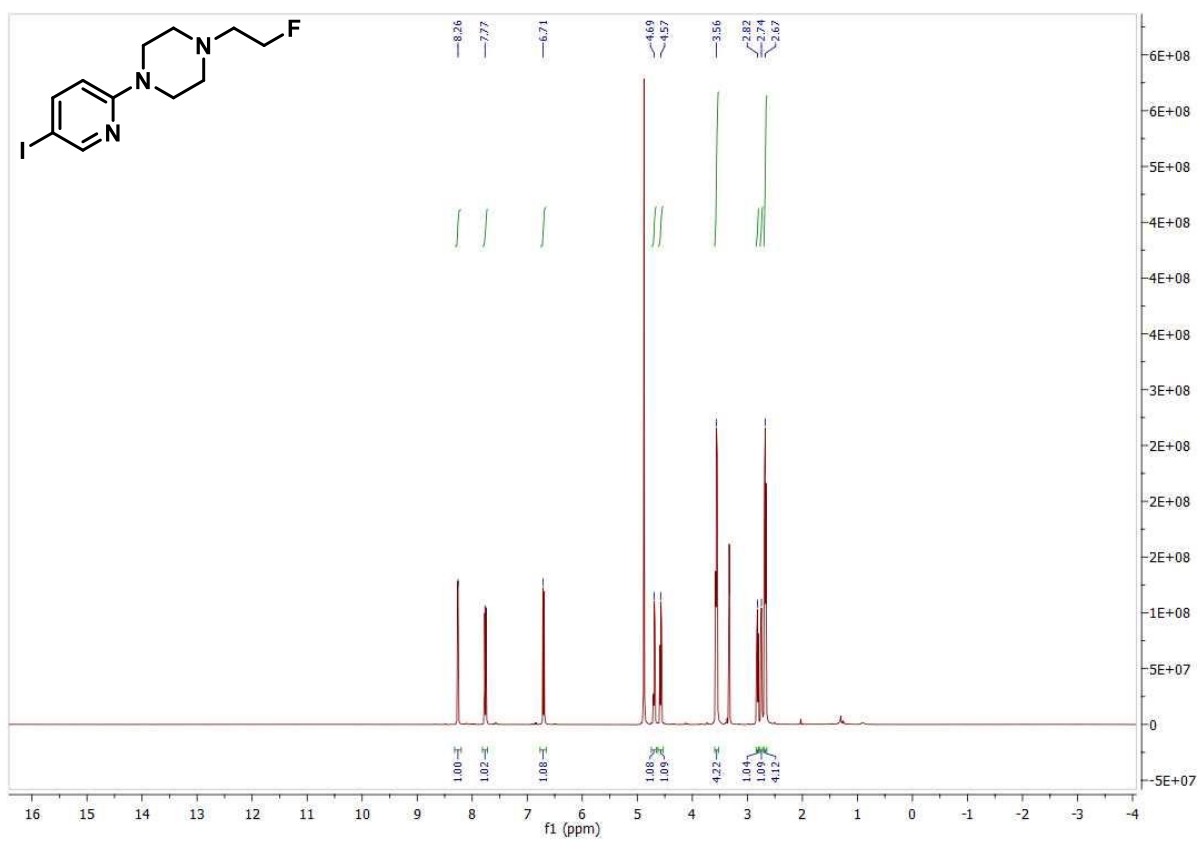
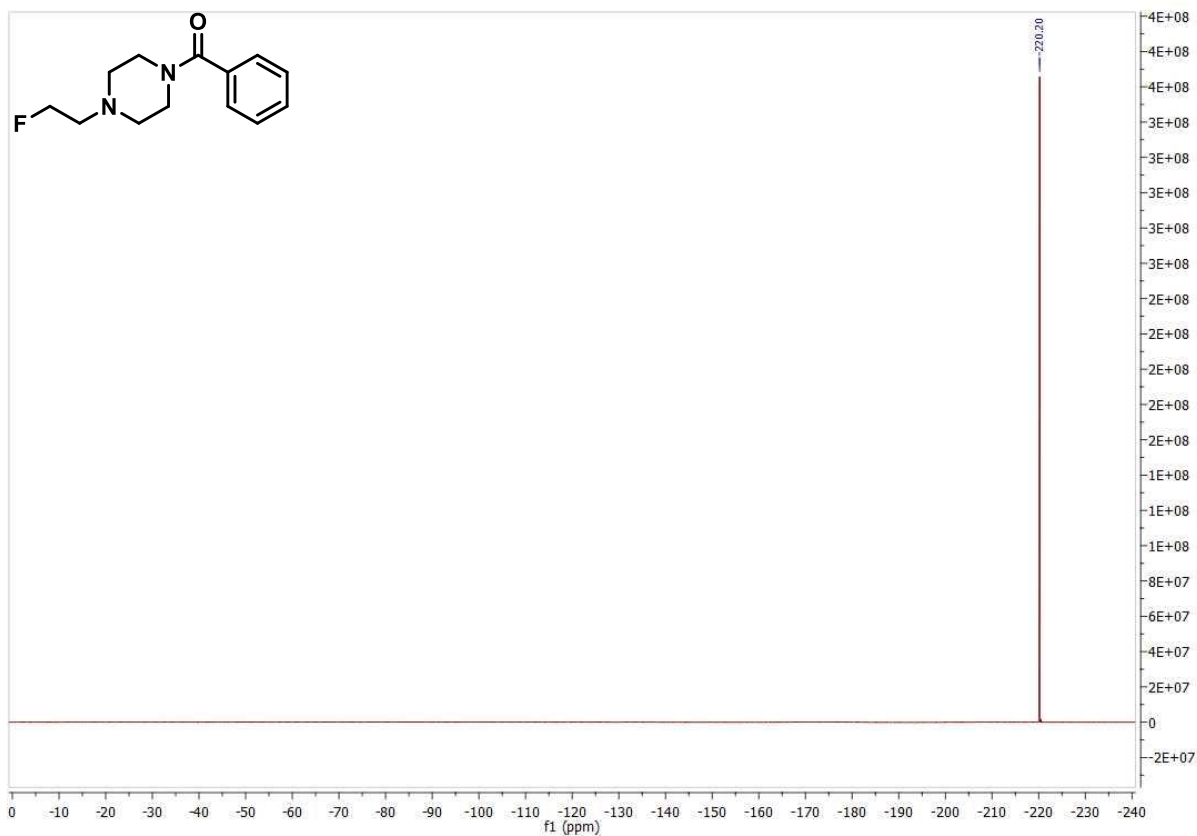
## 7 Experimental Part



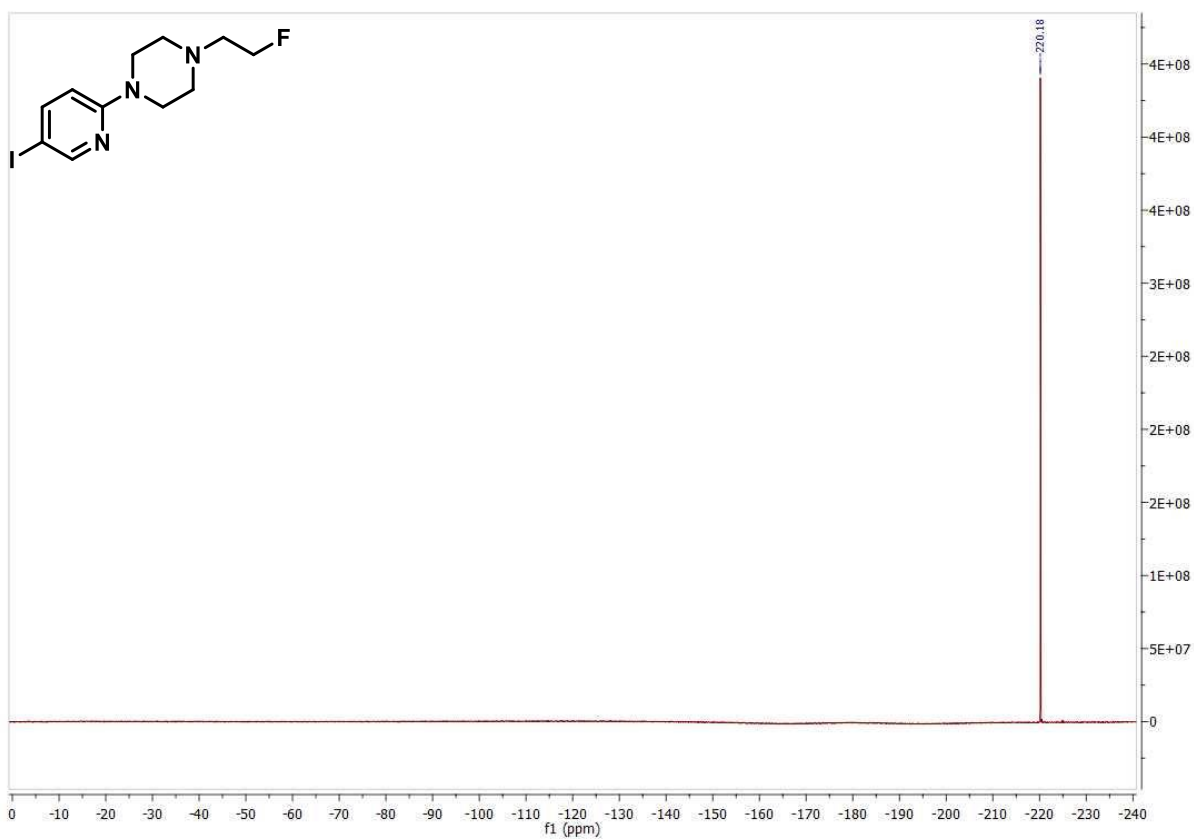
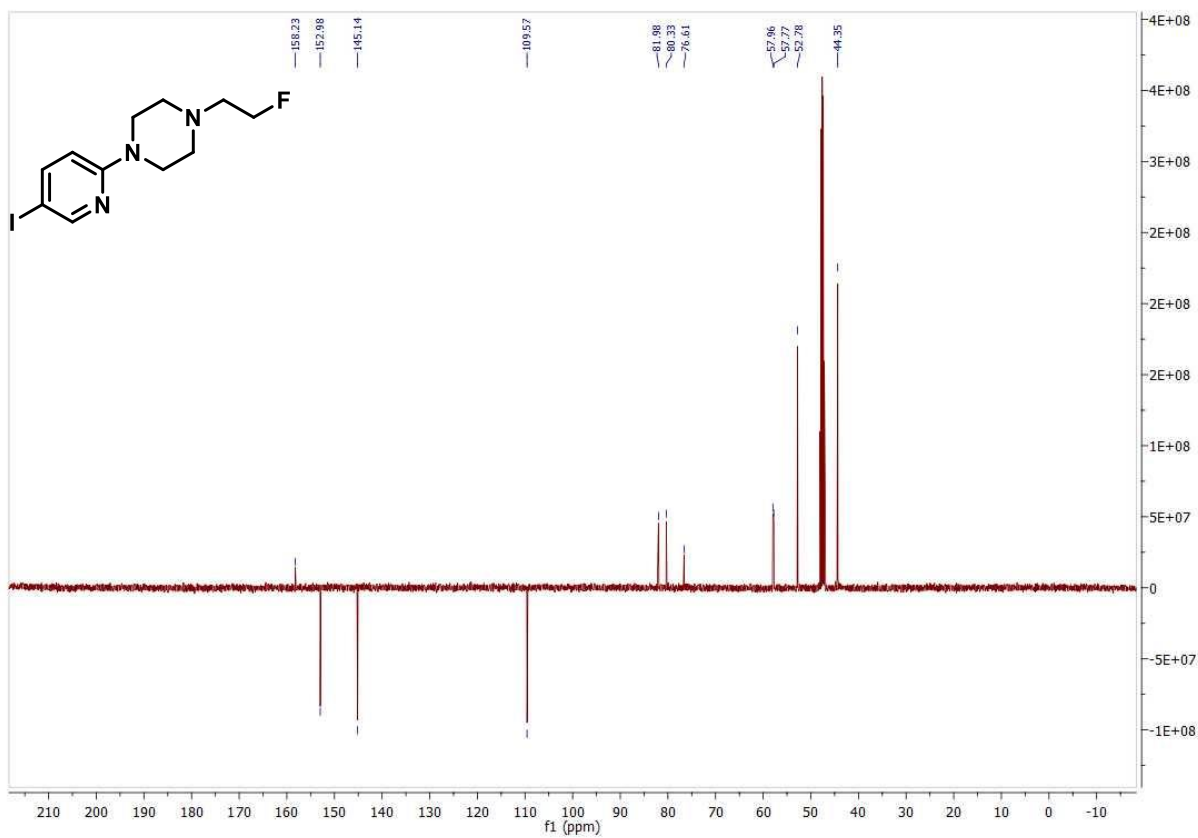
## 7 Experimental Part



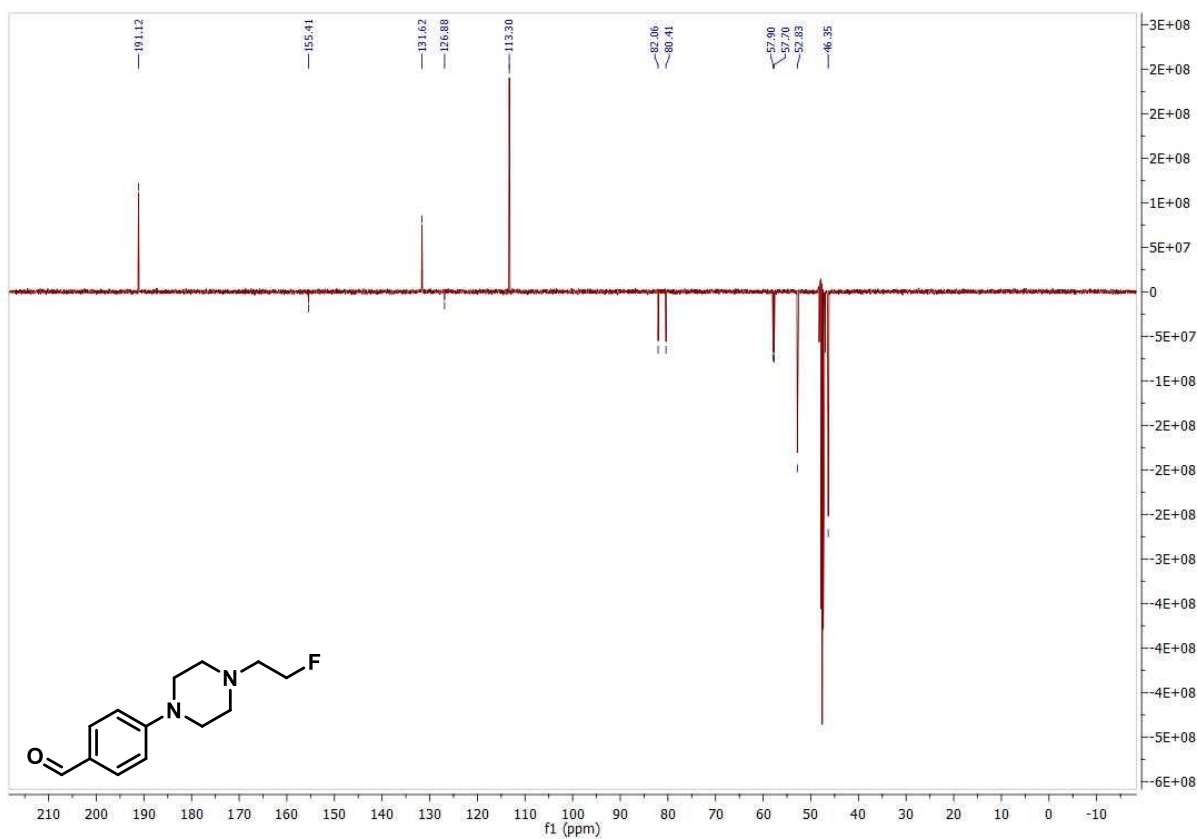
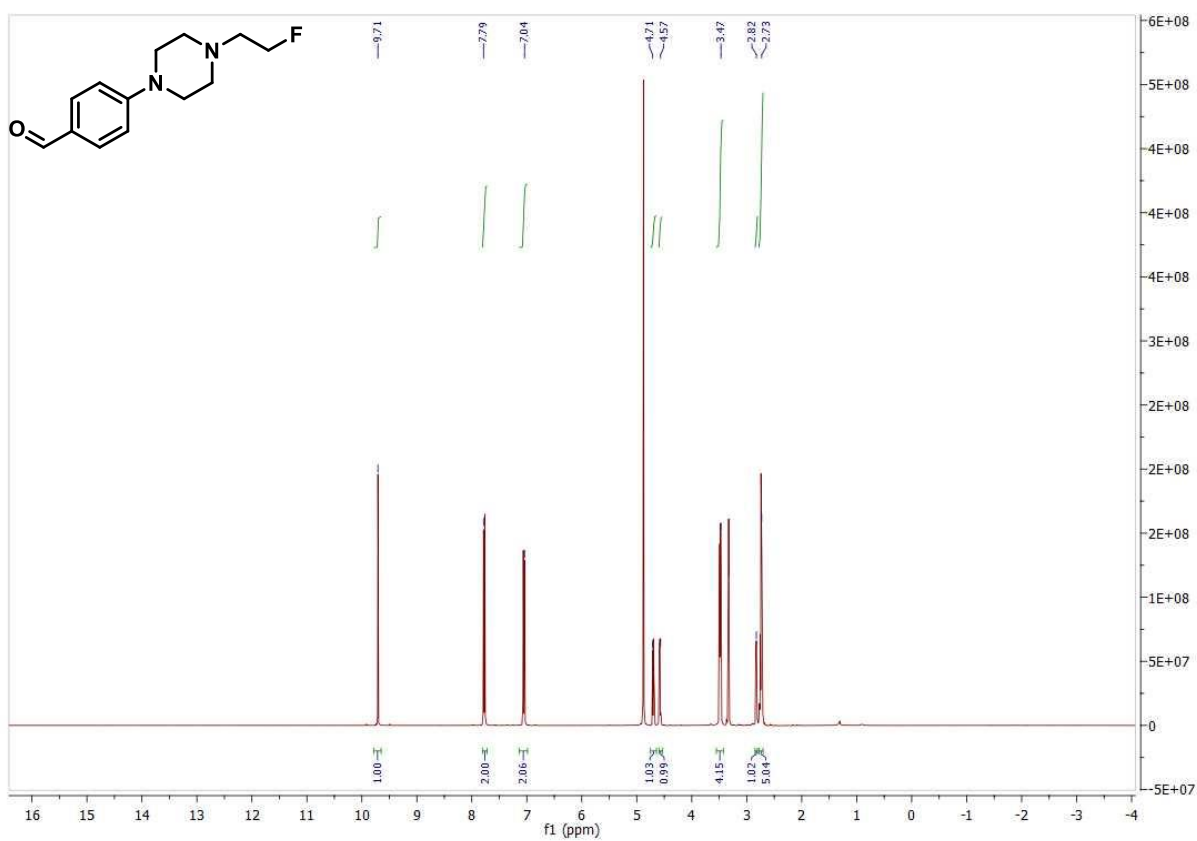
## 7 Experimental Part



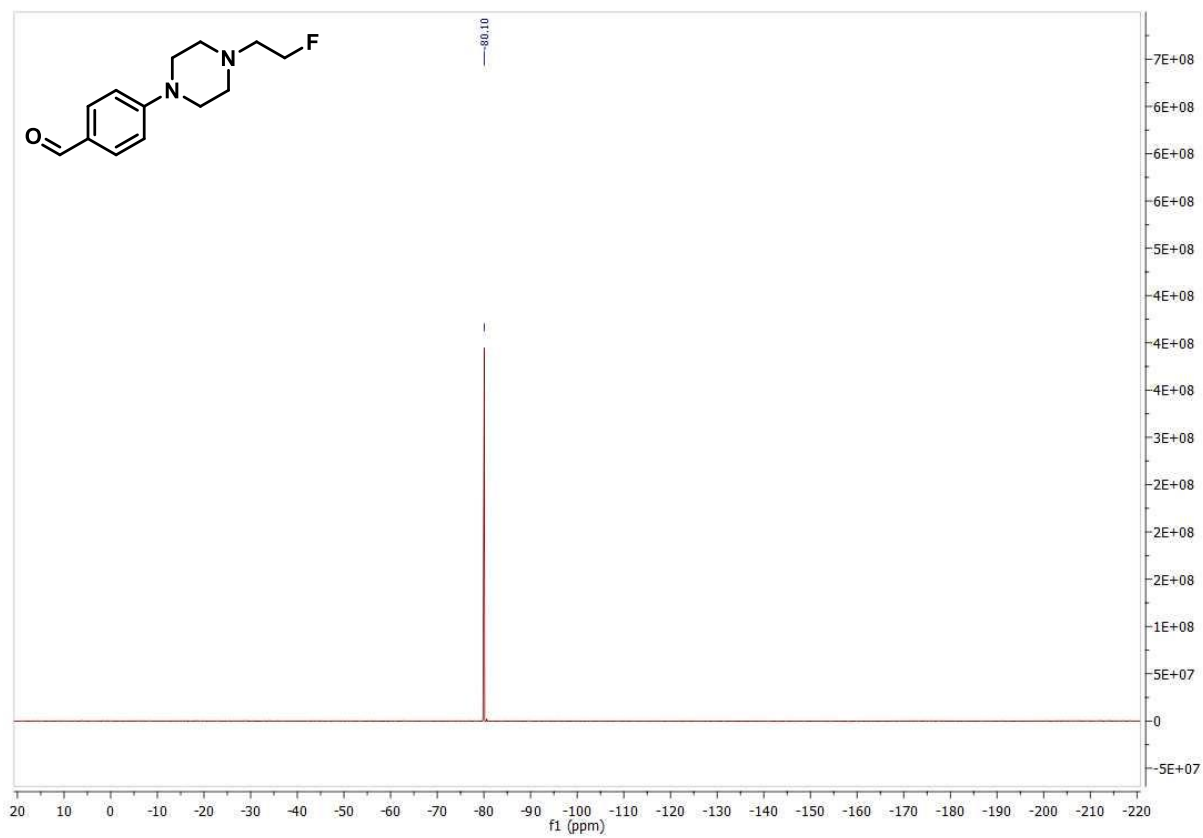
## 7 Experimental Part



## 7 Experimental Part



## 7 Experimental Part



## Radiosynthesis Procedures

All analysis was performed on a Knauer HPLC with a Knauer Azura UVD 2.1S UV-detector and a Berthold Herm LB 500 radiodetector, the determination of the RCCs was done in Clarity Chrome by comparing the decay corrected peak integral areas with the decay corrected peak integral areas of an injection bypassing the column in the fashion described in the next paragraph. Unless otherwise stated the HPLC chromatograms were recorded on a Luna 5  $\mu\text{m}$  PFP(2) 100 Å LC column 250x4.6 mm. Unless otherwise specified a gradient method with water and acetonitrile with 0.1% TFA was used as follows 0-8 min 5->20% MeCN, 8-17 min 20->95% MeCN, 17-25 min 95% flow: 1 mL/min.

For the determination of the RCCs the reaction was quenched with water shaken and analyzed by radio-HPLC determining the ratio of the area of the product peak and the injection behind the column signifying the whole activity of the reaction without potential adsorption of [ $^{18}\text{F}$ ]fluoride on the column.

## General Procedure for the Radiofluorination of DABCO-salts

The target water is diluted with distilled water and taken through a QMA cartridge (Waters Inc.). The cartridge is washed with dry MeOH (1.5 mL) from the male side. Afterwards the cartridge is dried with Argon from the female side for 30 s. The precursor (10  $\mu\text{mol}$ ) is dissolved in dry MeOH (0.5 mL) and the fixed [ $^{18}\text{F}$ ]fluoride is slowly eluted from the cartridge with the precursor solution from the female side of the cartridge into the reactor. The reactor is closed with a septum and the MeOH is evaporated at reduced pressure ( $\sim 300$  mBar) with a flow of argon at 60 °C. After the MeOH is removed ( $\sim 10$  min) the reaction solvent (0.5 mL) is given through the septum, and the reactor is vigorously shaken and placed in the Anton Parr inductive heater (Monowave 50). The heating program consists of two steps which each has two values. For the first step the heating method 'ASAP' is chosen while the reaction temperature is chosen as target temperature for heating. The next step is 'hold temperature', its value is chosen to be the reaction time. The final method is depicted in the method screen as shown in Table 11.

Table 11: Program of the Anton Parr inductive heater.

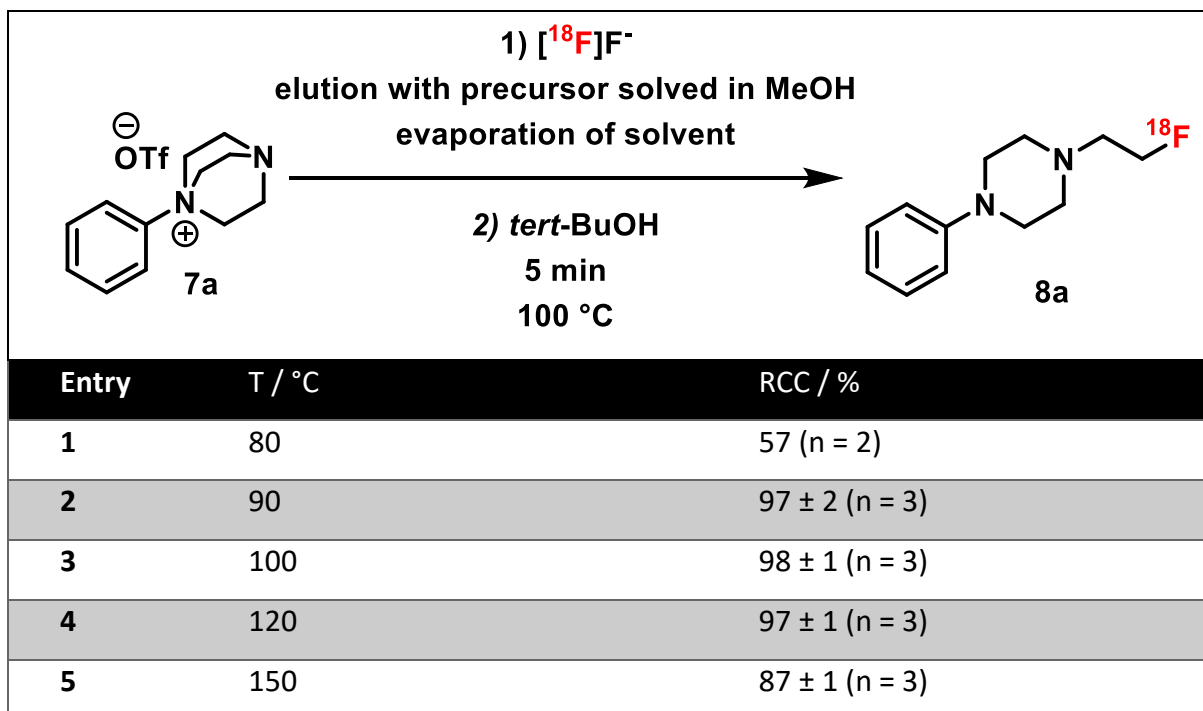
Modifier	Value
ASAP	Target temperature
Hold Temperature	Reaction time

After the heating process is complete the reactor is removed from the heater and the septum is removed. The reaction is diluted with water (1 mL) and the reactor is shaken for 30 seconds to account for eventually existing free fluoride sticking to the walls. Afterwards, the mixture is taken in a syringe and analyzed by radio-HPLC to determine the RCC.

### **Procedure for the Radiofluorination of mesityl(3-nitrophenyl)iodonium trifluoromethanesulfonate**

The iodonium salt (20  $\mu\text{mol}$ ) is dissolved in MeCN and DABCO (2 equiv.) is added in one portion. The solution is then heated at 110 °C for 30 min in an inductive heating reactor (Monowave 50). Afterwards, the MeCN is removed under reduced pressure with an argon flow at 60 °C. The residue is dissolved in MeOH (0.5 mL) and used as precursor solution for the elution of [ $^{18}\text{F}$ ]fluorine. For this the target water is diluted with distilled water and taken through a QMA cartridge (Waters Inc.). The cartridge is washed with dry MeOH (1.5 mL) from the male side. Afterwards the cartridge is dried with Argon from the female side for 30 s. The fixed [ $^{18}\text{F}$ ]fluoride is slowly eluted from the cartridge with the precursor solution from the female side of the cartridge into the reactor. The reactor is closed with a septum and the MeOH is evaporated at reduced pressure with an argon flow at 60 °C. After the MeOH is removed (~10 min) the reaction solvent (0.5 mL) is given through the septum and the reactor is shaken and placed in the Anton Parr inductive heater (Monowave 50). After the heating process is complete the reactor is removed from the heater and the septum is removed. The reaction is quenched with water (1 mL) and the reactor is shaken to account for eventually existing free fluoride sticking to the walls. Afterwards, the mixture is taken in a syringe and analyzed by radio-HPLC to determine the RCC.

## Optimization of Conditions for Aromatic Radiofluorination



### Isolation of [<sup>18</sup>F]1-(2-fluoroethyl)-4-phenylpiperazine

The radiofluorination was done according to the general procedure for radiofluorination of DABCO salts. Afterwards, the quenched reaction mixture was acidified with TFA and given on a semipreparative HPLC column (Synergi 10u Hydro-RP 80A 250 x 10 mm 10 micron) and purified by semipreparative-HPLC (20% MeCN + 0.1% TFA; flow rate: 3.7 mL/min). The purified radiolabelled product was analyzed with an analytical radio HPLC to determine the molar activity and the radiochemical purity. The molar activity was determined by comparison of the UV Peak of the radioproduct with the UV peaks of an external calibration curve of the reference compound.

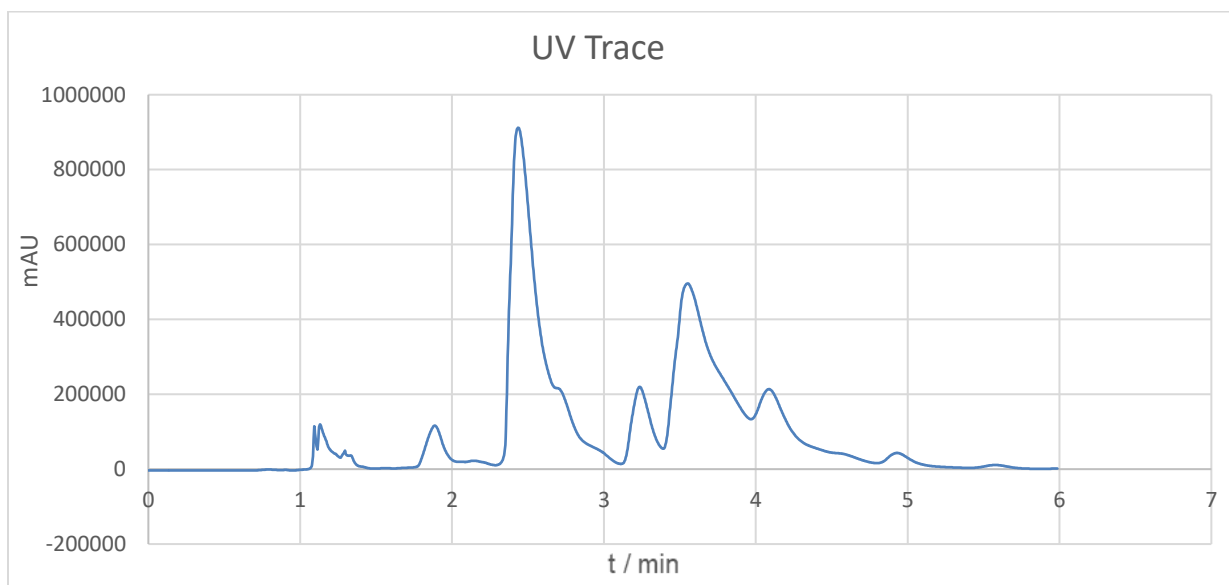
**Chromatogram of the Semipreparative HPLC:**

Figure 62: UV trace of the semipreparative HPLC; column: Synergi 10u Hydro-RP 80A 250 x 10 mm 10 micron; eluent: 20% MeCN (0.1% TFA); flow rate: 3.7 mL/min.

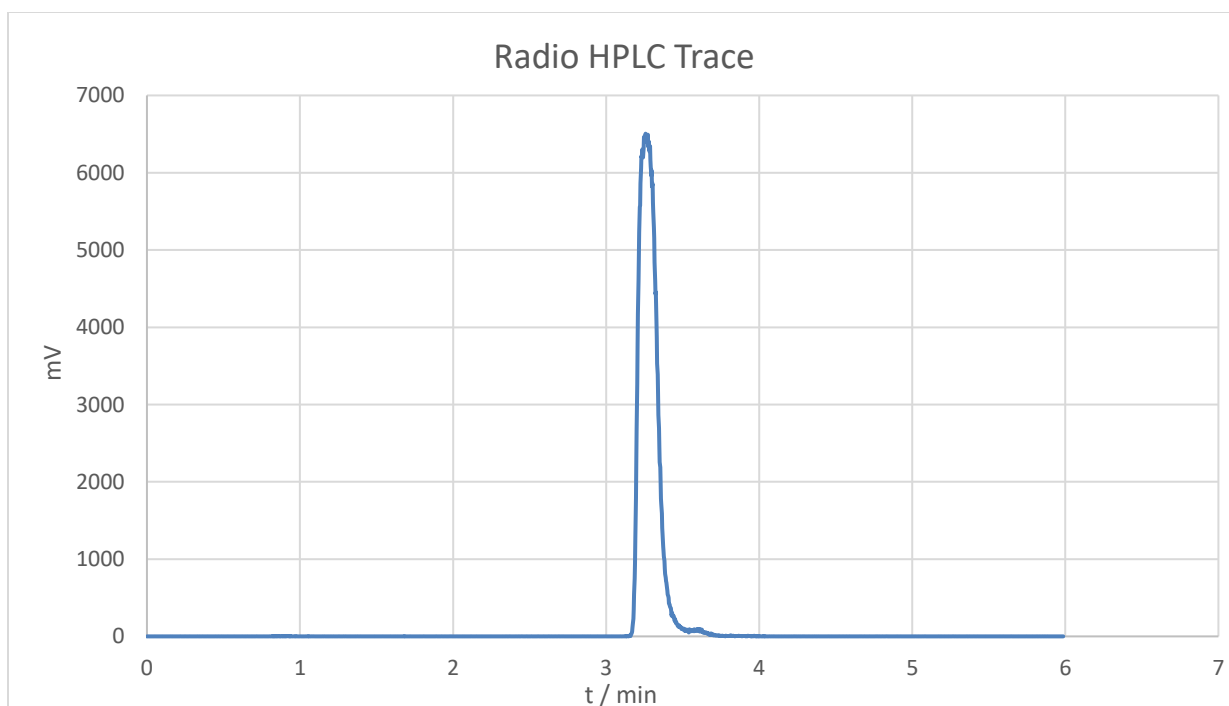


Figure 63: Radio HPLC trace of the semipreparative HPLC; column: Synergi 10u Hydro-RP 80A 250 x 10 mm 10 micron; eluent: 20% MeCN (0.1% TFA); flow rate: 3.7 mL/min.

**Determination of molar activity by use of an external calibration curve:**

Table 1: UV integrals of different concentrations of the non-radioactive reference compound.

Concentration nmol/mL	n/ nmol per injection	Area / mAU	Standard deviation
100	2	10.5781333	0.2409525
50	1	5.31266667	0.07608107
25	0,5	2.6957	0.0237
12.5	0.25	1.29976667	0.02034803
6.25	0.125	0.65293333	0.01078899
3.125	0.0625	0.31183333	0.00314572
1.5625	0.03125	0.1426	0.00268701
0.78125	0.015625	0.06773333	0.00459879
0.390625	0.0078125	0.0285	0.00071181
0.1953125	0.00390625	0.0122	0.00042426

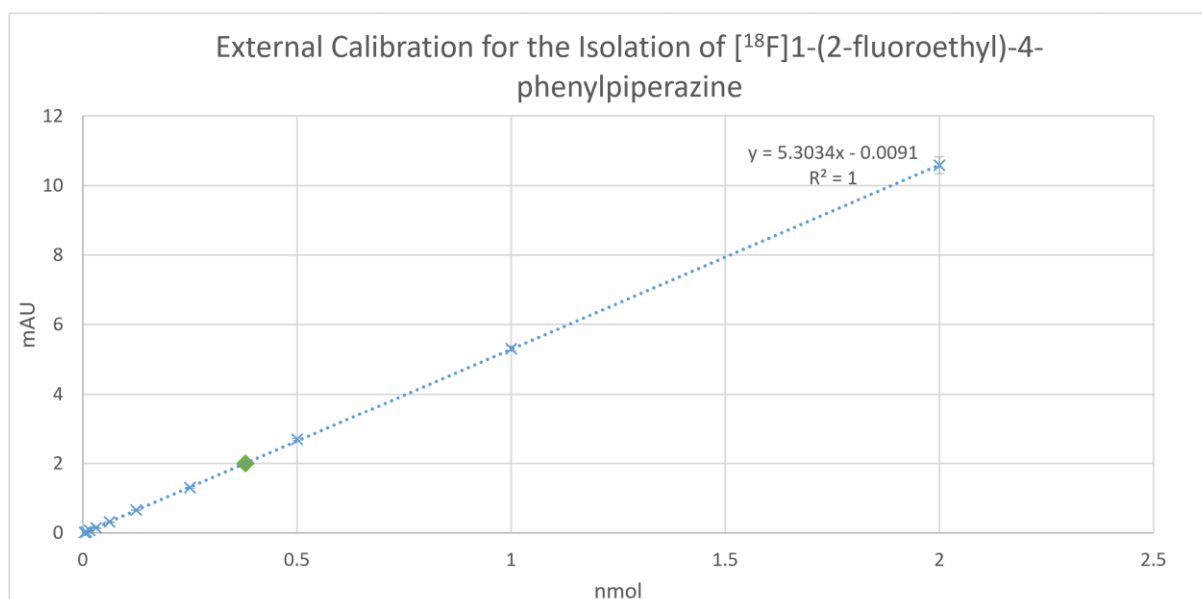


Figure 64: Calibration curve of the non-radioactive reference compound (blue) and measured UV-absorption of the isolated radiolabeled compound (green).

## 7 Experimental Part

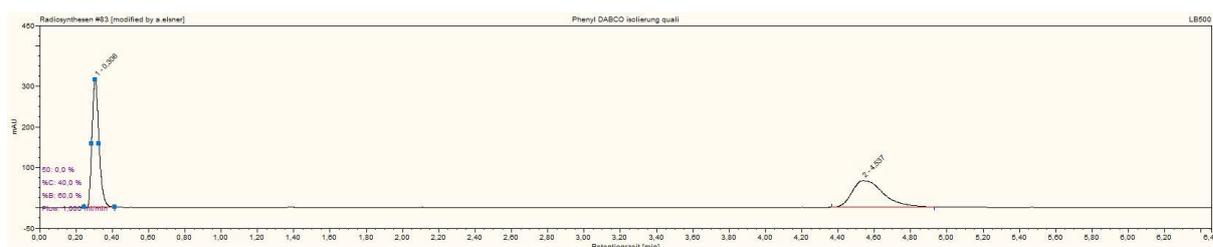


Figure 65: Radio trace of the quality control of the isolated product. Eluent: 30% MeCN (0.1% TFA), Flow rate: 1 mL/min isocratic. Luna 5  $\mu\text{m}$  PFP(2) 100 Å LC column 250x4.6 mm p.c.i. = post column injection.

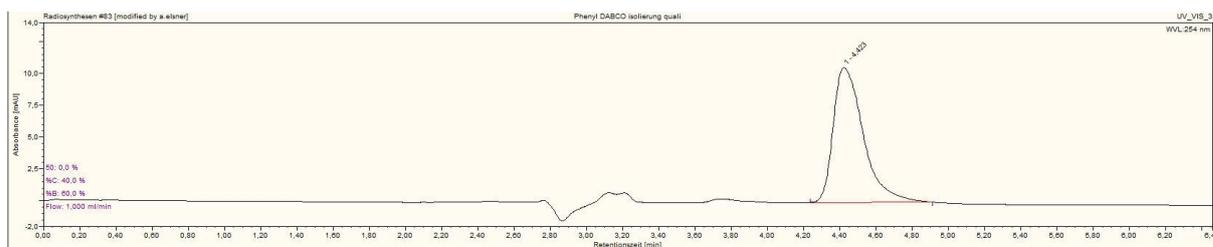


Figure 66: UV trace of the quality control of the isolated product. Eluent: 30% MeCN (0.1% TFA), Flow rate: 1 mL/min isocratic. Luna 5  $\mu\text{m}$  PFP(2) 100 Å LC column 250x4.6 mm; UV: 234 nm.

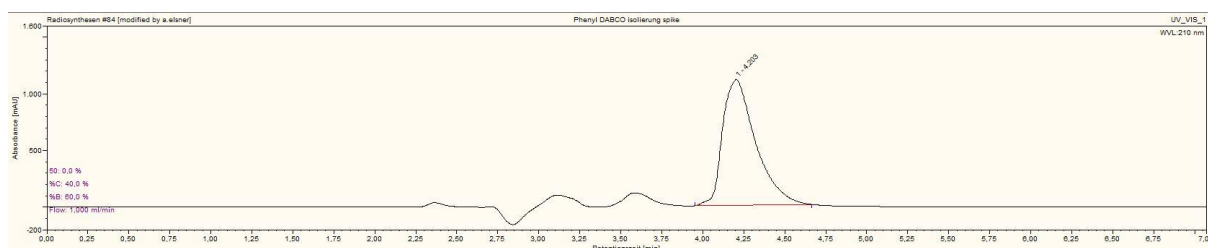


Figure 67: UV trace of the isolated product spiked with the non-radioactive reference compound. Eluent: 30% MeCN (0.1% TFA), Flow rate: 1 mL/min isocratic. Luna 5  $\mu\text{m}$  PFP(2) 100 Å LC column 250x4.6 mm; UV: 234 nm.

<b>UV Absorption of the isolated product</b>	2.035 mAU
<b>Amount of carrier in injection</b>	0.38 nmol
<b>Activity concentration</b>	309 MBq/mL
<b>Molar activity</b>	16.1 GBq/ $\mu\text{mol}$
<b>Radiochemical purity</b>	>95%
<b>Starting activity</b>	2 GBq
<b>Isolated activity</b>	647 MBq
<b>Reaction time</b>	63 min
<b>Activity yield</b>	32%
<b>RCY</b>	48%

## Conjugation of 1-(pent-4-yn-1-yl)-1,4-diazabicyclo[2.2.2]octan-1-ium 4-methylbenzenesulfonate (2c) Azide-Alkyne Huisgen Cycloaddition

For the conjugation of 1-(pent-4-yn-1-yl)-1,4-diazabicyclo[2.2.2]octan-1-ium 4-methylbenzenesulfonate it is radiofluorinated following the general procedure for the radiofluorination of DABCO-salts. Afterwards, the reaction is diluted with 20 mL of water and fixed on a HLB cartridge. The cartridge is washed with 10% MeCN in water (5 mL). The click-conjugation is performed according to a method used by Mamat et al.<sup>[46]</sup>. The cartridge is elude with 1 mL of Ethanol. Afterwards, the benzylazide (1  $\mu$ mol) was added to the solution, Na-ascorbate (30  $\mu$ mol, 0.6 M) and Copper(II) sulfate pentahydrate (20 mol, 0.4 M) were added as well. The solution was stirred at 40°C for 10 minutes. After stirring the reaction mixture was injected into a HPLC to measure the RCC.

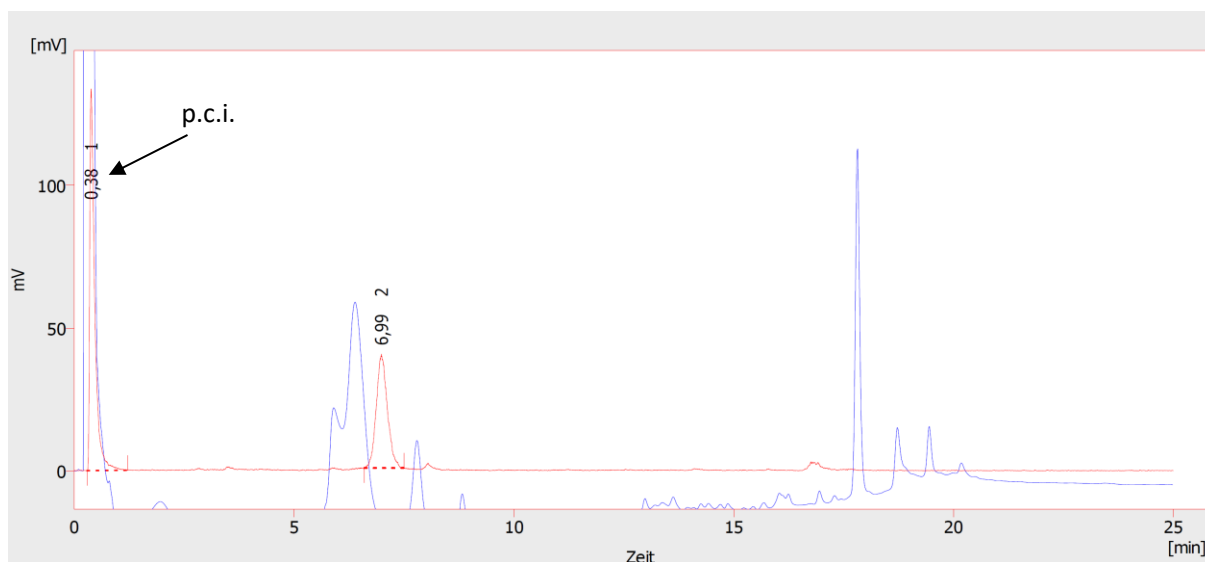


Figure 68: HPLC-chromatogram after the cartridge purification step. Eluent: 0–8 min: 5→20% MeCN (0.1% TFA), 8–17 min: 20→95% MeCN (0.1% TFA), 17–25 min: 95% MeCN (0.1% TFA); Flow rate: 1 mL/min; Luna 5  $\mu$ m PFP(2) 100 Å LC column 250x4.6 mm; p.c.i. = post column injection. Red: Radio HPLC trace, blue: UV trace 234 nm.

## 7 Experimental Part

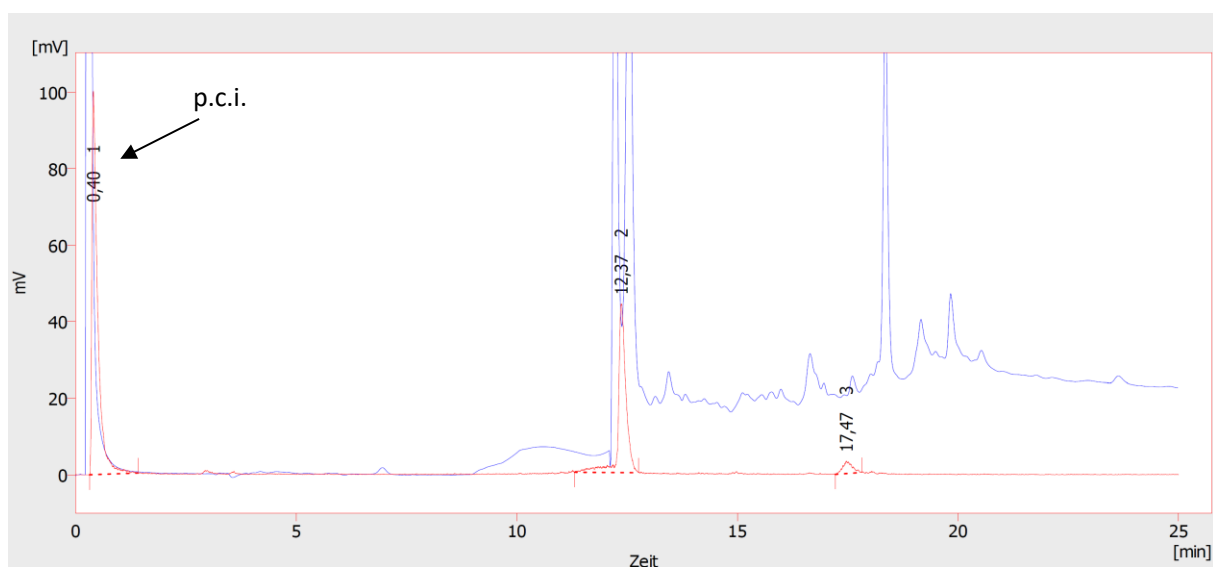
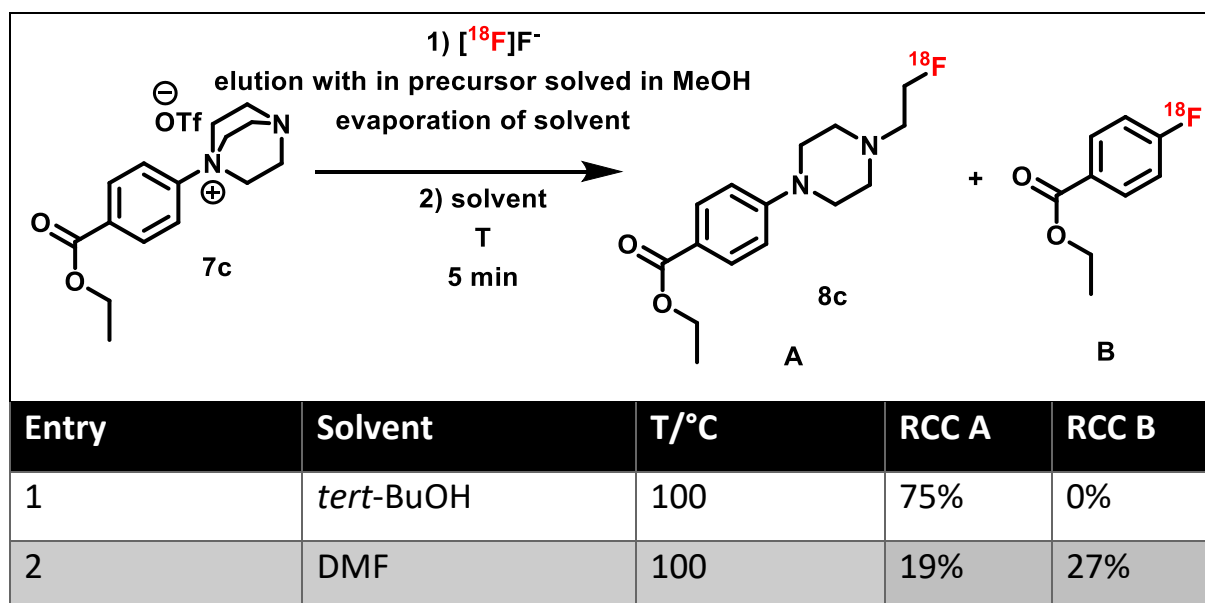


Figure 69: HPLC-chromatogram after the conjugation step. Eluent: 0–8 min: 5–>20% MeCN (0.1% TFA), 8–17 min: 20–>95% MeCN (0.1% TFA), 17–25 min: 95% MeCN (0.1% TFA); Flow rate: 1 mL/min; Luna 5  $\mu\text{m}$  PFP(2) 100 Å LC column 250x4.6 mm; p.c.i. = post column injection. Red: Radio HPLC trace, blue: UV trace 234 nm.

### Solvent Influence on the Radiofluorination of Highly Activated Aromatic

#### DABCO Salts.



## Chromatograms

### HPLC Chromatograms of the Crude Radiofluorination Reaction Mixtures and the Corresponding Reference Compounds

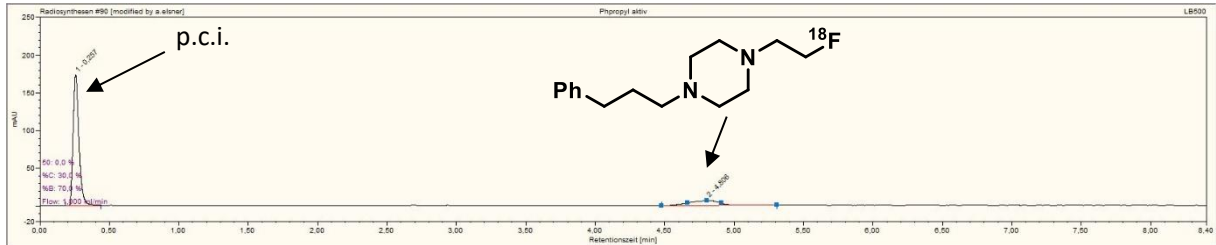


Figure 70: Eluent: 30% MeCN (0.1% TFA), Flow rate: 1 mL/min isocratic. Luna 5  $\mu$ m PFP(2) 100 Å LC column 250x4.6 mm p.c.i. = post column injection.

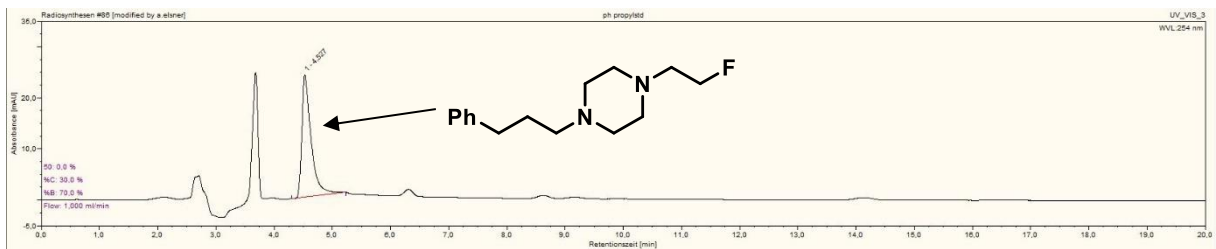


Figure 71: Eluent: 30% MeCN (0.1% TFA), Flow rate: 1 mL/min isocratic. Luna 5  $\mu$ m PFP(2) 100 Å LC column 250x4.6 mm, UV trace 234 nm.

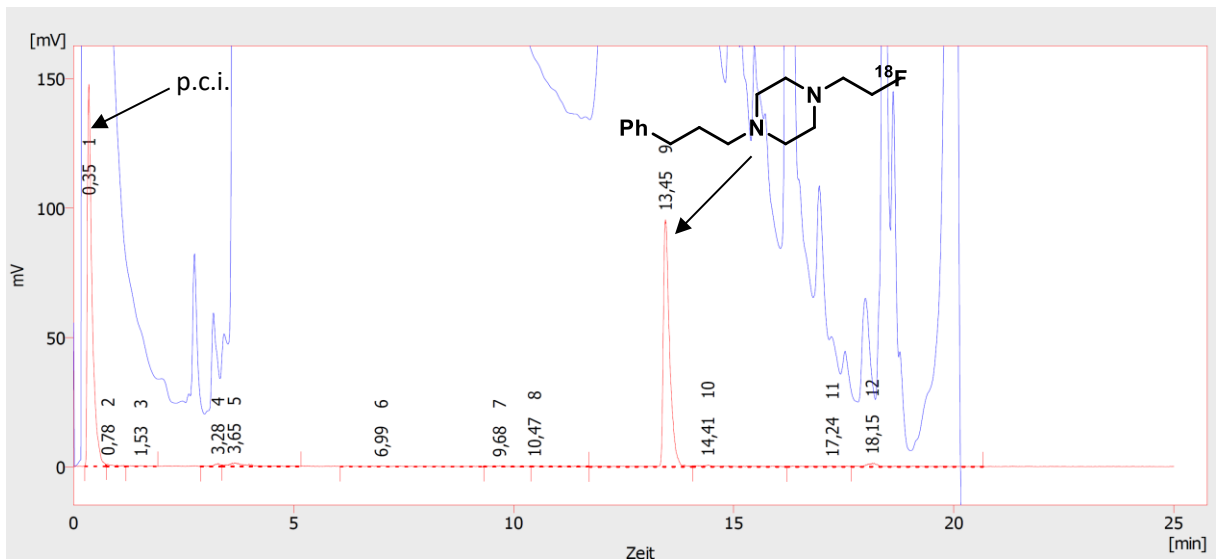


Figure 72: Eluent: 0–8 min: 5→20% MeCN (0.1% TFA), 8–17 min: 20→95% MeCN (0.1% TFA), 17–25 min: 95% MeCN (0.1% TFA); Flow rate: 1 mL/min; Luna 5  $\mu$ m PFP(2) 100 Å LC column 250x4.6 mm; p.c.i. = post column injection. Red: Radio HPLC trace, blue: UV trace 234 nm.

## 7 Experimental Part

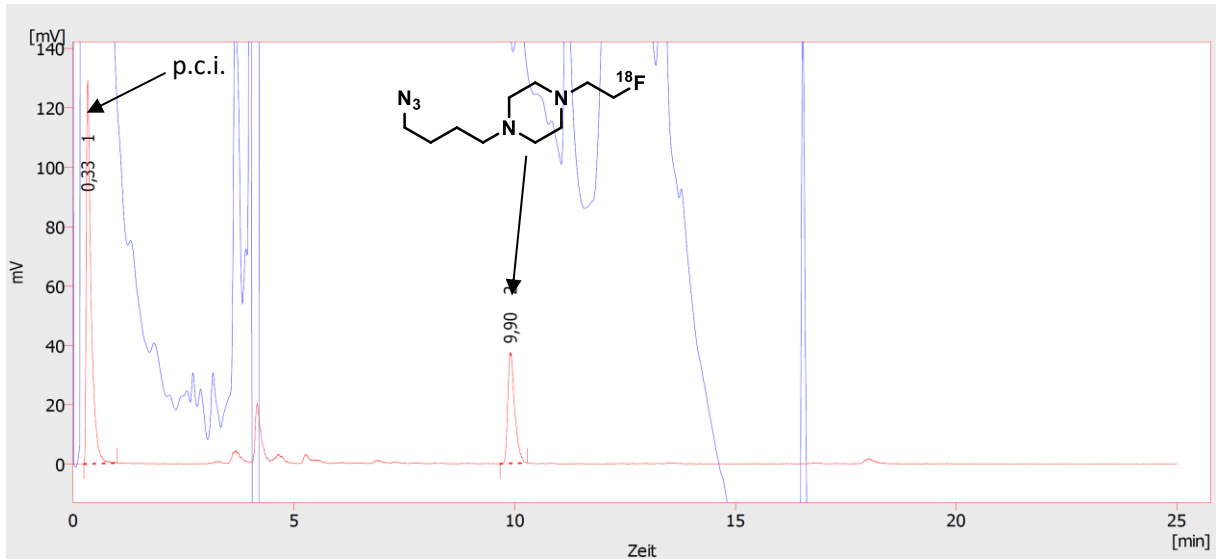


Figure 73: Eluent: 0–8 min: 5→20% MeCN (0.1% TFA), 8–17 min: 20→95% MeCN (0.1% TFA), 17–25 min: 95% MeCN (0.1% TFA); Flow rate: 1 mL/min; Luna 5 μm PFP(2) 100 Å LC column 250x4.6 mm; p.c.i. = post column injection. Red: Radio HPLC trace, blue: UV trace 234 nm.

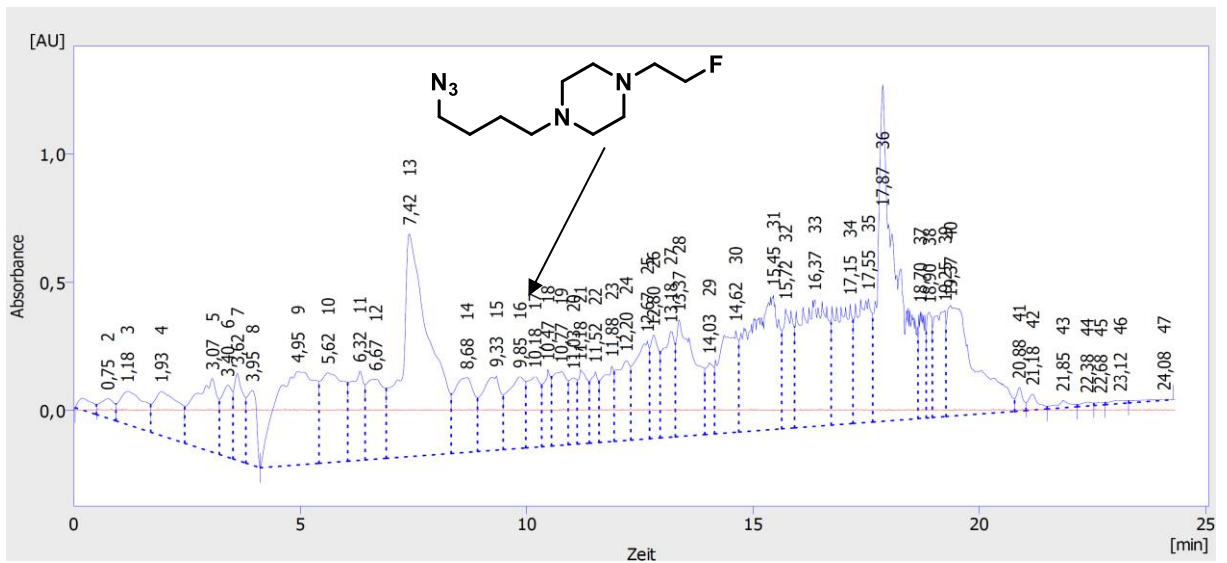


Figure 74: Eluent: 0–8 min: 5→20% MeCN (0.1% TFA), 8–17 min: 20→95% MeCN (0.1% TFA), 17–25 min: 95% MeCN (0.1% TFA); Flow rate: 1 mL/min; Luna 5 μm PFP(2) 100 Å LC column 250x4.6 mm; p.c.i. = post column injection. Red: Radio HPLC trace, blue: UV trace 234 nm.

## 7 Experimental Part

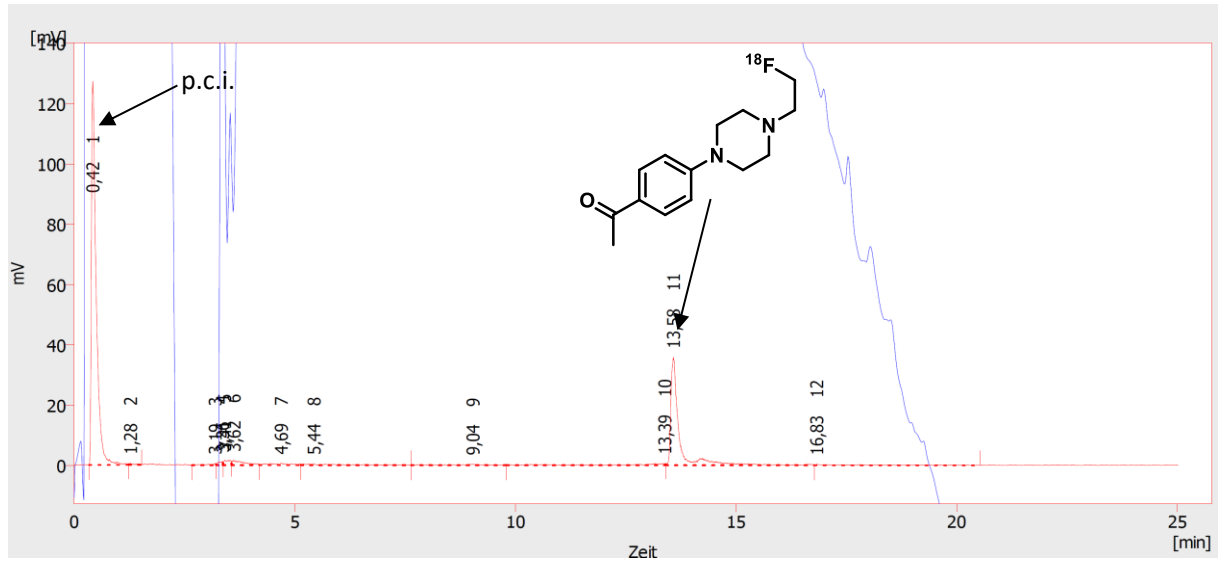


Figure 75: Eluent: 0–8 min: 5→20% MeCN (0.1% TFA), 8–17 min: 20→95% MeCN (0.1% TFA), 17–25 min: 95% MeCN (0.1% TFA); Flow rate: 1 mL/min; Luna 5  $\mu\text{m}$  PFP(2) 100 Å LC column 250x4.6 mm; p.c.i. = post column injection. Red: Radio HPLC trace, blue: UV trace 234 nm.

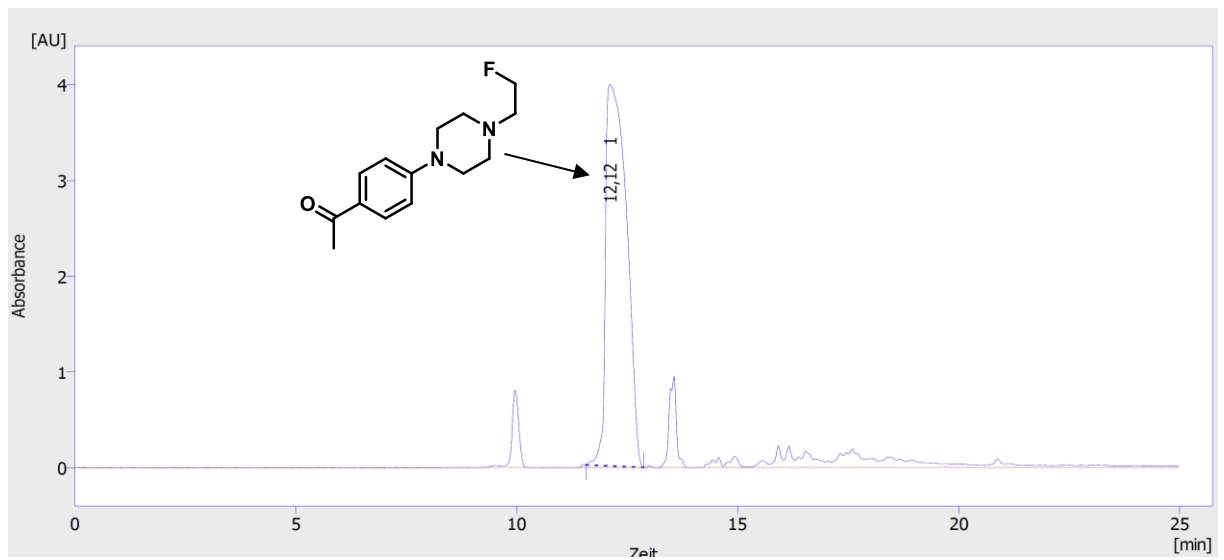


Figure 76: Eluent: 0–8 min: 5→20% MeCN (0.1% TFA), 8–17 min: 20→95% MeCN (0.1% TFA), 17–25 min: 95% MeCN (0.1% TFA); Flow rate: 1 mL/min; Luna 5  $\mu\text{m}$  PFP(2) 100 Å LC column 250x4.6 mm; p.c.i. = post column injection. Red: Radio HPLC trace, blue: UV trace 234 nm.

## 7 Experimental Part

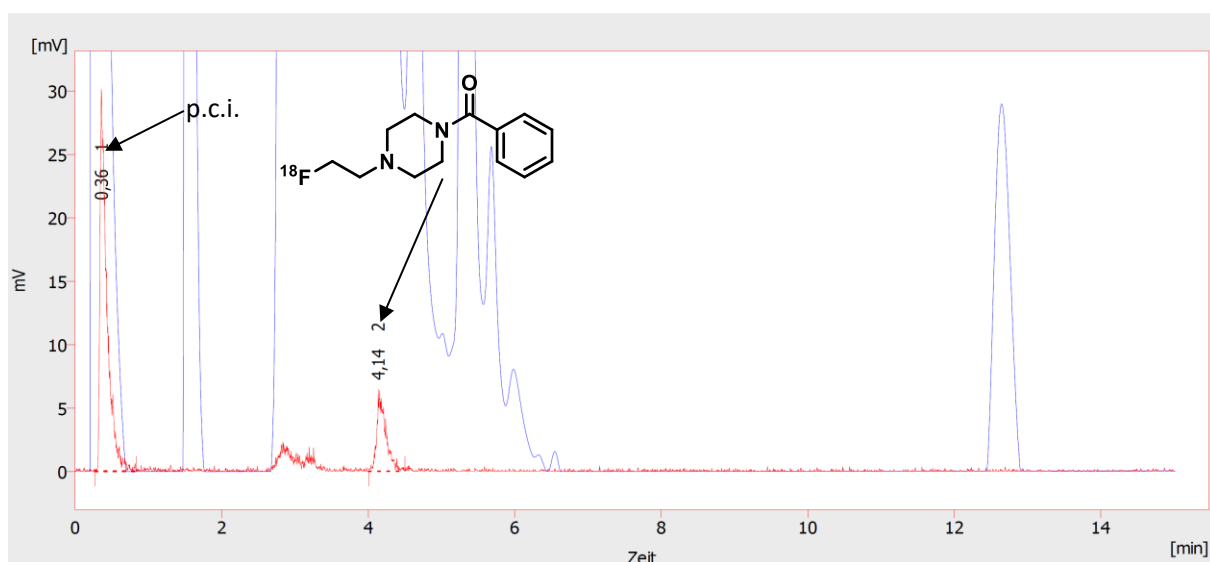


Figure 77: Eluent: 25% MeCN (0.1% TFA); Flow rate: 1 mL/min; Luna 5  $\mu\text{m}$  PFP(2) 100 Å LC column 250x4.6 mm p.c.i. = post column injection. Red: Radio HPLC trace, blue: UV trace 234 nm.

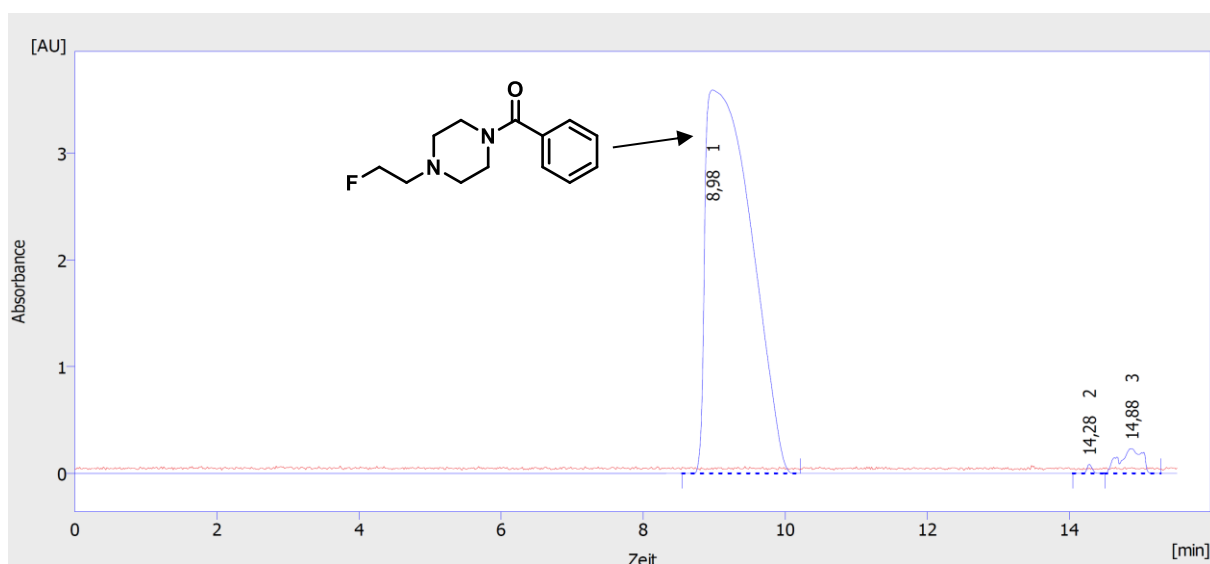


Figure 78: Eluent: 0–8 min: 5→20% MeCN (0.1% TFA), 8–17 min: 20→95% MeCN (0.1% TFA), 17–25 min: 95% MeCN (0.1% TFA); Flow rate: 1 mL/min; Luna 5  $\mu\text{m}$  PFP(2) 100 Å LC column 250x4.6 mm; p.c.i. = post column injection. Red: Radio HPLC trace, blue: UV trace 234 nm.

## 7 Experimental Part

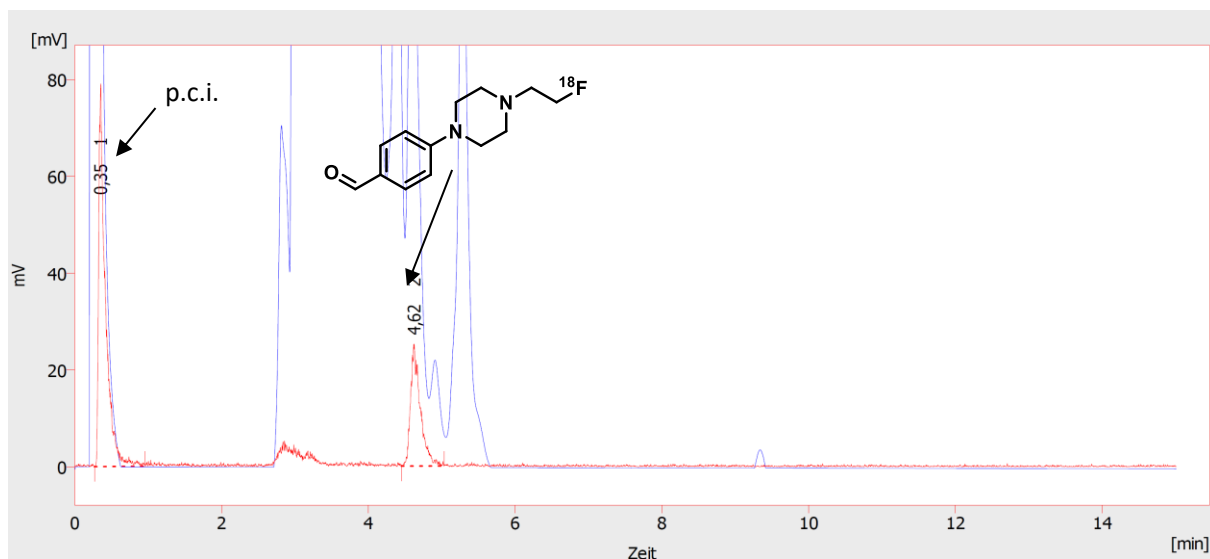


Figure 79: Eluent: 25% MeCN (0.1% TFA); Flow rate: 1 mL/min; Luna 5  $\mu$ m PFP(2) 100 Å LC column 250x4.6 mm p.c.i. = post column injection. Red: Radio HPLC trace, blue: UV trace 234 nm.

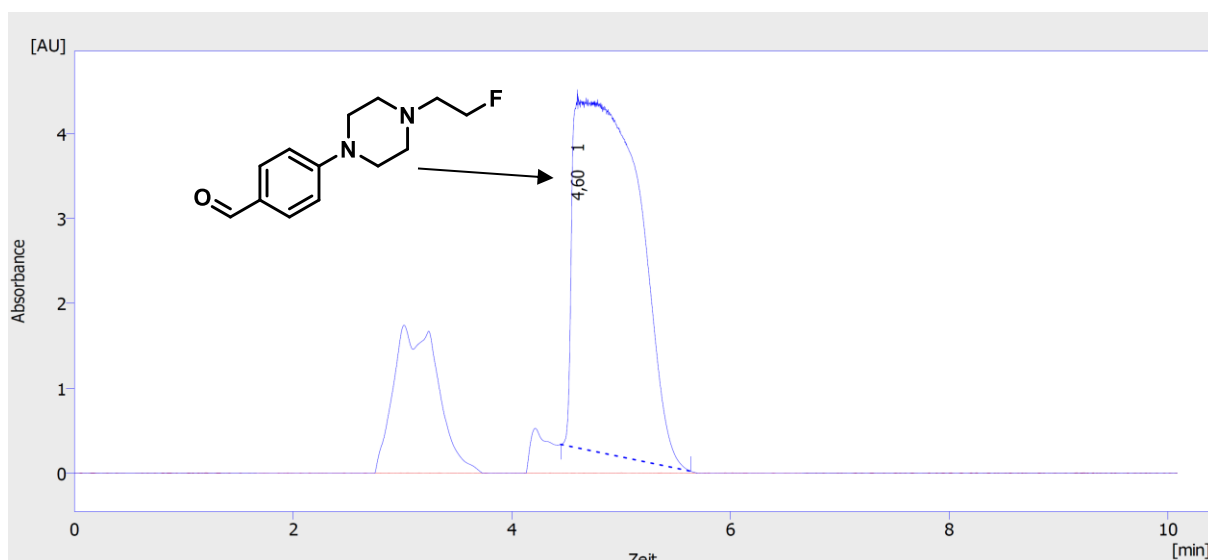


Figure 80: Eluent: 25% MeCN (0.1% TFA); Flow rate: 1 mL/min; Luna 5  $\mu$ m PFP(2) 100 Å LC column 250x4.6 mm. p.c.i. = post column injection. Red: Radio HPLC trace, blue: UV trace 234 nm.

## 7 Experimental Part

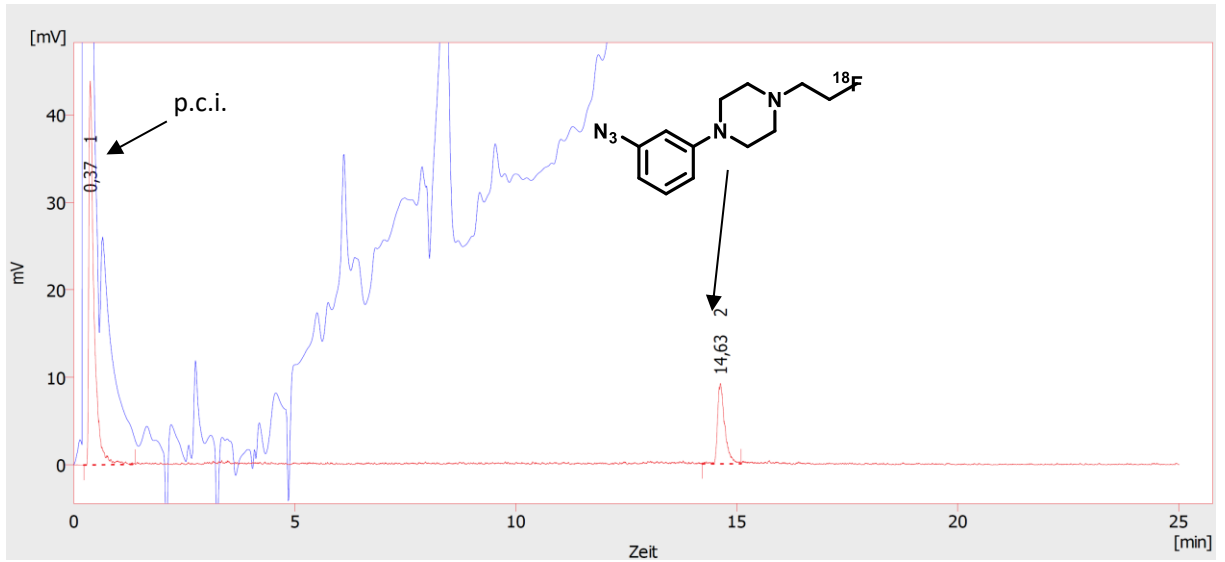


Figure 81: Eluent: 0–8 min: 5→20% MeCN (0.1% TFA), 8–17 min: 20→95% MeCN (0.1% TFA), 17–25 min: 95% MeCN (0.1% TFA); Flow rate: 1 mL/min; Luna 5  $\mu$ m PFP(2) 100 Å LC column 250x4.6 mm; p.c.i. = post column injection. Red: Radio HPLC trace, blue: UV trace 234 nm.

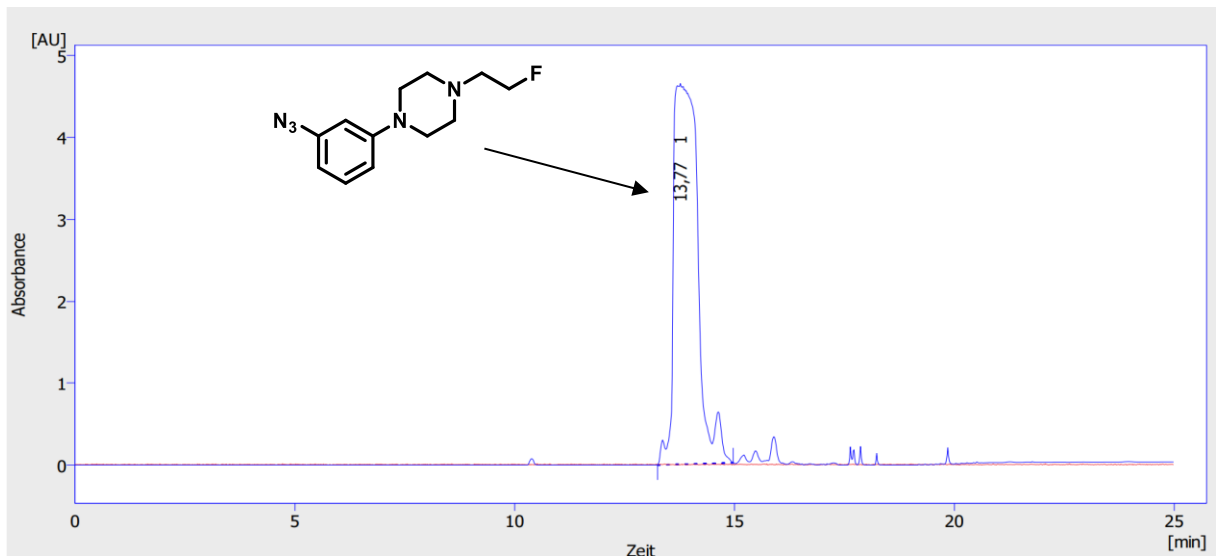


Figure 82: Eluent: 0–8 min: 5→20% MeCN (0.1% TFA), 8–17 min: 20→95% MeCN (0.1% TFA), 17–25 min: 95% MeCN (0.1% TFA); Flow rate: 1 mL/min; Luna 5  $\mu$ m PFP(2) 100 Å LC column 250x4.6 mm; p.c.i. = post column injection. Red: Radio HPLC trace, blue: UV trace 234 nm.

## 7 Experimental Part

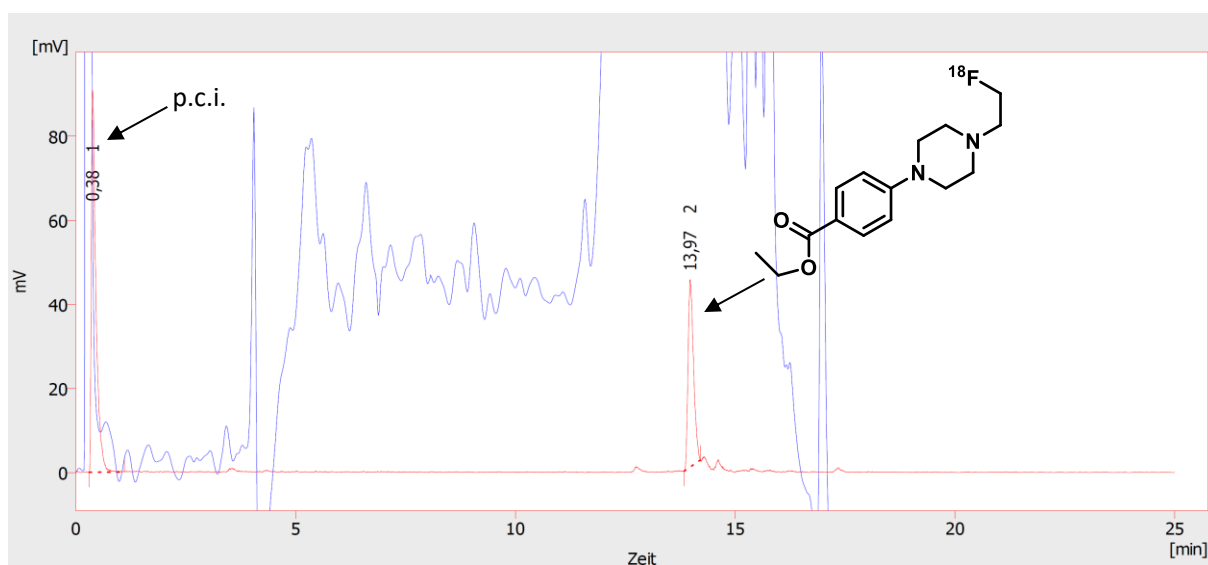


Figure 83: Eluent: 0–8 min: 5→20% MeCN (0.1% TFA), 8–17 min: 20→95% MeCN (0.1% TFA), 17–25 min: 95% MeCN (0.1% TFA); Flow rate: 1 mL/min; Luna 5  $\mu\text{m}$  PFP(2) 100 Å LC column 250x4.6 mm; p.c.i. = post column injection. Red: Radio HPLC trace, blue: UV trace 234 nm.

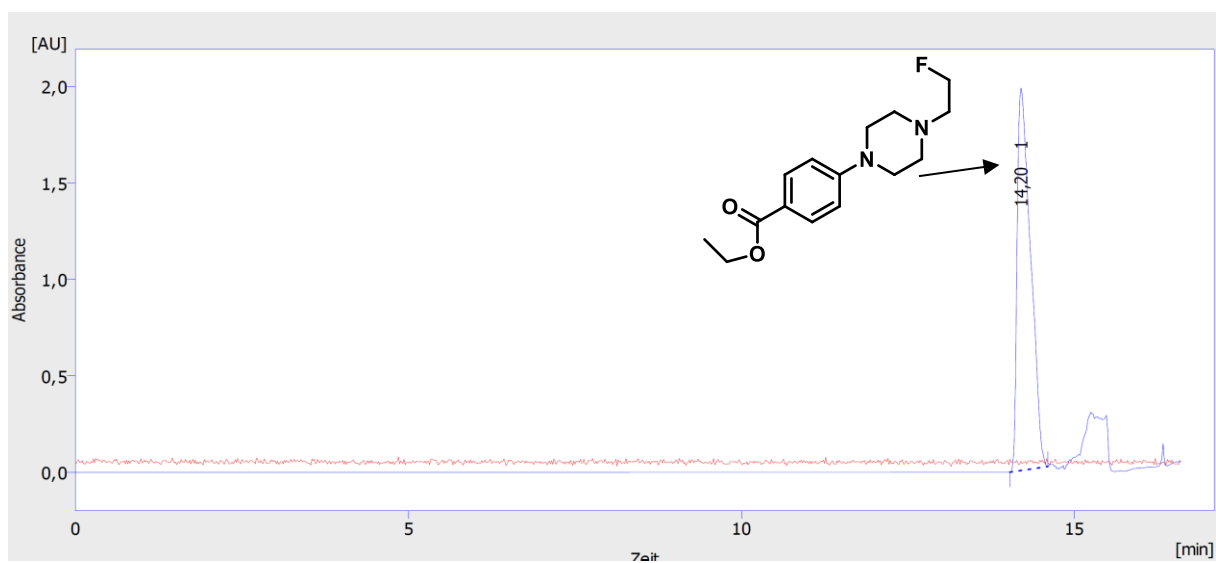


Figure 84: Eluent: 0–8 min: 5→20% MeCN (0.1% TFA), 8–17 min: 20→95% MeCN (0.1% TFA), 17–25 min: 95% MeCN (0.1% TFA); Flow rate: 1 mL/min; Luna 5  $\mu\text{m}$  PFP(2) 100 Å LC column 250x4.6 mm; p.c.i. = post column injection. Red: Radio HPLC trace, blue: UV trace 234 nm.

## 7 Experimental Part

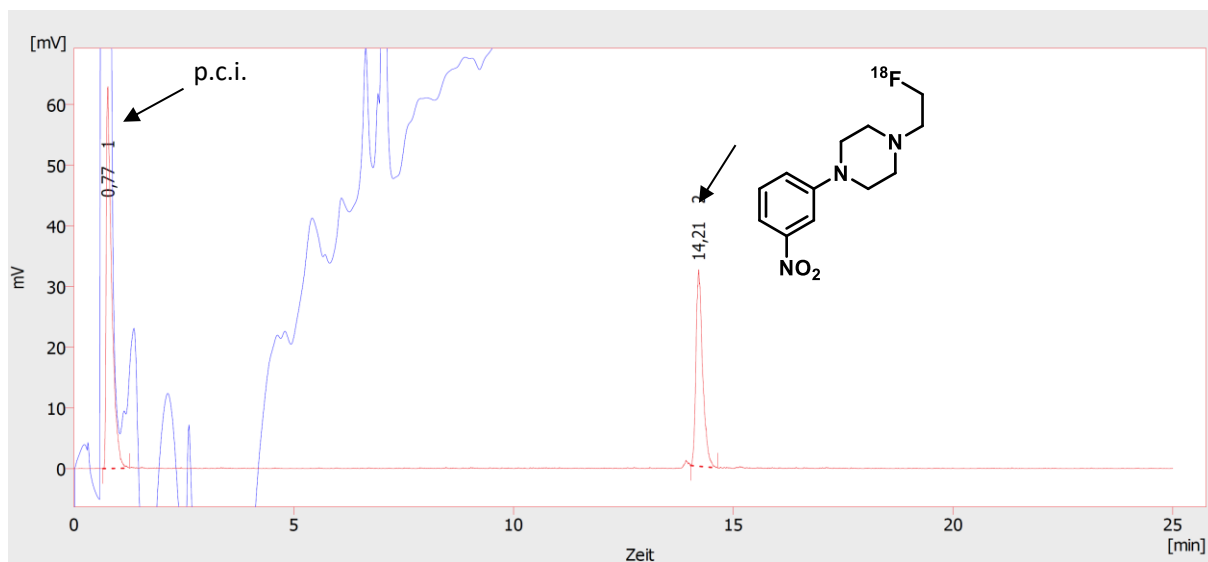


Figure 85: Eluent: 0–8 min: 5→20% MeCN (0.1% TFA), 8–17 min: 20→95% MeCN (0.1% TFA), 17–25 min: 95% MeCN (0.1% TFA); Flow rate: 1 mL/min; Luna 5  $\mu\text{m}$  PFP(2) 100 Å LC column 250x4.6 mm; p.c.i. = post column injection. Red: Radio HPLC trace, blue: UV trace 234 nm.

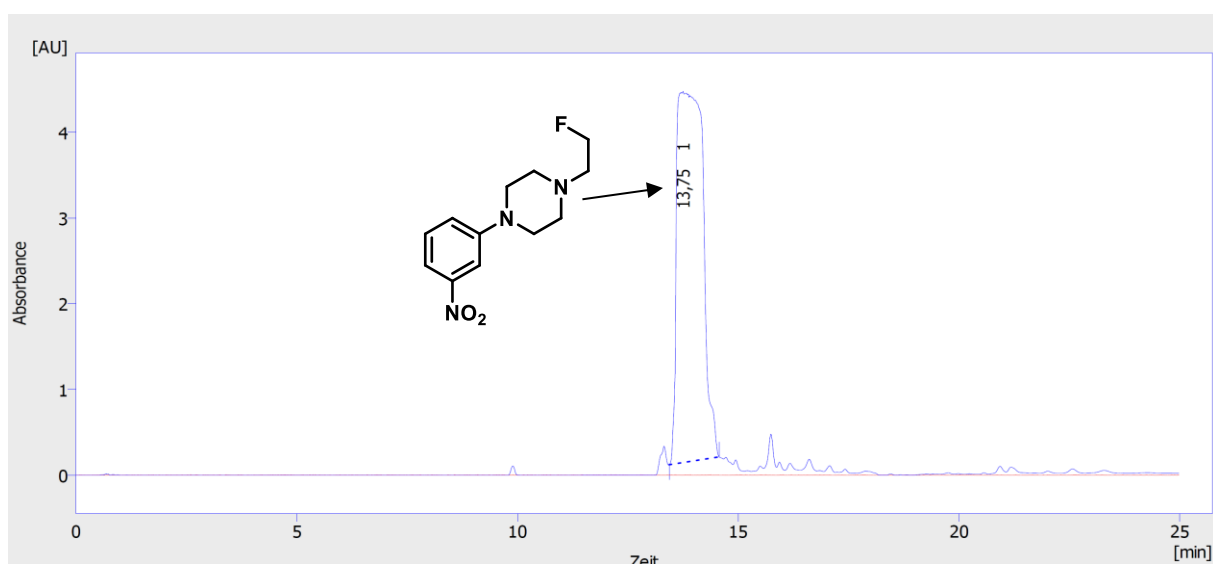


Figure 86: Eluent: 0–8 min: 5→20% MeCN (0.1% TFA), 8–17 min: 20→95% MeCN (0.1% TFA), 17–25 min: 95% MeCN (0.1% TFA); Flow rate: 1 mL/min; Luna 5  $\mu\text{m}$  PFP(2) 100 Å LC column 250x4.6 mm; p.c.i. = post column injection. Red: Radio HPLC trace, blue: UV trace 234 nm.

## 7 Experimental Part

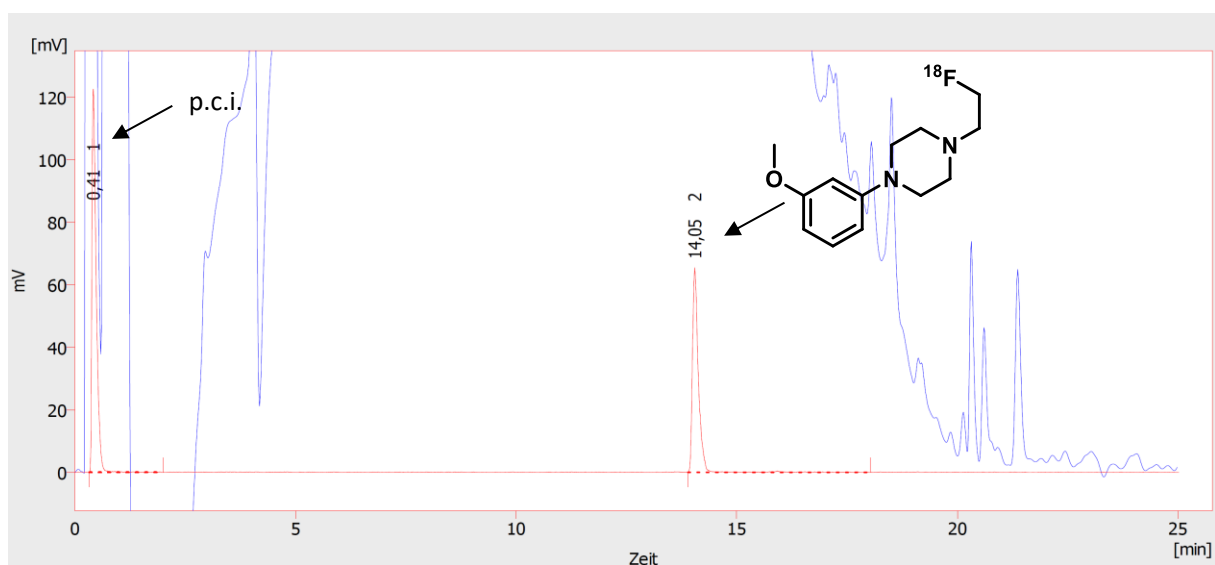


Figure 87: Eluent: 0–8 min: 5→20% MeCN (0.1% TFA), 8–17 min: 20→95% MeCN (0.1% TFA), 17–25 min: 95% MeCN (0.1% TFA); Flow rate: 1 mL/min; Luna 5  $\mu$ m PFP(2) 100 Å LC column 250x4.6 mm; p.c.i. = post column injection. Red: Radio HPLC trace, blue: UV trace 234 nm.

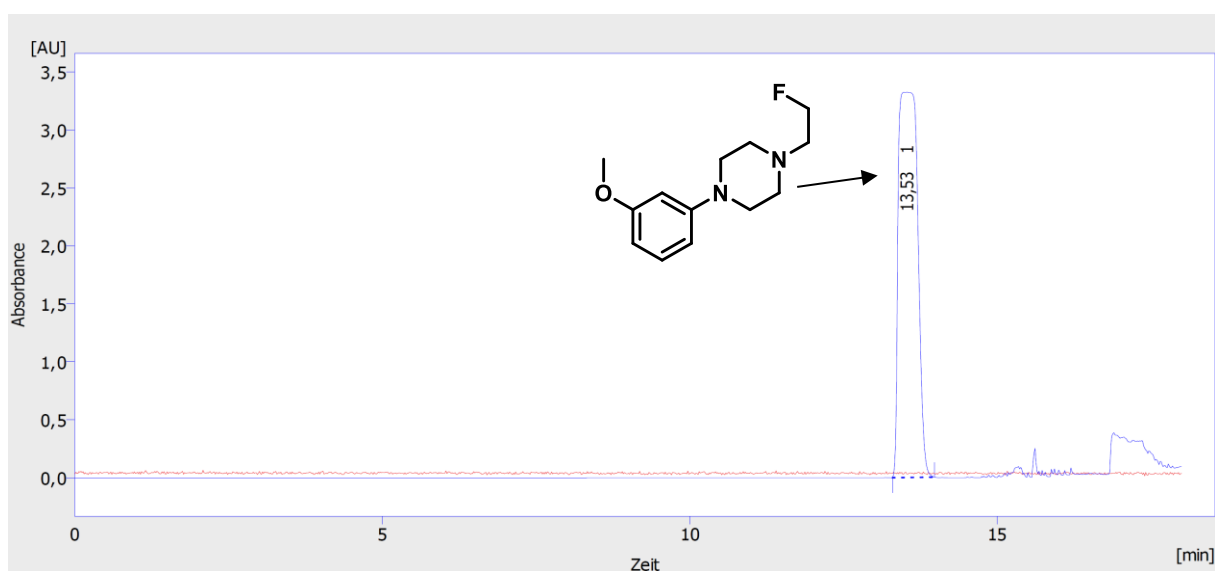


Figure 88: Eluent: 0–8 min: 5→20% MeCN (0.1% TFA), 8–17 min: 20→95% MeCN (0.1% TFA), 17–25 min: 95% MeCN (0.1% TFA); Flow rate: 1 mL/min; Luna 5  $\mu$ m PFP(2) 100 Å LC column 250x4.6 mm; p.c.i. = post column injection. Red: Radio HPLC trace, blue: UV trace 234 nm.

## 7 Experimental Part

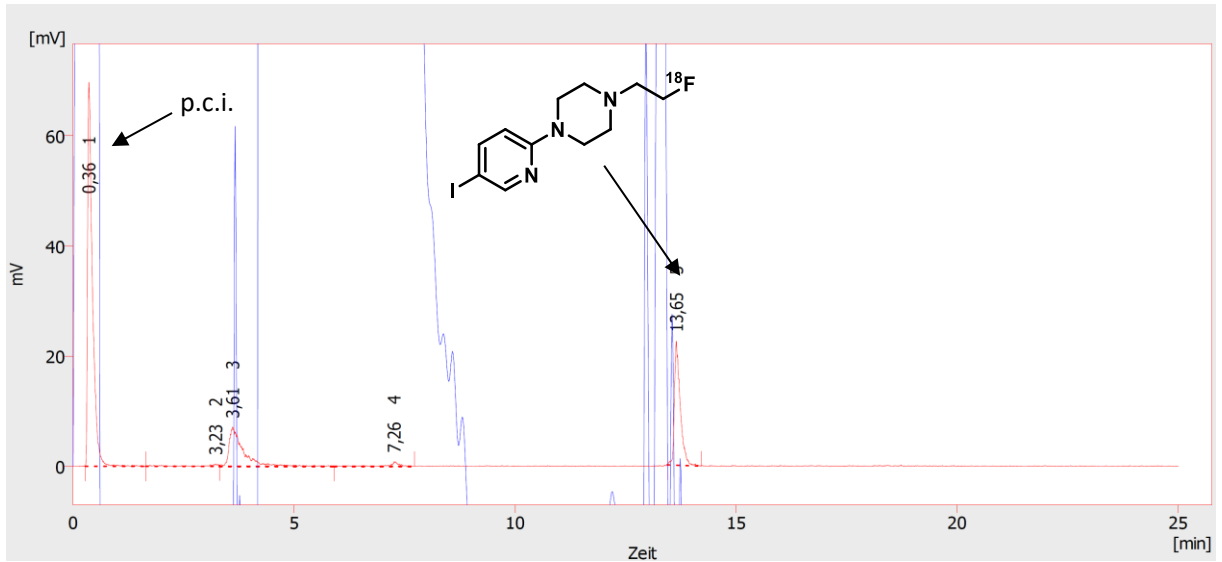


Figure 89: Eluent: 0–8 min: 5→20% MeCN (0.1% TFA), 8–17 min: 20→95% MeCN (0.1% TFA), 17–25 min: 95% MeCN (0.1% TFA); Flow rate: 1 mL/min; Luna 5  $\mu\text{m}$  PFP(2) 100 Å LC column 250x4.6 mm; p.c.i. = post column injection. Red: Radio HPLC trace, blue: UV trace 234 nm.

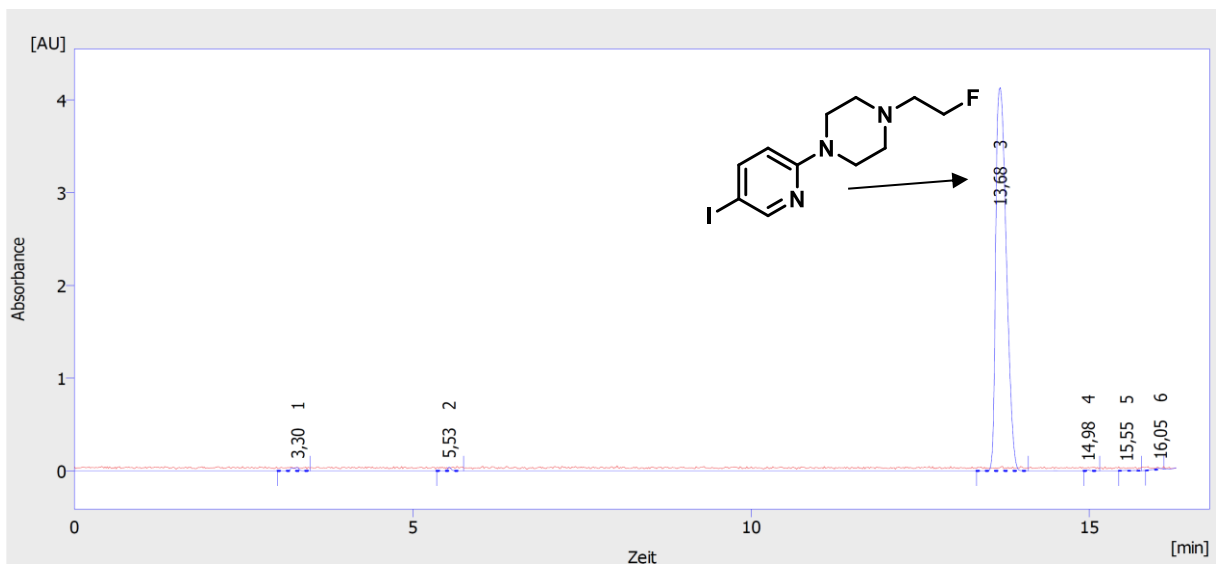


Figure 90: Eluent: 0–8 min: 5→20% MeCN (0.1% TFA), 8–17 min: 20→95% MeCN (0.1% TFA), 17–25 min: 95% MeCN (0.1% TFA); Flow rate: 1 mL/min; Luna 5  $\mu\text{m}$  PFP(2) 100 Å LC column 250x4.6 mm; p.c.i. = post column injection. Red: Radio HPLC trace, blue: UV trace 234 nm.

## 7 Experimental Part

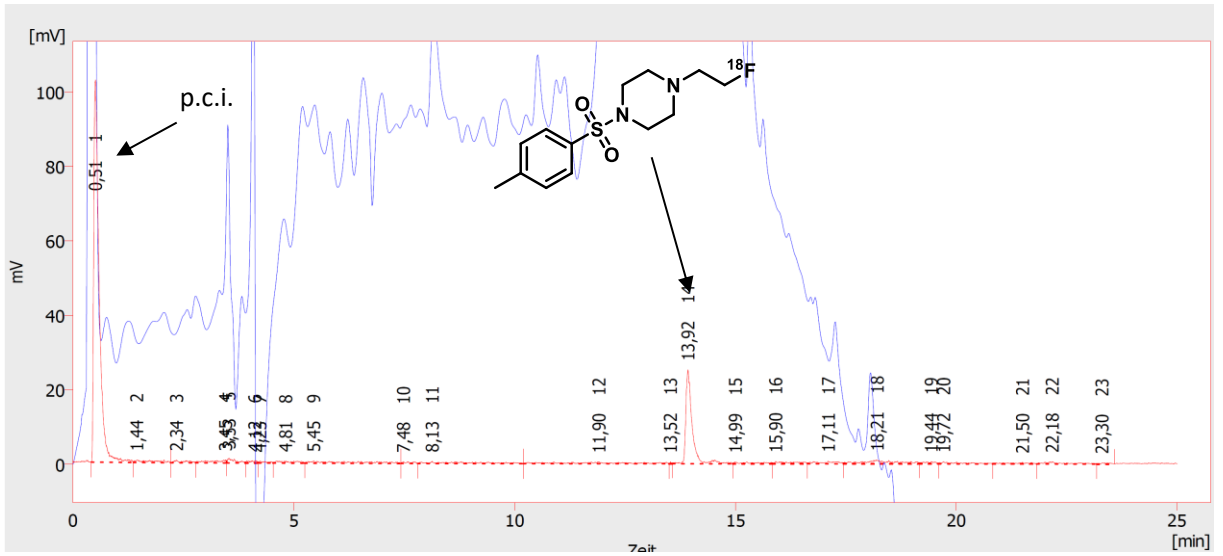


Figure 91: Eluent: 0–8 min: 5→20% MeCN (0.1% TFA), 8–17 min: 20→95% MeCN (0.1% TFA), 17–25 min: 95% MeCN (0.1% TFA); Flow rate: 1 mL/min; Luna 5  $\mu\text{m}$  PFP(2) 100  $\text{\AA}$  LC column 250x4.6 mm; p.c.i. = post column injection. Red: Radio HPLC trace, blue: UV trace 234 nm.

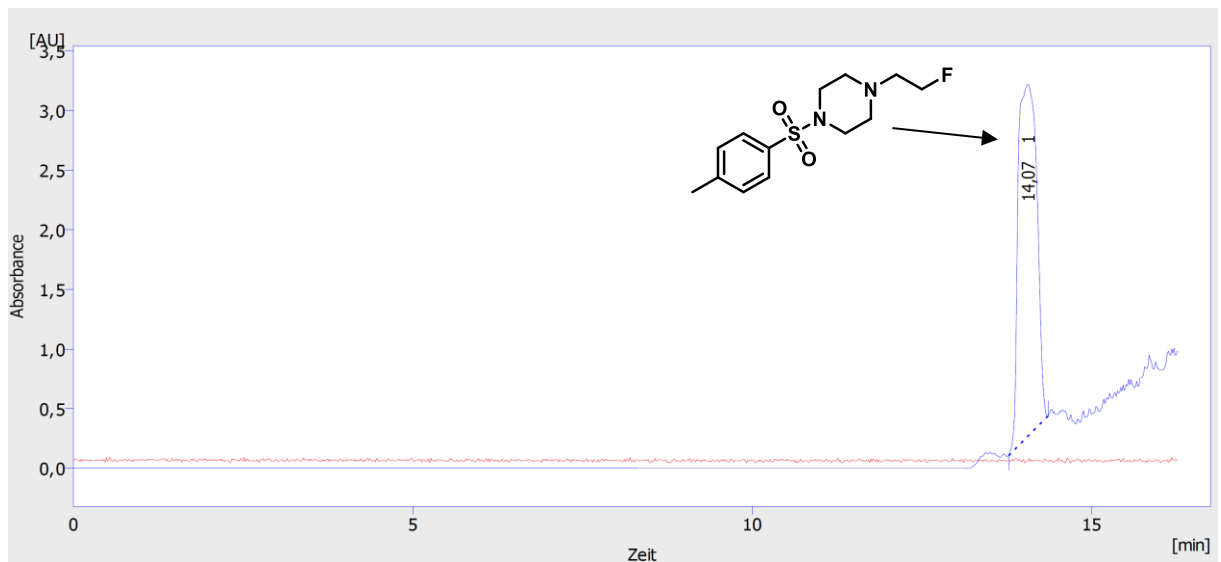
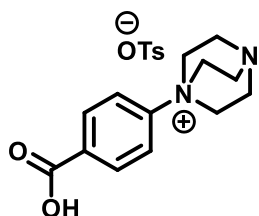


Figure 92: Eluent: 0–8 min: 5→20% MeCN (0.1% TFA), 8–17 min: 20→95% MeCN (0.1% TFA), 17–25 min: 95% MeCN (0.1% TFA); Flow rate: 1 mL/min; Luna 5  $\mu\text{m}$  PFP(2) 100  $\text{\AA}$  LC column 250x4.6 mm; p.c.i. = post column injection. Red: Radio HPLC trace, blue: UV trace 234 nm.

## 7.2 Experimental Part for DABCO Salts

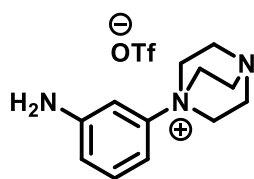
### 1-(4-Carboxyphenyl)-1,4-diazabicyclo[2.2.2]octan-1-ium tosylate (7)



1-(4-Carboxyphenyl)-1,4-diazabicyclo[2.2.2]octan-1-ium tosylate was synthesized starting from (4-(ethoxycarbonyl)phenyl)(mesityl)iodonium trifluoromethanesulfonate (0.25 mmol, 100 mg, 1 equiv.) it was dissolved in TFA (2.5 mmol, 288 mg, 192  $\mu$ L, 10 equiv.) and water (4 mL). The reaction mixture was heated for 3 h at 80 °C. Afterwards the TFA was removed under reduced pressure and the water was removed by lyophilization to give the title compound as a colorless solid (0.23 mmol, 89 mg, 90%).

$^1\text{H}$  NMR (400 MHz,  $\text{CD}_3\text{OD}$ )  $\delta$  = 8.20 – 8.09 (m, 2H), 7.88 – 7.78 (m, 2H), 3.99 – 3.88 (m, 6H), 3.44 – 3.36 (m, 6H).

### 1-(3-Aminophenyl)-1,4-diazabicyclo[2.2.2]octan-1-ium triflate (11)

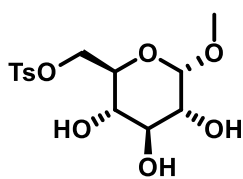


1-(3-Aminophenyl)-1,4-diazabicyclo[2.2.2]octan-1-ium triflate was synthesized starting from 1-(3-nitrophenyl)-1,4-diazabicyclo[2.2.2]octan-1-ium triflate (0.39 mmol, 150 mg, 1 equiv.). It was dissolved in ethanol (26 mL) and treated with iron powder (1.6 mmol, 87 mg, 4 equiv.) and acetic acid (12.6 g, 12 mL). The reaction mixture was stirred for 16 h at 100 °C. Afterwards, the solvents were removed under reduced pressure and the residue taken up in MeOH. The mixture was washed with a solution of  $\text{NaHCO}_3$  in water. The formed black solid is filtered off and the resulting organic phase is dried and evaporated under reduced pressure giving the title compound as clear oil (0.13 mmol, 46 mg, 34%).

$^1\text{H}$  NMR (400 MHz,  $\text{CD}_3\text{OD}$ )  $\delta$  = 8.62 (dd,  $J$  = 2.5, 1.6 Hz, 1H), 8.33 – 8.22 (m, 1H), 8.09 (dd,  $J$  = 8.2, 2.5 Hz, 1H), 7.93 (t,  $J$  = 8.2 Hz, 1H), 4.10 – 4.02 (m, 6H), 3.48 – 3.41 (m, 6H).

$^{19}\text{F}$  NMR (376 MHz,  $\text{CD}_3\text{OD}$ )  $\delta$  = -80.02.

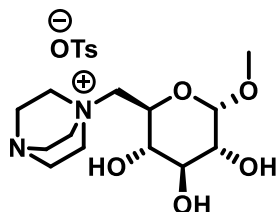
**((2R,3S,4S,5R,6S)-3,4,5-Trihydroxy-6-methoxytetrahydro-2H-pyran-2-yl)methyl 4-methylbenzenesulfonate (16)**



The title compound was synthesized starting from ((2R,3S,4S,5R,6S)-2-(Hydroxymethyl)-6-methoxytetrahydro-2H-pyran-3,4,5-triol (7.2 mmol, 1.4 g, 1 equiv.). It was dissolved in pyridine (14 mL) and treated with *p*-toluenesulfonyl chloride (9 mmol, 1.718 g, 1.25 equiv.). The reaction mixture was stirred at room temperature for 16 h. Afterwards, the pyridine was removed under reduced pressure and the residue purified by column chromatography (EtOAc:cyclohexane 30:70) giving the product as colorless solid (3.32 mmol, 1.150 g, 46%). The compound is already described in the literature<sup>[47]</sup>.

<sup>1</sup>H NMR (400 MHz, CD<sub>3</sub>OD) δ 7.85 – 7.75 (m, 2H), 7.46 (dd, *J* = 8.6, 0.6 Hz, 2H), 4.58 (d, *J* = 3.7 Hz, 1H), 4.33 (dd, *J* = 10.8, 2.0 Hz, 1H), 4.23 – 4.09 (m, 1H), 3.67 (ddd, *J* = 10.0, 6.0, 1.8 Hz, 1H), 3.61 – 3.53 (m, 1H), 3.36 – 3.30 (m, 4H), 3.19 (dt, *J* = 16.7, 8.3 Hz, 1H), 2.47 (s, 3H).

**1-(((2R,3S,4S,5R,6S)-3,4,5-Trihydroxy-6-methoxytetrahydro-2H-pyran-2-yl)methyl)-1,4-diazabicyclo[2.2.2]octan-1-ium tosylate (17)**

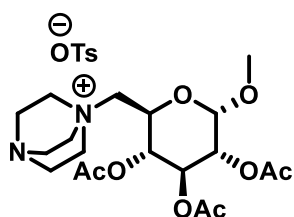


The title compound was synthesized starting from ((2R,3S,4S,5R,6S)-3,4,5-trihydroxy-6-methoxytetrahydro-2H-pyran-2-yl)methyl 4-methylbenzenesulfonate (0.32 mmol, 111 mg, 1 equiv.). It was dissolved in THF (4 mL) and DABCO (0.32 mmol, 36 mg, 1 equiv.) was added. The reaction mixture was stirred for 36 h at room temperature until a colorless oil formed. The solvent was removed under reduced pressure and the oil was washed with THF (5 mL) and diethylether (5 mL) under ultrasonication. The remaining oil was dried in a vacuum to yield the target salt as a colorless solid (0.22 mmol, 99 mg, 67%).

<sup>1</sup>H NMR (400 MHz, CD<sub>3</sub>OD) δ 7.79 – 7.66 (m, 2H), 7.25 (d, *J* = 0.6 Hz, 1H), 4.73 (t, *J* = 3.4 Hz, 1H), 4.18 (dd, *J* = 15.5, 6.5 Hz, 1H), 3.70 – 3.62 (m, 2H), 3.54 (s, 3H), 3.49 (dd, *J* = 9.5, 4.3 Hz, 6H), 3.41 (dd, *J* = 9.8, 3.7 Hz, 1H), 3.27 – 3.20 (m, 6H), 3.15 – 3.08 (m, 1H), 2.39 (s, 3H), 1.20 (t, *J* = 7.0 Hz, 1H).

m/z: [M<sup>+</sup>] calcd. for C<sub>13</sub>H<sub>25</sub>N<sub>2</sub>O<sub>5</sub>, 289.18; found, 289.31.

**1-(((2R,3R,4S,5R,6S)-3,4,5-Triacetoxy-6-methoxytetrahydro-2H-pyran-2-yl)methyl)-1,4-diazabicyclo[2.2.2]octan-1-ium tosylate (18)**

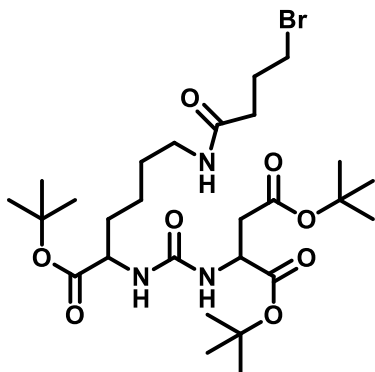


The title compound was synthesized starting from 1-(((2R,3S,4S,5R,6S)-3,4,5-trihydroxy-6-methoxytetrahydro-2H-pyran-2-yl)methyl)-1,4-diazabicyclo[2.2.2]octan-1-ium tosylate (0.16 mmol, 95 mg, 1 equiv.). It was dissolved in a mixture of acetic anhydride (300  $\mu$ L) and pyridine (300  $\mu$ L). After stirring for 16 h at room temperature the solvents were removed under reduced pressure and the residue was dissolved in water (3 mL) and lyophilized to give the title compound as colorless solid (0.13 mmol, 97 mg, 80%).

$^1\text{H}$  NMR (400 MHz,  $\text{CD}_3\text{OD}$ )  $\delta$  7.73 (d,  $J$  = 8.2 Hz, 2H), 7.27 (d,  $J$  = 7.9 Hz, 2H), 5.54 – 5.42 (m, 1H), 5.04 (d,  $J$  = 3.6 Hz, 1H), 4.99 – 4.89 (m, 3H), 4.61 (t,  $J$  = 9.1 Hz, 1H), 3.62 (dt,  $J$  = 13.9, 7.0 Hz, 1H), 3.56 (d,  $J$  = 7.1 Hz, 3H), 3.56 – 3.41 (m, 6H), 3.30 – 3.22 (m, 6H), 2.39 (s, 3H), 2.10 – 1.98 (m, 9H).

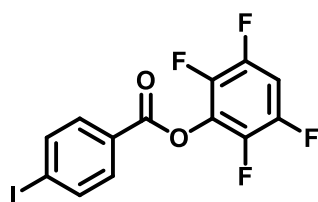
$m/z$ : [ $\text{M}^+$ ] calcd. for  $\text{C}_{19}\text{H}_{31}\text{N}_2\text{O}_8$ , 415.21; found, 415.27.

**Di-*tert*-butyl ((6-(4-bromobutanamido)-1-(*tert*-butoxy)-1-oxohexan-2-yl)carbamoyl)aspartate (21)**



The title compound was prepared starting from di-*tert*-butyl ((6-amino-1-(*tert*-butoxy)-1-oxohexan-2-yl)carbamoyl)aspartate. For this bromobutanic anhydride (0.5 mmol, 142 mg, 1.1 equiv.) was given to a solution of di-*tert*-butyl ((6-amino-1-(*tert*-butoxy)-1-oxohexan-2-yl)carbamoyl)aspartate (0.45 mmol, 200 mg, 1 equiv.) and  $\text{NEt}_3$  (0.9 mmol, 91 mg, 2 equiv.) in DCM (5 mL) at 0  $^\circ\text{C}$ . The reaction mixture was warmed to room temperature over 1 h and stirred for 16 h at room temperature. The reaction mixture was washed with water and brine and the organic phase dried with  $\text{NaSO}_4$ . The solvent was removed under reduced pressure and the residue purified by column chromatography (15% EtOAc in cyclohexane) to give the product as a colorless oil (0.41 mmol, 0.235 g, 92%).

$^1\text{H}$  NMR (400 MHz,  $\text{CD}_3\text{OD}$ )  $\delta$  = 4.37 (t,  $J$  = 7.1 Hz, 2H), 4.24 – 4.11 (m, 2H), 3.04 (q,  $J$  = 7.0 Hz, 1H), 2.69 – 2.20 (m, 8H), 2.14 – 1.59 (m, 6H), 1.50 – 1.46 (m, 27H), 1.43 – 1.26 (m, 2H), 1.07 (t,  $J$  = 7.2 Hz, 1H).

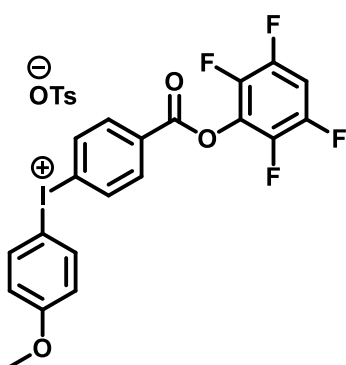
**2,3,5,6-Tetrafluorophenyl 4-iodobenzoate (24)**

The title compound was prepared from 4-iodobenzoic acid (16 mmol, 2 g, 1 equiv.) which was given to 2,3,5,6-tetrafluorophenol (8 mmol, 1.33 g, 1 equiv.) and *N,N'*-Dicyclohexylcarbodiimid (12 mmol, 2.5 g, 1.5 equiv.) in DCM (15 mL). The mixture was stirred for 16 h at room temperature. The solvent was washed with water (10 mL) and brine (10 mL) and the organic phase dried with NaSO<sub>4</sub>. The solvent was removed under reduced pressure to give the product as a colorless solid (3.68 mmol, 1.45 g, 46%). The compound is already described in the literature<sup>[13]</sup>.

<sup>1</sup>H NMR (400 MHz, CDCl<sub>3</sub>) δ = 7.99 – 7.89 (m, 4H), 7.14 – 7.02 (m, 1H).

<sup>19</sup>F NMR (376 MHz, CDCl<sub>3</sub>) δ = -138.75 (dd, *J* = 21.9, 9.7 Hz), -152.66 (dd, *J* = 21.6, 9.8 Hz).

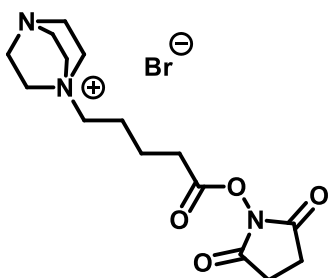
**(4-Methoxyphenyl)(4-((2,3,5,6-tetrafluorophenoxy)carbonyl)phenyl)iodonium tosylate (25)**



The title compound was prepared from 2,3,5,6-tetrafluorophenyl 4-iodobenzoate (2.28 mmol, 0.900 g, 1 equiv.) which was dissolved in DCM (5 mL) and 2,2,2-trifluoroethanol (5 mL) with *p*-toluenesulfonic acid (3.4 mmol, 0.586 g, 1.5 equiv.), mCPBA (6.8 mmol, 1.172 g, 3 equiv.) and anisole (4.3 mmol, 0.467 g, 1.9 equiv.). The reaction mixture was stirred at room temperature for 16 h before Et<sub>2</sub>O (20 mL) was added. The formed suspension was stirred for an additional hour and filtrated to give the title compound as a colorless solid (1.25 mmol, 0.835 g, 55%). The compound is already described in the literature<sup>[13]</sup>.

<sup>1</sup>H NMR (400 MHz, CDCl<sub>3</sub>) δ = 8.17 (d, *J* = 8.5 Hz, 2H), 7.99 (dt, *J* = 19.5, 9.7 Hz, 4H), 7.39 (d, *J* = 8.0 Hz, 2H), 7.08 (dq, *J* = 9.8, 7.1 Hz, 1H), 6.99 (d, *J* = 7.9 Hz, 2H), 6.82 (d, *J* = 8.9 Hz, 2H), 3.79 (s, *J* = 5.5 Hz, 3H), 2.30 (s, 3H).

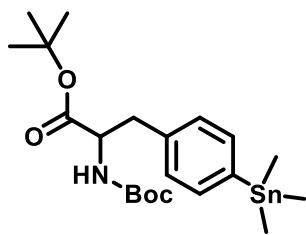
**1-(5-((2,5-Dioxopyrrolidin-1-yl)oxy)-5-oxopentyl)-1,4-diazabicyclo[2.2.2]octan-1-ium bromide (23c)**



For the synthesis of 1-(5-((2,5-dioxopyrrolidin-1-yl)oxy)-5-oxopentyl)-1,4-diazabicyclo[2.2.2]octan-1-ium bromide, 5-bromopentanoic acid (11.1 mmol, 2 g, 1 equiv.) was dissolved in DCM (11 mL) and *N,N'*-dicyclohexylcarbodiimid (16.6 mmol, 3.419 g, 1.5 equiv.) and *N*-hydroxysuccinimid (13.2 mmol, 1.526 g, 1.2 equiv.) were added to the solution. The reaction mixture was stirred for 16 h and washed with water (10 mL). The organic phase was separated and the solvent removed under reduced pressure giving a colorless oil (9 mmol, 2.4 g, 82%). The oil (1.7 mmol, 0.500 g, 1 equiv.) was dissolved in THF (8 mL) and DABCO (1.7 mmol, 192 mg, 1 equiv.) was given to the solution. After stirring for 40 h a colorless solid formed. It was filtered off and washed with Et<sub>2</sub>O to give the title compound as colorless solid (1.1 mmol, 0.440 g, 65%).

<sup>1</sup>H NMR (400 MHz, CD<sub>3</sub>OD) δ 3.49 – 3.38 (m, 6H), 3.36 – 3.30 (m, 4H), 3.22 (dd, *J* = 10.0, 4.9 Hz, 6H), 2.87 (s, 4H), 2.80 (t, *J* = 6.9 Hz, 2H), 1.96 (ddd, *J* = 11.5, 10.2, 6.0 Hz, 2H), 1.88 – 1.80 (m, 2H).

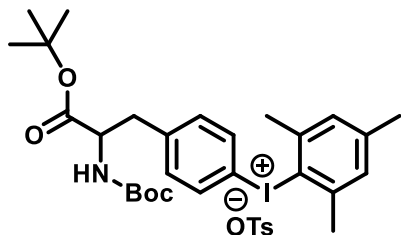
***tert*-Butyl-2-((*tert*-butoxycarbonyl)amino)-3-(4-**



**(trimethylstannyl)phenyl)propanoate (27)**

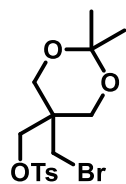
The title compound was prepared from *tert*-butyl 2-((*tert*-butoxycarbonyl)amino)-3-(4-iodophenyl)propanoate (1.1 mmol, 0.420 g, 1 equiv.) which was dissolved in dioxan (5 mL) and Sn<sub>2</sub>Me<sub>6</sub> (2.6 mmol, 0.844 g, 2.4 equiv.) and Pd(Ph<sub>3</sub>)<sub>4</sub> (0.11 mmol, 124 mg, 0.1 equiv.) were added. The mixture was stirred for 3 h at 80 °C filtered through celite and the organic solvent was removed under reduced pressure to give the title compound as colorless oil (0.1 mmol, .420 g, 92%).

**(4-(3-(*tert*-Butoxy)-2-((*tert*-butoxycarbonyl)amino)-3-oxopropyl)phenyl)(mesityl)iodonium tosylate (28)**



The title compound was prepared from *tert*-butyl 2-((*tert*-butoxycarbonyl)amino)-3-(4-(trimethylstannyl)phenyl)propanoate (0.1 mmol, 0.420 g, 1 equiv.) which was dissolved in DCM (10 mL). Hydroxy(tosyloxy)iodobenzene (0.1 mmol, 0.279 g, 1 equiv.) was added and the mixture was stirred for 16 h. The solvent was removed under reduced pressure and the residue purified by RP-column chromatography (20% MeCN in water) to give the title compound as colorless solid (0.02 mmol, 154 mg, 21%). The compound is already described in the literature<sup>[48]</sup>. The analytical data are in accordance with the published data.

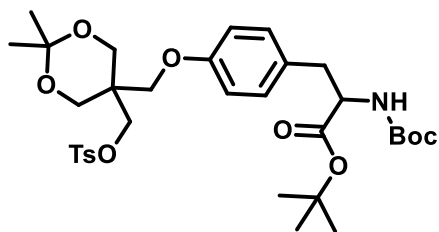
**(5-(Bromomethyl)-2,2-dimethyl-1,3-dioxan-5-yl)methyl 4-methylbenzenesulfonate (29)**



The title compound was prepared from 2-(bromomethyl)-2-(hydroxymethyl)propane-1,3-diol (5 mmol, 1 equiv., 1 g). It was dissolved in acetone (1.25 M, 6.25 mL) and treated with *p*-toluenesulfonic acid (0.05 mmol, 8.6 mg, 0.01 equiv.). The mixture was stirred for 16 h and treated with K<sub>2</sub>CO<sub>3</sub> (0.1 mmol, 13.8 mg, 0.02 equiv.). The mixture was stirred for an additional 1 h and diluted with water (10 mL) and extracted with EtOAc (20 mL). The organic phase was separated, dried with NaSO<sub>4</sub> and the solvent was removed under reduced pressure. The residue was dissolved in DCM (10 mL) and *p*-toluenesulfonic acid (5 mmol, 0.950g, 1 equiv.) and triethylamine (5 mmol, 0.505g, 1 equiv.) were added. The mixture was stirred for 16 h at room temperature. The solvent was removed under reduced pressure and the residue purified via column chromatography (20% EtOAc in cyclohexane) to give the title compound as colorless oil (2.5 mmol, 1.021 g, 52%).

<sup>1</sup>H NMR (400 MHz, CDCl<sub>3</sub>) δ = 7.87 – 7.78 (m, 2H), 7.39 (dd, *J* = 8.6, 0.6 Hz, 2H), 4.12 (s, 2H), 3.71 (s, 4H), 3.43 (s, 2H), 2.48 (s, 3H), 1.40 (s, 3H), 1.33 (s, 3H).

***tert*-Butyl 2-((*tert*-butoxycarbonyl)amino)-3-(4-((2,2-dimethyl-5-((tosyloxy)methyl)-1,3-dioxan-5-yl)methoxy)phenyl)propanoate (30)**

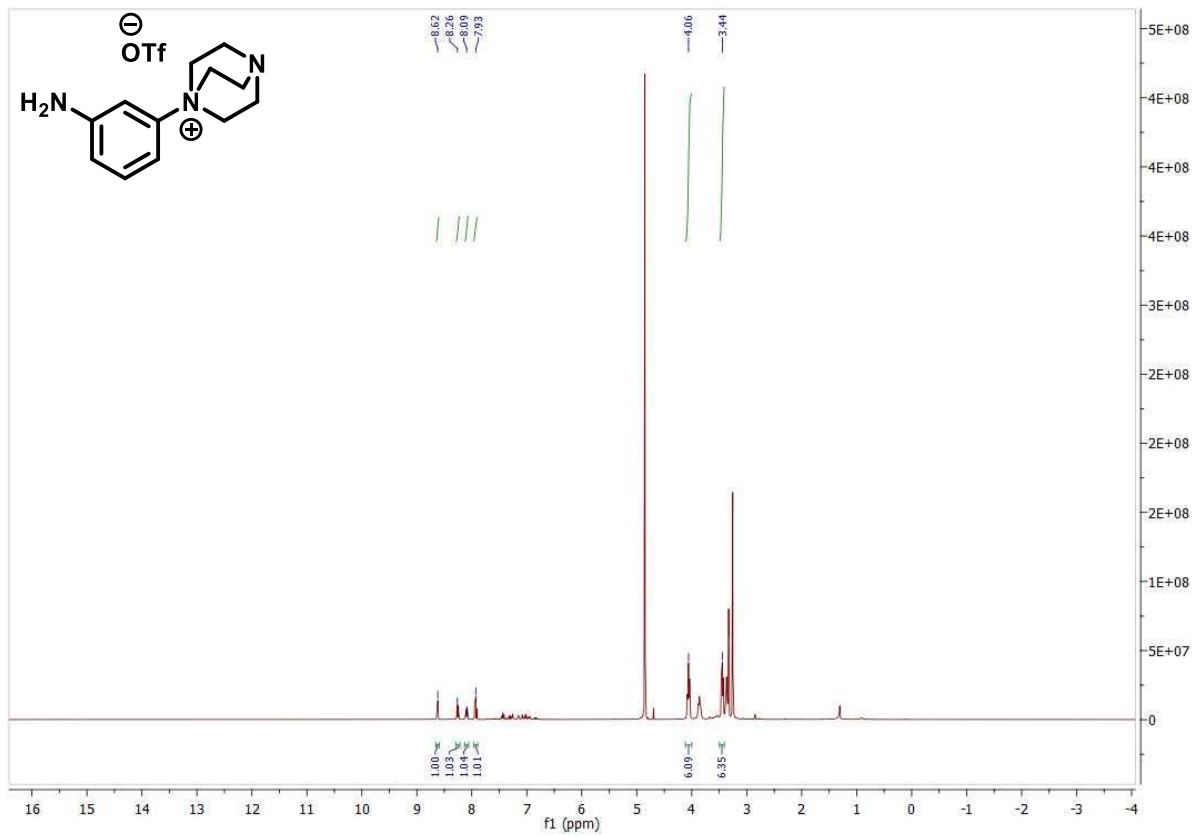
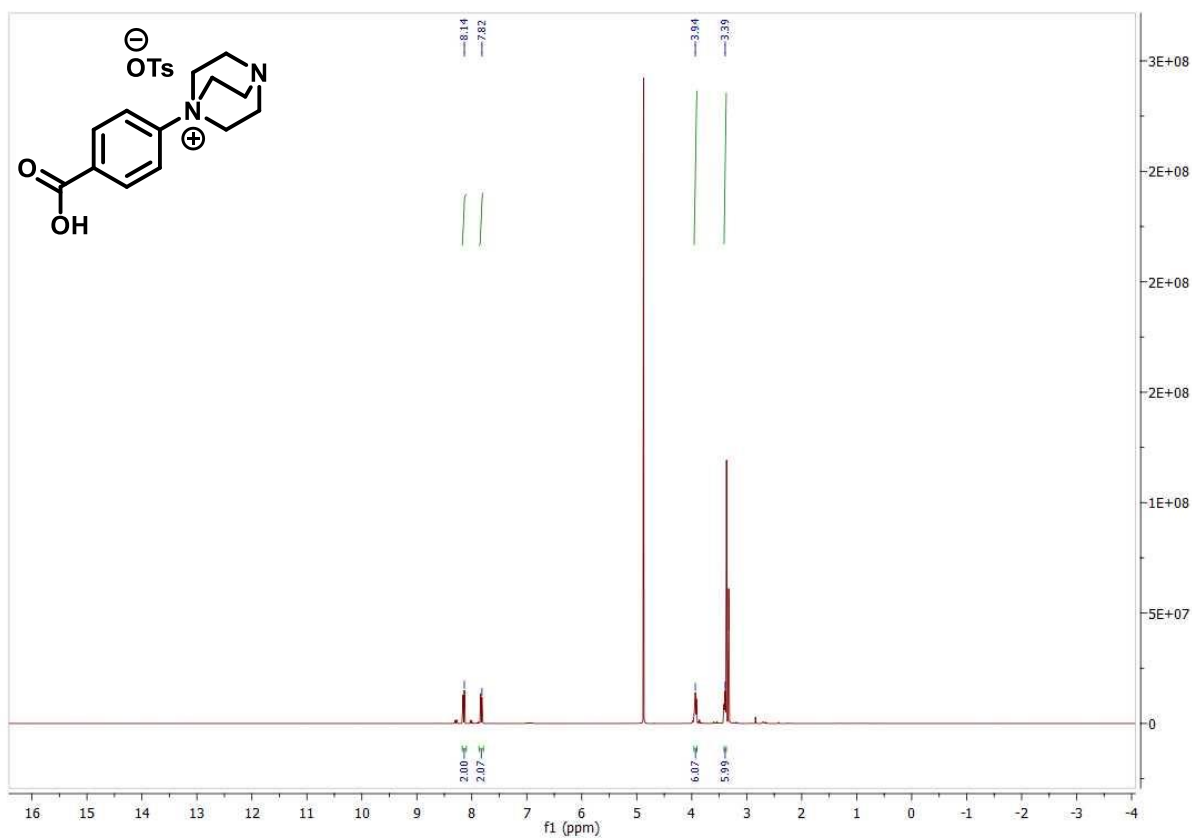


The title compound was synthesized starting from (5-(bromomethyl)-2,2-dimethyl-1,3-dioxan-5-yl)methyl 4-methylbenzenesulfonate (0.2 mmol, 50 mg, 1 equiv.) which was dissolved in DMF (3 mL).  $K_2CO_3$  (0.4 mmol, 55 mg, 2 equiv.) and *tert*-butyl (*tert*-butoxycarbonyl)tyrosinate (0.2 mmol, 57 mg, 1 equiv.) were added. The mixture was stirred for 16 h and quenched with water (3 mL). The mixture was extracted with EtOAc (3x10 mL) and the organic phase was dried with  $Na_2SO_4$ . The solvent was removed under reduced pressure and the residue purified by column chromatography (25% EtOAc in cyclohexane) to give the title compound as colorless oil (0.07 mmol, 35 mg, 43%).

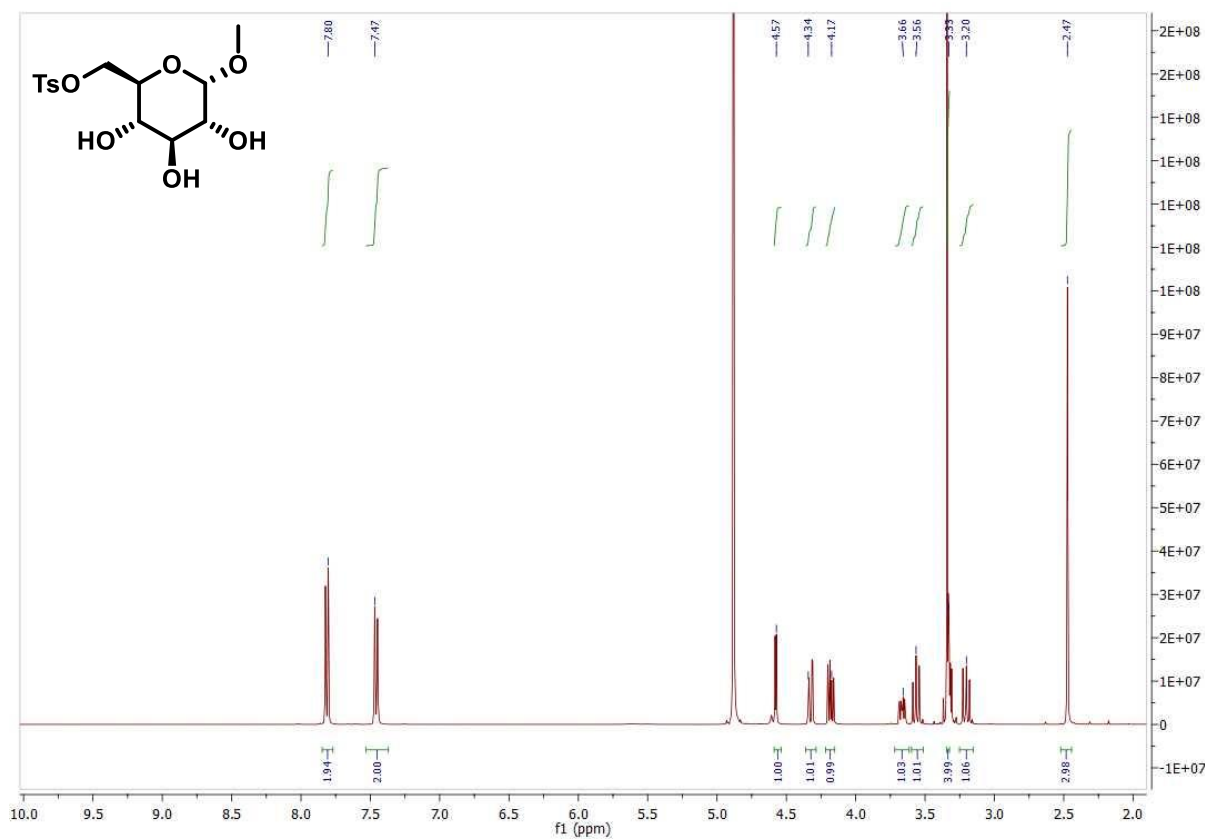
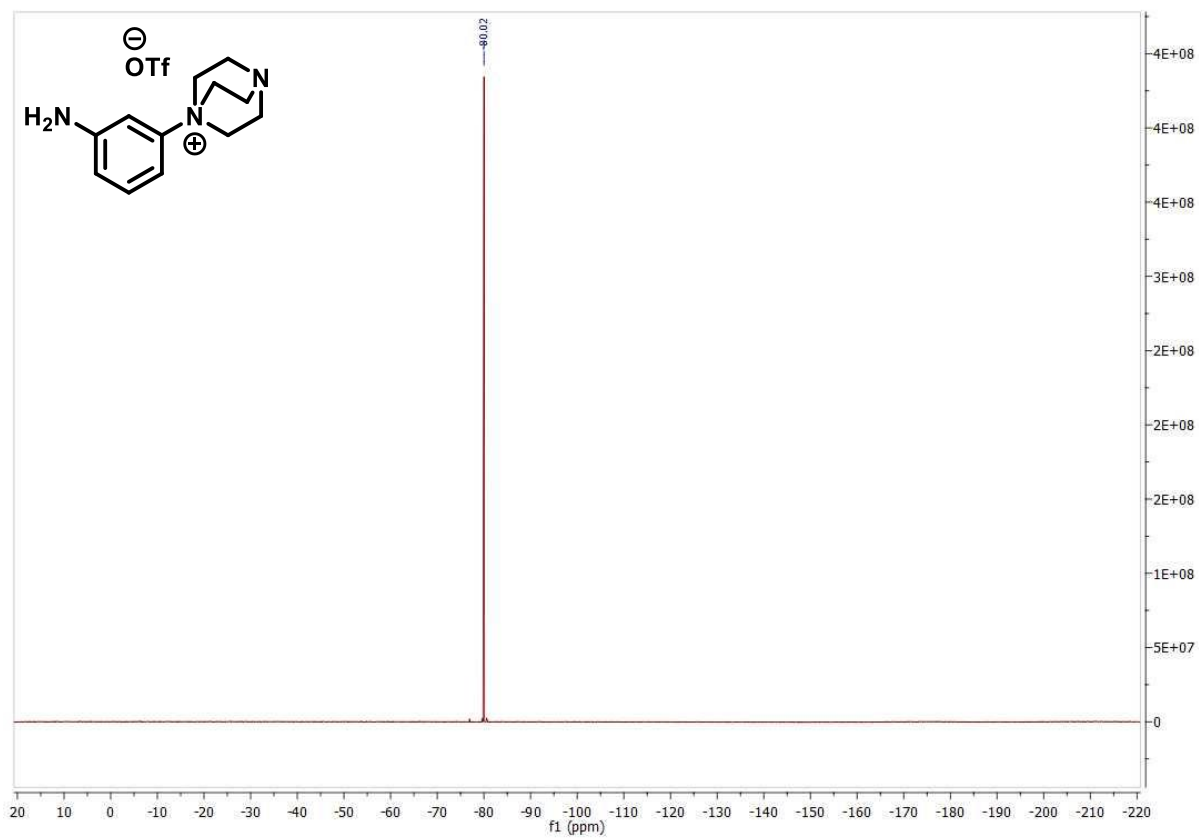
$^1H$  NMR (400 MHz,  $CDCl_3$ )  $\delta$  = 7.72 (dd,  $J$  = 16.0, 8.3 Hz, 2H), 7.24 (dd,  $J$  = 8.3, 4.0 Hz, 2H), 7.03 (t,  $J$  = 7.3 Hz, 2H), 6.70 (d,  $J$  = 8.6 Hz, 2H), 4.99 (d,  $J$  = 7.9 Hz, 1H), 4.60 – 4.52 (m, 1H), 4.17 (d,  $J$  = 6.0 Hz, 2H), 3.85 (d,  $J$  = 5.4 Hz, 2H), 3.82 – 3.80 (m, 2H), 3.77 (s, 1H), 3.74 (s, 3H), 3.05 (tt,  $J$  = 13.8, 6.9 Hz, 2H), 2.40 (s, 3H), 1.44 (s, 9H), 1.40 (s, 3H), 1.36 (s, 3H).

## 7 Experimental Part

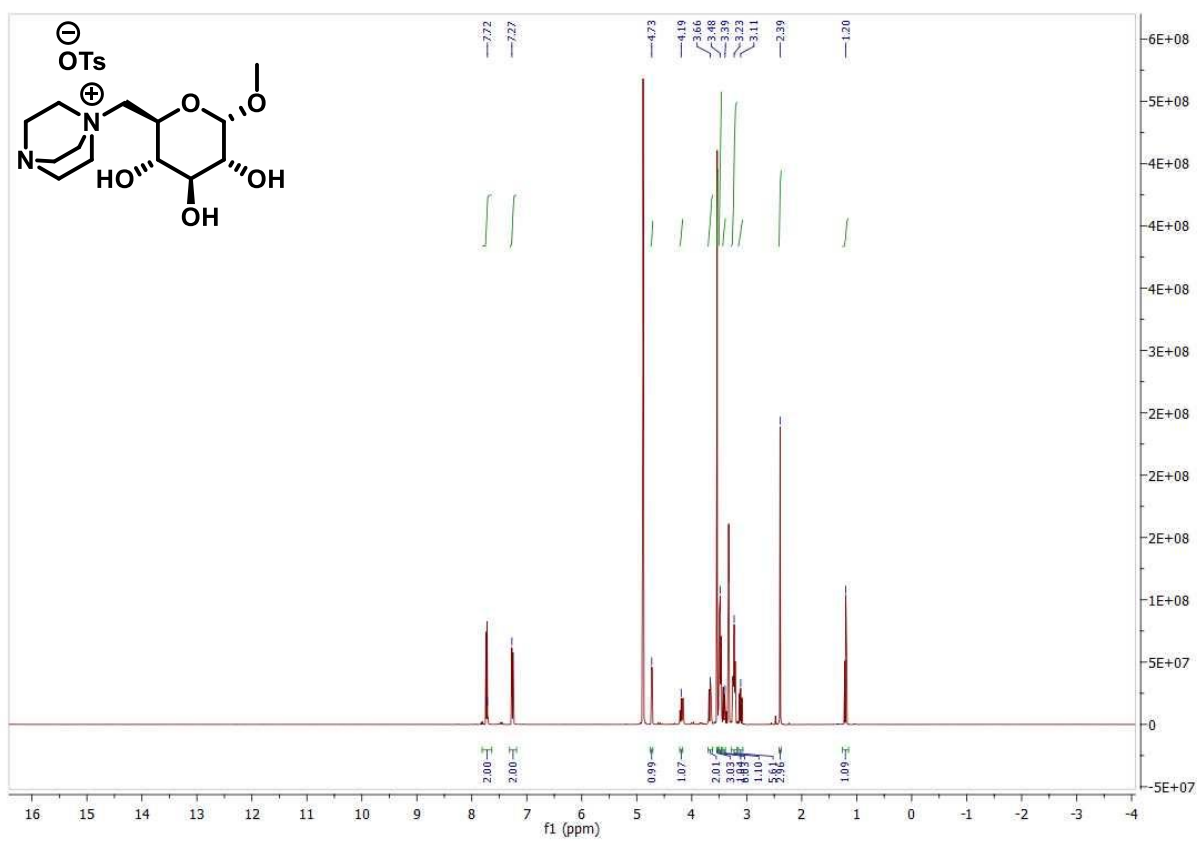
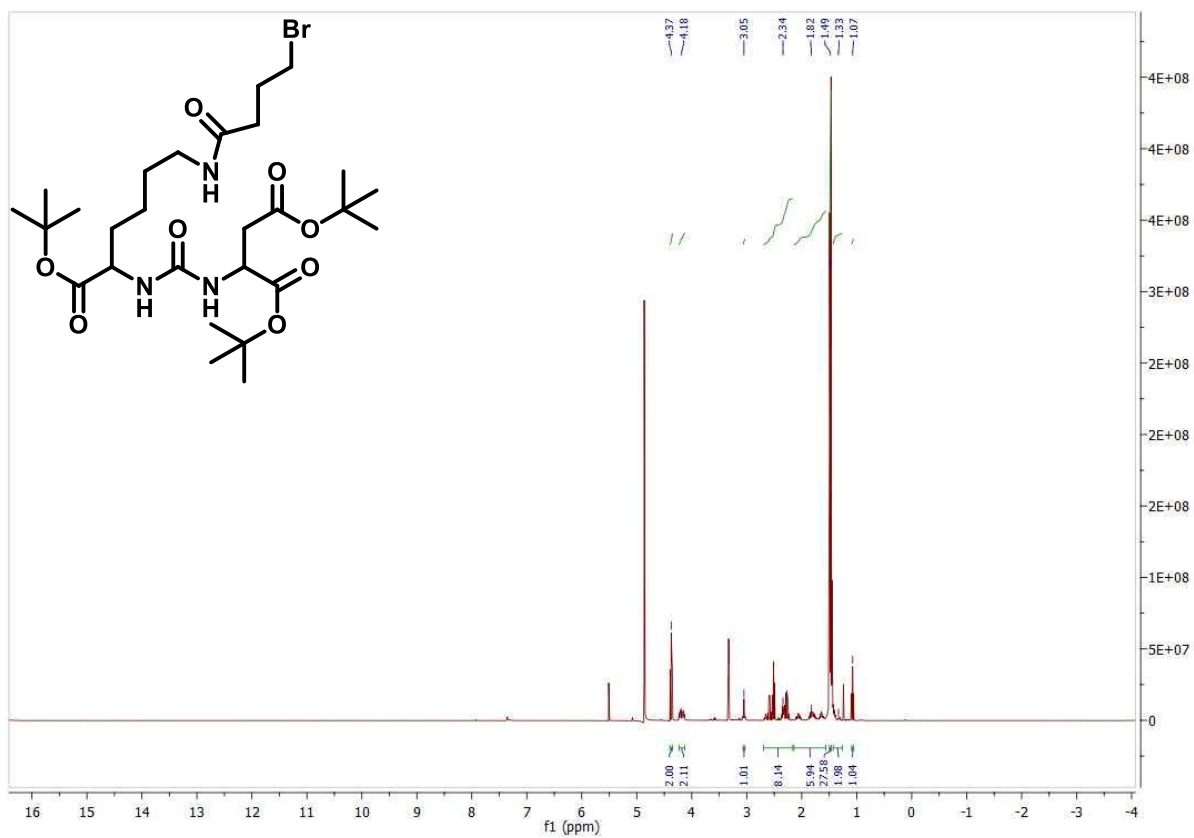
### NMR Spectra



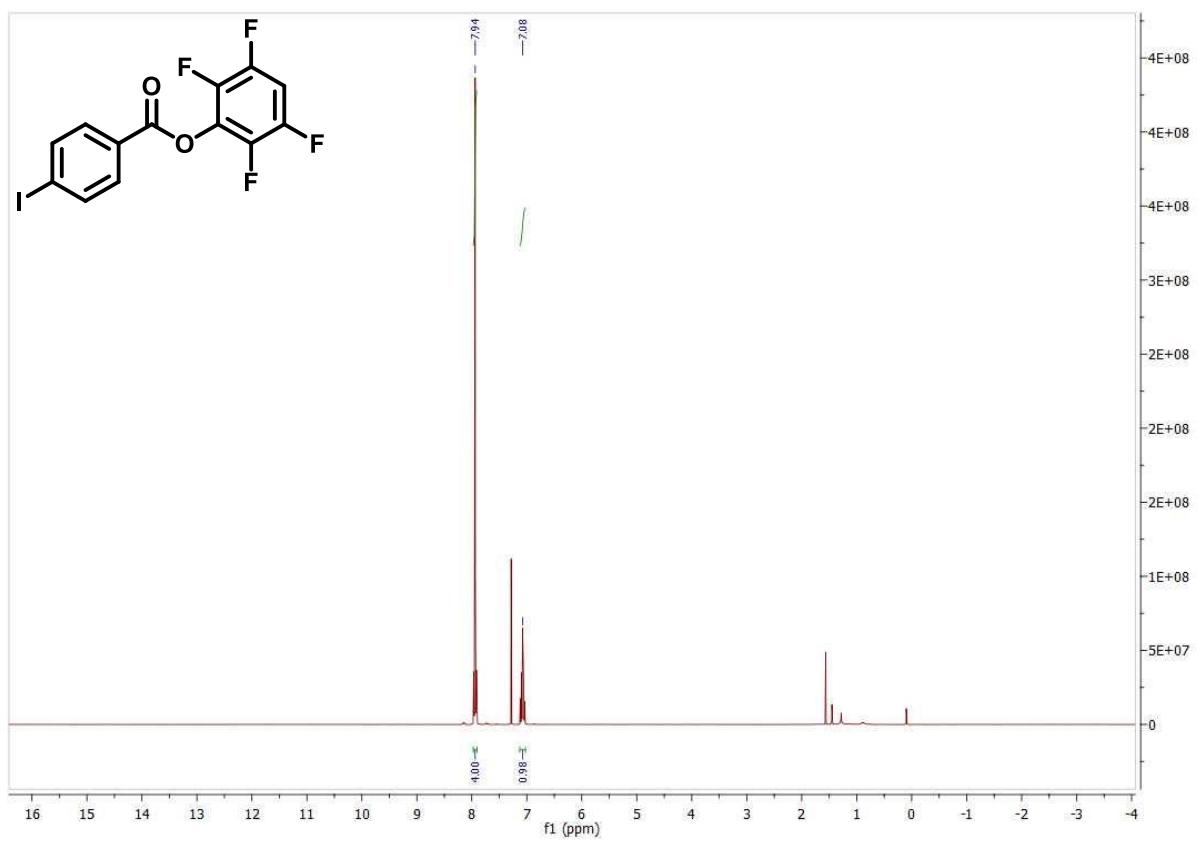
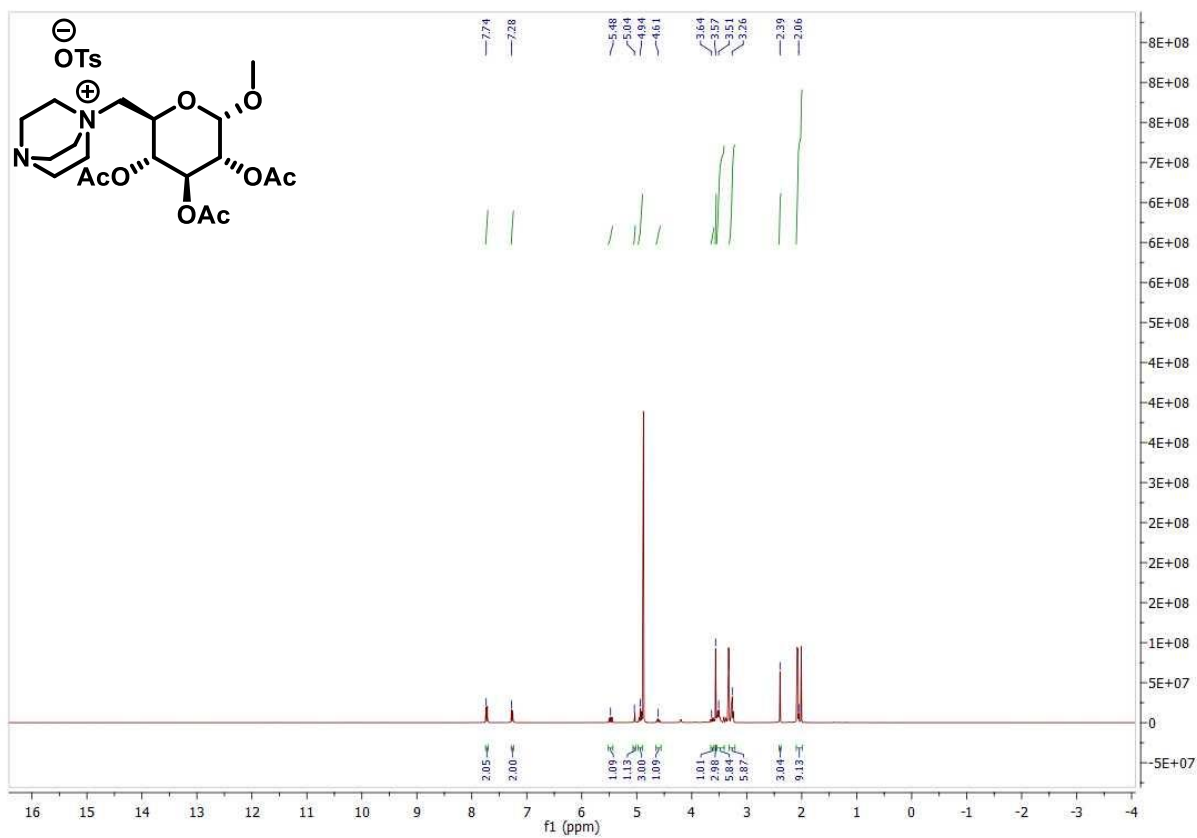
## 7 Experimental Part



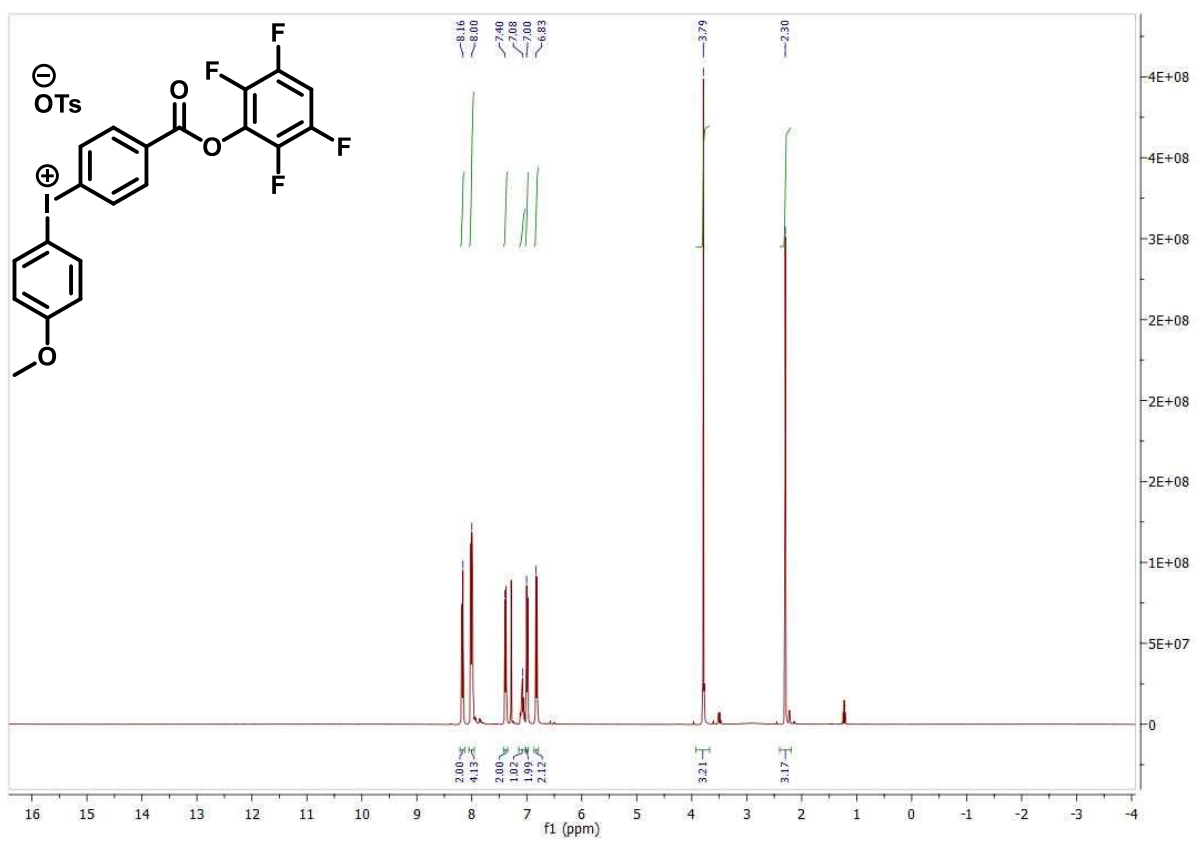
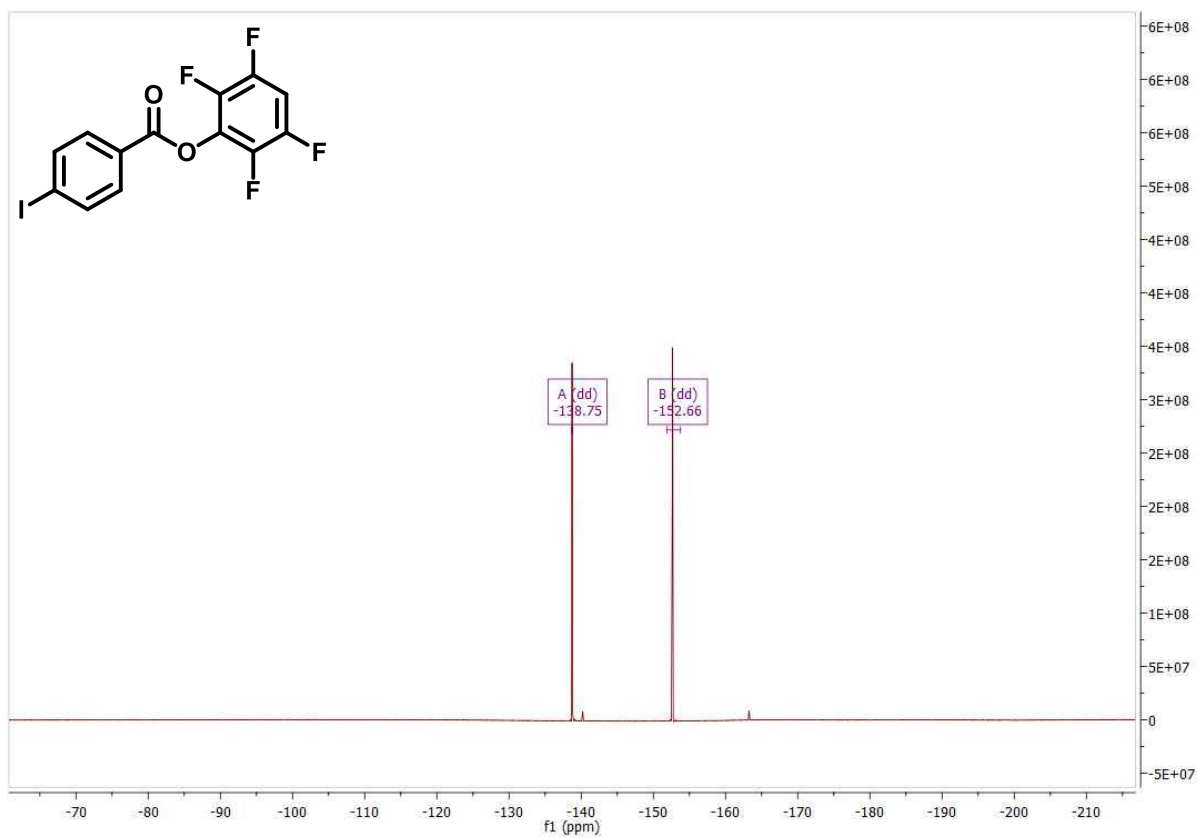
## 7 Experimental Part



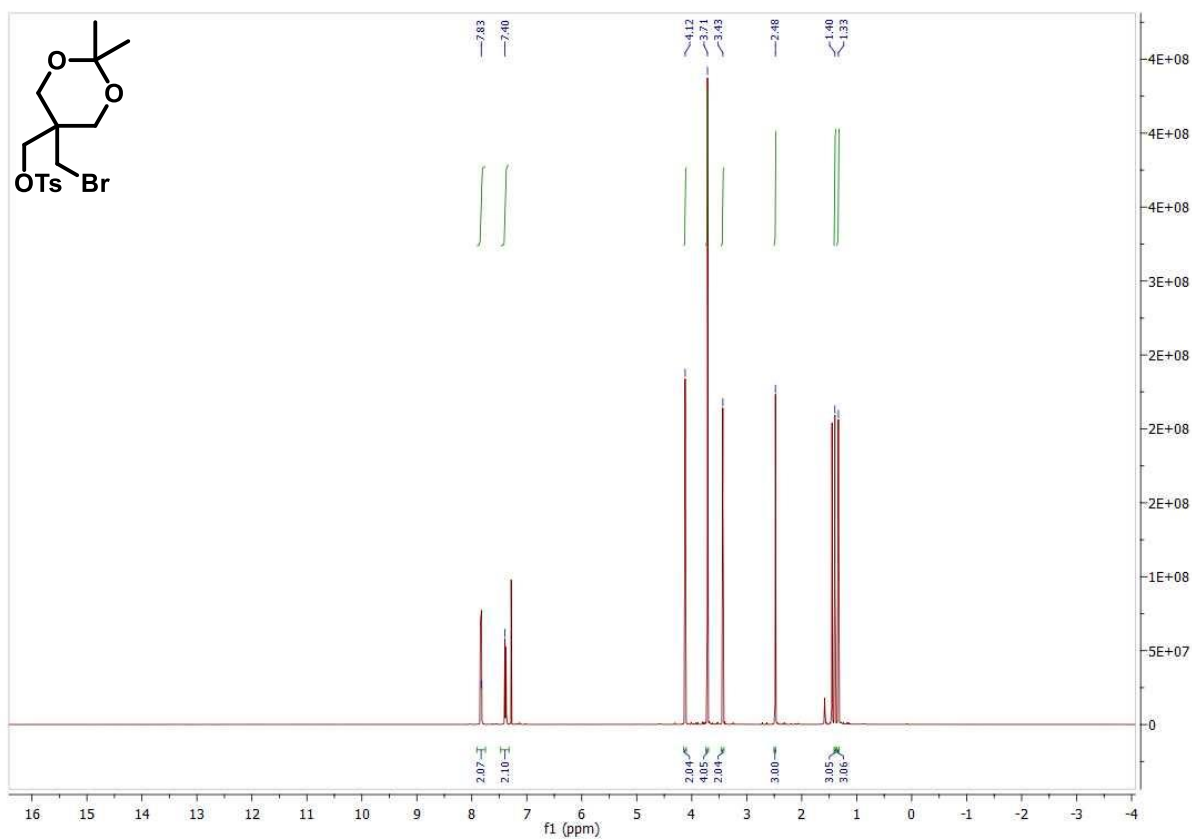
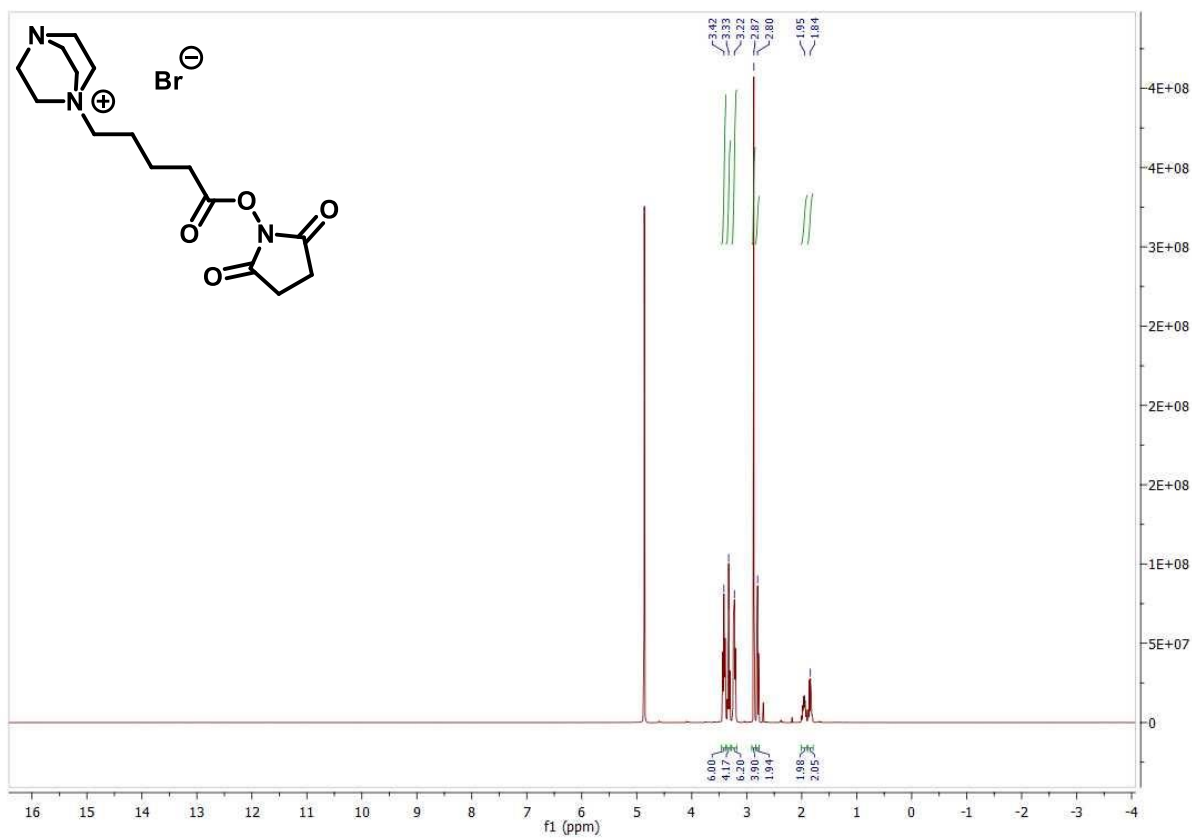
## 7 Experimental Part



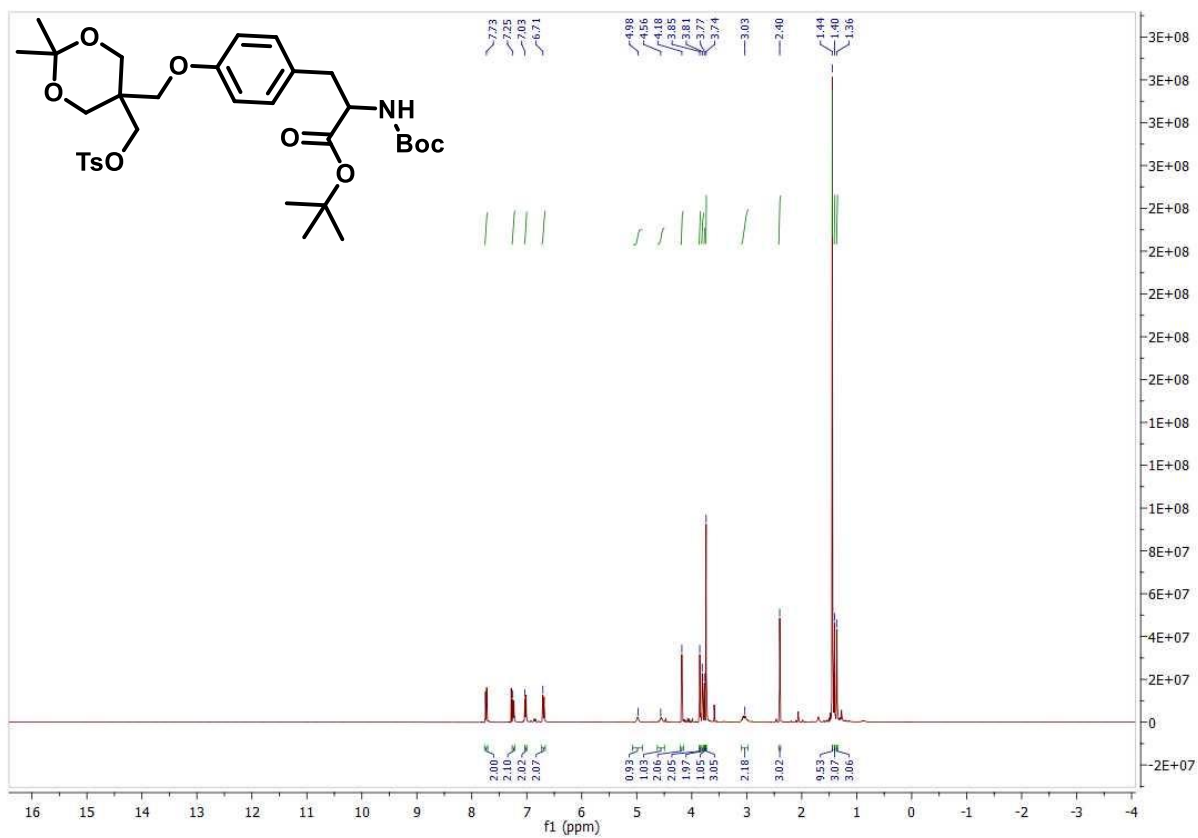
## 7 Experimental Part



## 7 Experimental Part

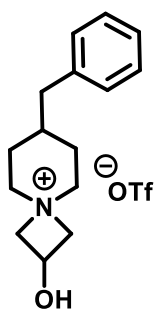


# 7 Experimental Part



### 7.3 Experimental Part for 3-Hydroxyazetidinium Salts

#### 7-Benzyl-2-hydroxy-4-azaspiro[3.5]nonan-4-ium triflate (32)



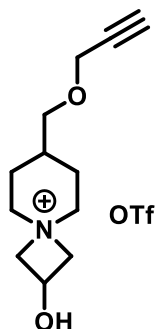
7-Benzyl-2-hydroxy-4-azaspiro[3.5]nonan-4-ium tosylate was synthesized starting from 4-benzylpiperidine. 4-Benzylpiperidine (5.7 mmol, 1 g, 1 equiv.) was stirred for 16 h with epichlorohydrin (5.7 mmol, 0.526 g, 445  $\mu$ L, 1 equiv.). Afterwards, the reaction mixture was diluted with EtOAc and the solvent mixture removed under reduced pressure until a colorless solid formed. The solid was filtered off and washed with EtOAc and used without further purification for the next step. The solid was dissolved in MeOH with AgOTf (5.7 mmol, 1.288 g, 1 equiv.) and stirred for 30 min. The formed solid was filtered off with cotton and the filtrate was evaporated to give the analytically pure triflate (5 mmol, 1.9 g, 88%).

$^1\text{H}$  NMR (400 MHz,  $\text{CDCl}_3$ )  $\delta$  = 7.34 – 7.27 (m, 2H), 7.22 (ddt,  $J$  = 7.3, 6.0, 3.0 Hz, 1H), 7.15 – 7.10 (m, 2H), 4.86 – 4.78 (m, 1H), 4.49 (dt,  $J$  = 12.2, 7.3 Hz, 2H), 4.18 – 4.02 (m, 3H), 3.86 (d,  $J$  = 12.6 Hz, 1H), 3.65 (d,  $J$  = 12.6 Hz, 1H), 3.34 – 3.14 (m, 2H), 2.57 (d,  $J$  = 6.8 Hz, 2H), 1.87 – 1.73 (m, 3H), 1.55 – 1.36 (m, 2H).

$^{13}\text{C}$  NMR (101 MHz,  $\text{CDCl}_3$ )  $\delta$  = 138.48, 129.01, 128.61, 126.56, 73.47, 68.75, 62.20, 60.79, 59.08, 41.46, 34.45, 27.20, 26.78. The additional aliphatic signals are due to an equilibrium with the open chained 3-(4-benzylpiperidin-1-yl)-2-hydroxypropyl trifluoromethanesulfonate.

$^{19}\text{F}$  NMR (376 MHz,  $\text{CDCl}_3$ )  $\delta$  = -78.48.

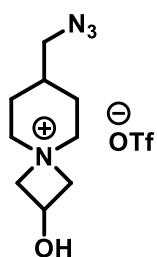
**2-Hydroxy-7-((prop-2-yn-1-yloxy)methyl)-4-azaspiro[3.5]nonan-4-ium triflate (34)**



2-Hydroxy-7-((prop-2-yn-1-yloxy)methyl)-4-azaspiro[3.5]nonan-4-ium triflate was synthesized starting from 4-((prop-2-yn-1-yloxy)methyl)piperidin-1-ium chloride. It (4.4 mmol, 0.830 g, 1 equiv.) was stirred for 16 h with epichlorohydrin (4.8 mmol, 0.447 g, 379  $\mu$ L, 1.1 equiv.) and  $\text{NEt}_3$  (4.4 mmol, 0.444 g, 584  $\mu$ L, 1.0 equiv.). Afterwards, the reaction mixture was diluted with EtOAc and the solvent mixture removed under reduced pressure until a colorless solid formed. The solid was filtered off and washed with EtOAc and used without further purification for the next step. The solid was dissolved in MeOH with AgOTf (0.2 mmol, 50 mg) and stirred for 30 min. The formed solid was filtered off with cotton and the filtrate was evaporated to give the analytically pure triflate (0.18 mmol, 57 mg, 4%).

$^1\text{H}$  NMR (400 MHz,  $\text{CD}_3\text{OD}$ )  $\delta$  = 4.76 (ddd,  $J$  = 11.5, 6.8, 4.9 Hz, 1H), 4.60 – 4.48 (m, 2H), 4.21 – 4.14 (m, 2H), 4.13 – 4.06 (m, 2H), 3.88 – 3.79 (m, 1H), 3.74 – 3.65 (m, 1H), 3.49 – 3.42 (m, 3H), 3.29 – 3.19 (m, 3H), 2.02 – 1.89 (m, 2H), 1.71 – 1.53 (m, 2H).

**7-(Azidomethyl)-2-hydroxy-4-azaspiro[3.5]nonan-4-ium triflate (36)**



7-(azidomethyl)-2-hydroxy-4-azaspiro[3.5]nonan-4-ium triflate was synthesized starting from 4-(azidomethyl)piperidin-1-ium chloride. It (3.4 mmol, 1 equiv., 600 mg) was stirred for 16 h with epichlorohydrin (5.1 mmol, 0.471 g, 428  $\mu$ L, 1.5 equiv.) and  $\text{NEt}_3$  (3.7 mmol, 0.378 g, 500  $\mu$ L, 1.1 equiv.). Afterwards, the reaction mixture was diluted with EtOAc and the solvent mixture removed under reduced pressure until a colorless solid formed. The solid was filtered off and washed with EtOAc and used without further purification for the next step. The solid was dissolved in MeOH with AgOTf (3.4 mmol, 0.900 g, 1 equiv.) and stirred for 30 min. The formed solid was filtered off with cotton and the filtrate was evaporated to give the analytically pure triflate (1.7 mmol, 0.560 g, 49%)

$^1\text{H}$  NMR (400 MHz,  $\text{CD}_3\text{OD}$ )  $\delta$  = 4.76 (ddd,  $J$  = 11.5, 6.7, 4.9 Hz, 1H), 4.63 – 4.46 (m, 2H), 4.10 (ddd,  $J$  = 11.2, 6.5, 2.6 Hz, 2H), 3.85 (dd,  $J$  = 12.4, 2.1 Hz, 1H), 3.74 – 3.67 (m, 1H), 3.47 (d,  $J$  = 6.2 Hz, 2H), 3.38 – 3.30 (m, 3H), 1.94 (d,  $J$  = 15.0 Hz, 2H), 1.66 – 1.47 (m, 2H).

### Radiofluorination

All analysis was performed on a Knauer HPLC with a Knauer Azura UVD 2.1S UV-detector and a Berthold Herm LB 500 radiodetector, the determination of the RCCs was done in Clarity Chrome by comparing the decay corrected peak integral areas with the decay corrected peak integral areas of an injection bypassing the column. The HPLC chromatograms were recorded on a Luna 5  $\mu\text{m}$  PFP(2) 100 Å LC column 250x4.6 mm. Unless otherwise specified a gradient method with water and acetonitrile with 0.1% TFA was used as follows 0-8 min 5->20% MeCN, 8-17 min 20->95% MeCN, 17-25 min 95% 1 mL/min.

For the determination of the RCCs the reaction was quenched with water shaken and analyzed by radio-HPLC determining the ratio of the area of the product peak and the injection behind the column signifying the whole activity of the reaction without potential adsorption of [ $^{18}\text{F}$ ]fluoride on the column.

### General Procedure for Radiofluorination of 3-Hydroxyazetidinium Salts

The target water is diluted with distilled water and taken through a QMA cartridge (Waters Inc.). The cartridge is washed with dry MeOH (1.5 mL) from the male side. Afterwards the cartridge is dried with Argon from the female side for 30 s. The precursor (10  $\mu\text{mol}$ ) is dissolved in dry MeOH (0.5 mL) and the fixed [ $^{18}\text{F}$ ]fluoride is slowly eluted from the cartridge with the precursor solution from the female side of the cartridge into the reactor. The reactor is closed with a septum and the MeOH is evaporated at reduced pressure ( $\sim 300$  mBar) with a flow of argon at 60 °C. After the MeOH is removed ( $\sim 10$  min) the reaction solvent (0.5 mL) is given through the septum, and the reactor is vigorously shaken and placed in the Anton Parr inductive heater (Monowave 50).

After the heating process is complete the reactor is removed from the heater and the septum is removed. The reaction is diluted with water (1 mL) and the reactor is shaken for 30 seconds to account for eventually existing free fluoride sticking to the walls. Afterwards, the mixture is taken in a syringe and analyzed by radio-HPLC to determine the RCC.

## 7 Experimental Part

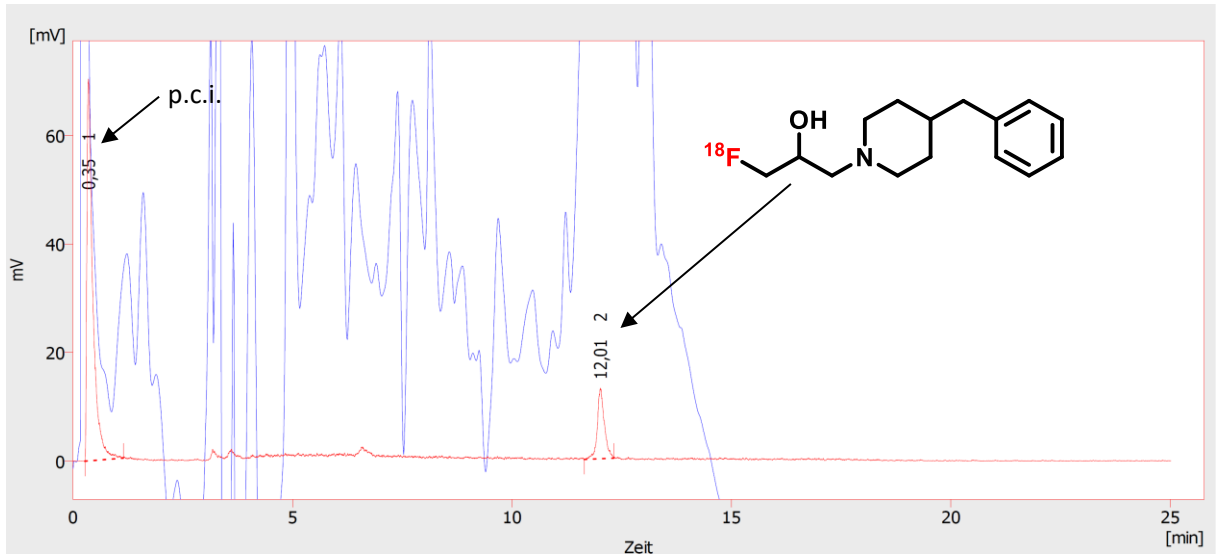


Figure 93: Eluent: 0–8 min: 5→20% MeCN (0.1% TFA), 8–17 min: 20→95% MeCN (0.1% TFA), 17–25 min: 95% MeCN (0.1% TFA); Flow rate: 1 mL/min; Luna 5 µm PFP(2) 100 Å LC column 250x4.6 mm; p.c.i. = post column injection. Red: Radio HPLC trace, blue: UV trace 234 nm.

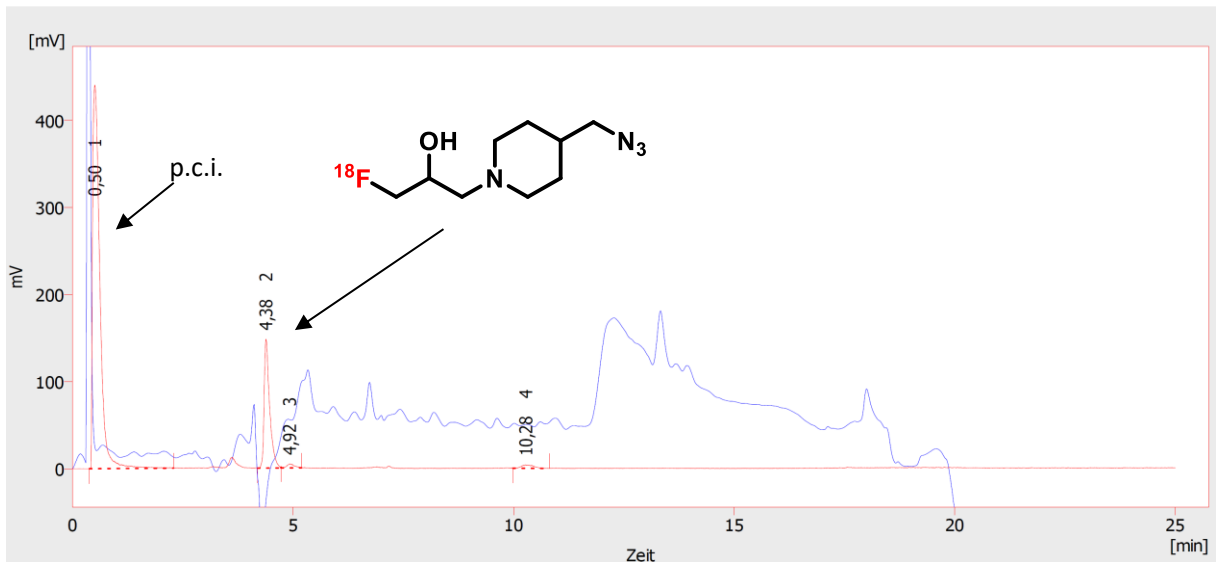
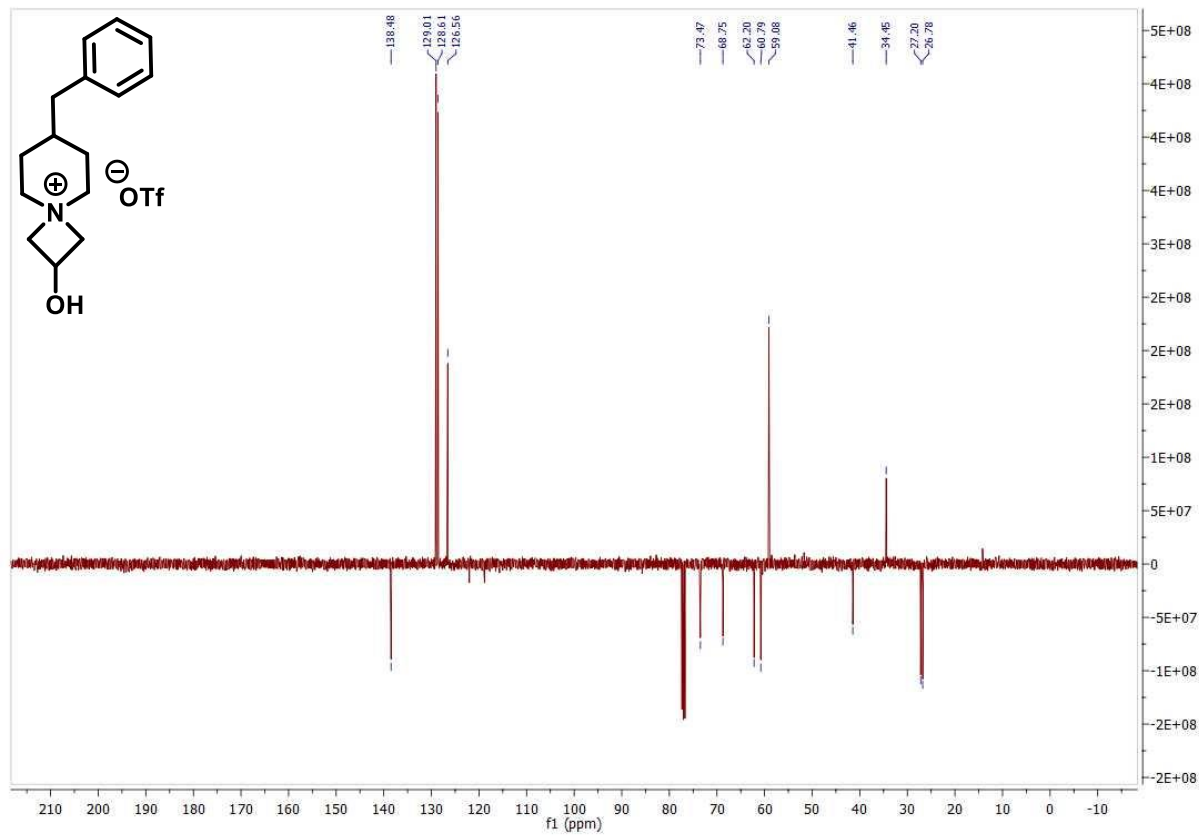
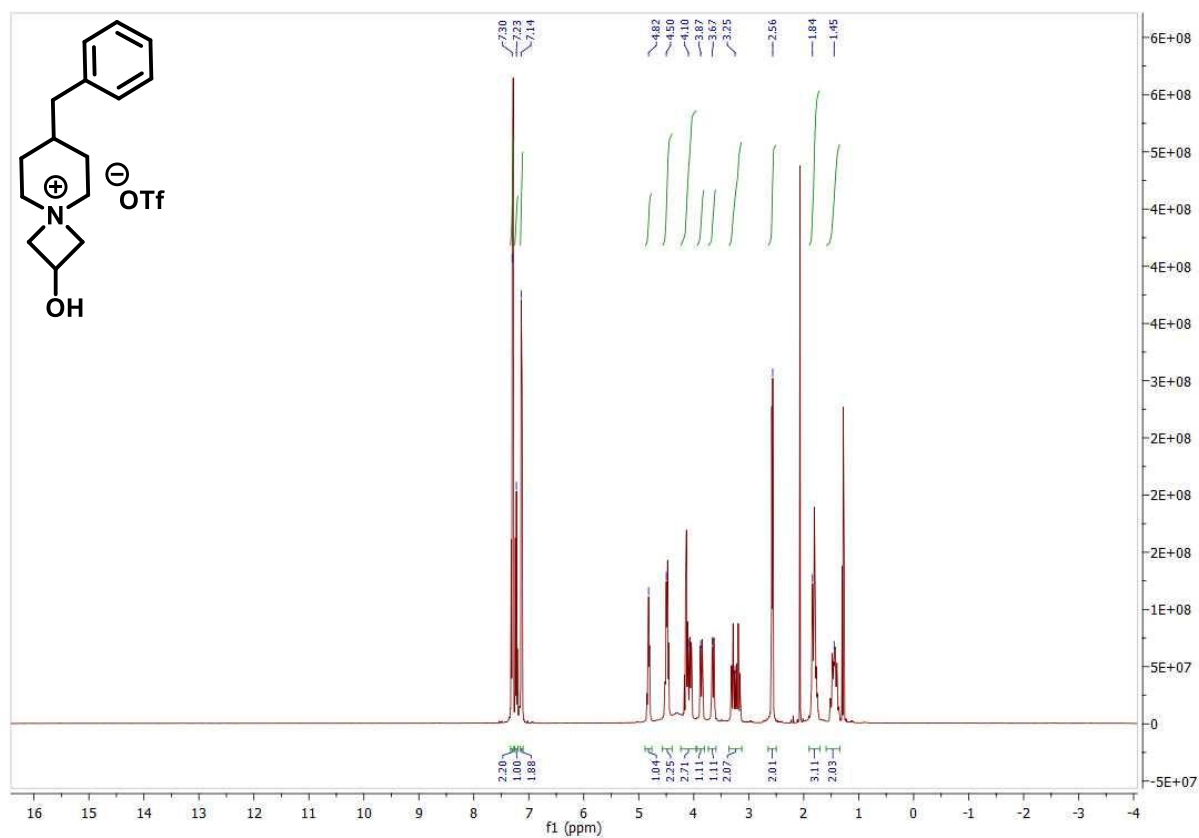


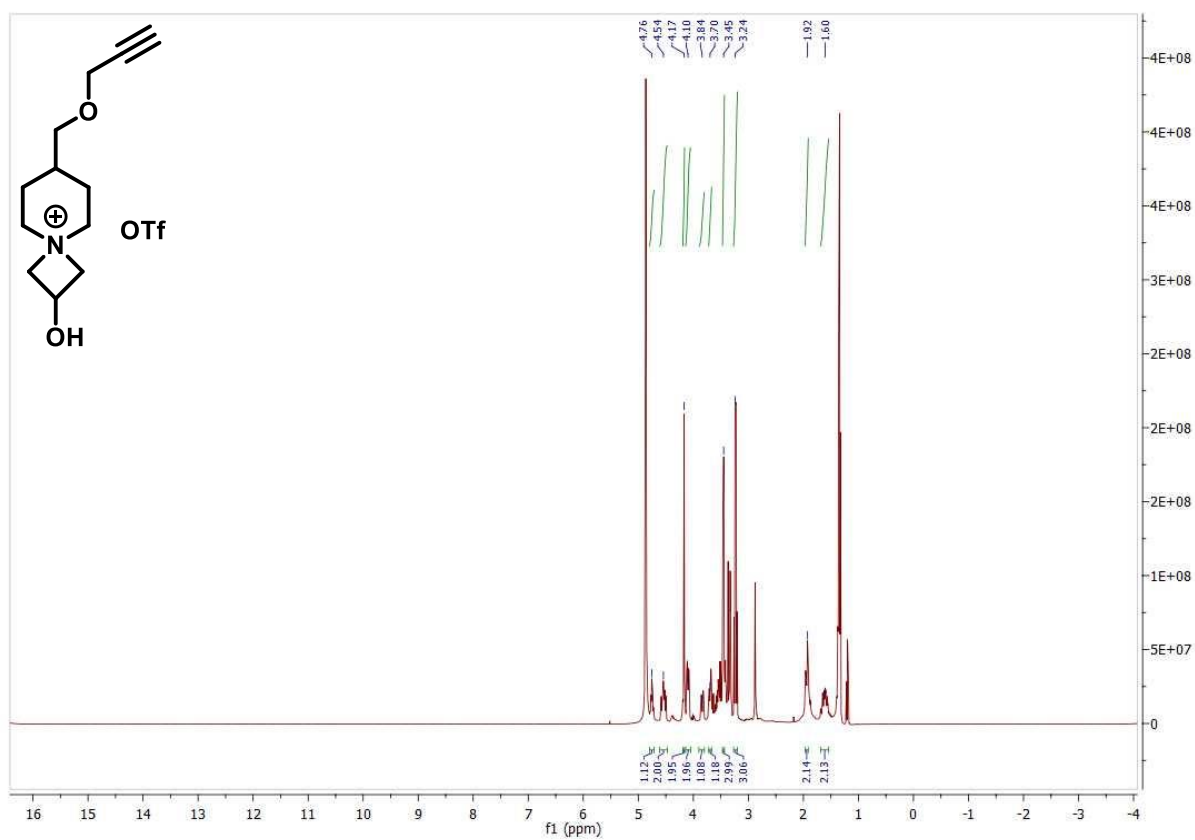
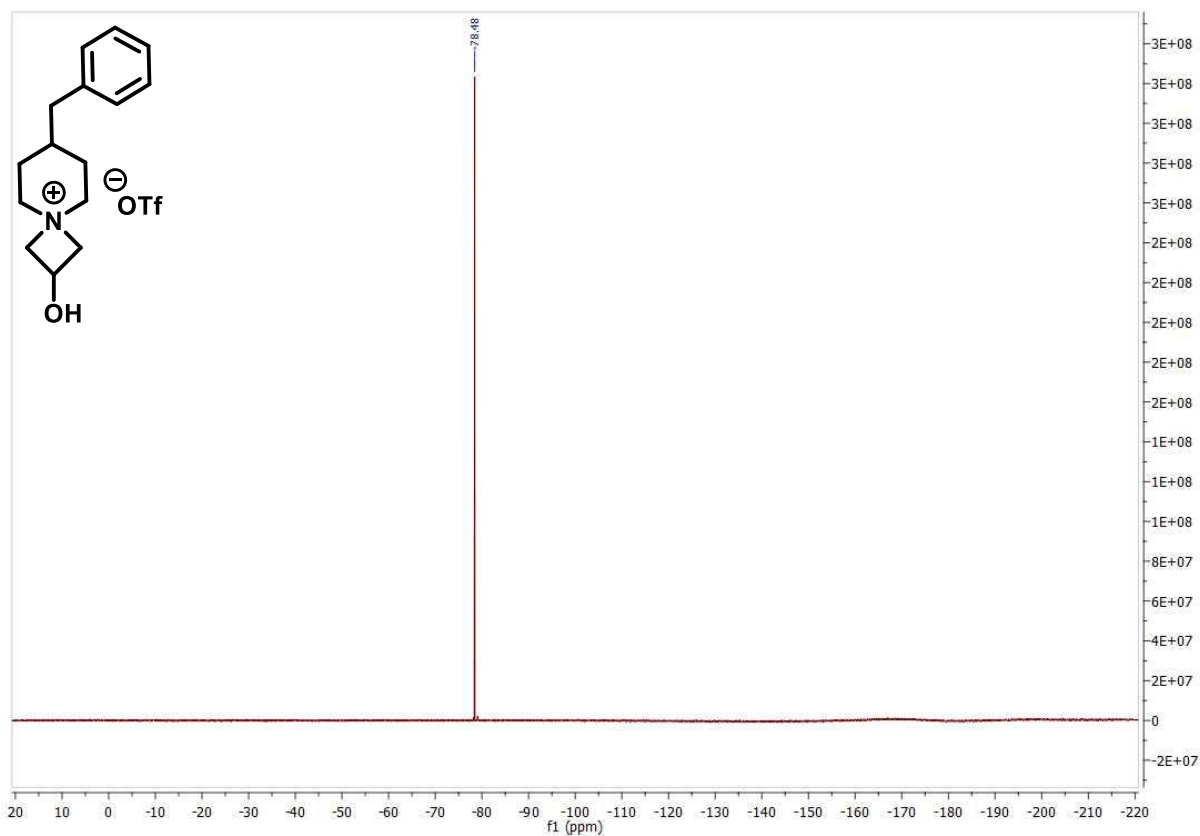
Figure 94: Eluent: 0–8 min: 5→20% MeCN (0.1% TFA), 8–17 min: 20→95% MeCN (0.1% TFA), 17–25 min: 95% MeCN (0.1% TFA); Flow rate: 1 mL/min; Luna 5 µm PFP(2) 100 Å LC column 250x4.6 mm; p.c.i. = post column injection. Red: Radio HPLC trace, blue: UV trace 234 nm.

## 7 Experimental Part

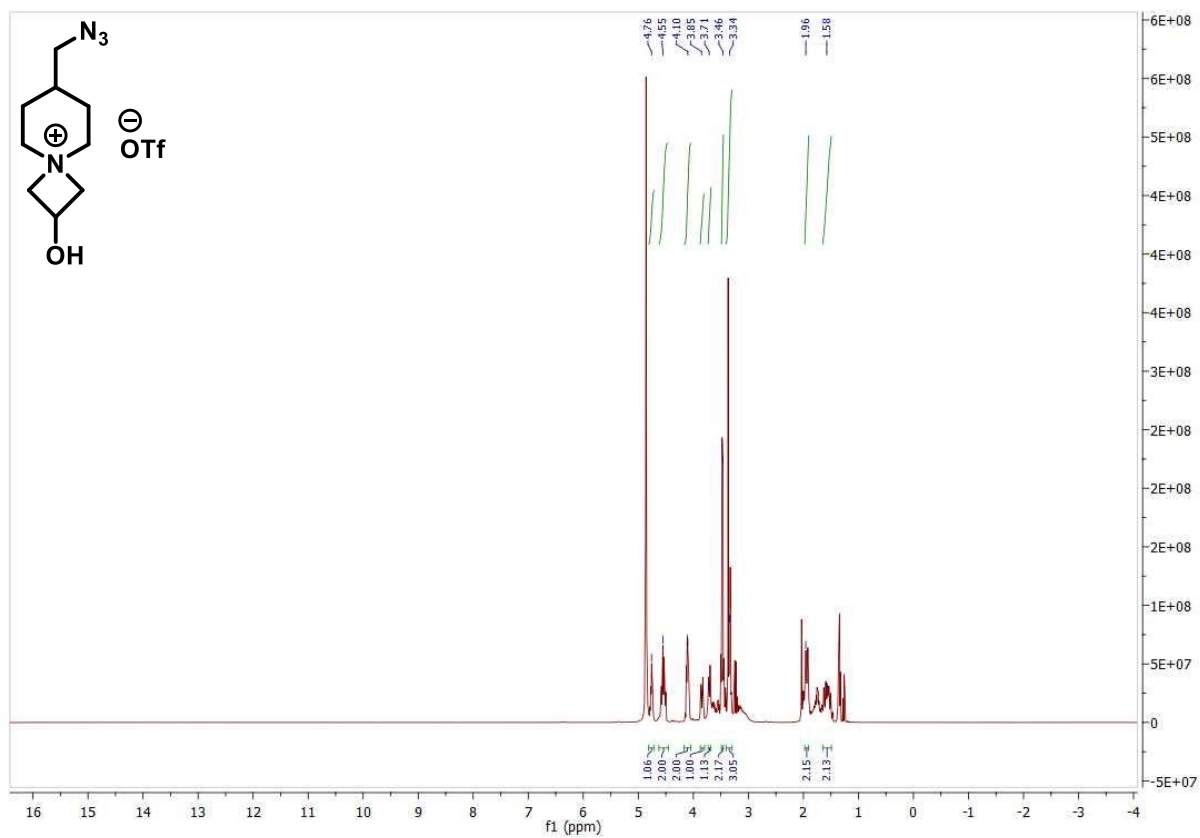
### NMR spectra



## 7 Experimental Part



## 7 Experimental Part



## 8 References

- [1] J.-V. Kratz, K. H. Lieser (Hrsg.) *Nuclear and Radiochemistry. Fundamentals and applications using ICP-MS*, Wiley, Weinheim, **2013**.
- [2] P. Moskal, D. Kisiełowska, C. Curceanu, E. Czerwiński, K. Dulski, A. Gajos, M. Gorgol, B. Hiesmayr, B. Jasińska, K. Kacprzak et al., *Physics in medicine and biology* **2019**, *64*, 55017.
- [3] P. Moskal, B. Jasińska, E. Ł. Stępień, S. D. Bass, *Nat Rev Phys* **2019**, *1*, 527.
- [4] M. D. Harpen, *Medical physics* **2004**, *31*, 57.
- [5] D. Prakash, D. Tafti, *Nuclear Medicine Computed Tomography Physics*, StatPearls Publishing, Treasure Island (FL), **2024**.
- [6] G. Blessing, H.H. Coenen, K. Franken, S.M. Qaim, *International Journal of Radiation Applications and Instrumentation. Part A. Applied Radiation and Isotopes* **1986**, 1135.
- [7] H. H. Coenen, *Ernst Schering Research Foundation workshop* **2007**, 15.
- [8] C.-G. Zhan, D. A. Dixon, *J. Phys. Chem. A* **2004**, *108*, 2020.
- [9] S. J. Lee, M. T. Morales-Colón, A. F. Brooks, J. S. Wright, K. J. Makaravage, P. J. H. Scott, M. S. Sanford, *The Journal of organic chemistry* **2021**, *86*, 14121.
- [10] D. J. Schlyer, M. L. Firouzbakht, A. P. Wolf, *Applied radiation and isotopes : including data, instrumentation and methods for use in agriculture, industry and medicine* **1993**, *44*, 1459.
- [11] S. Yu, *Biomedical imaging and intervention journal* **2006**, *2*, e57.
- [12] E. E. Kwan, Y. Zeng, H. A. Besser, E. N. Jacobsen, *Nature chemistry* **2018**, *10*, 917.
- [13] R. Richarz, P. Krapf, F. Zarrad, E. A. Urusova, B. Neumaier, B. D. Zlatopolskiy, *Org. Biomol. Chem.* **2014**, *12*, 8094.
- [14] B. D. Zlatopolskiy, J. Zischler, P. Krapf, R. Richarz, K. Lauchner, B. Neumaier, *Journal of labelled compounds & radiopharmaceuticals* **2019**, *62*, 404.
- [15] H. Sun, S. G. DiMagno, *Journal of Fluorine Chemistry* **2007**, *128*, 806.
- [16] J. Ford, S. Ortalli, Z. Chen, J. B. I. Sap, M. Tredwell, V. Gouverneur, *Angewandte Chemie (International ed. in English)* **2024**, *63*, e202404945.
- [17] D. I. Bugaenko, M. A. Yurovskaya, A. V. Karchava, *Organic letters* **2018**, *20*, 6389.
- [18] S. Humpert, M. A. Omrane, E. A. Urusova, L. Gremer, D. Willbold, H. Endepols, R. N. Krasikova, B. Neumaier, B. D. Zlatopolskiy, *Chemical communications (Cambridge, England)* **2021**, *57*, 3547.

## 8 References

- [19] V. W. Pike, *Labelled Comp Radiopharmac* **2018**, *61*, 196.
- [20] Y.-S. Lee, J.-H. Chun, M. Hodošček, V. W. Pike, *Chemistry (Weinheim an der Bergstrasse, Germany)* **2017**, *23*, 4353.
- [21] J.-H. Chun, V. W. Pike, *J. Org. Chem.* **2012**, *77*, 1931.
- [22] a) V. W. Pike, F. Butt, A. Shah, D. A. Widdowson, *J. Chem. Soc., Perkin Trans. 1* **1999**, 245; b) Gerald F. Koser/Richard H. Wettach.
- [23] A. Shah, V. W. Pike, D. A. Widdowson, *J. Chem. Soc., Perkin Trans. 1* **1997**, 2463.
- [24] Gerald F. Koser/Richard H. Wettach/Carol S. Smith.
- [25] W.-J. Kuik, I. P. Kema, A. H. Brouwers, R. Zijlma, K. D. Neumann, R. A. J. O. Dierckx, S. G. DiMugno, P. H. Elsinga, *Journal of nuclear medicine : official publication, Society of Nuclear Medicine* **2015**, *56*, 106.
- [26] B. H. Rotstein, L. Wang, R. Y. Liu, J. Patteson, E. E. Kwan, N. Vasdev, S. H. Liang, *Chemical science* **2016**, *7*, 4407.
- [27] K. Sander, T. Gendron, E. Yiannaki, K. Cybulska, T. L. Kalber, M. F. Lythgoe, E. Årstad, *Scientific reports* **2015**, *5*, 9941.
- [28] P. Xu, Da Zhao, F. Berger, A. Hamad, J. Rickmeier, R. Petzold, M. Kondratiuk, K. Bohdan, T. Ritter, *Angewandte Chemie (International ed. in English)* **2020**, *59*, 1956.
- [29] P. R. Khoury, J. D. Goddard, W. Tam, *Tetrahedron* **2004**, *60*, 8103.
- [30] D. O. Kiesewetter, W. C. Eckelman, *Labelled Comp Radiopharmac* **2004**, *47*, 953.
- [31] F. Reissig, C. Mamat, *ChemistryOpen* **2022**, *11*, e202200039.
- [32] CHI DAE-YOON, WO\_2012050315\_A2.
- [33] S. D. Ross, J. J. Bruno, R. C. Petersen, *J. Am. Chem. Soc.* **1963**, *85*, 3999.
- [34] N. Maraš, S. Polanc, M. Kočever, *Organic & biomolecular chemistry* **2012**, *10*, 1300.
- [35] J. Seo, D. Kim, H. M. Ko, *Adv Synth Catal* **2020**, *362*, 2739.
- [36] F. Wuest, C. Hultsch, M. Berndt, R. Bergmann, *Bioorganic & medicinal chemistry letters* **2009**, *19*, 5426.
- [37] Mohamed Aymen Omrane. Entwicklung von neuen Radiofluorierungsmethoden für die effiziente Produktion von klinisch relevanten PET-Tracern. Universität zu Köln.
- [38] A. Sivo, V. Ruta, G. Vilé, *The Journal of organic chemistry* **2021**, *86*, 14113.
- [39] C.-L. Ma, X.-L. Yu, X.-L. Zhu, Y.-Z. Hu, X.-W. Dong, B. Tan, X.-Y. Liu, *Adv Synth Catal* **2015**, *357*, 569.

## 8 References

- [40] R. Chekol, O. Gheysens, M. Ahamed, J. Cleynhens, P. Pokreisz, G. Vanhoof, S. Janssens, A. Verbruggen, G. Bormans, *Journal of medicinal chemistry* **2017**, *60*, 486.
- [41] Michael Härter, Hartmut Beck, Peter Ellinghaus, Kerstin Berhörster, Susanne Greschat, Karl-Heinz Thierauch, Frank Süßmeier, US20130196964A1.
- [42] G. Laudadio, H. P. L. Gemoets, V. Hessel, T. Noël, *J. Org. Chem.* **2017**, *82*, 11735.
- [43] CAMA LOVJI D (US), WILKENING ROBERT R (US), RATCLIFFE RONALD W (US), WILDONGER KENNETH J (US), SUN WANYING (US), US6140318A.
- [44] D. I. Bugaenko, M. A. Yurovskaya, A. V. Karchava, *J. Org. Chem.* **2017**, *82*, 2136.
- [45] S. BUSS, GIESE ARMIN, C. GRIESINGER, K. HERFERT, L. KUBLER, A. LEONOV, A. MAURER, B. PICHLER, S. RYAZANOV, F. SCHMIDT et al., CA3160364A1.
- [46] M. Pretze, C. Mamat, *Journal of Fluorine Chemistry* **2013**, *150*, 25.
- [47] A. A. Lee, Y.-C. S. Chen, E. Ekalestari, S.-Y. Ho, N.-S. Hsu, T.-F. Kuo, T.-S. A. Wang, *Angewandte Chemie (International ed. in English)* **2016**, *55*, 12338.
- [48] V. V. Orlovskaya, D. J. Modemann, O. F. Kuznetsova, O. S. Fedorova, E. A. Urusova, N. Kolks, B. Neumaier, R. N. Krasikova, B. D. Zlatopolskiy, *Molecules (Basel, Switzerland)* **2019**, *24*.

## 9 List of Abbreviations

Ac: Acetate

AY: Activity yield

Boc: *tert*-Butyloxycarbonyl

DABCO: 1,4-Diazabicyclo[2.2.2]octane

DCM: Dichloromethane

DMF: Dimethylformamide

EDC: 1-Ethyl-3-(3-dimethylaminopropyl)carbodiimide hydrochlorid

HATU: *O*-(7-Azabenzotriazol-1-yl)-*N,N,N',N'*-tetramethyluronium-hexafluorophosphat

LG: Leaving group

mCPBA: *m*-Chloroperoxybenzoic acid

n.c.a.: Non-carrier-added

Nu: Nucleophile

p.c.i.: Post column injection

RCC: Radiochemical conversion

RCY: Radiochemical yield

PSMA: Prostate-specific membrane antigen

r.t.: Room temperature

TBAT: Tetrabutylammoniumdifluorotriphenylsilicate

Tf: Triflyl

TFA: Trifluoroacetic acid

Ts: Tosyl

## 10 List of Figures

Figure 1: Radioactive decay options for proton rich nuclides.....	7
Figure 2: Scheme of $\beta^+$ -decay with positronium variants <sup>[3,2,4]</sup> .....	8
Figure 3: Coordination of water molecules around fluorine in water. ....	11
Figure 4: Preparation of [ <sup>18</sup> F]FDG by nucleophilic radiofluorination <sup>[11]</sup> .....	11
Figure 5: Mechanism of the S <sub>N</sub> 2 reaction. ....	13
Figure 6: Mechanisms of the S <sub>N</sub> Ar reaction.....	14
Figure 7: Example for S <sub>N</sub> Ar radiofluorination <sup>[9]</sup> . ....	14
Figure 8: [ <sup>18</sup> F]Fluoride workup with onium salt precursors as elution salts. ....	15
Figure 9: Minimalist radiofluorination of trimethylammonium benzaldehyde triflate. ....	15
Figure 10: Minimalist radiofluorination of an active ester. ....	16
Figure 11: Radiofluorination of a derivative of a PSMA inhibitor with the green minimalist approach.....	17
Figure 12: Overview of onium salt precursors conveniently used for nucleophilic aromatic radiofluorination. ....	18
Figure 13: Formation of undesired side products in radiofluorination of <i>N, N, N</i> -trimethylammonium salts <sup>[15]</sup> .....	18
Figure 14: Use of a pyridinium salt as precursor for nucleophilic radiofluorination <sup>[16]</sup> .....	19
Figure 15: Use of a DABCO salt as leaving group for nucleophilic radiofluorination <sup>[18]</sup> . ....	20
Figure 16: Mechanism of the copper-free radiofluorination of iodonium salts <sup>[19]</sup> .....	21
Figure 17: Selection of synthesis routes for asymmetric iodonium salts <sup>[19]</sup> . ....	22
Figure 18: Synthesis of 6-[ <sup>18</sup> F]FDOPA from an asymmetric iodonium salt precursor <sup>[25]</sup> . ...	23
Figure 19: Radiofluorination of an ylide precursor <sup>[26]</sup> .....	23
Figure 20: Synthesis and radiofluorination of a sulfonium salt precursor <sup>[27]</sup> .....	24
Figure 21: Radiofluorination of a triarylsulfonium salt following the minimalist protocol <sup>[13]</sup> . .....	24
Figure 22: Radiofluorination of a dibenzothiophenium salt precursor.....	25
Figure 23: Synthesis of an azetidinium salt <sup>[30]</sup> .....	26
Figure 24: Mechanism of the nucleophilic ring opening of azetidinium salts <sup>[31]</sup> . ....	27
Figure 25: Radiofluorination of an azetidinium salt <sup>[30]</sup> .....	27
Figure 26: Preparation of [ <sup>18</sup> F]FP-CIT by nucleophilic radiofluorination of an azetidinium salt <sup>[32]</sup> .....	28

## 10 List of Figures

Figure 27: Pathways for the nucleophilic attack on DABCO salts. ....	29
Figure 28: Reaction pathway in the ring opening of an aromatic DABCO salt <sup>[33]</sup> . ....	30
Figure 29: Ring opening of DABCO salts with nucleophiles <sup>[34]</sup> . ....	31
Figure 30: Scheme of the synthesis of ethyl piperazines via benzyne. ....	31
Figure 31: Example of the ring opening reaction for a in situ generated DABCO salt starting from the benzyne precursor <sup>[35]</sup> . ....	32
Figure 32. Radiofluorination of aliphatic DABCO-salts. ....	36
Figure 33. Proposed mechanism for the formation of ethylpiperazyl-DABCO salts. ....	37
Figure 34. Radiofluorination of ethylpiperazyl DABCO salts. ....	37
Figure 35: Synthesis of ethylpiperazyl DABCO salts starting from benzoyl bromide and tosyl chloride. ....	38
Figure 36: Radiofluorination of ethylpiperazyl-DABCO salts. ....	39
Figure 37: Synthesis of aromatic DABCO salts. ....	39
Figure 38. Scope of aromatic [ <sup>18</sup> F]fluoroethylpiperazyl substrates. ....	40
Figure 39: One-pot synthesis and radiofluorination of aromatic DABCO salts. ....	42
Figure 40: Synthesis of the model precursor. ....	44
Figure 41: Synthesis of the free acid starting from the ethyl ester. ....	49
Figure 42: Synthesis of amine bearing DABCO salt by reduction with hydrogen. ....	49
Figure 43: Reduction of the nitro bearing DABCO salt with zinc and ammoniumchloride. ....	50
Figure 44: Reduction of the nitro bearing DABCO salt with tin and hydrogenchloride. ....	50
Figure 45: Reduction of the nitro bearing DABCO salt with iron and acetic acid. ....	50
Figure 46: Conjugation of the amine DABCO salt with model compounds. ....	51
Figure 47: Conjugation of the amine DABCO salt with boc-glutaric anhydride. ....	52
Figure 48: Mechanism of the conjugation of the target molecule with an aminoxy peptide. ....	52
Figure 49: Synthesis of a ribose DABCO salt. ....	53
Figure 50: Radiofluorination attempt of the ribose DABCO salt. ....	53
Figure 51: Synthesis of DABCO-substituted PSMA ligand. ....	54
Figure 52: Proposed side reaction preventing isolation of the DABCO-substituted PSMA ligand. ....	55
Figure 53: Synthesis of DABCO bearing active esters. ....	55
Figure 54: Synthesis of a DABCO salt bearing PSMA precursor. ....	56

## 10 List of Figures

Figure 55: Synthesis of a tyrosine DABCO salt via a tyrosine iodonium salt.....	57
Figure 56: Synthesis of a tyrosine DABCO salt with a linker. ....	58
Figure 57: Synthesis scheme of 7-benzyl-2-hydroxy-4-azaspiro[3.5]nonan-4-ium tosylate. .....	60
Figure 58: Schematic depiction of the silanization of a reactor wall. ....	62
Figure 59: Results of the radiofluorination with an inductive heater. ....	64
Figure 60: Radiofluorination attempt of alkyne-substituted 3-hydroxyazetidinium salt. ..	65
Figure 61: Radiofluorination of azide-substituted 3-hydroxyazetidinium salt. ....	65
Figure 62: UV trace of the semipreparative HPLC; column: Synergi 10u Hydro-RP 80A 250 x 10 mm 10 micron; eluent: 20% MeCN (0.1% TFA); flow rate: 3.7 mL/min. ....	129
Figure 63: Radio HPLC trace of the semipreparative HPLC; column: Synergi 10u Hydro-RP 80A 250 x 10 mm 10 micron; eluent: 20% MeCN (0.1% TFA); flow rate: 3.7 mL/min.....	129
Figure 64: Calibration curve of the non-radioactive reference compound (blue) and measured UV-absorption of the isolated radiolabeled compound (green). ....	130
Figure 65: Radio trace of the quality control of the isolated product Eluent: 30% MeCN (0.1% TFA), Flow rate: 1 mL/min isocratic. Luna 5 µm PFP(2) 100 Å LC column 250x4.6 mm p.c.i. = post column injection. ....	131
Figure 66: UV trace of the quality control of the isolated product. Eluent: 30% MeCN (0.1% TFA), Flow rate: 1 mL/min isocratic. Luna 5 µm PFP(2) 100 Å LC column 250x4.6 mm; UV: 234 nm.....	131
Figure 67: UV trace of the isolated product spiked with the non-radioactive reference compound. Eluent: 30% MeCN (0.1% TFA), Flow rate: 1 mL/min isocratic. Luna 5 µm PFP(2) 100 Å LC column 250x4.6 mm; UV: 234 nm.....	131
Figure 68: HPLC-chromatogram after the cartridge purification step. Eluent: 0–8 min: 5– >20% MeCN (0.1% TFA), 8–17 min: 20–>95% MeCN (0.1% TFA), 17–25 min: 95% MeCN (0.1% TFA); Flow rate: 1 mL/min; Luna 5 µm PFP(2) 100 Å LC column 250x4.6 mm; p.c.i. = post column injection. Red: Radio HPLC trace, blue: UV trace 234 nm.....	132
Figure 69: HPLC-chromatogram after the conjugation step. Eluent: 0–8 min: 5–>20% MeCN (0.1% TFA), 8–17 min: 20–>95% MeCN (0.1% TFA), 17–25 min: 95% MeCN (0.1% TFA); Flow rate: 1 mL/min; Luna 5 µm PFP(2) 100 Å LC column 250x4.6 mm; p.c.i. = post column injection. Red: Radio HPLC trace, blue: UV trace 234 nm.....	133

## 10 List of Figures

- Figure 70: Eluent: 30% MeCN (0.1% TFA), Flow rate: 1 mL/min isocratic. Luna 5  $\mu$ m PFP(2) 100 Å LC column 250x4.6 mm p.c.i. = post column injection. .... 134
- Figure 71: Eluent: 30% MeCN (0.1% TFA), Flow rate: 1 mL/min isocratic. Luna 5  $\mu$ m PFP(2) 100 Å LC column 250x4.6 mm, UV trace 234 nm..... 134
- Figure 72: Eluent: 0–8 min: 5→20% MeCN (0.1% TFA), 8–17 min: 20→95% MeCN (0.1% TFA), 17–25 min: 95% MeCN (0.1% TFA); Flow rate: 1 mL/min; Luna 5  $\mu$ m PFP(2) 100 Å LC column 250x4.6 mm; p.c.i. = post column injection. Red: Radio HPLC trace, blue: UV trace 234 nm..... 134
- Figure 73: Eluent: 0–8 min: 5→20% MeCN (0.1% TFA), 8–17 min: 20→95% MeCN (0.1% TFA), 17–25 min: 95% MeCN (0.1% TFA); Flow rate: 1 mL/min; Luna 5  $\mu$ m PFP(2) 100 Å LC column 250x4.6 mm; p.c.i. = post column injection. Red: Radio HPLC trace, blue: UV trace 234 nm..... 135
- Figure 74: Eluent: 0–8 min: 5→20% MeCN (0.1% TFA), 8–17 min: 20→95% MeCN (0.1% TFA), 17–25 min: 95% MeCN (0.1% TFA); Flow rate: 1 mL/min; Luna 5  $\mu$ m PFP(2) 100 Å LC column 250x4.6 mm; p.c.i. = post column injection. Red: Radio HPLC trace, blue: UV trace 234 nm..... 135
- Figure 75: Eluent: 0–8 min: 5→20% MeCN (0.1% TFA), 8–17 min: 20→95% MeCN (0.1% TFA), 17–25 min: 95% MeCN (0.1% TFA); Flow rate: 1 mL/min; Luna 5  $\mu$ m PFP(2) 100 Å LC column 250x4.6 mm; p.c.i. = post column injection. Red: Radio HPLC trace, blue: UV trace 234 nm..... 136
- Figure 76: Eluent: 0–8 min: 5→20% MeCN (0.1% TFA), 8–17 min: 20→95% MeCN (0.1% TFA), 17–25 min: 95% MeCN (0.1% TFA); Flow rate: 1 mL/min; Luna 5  $\mu$ m PFP(2) 100 Å LC column 250x4.6 mm; p.c.i. = post column injection. Red: Radio HPLC trace, blue: UV trace 234 nm..... 136
- Figure 77: Eluent: 25% MeCN (0.1% TFA); Flow rate: 1 mL/min; Luna 5  $\mu$ m PFP(2) 100 Å LC column 250x4.6 mm p.c.i. = post column injection. Red: Radio HPLC trace, blue: UV trace 234 nm..... 137
- Figure 78: Eluent: 0–8 min: 5→20% MeCN (0.1% TFA), 8–17 min: 20→95% MeCN (0.1% TFA), 17–25 min: 95% MeCN (0.1% TFA); Flow rate: 1 mL/min; Luna 5  $\mu$ m PFP(2) 100 Å LC column 250x4.6 mm; p.c.i. = post column injection. Red: Radio HPLC trace, blue: UV trace 234 nm..... 137

## 10 List of Figures

- Figure 79: Eluent: 25% MeCN (0.1% TFA); Flow rate: 1 mL/min; Luna 5  $\mu$ m PFP(2) 100 Å LC column 250x4.6 mm p.c.i. = post column injection. Red: Radio HPLC trace, blue: UV trace 234 nm..... 138
- Figure 80: Eluent: 25% MeCN (0.1% TFA); Flow rate: 1 mL/min; Luna 5  $\mu$ m PFP(2) 100 Å LC column 250x4.6 mm. p.c.i. = post column injection. Red: Radio HPLC trace, blue: UV trace 234 nm..... 138
- Figure 81: Eluent: 0–8 min: 5→20% MeCN (0.1% TFA), 8–17 min: 20→95% MeCN (0.1% TFA), 17–25 min: 95% MeCN (0.1% TFA); Flow rate: 1 mL/min; Luna 5  $\mu$ m PFP(2) 100 Å LC column 250x4.6 mm; p.c.i. = post column injection. Red: Radio HPLC trace, blue: UV trace 234 nm..... 139
- Figure 82: Eluent: 0–8 min: 5→20% MeCN (0.1% TFA), 8–17 min: 20→95% MeCN (0.1% TFA), 17–25 min: 95% MeCN (0.1% TFA); Flow rate: 1 mL/min; Luna 5  $\mu$ m PFP(2) 100 Å LC column 250x4.6 mm; p.c.i. = post column injection. Red: Radio HPLC trace, blue: UV trace 234 nm..... 139
- Figure 83: Eluent: 0–8 min: 5→20% MeCN (0.1% TFA), 8–17 min: 20→95% MeCN (0.1% TFA), 17–25 min: 95% MeCN (0.1% TFA); Flow rate: 1 mL/min; Luna 5  $\mu$ m PFP(2) 100 Å LC column 250x4.6 mm; p.c.i. = post column injection. Red: Radio HPLC trace, blue: UV trace 234 nm..... 140
- Figure 84: Eluent: 0–8 min: 5→20% MeCN (0.1% TFA), 8–17 min: 20→95% MeCN (0.1% TFA), 17–25 min: 95% MeCN (0.1% TFA); Flow rate: 1 mL/min; Luna 5  $\mu$ m PFP(2) 100 Å LC column 250x4.6 mm; p.c.i. = post column injection. Red: Radio HPLC trace, blue: UV trace 234 nm..... 140
- Figure 85: Eluent: 0–8 min: 5→20% MeCN (0.1% TFA), 8–17 min: 20→95% MeCN (0.1% TFA), 17–25 min: 95% MeCN (0.1% TFA); Flow rate: 1 mL/min; Luna 5  $\mu$ m PFP(2) 100 Å LC column 250x4.6 mm; p.c.i. = post column injection. Red: Radio HPLC trace, blue: UV trace 234 nm..... 141
- Figure 86: Eluent: 0–8 min: 5→20% MeCN (0.1% TFA), 8–17 min: 20→95% MeCN (0.1% TFA), 17–25 min: 95% MeCN (0.1% TFA); Flow rate: 1 mL/min; Luna 5  $\mu$ m PFP(2) 100 Å LC column 250x4.6 mm; p.c.i. = post column injection. Red: Radio HPLC trace, blue: UV trace 234 nm..... 141
- Figure 87: Eluent: 0–8 min: 5→20% MeCN (0.1% TFA), 8–17 min: 20→95% MeCN (0.1% TFA), 17–25 min: 95% MeCN (0.1% TFA); Flow rate: 1 mL/min; Luna 5  $\mu$ m PFP(2) 100 Å

## 10 List of Figures

LC column 250x4.6 mm; p.c.i. = post column injection. Red: Radio HPLC trace, blue: UV trace 234 nm.....	142
Figure 88: Eluent: 0–8 min: 5→20% MeCN (0.1% TFA), 8–17 min: 20→95% MeCN (0.1% TFA), 17–25 min: 95% MeCN (0.1% TFA); Flow rate: 1 mL/min; Luna 5 μm PFP(2) 100 Å	
LC column 250x4.6 mm; p.c.i. = post column injection. Red: Radio HPLC trace, blue: UV trace 234 nm.....	142
Figure 89: Eluent: 0–8 min: 5→20% MeCN (0.1% TFA), 8–17 min: 20→95% MeCN (0.1% TFA), 17–25 min: 95% MeCN (0.1% TFA); Flow rate: 1 mL/min; Luna 5 μm PFP(2) 100 Å	
LC column 250x4.6 mm; p.c.i. = post column injection. Red: Radio HPLC trace, blue: UV trace 234 nm.....	143
Figure 90: Eluent: 0–8 min: 5→20% MeCN (0.1% TFA), 8–17 min: 20→95% MeCN (0.1% TFA), 17–25 min: 95% MeCN (0.1% TFA); Flow rate: 1 mL/min; Luna 5 μm PFP(2) 100 Å	
LC column 250x4.6 mm; p.c.i. = post column injection. Red: Radio HPLC trace, blue: UV trace 234 nm.....	143
Figure 91: Eluent: 0–8 min: 5→20% MeCN (0.1% TFA), 8–17 min: 20→95% MeCN (0.1% TFA), 17–25 min: 95% MeCN (0.1% TFA); Flow rate: 1 mL/min; Luna 5 μm PFP(2) 100 Å	
LC column 250x4.6 mm; p.c.i. = post column injection. Red: Radio HPLC trace, blue: UV trace 234 nm.....	144
Figure 92: Eluent: 0–8 min: 5→20% MeCN (0.1% TFA), 8–17 min: 20→95% MeCN (0.1% TFA), 17–25 min: 95% MeCN (0.1% TFA); Flow rate: 1 mL/min; Luna 5 μm PFP(2) 100 Å	
LC column 250x4.6 mm; p.c.i. = post column injection. Red: Radio HPLC trace, blue: UV trace 234 nm.....	144
Figure 93: Eluent: 0–8 min: 5→20% MeCN (0.1% TFA), 8–17 min: 20→95% MeCN (0.1% TFA), 17–25 min: 95% MeCN (0.1% TFA); Flow rate: 1 mL/min; Luna 5 μm PFP(2) 100 Å	
LC column 250x4.6 mm; p.c.i. = post column injection. Red: Radio HPLC trace, blue: UV trace 234 nm.....	162
Figure 94: Eluent: 0–8 min: 5→20% MeCN (0.1% TFA), 8–17 min: 20→95% MeCN (0.1% TFA), 17–25 min: 95% MeCN (0.1% TFA); Flow rate: 1 mL/min; Luna 5 μm PFP(2) 100 Å	
LC column 250x4.6 mm; p.c.i. = post column injection. Red: Radio HPLC trace, blue: UV trace 234 nm.....	162

## 11 List of Tables

Table 1: Physical properties of radionuclides commonly used in positron emission tomography <sup>[5]</sup> .....	9
Table 2: Influence of the reaction temperature and the heating method on the radiochemical conversions (RCCs). ....	35
Table 3: Optimization of reaction temperature and heating method. ....	45
Table 4: Example reactions to investigate the influence of silanization and presence of a stirring bar on the RCC. ....	46
Table 5: Determination of optimal precursor amount.....	47
Table 6: Influence of solvents on the ratio of ring opening and aromatic substitution reaction. ....	48
Table 7: Preliminary experiments for the determination of RCC.....	61
Table 8: Determination of the effect of precursor loading and solvent volume on radiochemical conversion. ....	61
Table 9: Optimization of non-stirred 3-hydroxyazetidinium salt radiofluorinations.....	62
Table 10: Investigation of microwave heating on the reaction. ....	63
Table 11: Program of the Anton Parr inductive heater.....	126

## **12 Attachment: Erklärung gemäß § 7 Absatz 8**

„Hiermit versichere ich an Eides statt, dass ich die vorliegende Dissertation selbstständig und ohne die Benutzung anderer als der angegebenen Hilfsmittel und Literatur angefertigt habe. Alle Stellen, die wörtlich oder sinngemäß aus veröffentlichten und nicht veröffentlichten Werken dem Wortlaut oder dem Sinn nach entnommen wurden, sind als solche kenntlich gemacht. Ich versichere an Eides statt, dass diese Dissertation noch keiner anderen Fakultät oder Universität zur Prüfung vorgelegen hat; dass sie - abgesehen von unten angegebenen Teilpublikationen und eingebundenen Artikeln und Manuskripten - noch nicht veröffentlicht worden ist sowie, dass ich eine Veröffentlichung der Dissertation vor Abschluss der Promotion nicht ohne Genehmigung des Promotionsausschusses vornehmen werde. Die Bestimmungen dieser Ordnung sind mir bekannt. Darüber hinaus erkläre ich hiermit, dass ich die Ordnung zur Sicherung guter wissenschaftlicher Praxis und zum Umgang mit wissenschaftlichem Fehlverhalten der Universität zu Köln gelesen und sie bei der Durchführung der Dissertation zugrundeliegenden Arbeiten und der schriftlich verfassten Dissertation beachtet habe und verpflichte mich hiermit, die dort genannten Vorgaben bei allen wissenschaftlichen Tätigkeiten zu beachten und umzusetzen. Ich versichere, dass die eingereichte elektronische Fassung der eingereichten Druckfassung vollständig entspricht.“

Yannick Keuthen